

**Tetsuo Sasao and André B. Fletcher**  
**Introduction to VLBI Systems**  
**Chapter 3**

Lecture Notes for KVN Students  
Partly Based on Ajou University Lecture Notes  
Issued July 14, 2005  
revised September 25, 2005  
revised October 28, 2005  
revised November 11, 2005  
(to be further edited)

# Radio Interferometry

## Contents

<b>1</b>	<b>Fundamentals of Radio Interferometry</b>	<b>4</b>
1.1	Two Explanations of VLBI . . . . .	4
1.1.1	VLBI System . . . . .	4
1.1.2	“Geodetic” Explanation — Noise Approach . . . . .	5
1.1.3	“Astrophysical” Explanation — Monochromatic Wave Approach . . . . .	6
1.1.4	Superposition of Monochromatic Waves . . . . .	7
1.1.5	Fringe Pattern Appears within an Envelope . . . . .	9
1.1.6	Peak of the Envelope . . . . .	9
1.1.7	Fringe Pattern Enclosed by the Envelope . . . . .	10
1.2	Elements of Stationary Random Processes . . . . .	12
1.2.1	Basic Concepts . . . . .	13
1.2.2	Random Processes in Linear Systems . . . . .	26
1.2.3	Stationary Random Processes . . . . .	28
1.2.4	Ergodicity . . . . .	30
1.2.5	Stationary Random Processes in Linear Systems . . . . .	33
1.2.6	Spectra of Stationary Random Processes . . . . .	35
1.2.7	Spectra of Outputs of Linear Systems . . . . .	41
1.2.8	Two Designs of Spectrometers . . . . .	43
1.2.9	Fourier Transforms of Stationary Random Processes . . . . .	45

1.3	The White Fringe . . . . .	49
1.3.1	A Simple Interferometer . . . . .	49
1.3.2	Received Voltages as Stationary Random Processes . .	50
1.3.3	Cross-Correlation of Received Voltages . . . . .	51
1.3.4	Fringe Pattern Enclosed by Bandwidth Pattern . . . .	55
1.3.5	Amplitude and Phase Spectra of the Correlated Signals	58
1.3.6	Coherence Interval in the Sky . . . . .	59
1.3.7	Fringe Spacing in the Sky . . . . .	60
<b>2</b>	<b>A Realistic Radio Interferometer</b>	<b>61</b>
2.1	Source Structure, Visibility and Intensity . . . . .	63
2.1.1	Source Coherence Function . . . . .	63
2.1.2	Power of Electric Field Incident from a Certain Direction	65
2.1.3	Poynting Flux . . . . .	66
2.1.4	Electric Field and Radio Source Intensity — Electro-	
	magnetics and Astronomy . . . . .	69
2.1.5	Field of View of a Radio Telescope . . . . .	70
2.1.6	Power Pattern of a Receiving Antenna . . . . .	72
2.1.7	New Dimensions of Voltage and Electric Field . . . . .	74
2.1.8	How Does A Radio Interferometer View the Universe?	75
2.1.9	Complex Visibility . . . . .	79
2.2	Frequency Conversion in Radio Interferometers . . . . .	80
2.2.1	Response of RF Filters . . . . .	81
2.2.2	Fourier Transform of IF Voltage Signal . . . . .	83
2.2.3	Cross-Correlation of Fourier Transforms of IF Signals .	84
2.2.4	Roles of Low-Pass Filters . . . . .	86
2.2.5	Relationship between RF Spectrum and IF Spectrum .	88
2.3	Delay Tracking and Fringe Stopping . . . . .	91
2.3.1	General Form of Cross-Power Spectrum of IF Signals .	91
2.3.2	“Expected Correlation” of IF Signals . . . . .	95
2.3.3	Radio Source Tracking by an Interferometer . . . . .	98
2.3.4	Requirements to the Delay Tracking and Fringe Stopping	100
2.3.5	Insertion of Instrumental Delay at IF Band . . . . .	104
2.3.6	Separation of Delay Tracking and Fringe Stopping Due	
	to Frequency Conversion . . . . .	106
2.3.7	Actual Implementations of Delay Tracking . . . . .	108
2.3.8	Actual Implementations of Fringe Stopping . . . . .	109
2.4	Correlator Outputs . . . . .	113
2.4.1	Multiplier and Integrator . . . . .	113
2.4.2	Single Sideband (USB or LSB) Reception . . . . .	115
2.4.3	Correlator Outputs in Single Sideband Reception . . .	117

2.4.4	Fringe Amplitude and Fringe Phase . . . . .	119
2.4.5	Group Delay and Fringe Frequency . . . . .	120
2.4.6	Complex Correlator . . . . .	122
2.4.7	Projected Baseline . . . . .	124
<b>3</b>	<b>Source Structure and Correlated Flux Density</b>	<b>125</b>
3.1	Basic Equations of Image Synthesis . . . . .	126
3.1.1	Complex Visibility as an Observable . . . . .	126
3.1.2	Visibility and Intensity in EW–NS Coordinate System	126
3.1.3	Approximation of a Celestial Sphere by a Tangent Plane	129
3.1.4	Interferometer is a Fourier Transformer . . . . .	133
3.2	<i>uv</i> –Coverage . . . . .	134
3.2.1	<i>uv</i> –Trajectories . . . . .	135
3.2.2	Synthesized Beams . . . . .	139
3.3	Correlated Flux Density of a Source with Gaussian Intensity (Brightness) Distribution . . . . .	142
3.4	What Can VLBI Observe? . . . . .	146
<b>4</b>	<b>Signal–to–Noise Ratio in Radio Interferometry</b>	<b>147</b>
4.1	Statistical Model of a Correlator Output . . . . .	148
4.1.1	Signal + Noise Inputs to a Correlator . . . . .	148
4.1.2	Integration of the Multiplier Output . . . . .	148
4.1.3	Statistical Expectation of the Correlator Output . . . .	149
4.1.4	Dispersion of the Correlator Output . . . . .	150
4.2	Useful Formulae Related to the Correlator Output . . . . .	150
4.2.1	Fourth Order Moment Relation . . . . .	151
4.2.2	Multiplier Output as a Stationary Random Process . .	155
4.2.3	Time Averaging Operator . . . . .	156
4.2.4	Power Spectrum of Multiplier Output . . . . .	157
4.2.5	Power and Cross–Power Spectra of Input Voltages . . .	158
4.2.6	Antenna Temperature and System Noise Temperature .	159
4.3	Sensitivity of a Radio Interferometer . . . . .	160
4.3.1	Standard Deviation Due to the Noise . . . . .	160
4.3.2	Signal in the Correlator Output . . . . .	162
4.3.3	Signal–to–Noise Ratio of the Correlator Output . . . .	163
4.3.4	Additional Remarks on the <i>SNR</i> Formula . . . . .	164
4.3.5	A Simple Interpretation of the $\sqrt{B\tau_a}$ Factor . . . . .	165
4.3.6	Formulae for <i>SNR</i> and Minimum Detectable Flux Den- sity . . . . .	166

# 1 Fundamentals of Radio Interferometry

## 1.1 Two Explanations of VLBI

Two quite different explanations on the principles of Very Long Baseline Interferometry (VLBI) are given in the literature. The two alternative explanations are illustrated in Figure 1.

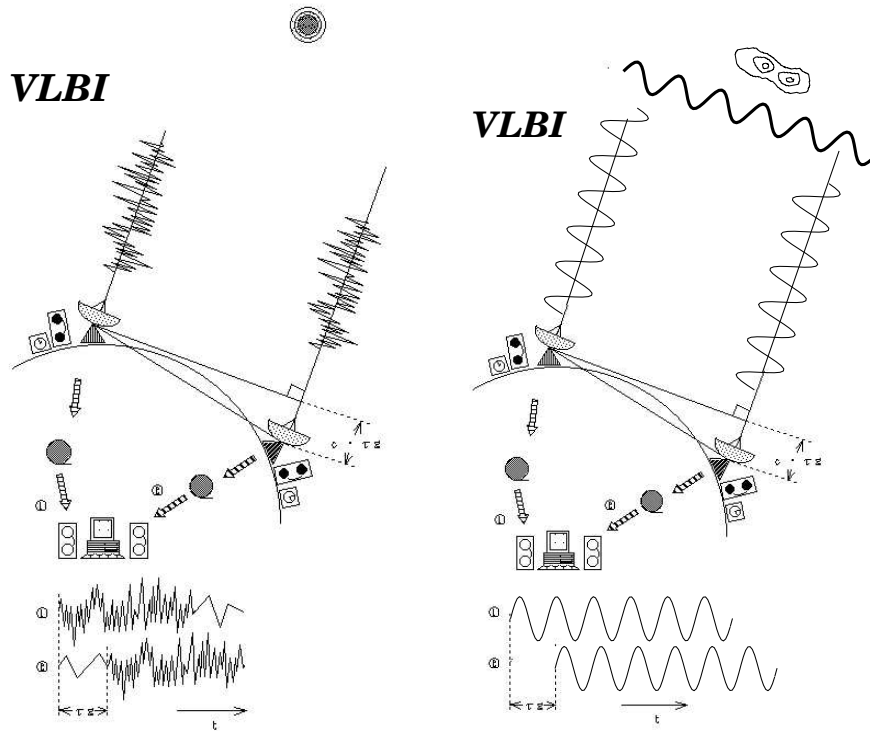


Figure 1: Receptions of noise (left) and monochromatic wave (right) with VLBI. This picture is based on a drawing originally provided by Dr. Katsuhisa Sato.

### 1.1.1 VLBI System

The VLBI system itself is described in almost the same way in these two explanations:

Two or more antennas are located at distant stations. They observe the same radio source at the same time. The observed data

are recorded on magnetic media, such as magnetic tapes, with accurate time marks generated by independent, but highly stable and well synchronized, clocks (or, better to say, frequency standards). The recorded media are sent to a correlation center, where they are played back and mutually multiplied and averaged (integrated) for some duration of time. This “multiplication and integration” procedure is called “correlation processing”.

The geometry of the observation is also presented in a similar way:

The radio wave from the same radio source must travel slightly further to reach antenna ② (right hand one in Figure 1) than antenna ① (left hand one), with a small time delay  $\tau_g$ . The delay  $\tau_g$  is determined by the geometric configuration of the antennas and the radio source, and hence it is called the “geometric delay”.

The difference begins with the treatment of the signal from the radio source.

### 1.1.2 “Geodetic” Explanation — Noise Approach

One explanation, shown in the left panel of Figure 1, which is favored in geodetic VLBI, regards the signal **as a random noise time series**.

If we simply multiply and average the two played-back data streams recorded at the same time, we must get a nearly zero result in most cases, since we are in effect averaging products of two random noise time series, which is also random noise, with all possible positive and negative values. But if, and only if, we shift the playback timing of the record from the antenna ② exactly by the geometric delay  $\tau_g$ , while keeping the playback timing of the record from the antenna ① unchanged, then the noise patterns from the same source in the two records ① and ② coincide. Therefore, the product of the two time series always gives positive values (since plus times plus is plus, and minus times minus is also plus) and the integration yields some finite positive value. Thus, we “get the correlation” of the two records. By carefully adjusting the time shift value so that the maximum correlation is obtained, we precisely determine the geometric delay with an accuracy of 0.1 nsec ( $10^{-10}$  sec) or better, which is sufficient to determine the plate movements of the continents with typical speeds of a few cm / year.

### 1.1.3 “Astrophysical” Explanation — Monochromatic Wave Approach

Another explanation, shown in the right panel of Figure 1, which is favored in astronomical VLBI for very high angular resolution imaging of radio sources, regards the signal as a **monochromatic sine wave**.

Two waves from the same source with an angular sky frequency  $\omega$  arrive at two antennas, giving rise to sinusoidal oscillations with a small time offset  $\tau_g$  due to the geometric delay. Therefore, the played-back data records from antennas ① and ② are proportional to  $\sin(\omega t)$  and  $\sin(\omega(t - \tau_g))$ , respectively. Their product is then proportional to

$$\sin(\omega t) \sin(\omega(t - \tau_g)) = \frac{1}{2} \{ \cos(\omega \tau_g) - \cos(2\omega t - \omega \tau_g) \}. \quad (1)$$

It is clear that the contribution of the rapidly oscillating second term in the right hand side of equation (1), at a frequency twice as large as the sky frequency, is almost nullified after time averaging (integration) over some duration. Therefore, only the first term, which is proportional to  $\cos(\omega \tau_g)$ , is left after the correlation processing.

This term expresses a sinusoidal interferometric fringe pattern on the sky, because the argument  $\omega \tau_g$  varies with the source direction in the sky. In particular, since  $\omega \tau_g = 2\pi c \tau_g / \lambda$ , where  $c$  is the light velocity, and  $\lambda = 2\pi c / \omega$  is the wavelength, the fringe pattern reverses its sign when the path length difference  $c \tau_g$  changes by a half wavelength  $\lambda/2$ , as expected from the standard theory of interferometry. The angular distance corresponding to the separation between two successive peaks of the fringe pattern is called the “fringe spacing”. If the radio source is more extended than the fringe spacing, contributions from various elements of the source are mutually compensated in the correlation processing, due to the different signs of the fringe pattern over the extended source. Therefore, the strength of an extended radio source is significantly diminished in the VLBI output. If the source is sufficiently compact compared with the fringe spacing, on the other hand, the amplitude of the source strength is almost the same as what is measured by a single dish radio telescope. Thus, the VLBI output contains information on the source structure. By analysing the VLBI data obtained with various fringe patterns,

we can obtain a detailed image of the source structure, with surprisingly high angular resolutions of 1 milliarcsecond, or better.

Each of these two explanations, if examined separately, seems clear and internally consistent. But it looks as if they are explaining completely different observational technologies, having no common feature at all. Nevertheless, they are the explanations of the same VLBI instrument, observing the same radio source, with the same antennas, receivers, frequency standards, magnetic tapes, and correlators. Then, how can we understand the two explanations from a unified point of view?

#### 1.1.4 Superposition of Monochromatic Waves

Both of the above two explanations deviate from reality on the same point, but in opposite directions. This point is the spectrum of the received signal.

The noise approach implicitly assumes that the spectrum of the signal is white, i.e. the amplitude of the spectrum is finite, and more or less constant, in a very wide range of frequency. While this assumption may not be too bad for the radio wave propagating in space, it is certainly not valid for the received signal, which must be band-limited due to the frequency characteristics of the optical and receiving systems of element antennas.

The monochromatic-wave approach, on the other hand, assumes an infinitely narrow bandwidth, when it talks about a wave having a certain frequency. But this is, of course, far from the reality (Figure 2).

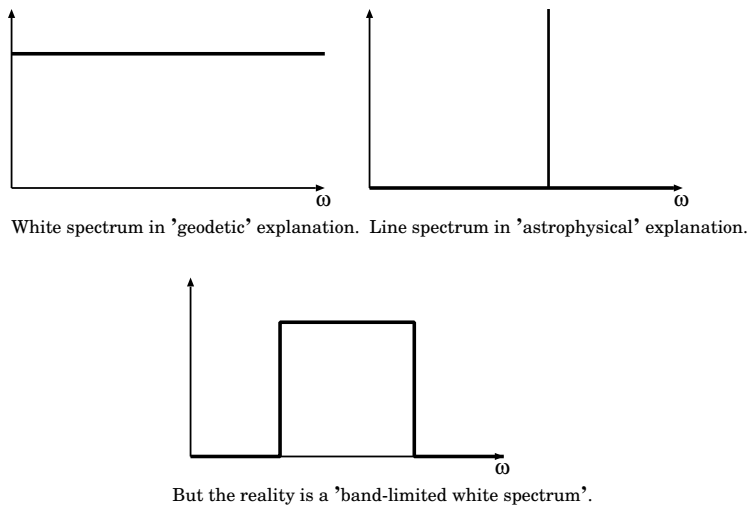


Figure 2: Different source signal spectra assumed in the two explanations.

So, what will come out, if we take a more realistic picture, by summing up the monochromatic waves with different frequencies, spread within a certain bandwidth? Figure 3 shows an answer.

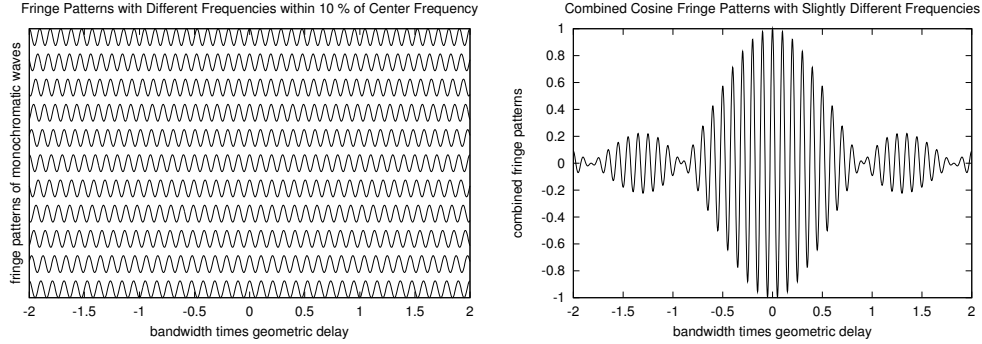


Figure 3: Fringe patterns of 11 monochromatic waves with slightly different frequencies within a bandwidth which is 10 % of the central frequency (left), and their superposition (right).

Here, we summed up 11 fringe patterns of monochromatic waves (left panel of Figure 3), which have slightly different frequencies, distributed at even intervals within a bandwidth  $B$ , centered at  $\nu_0 = \omega_0/2\pi$ , to generate the superposed pattern shown in the right panel of the same figure. The lowermost curve, in the left panel of Figure 3, shows the fringe pattern  $\cos(\omega_l\tau_g)$  with the lowest angular frequency  $\omega_l = 2\pi(\nu_0 - B/2)$ , while the uppermost one shows the fringe pattern  $\cos(\omega_u\tau_g)$  with the highest angular frequency  $\omega_u = 2\pi(\nu_0 + B/2)$ .

The horizontal axes of both panels in Figure 3 show the geometric delay  $\tau_g$ , multiplied by the bandwidth  $B$ , within a range of  $-2 \leq B\tau_g \leq 2$ . We took the center of the horizontal axis at  $\tau_g = 0$ , since the noise approach predicts that the finite correlation is obtained only when the playback timing of one record is shifted by the geometric delay. This shift is made to align the two records, as if the same wave front is received at the same time by the two antennas. This is obviously equivalent to effectively reducing the geometric delay to zero. Therefore, we assume the simplest case, where the source direction is nearly perpendicular to the baseline, so that  $\tau_g \simeq 0$  from the beginning.

We assumed here that the bandwidth is equal to 10 % of the central frequency ( $\nu_0 = 10B$ ).

### 1.1.5 Fringe Pattern Appears within an Envelope

The right panel of Figure 3 shows a rapid oscillation, enclosed by a more slowly varying envelope. The rapid oscillation has 10 peaks and valleys, within an interval of  $\Delta(B\tau_g) = 1$ . The number 10 here is nothing but the ratio  $\nu_0/B$ . So, this corresponds to the fringe pattern  $\cos(\omega_0\tau_g)$  at the central angular frequency  $\omega_0 = 2\pi\nu_0$ , as expected in the monochromatic-wave approach.

But the fringe pattern here does not have a constant amplitude. Instead, it is enclosed by an envelope which takes a maximum value at  $\tau_g = 0$ , when the two time series, obtained from the same source with two antennas, are most coincident with each other. This reminds us of the explanation of the correlation result in the noise approach.

### 1.1.6 Peak of the Envelope

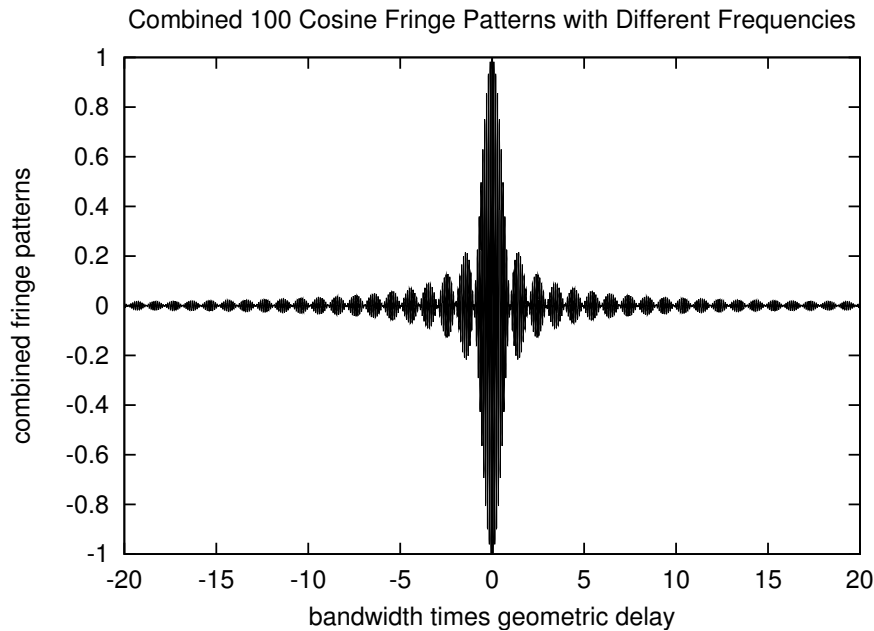


Figure 4: Superposed fringe patterns of 100 monochromatic waves, with slightly different frequencies, contained within a bandwidth equal to 10 % of the central frequency.

In order to see the point more clearly, we make our model still closer to an actual continuum spectrum, by increasing the number of monochromatic

waves to 100, but keeping the same bandwidth ( $B = \nu_0/10$ ), and show the superposed fringe patterns over a wider range of the horizontal axis:  $-20 \leq B\tau_g \leq 20$ . The result is given in Figure 4.

Now it is clear that the correlation result of the superposed monochromatic waves has sufficiently large amplitude only within a small range of the geometric delay around  $\tau_g = 0$ , which is roughly given by  $-1/B \leq \tau_g \leq 1/B$ . Although there are a number of sidelobes due to the finite bandwidth, the amplitude of these sidelobes rapidly decreases with increasing  $|\tau_g|$ . Therefore, Figure 4 is actually quite close to what is expected in the noise approach.

As a matter of fact, in a standard procedure for geodetic VLBI, the peak position of the envelope of the fringe pattern, such as the one shown in Figure 4, is searched by effectively shifting the playback timing of one record against the another. The peak is obtained at the time shift value which makes the two records most coincident, as if the same wave front was received at the same time by the two antennas. The best time shift value thus obtained yields an estimate of a quantity called the “group delay”, which will be explained later in more detail. After some corrections for systematic effects, the group delay serves as a good estimate of the geometric delay, which is further analysed to obtain scientific results in geodesy, geophysics, and astronomy.

Since the horizontal axis of the Figure 4 stands for  $B\tau_g$ , the larger the bandwidth, the narrower the envelope is, in terms of the geometric delay  $\tau_g$ . Therefore, the accuracy (or statistical error) of determination of the geometric delay in geodetic VLBI will be proportional to  $1/B$ . Also, the accuracy must be inversely proportional to the signal-to-noise ratio  $S/N$  of the observation, since the higher the  $S/N$ , the finer we can determine the peak position of the envelope. Although we do not know the exact number of the proportionality coefficient yet, we just assume that the coefficient is close to 1, for the purpose of a rough estimation.

So, if the bandwidth  $B$  is 500 MHz and the  $S/N$  is 20, then the expected accuracy is around

$$\frac{1}{(S/N)B} = \frac{1}{20 \times 5 \times 10^8} = 10^{-10} = 0.1 \text{ nsec.}$$

Therefore, we can already understand, at least qualitatively, how a 0.1 nsec accuracy is achieved in geodetic VLBI.

### 1.1.7 Fringe Pattern Enclosed by the Envelope

Now, as an opposite extreme, let us adopt a narrower bandwidth  $B = \nu_0/40$ , compared with the central frequency  $\nu_0$ , and look at a narrower range:  $-0.2 \leq B\tau_g \leq 0.2$ . The result is given in Figure 5, which clearly shows

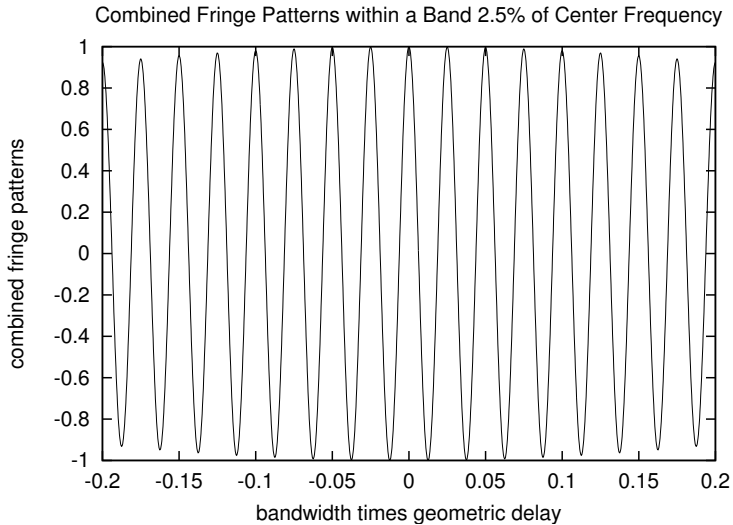


Figure 5: Superposed fringe patterns of monochromatic waves, with slightly different frequencies, contained within a bandwidth equal to 2.5 % of the central frequency.

the fringe pattern  $\cos(\omega_0\tau_g)$ , at the central angular frequency  $\omega_0 = 2\pi\nu_0$  of the band, which is quite similar to the one expected in the monochromatic-wave approach.

Therefore, we can conclude that the two explanations are talking about two extreme cases, corresponding to the very wide and very narrow bandwidths, of a common signal, which is composed of the fringe pattern at the central frequency enclosed by the envelope pattern, whose sharpness is determined by the bandwidth. Geodetic VLBI uses the envelope pattern to determine the peak position, where the signals obtained at two antennas are most coincident with each other, to get a good estimate of the geometric delay  $\tau_g$ . VLBI source imaging uses the fringe pattern, which appears within a limited central range of the envelope pattern, to derive the high angular resolution structures of astronomical radio sources. Both tasks can be done with the same VLBI telescope.

Although we could obtain, at least qualitatively, a unified view on the apparently quite different two approaches, the above discussion assumed the ensemble of a finite number of monochromatic waves, which are still not very realistic. More rigorous treatment of the signals with band-limited

continuum spectra can be obtained in the so-called “white fringe theory” (e.g., Thompson, Moran and Swenson, 2001), which is based on the statistical theory of the stationary random processes.

## 1.2 Elements of Stationary Random Processes

The radio waves coming from astronomical sources are mostly generated by chaotic processes occurring in the source regions. For example, the thermal radiation is caused by the thermal random motions of the atoms, molecules and free electrons, while the synchrotron radiation emerges from the random explosive processes, which accelerate relativistic electrons in magnetic fields. Hence, the electromagnetic fields, or the voltages in the receiving systems, associated with the cosmic radio waves, mostly show characteristics of the Gaussian random noise time series, as the “geodetic explanation” assumed. A mathematical tool, which well describes such a random noise time series, is the statistical theory of the stationary random processes. Therefore, we briefly introduce here basic elements of the theory, to the extent which will be needed in following discussions. For deeper understanding, one can consult with standard textbooks, for example, “Probability, Random Variables, and Stochastic Processes, 2nd Edition” by Athanasios Papoulis (1984) .

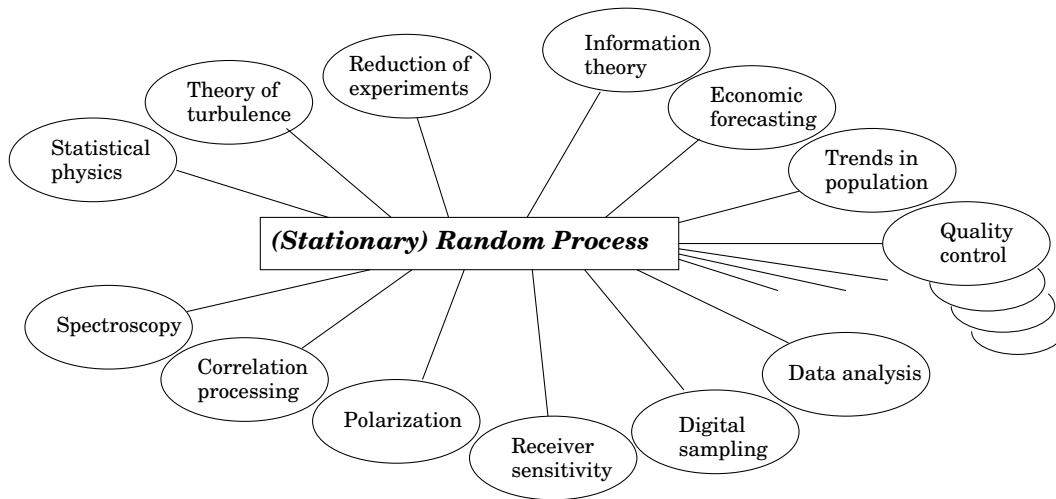


Figure 6: Statistical theory of random processes is a powerful tool for a variety of scientific disciplines.

The statistical theory of the random (or Stochastic) processes has wide

applications to many disciplines of radio astronomy, as well as other natural and human sciences, as illustrated in Figure 6.

In the antenna theory, the basic framework was the electromagnetics, and the vector algebra was used as the main mathematical tool. In the theory of radio interferometry, however, we will no longer newly deal with the electromagnetics. Instead, we will intensively use the theory of the stationary random process as the fundamental tool for the mathematical development of the theory.

### 1.2.1 Basic Concepts

#### Random (or Stochastic) Process

A process  $x(t)$  is called “random (or Stochastic) process”, if it is a function of time  $t$ , and, if its value  $x(t)$  at any time  $t$  is a random variable, i.e., may vary from trial to trial (see Figure 7).

If we characterize each trial of an experiment by an outcome  $\zeta$  of the experiment, the random process can be represented as a function of both  $t$  and  $\zeta$ , i.e., as  $x(t, \zeta)$ .

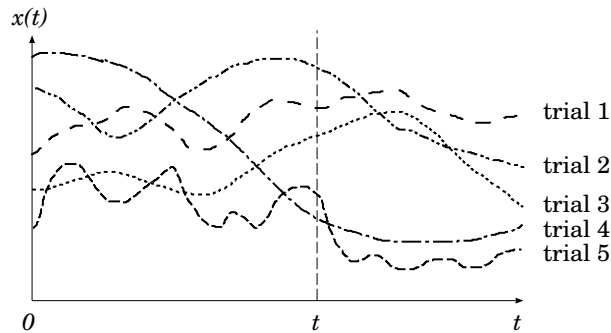


Figure 7: A random process is a function of time whose value at any time  $t$  is a random variable.

The random process is a mathematical model of any time-varying and, in general, deterministically unpredictable process. The properties of the random process are usually described in terms of statistical quantities, such as probability distribution, probability density, expectation, correlation, covariance, etc.

## Probability Distribution and Probability Density

Let us first consider a real random process  $x(t)$ .

Let us denote a probability for  $x(t)$  at a specific time  $t$  not to exceed a certain number  $x$ , as  $P\{x(t) \leq x\}$ . Also, let us denote a probability for occurrence of multiple events,  $x(t_1)$  not to exceed  $x_1$ ,  $x(t_2)$  not to exceed  $x_2$ ,  $\dots$ , and  $x(t_n)$  not to exceed  $x_n$ , as  $P\{x(t_1) \leq x_1, x(t_2) \leq x_2, \dots, x(t_n) \leq x_n\}$ .

Now, the first-order probability distribution  $F(x; t)$  of the random process  $x(t)$  is defined as:

$$F(x; t) = P\{x(t) \leq x\}. \quad (2)$$

Likewise, the second-order probability distribution  $F(x_1, x_2; t_1, t_2)$  is defined as:

$$F(x_1, x_2; t_1, t_2) = P\{x(t_1) \leq x_1, x(t_2) \leq x_2\}, \quad (3)$$

and the  $n$ -th-order probability distribution  $F(x_1, \dots, x_n; t_1, \dots, t_n)$  is defined as:

$$F(x_1, \dots, x_n; t_1, \dots, t_n) = P\{x(t_1) \leq x_1, \dots, x(t_n) \leq x_n\}. \quad (4)$$

On the other hand, the first-order probability density  $f(x; t)$  of the random process  $x(t)$  is defined as a derivative of the distribution  $F(x; t)$  with respect to  $x$ :

$$f(x; t) = \frac{\partial F(x; t)}{\partial x}. \quad (5)$$

Since, by definition,

$$\frac{\partial F(x; t)}{\partial x} = \lim_{\Delta x \rightarrow 0} \frac{F(x + \Delta x; t) - F(x; t)}{\Delta x},$$

the probability density has a meaning:

$$\begin{aligned} f(x; t) &= \lim_{\Delta x \rightarrow 0} \frac{P\{x(t) \leq x + \Delta x\} - P\{x(t) \leq x\}}{\Delta x} \\ &= \lim_{\Delta x \rightarrow 0} \frac{P\{x < x(t) \leq x + \Delta x\}}{\Delta x}. \end{aligned} \quad (6)$$

Likewise, the second-order probability density  $f(x_1, x_2; t_1, t_2)$  is defined as:

$$f(x_1, x_2; t_1, t_2) = \frac{\partial^2 F(x_1, x_2; t_1, t_2)}{\partial x_1 \partial x_2}, \quad (7)$$

and the  $n$ -th-order probability density  $f(x_1, \dots, x_n; t_1, \dots, t_n)$  is defined as:

$$f(x_1, \dots, x_n; t_1, \dots, t_n) = \frac{\partial^n F(x_1, \dots, x_n; t_1, \dots, t_n)}{\partial x_1 \cdots \partial x_n}. \quad (8)$$

Generally speaking, if  $t$  is continuous, we need infinite number of various orders of probability distributions, in order to properly describe a random process. In many practical cases, especially in cases of stationary random processes, however, it is sufficient to take into account first- and second-order distributions only, as we will see later.

Following general properties are satisfied for probability distributions and densities, as evident from their definitions:

- $F(\infty; t) = 1$ ,
- $F(x_1; t_1) = F(x_1, \infty; t_1, t_2)$ ,
- $f(x; t) \geq 0$  (i.e.,  $F(x; t)$  is a monotonically increasing function of  $x$ ),
- $\int_{x_1}^{x_2} f(x; t) dx = P\{x_1 < x(t) \leq x_2\}$ ,
- $f(x_1; t_1) = \int_{-\infty}^{\infty} f(x_1, x_2; t_1, t_2) dx_2$ ,
- $\int_{-\infty}^{\infty} f(x; t) dx = 1$ .

Now, let us consider a case, where a random process  $z(t)$  is a complex process:

$$z(t) = x(t) + i y(t),$$

where a real part  $x(t)$  and an imaginary part  $y(t)$  are real random processes, and  $i$  is the imaginary unit.

The probability distribution of the complex random process  $z(t)$  is defined by the joint probability distribution of  $x(t)$  and  $y(t)$ . Thus, the  $n$ -th-order probability distribution is defined as:

$$\begin{aligned} F(z_1, \dots, z_n; t_1, \dots, t_n) &= F(x_1, \dots, x_n; y_1, \dots, y_n; t_1, \dots, t_n) \\ &= P\{x(t_1) \leq x_1, \dots, x(t_n) \leq x_n, y(t_1) \leq y_1, \dots, y(t_n) \leq y_n\}, \end{aligned} \quad (9)$$

and the  $n$ -th order probability density is defined as:

$$\begin{aligned} f(z_1, \dots, z_n; t_1, \dots, t_n) &= f(x_1, \dots, x_n; y_1, \dots, y_n; t_1, \dots, t_n) \\ &= \frac{\partial^{2n} F(x_1, \dots, x_n; y_1, \dots, y_n; t_1, \dots, t_n)}{\partial x_1 \cdots \partial x_n \partial y_1 \cdots \partial y_n}. \end{aligned} \quad (10)$$

When we have two complex random processes  $x(t)$  and  $y(t)$ :

$$\begin{aligned}x(t) &= x^r(t) + i x^i(t), \\y(t) &= y^r(t) + i y^i(t),\end{aligned}$$

where real parts  $x^r(t)$  and  $y^r(t)$ , and imaginary parts  $x^i(t)$  and  $y^i(t)$ , are all real random processes, we introduce joint probability distributions and joint probability densities of the two complex random processes.

For example, the first order joint probability distribution of the complex random processes  $x(t)$  and  $y(t)$  at times  $t_1$  and  $t_2$ , respectively, is

$$\begin{aligned}F(x; y; t_1; t_2) &= F(x^r, x^i; y^r, y^i; t_1; t_2) \\&= P\{x^r(t_1) \leq x^r; x^i(t_1) \leq x^i; y^r(t_2) \leq y^r; y^i(t_2) \leq y^i\},\end{aligned}\quad (11)$$

and the corresponding joint probability density is

$$\begin{aligned}f(x; y; t_1; t_2) &= f(x^r, x^i; y^r, y^i; t_1; t_2) \\&= \frac{\partial^4 F(x^r, x^i; y^r, y^i; t_1; t_2)}{\partial x^r \partial x^i \partial y^r \partial y^i}.\end{aligned}\quad (12)$$

### Expectation (or Ensemble Average)

Expectation (or ensemble average)  $\eta_z(t)$  of a complex random process  $z(t) = x(t) + iy(t)$  at time  $t$  is defined as:

$$\eta_z(t) = \langle z(t) \rangle = \int_{-\infty}^{\infty} \int_{-\infty}^{\infty} [x(t) + iy(t)] f(x; y; t) dx dy, \quad (13)$$

where the symbol  $\langle \quad \rangle$ , which stands for the expectation, is often denoted also as  $E\{ \quad \}$ .

### Autocorrelation

Autocorrelation  $R_{zz}(t_1, t_2)$  of a complex random process  $z(t) = x(t) + iy(t)$  at times  $t_1$  and  $t_2$  is defined as:

$$\begin{aligned}R_{zz}(t_1, t_2) &= \langle z(t_1) z^*(t_2) \rangle \\&= \int_{-\infty}^{\infty} \int_{-\infty}^{\infty} \int_{-\infty}^{\infty} \int_{-\infty}^{\infty} z(t_1) z^*(t_2) f(x_1, x_2; y_1, y_2; t_1, t_2) dx_1 dx_2 dy_1 dy_2,\end{aligned}\quad (14)$$

where the symbol  $( \quad )^*$  stands for the complex conjugate.

Hereafter, we will usually omit suffices such as  $zz$ , for simplicity, when we express autocorrelations. Thus, autocorrelations  $R_{xx}(t_1, t_2)$ ,  $R_{yy}(t_1, t_2)$ ,  $R_{zz}(t_1, t_2)$ , and so on, will be all denoted simply as  $R(t_1, t_2)$ , except for cases, when we wish to explicitly specify the random processes under consideration.

Following general properties hold for autocorrelations.

- $R(t_2, t_1) = R^*(t_1, t_2)$ .
- $R(t, t) = \langle |z(t)|^2 \rangle \geq 0$ , i.e., real and positive.
- Positive definite, namely,

$$\sum_{i=1}^n \sum_{j=1}^n a_i a_j^* R(t_i, t_j) \geq 0 \quad \text{for any numbers } a_i \ (i = 1, 2, \dots, n).$$

*Proof:*

$$0 \leq \langle \left| \sum_{i=1}^n a_i z(t_i) \right|^2 \rangle = \sum_{i=1}^n \sum_{j=1}^n a_i a_j^* \langle z(t_i) z^*(t_j) \rangle = \sum_{i=1}^n \sum_{j=1}^n a_i a_j^* R(t_i, t_j).$$

- An inequality:

$$|R(t_1, t_2)|^2 \leq R(t_1, t_1) R(t_2, t_2). \quad (15)$$

*Proof:*

1. For any complex random variables  $v$  and  $w$ , we have

$$\langle |v| |w| \rangle^2 \leq \langle |v|^2 \rangle \langle |w|^2 \rangle.$$

*Proof:*

Since we always have

$$\langle (s|v| + |w|)^2 \rangle = s^2 \langle |v|^2 \rangle + 2s \langle |v| |w| \rangle + \langle |w|^2 \rangle \geq 0,$$

for any real variable  $s$ , the discriminant of the above quadratic equation with respect to  $s$  must be smaller than or equal to 0, i.e.,

$$\langle |v| |w| \rangle^2 - \langle |v|^2 \rangle \langle |w|^2 \rangle \leq 0,$$

and, hence,

$$\langle |v| |w| \rangle^2 \leq \langle |v|^2 \rangle \langle |w|^2 \rangle.$$

2. For any complex random variables  $v$  and  $w$ , we have

$$| \langle vw \rangle | \leq \langle |v| |w| \rangle.$$

*Proof:*

Let us first prove a general statement that, for any complex random variable  $A = a + ib$ , where  $a$  and  $b$  are real random variables, we have

$$| \langle A \rangle | \leq \langle |A| \rangle.$$

Let us denote the probability density of  $A$  as  $f(a, b)$ . Then  $| \langle A \rangle |$  and  $\langle |A| \rangle$  are expressed as

$$\begin{aligned} | \langle A \rangle | &= \left| \int \int A f(a, b) da db \right| \\ &= \lim_{\Delta a \rightarrow 0} \lim_{\Delta b \rightarrow 0} \left| \sum \sum A f(a, b) \Delta a \Delta b \right|, \end{aligned} \quad (16)$$

and

$$\begin{aligned} \langle |A| \rangle &= \int \int |A| f(a, b) da db \\ &= \lim_{\Delta a \rightarrow 0} \lim_{\Delta b \rightarrow 0} \sum \sum |A| f(a, b) \Delta a \Delta b \\ &= \lim_{\Delta a \rightarrow 0} \lim_{\Delta b \rightarrow 0} \sum \sum |A f(a, b) \Delta a \Delta b|, \end{aligned} \quad (17)$$

where we replaced the integrations by the infinite summations, which are performed in the same way in both equations (16) and (17), and we used a property of the probability density  $f(a, b)$  in equation (17), that it is always real and greater than or equal to zero.

Now, for any complex numbers  $B$  and  $C$ , we have

$$| B + C | \leq | B | + | C |,$$

since

$$\begin{aligned} | B + C | &= \sqrt{(B + C)(B + C)^*} = \sqrt{|B|^2 + B^*C + BC^* + |C|^2} \\ &= \sqrt{|B|^2 + 2|B||C|\cos\Phi + |C|^2}, \end{aligned}$$

where we introduced an angle  $\Phi$  satisfying

$$B^*C = |B||C|e^{i\Phi},$$

is always smaller than  $|B| + |C|$ , because  $\cos\Phi \leq 1$ . This relation is easily extended to the sum of arbitrary number  $n$  of complex numbers  $B_1, B_2, \dots, B_n$ , i.e.,

$$\left| \sum_{i=1}^n B_i \right| \leq \sum_{i=1}^n |B_i|,$$

because

$$\begin{aligned} \left| \sum_{i=1}^n B_i \right| &= \left| B_1 + \sum_{i=2}^n B_i \right| \leq |B_1| + \left| \sum_{i=2}^n B_i \right| = |B_1| + \left| B_2 + \sum_{i=3}^n B_i \right| \\ &\leq |B_1| + |B_2| + \left| \sum_{i=3}^n B_i \right| = \cdots \leq |B_1| + |B_2| + \cdots + |B_n|. \end{aligned}$$

Applying the above relation to the summations of equations (16) and (17), we confirm that  $|\langle A \rangle| \leq \langle |A|^2 \rangle$ .

This implies that  $|\langle vw \rangle| \leq \langle |v|^2 |w|^2 \rangle$ , since

$$|vw| = \sqrt{v w v^* w^*} = \sqrt{v v^*} \sqrt{w w^*} = |v| |w|.$$

3. From 1. and 2. above, we obtain

$$|\langle vw \rangle|^2 \leq \langle |v|^2 |w|^2 \rangle \leq \langle |v|^2 \rangle \langle |w|^2 \rangle,$$

i.e.,

$$|\langle vw \rangle|^2 \leq \langle |v|^2 \rangle \langle |w|^2 \rangle. \quad (18)$$

If we adopt here  $v = z(t_1)$  and  $w = z^*(t_2)$ , then we prove that

$$|R(t_1, t_2)|^2 \leq R(t_1, t_1) R(t_2, t_2).$$

### Autocovariance

Autocovariance  $C(t_1, t_2)$  of a complex random process  $z(t)$  at times  $t_1$  and  $t_2$  is defined as:

$$C(t_1, t_2) = R(t_1, t_2) - \eta(t_1) \eta^*(t_2), \quad (19)$$

where  $\eta(t) \equiv \eta_z(t) = \langle z(t) \rangle$  is the expectation of  $z(t)$  at time  $t$ .

The autocovariance of  $z(t)$  is equal to the autocorrelation of  $\tilde{z}(t) = z(t) - \eta(t)$ , i.e.,

$$C(t_1, t_2) = R_{\tilde{z}\tilde{z}} = \langle \tilde{z}(t_1) \tilde{z}^*(t_2) \rangle. \quad (20)$$

In fact,

$$\begin{aligned} \langle \tilde{z}(t_1) \tilde{z}^*(t_2) \rangle &= \langle [z(t_1) z^*(t_2) - z(t_1) \eta^*(t_2) - \eta(t_1) z^*(t_2) + \eta(t_1) \eta^*(t_2)] \rangle \\ &= R(t_1, t_2) - \eta(t_1) \eta^*(t_2). \end{aligned}$$

## Correlation Coefficient

Correlation coefficient  $r(t_1, t_2)$  of a complex random process  $z(t)$  at times  $t_1$  and  $t_2$  is defined as:

$$r(t_1, t_2) = \frac{C(t_1, t_2)}{\sqrt{C(t_1, t_1) C(t_2, t_2)}}. \quad (21)$$

It is evident that

- $r(t, t) = 1$ .

Also, the absolute value of the correlation coefficient is always smaller than or equal to 1:

- $|r(t_1, t_2)| \leq 1$ ,

since from equations (15) and (20), we have

$$|C(t_1, t_2)|^2 \leq C(t_1, t_1) C(t_2, t_2).$$

## Cross-Correlation

Cross-correlation  $R_{xy}(t_1, t_2)$  of two complex random processes  $x(t) = x^r(t) + i x^i(t)$  and  $y(t) = y^r(t) + i y^i(t)$  at times  $t_1$  and  $t_2$ , respectively, is defined as:

$$R_{xy}(t_1, t_2) = \langle x(t_1) y^*(t_2) \rangle = \int_{-\infty}^{\infty} \int_{-\infty}^{\infty} \int_{-\infty}^{\infty} \int_{-\infty}^{\infty} x(t_1) y^*(t_2) f(x^r, x^i; y^r, y^i; t_1; t_2) dx^r dx^i dy^r dy^i, \quad (22)$$

using the joint probability density of  $x(t)$  and  $y(t)$ , given in equation (12).

Following properties hold for cross-correlations.

- $R_{xy}(t_2, t_1) = R_{yx}^*(t_1, t_2)$ .  
This is evident from the above definition.
- $|R_{xy}(t_1, t_2)|^2 \leq R_{xx}(t_1, t_1) R_{yy}(t_2, t_2)$ .  
This is proven by adopting  $v = x(t_1)$  and  $w = y^*(t_2)$  in equation (18).

## Cross–Covariance

Cross–covariance  $C_{xy}(t_1, t_2)$  of two complex random processes  $x(t)$  and  $y(t)$  at times  $t_1$  and  $t_2$  is defined as:

$$C_{xy}(t_1, t_2) = R_{xy}(t_1, t_2) - \eta_x(t_1) \eta_y^*(t_2). \quad (23)$$

Following properties hold for cross-covariances.

- The cross–covariance of  $x(t)$  and  $y(t)$  is equal to the cross–correlation of  $\tilde{x}(t) = x(t) - \eta_x(t)$  and  $\tilde{y}(t) = y(t) - \eta_y(t)$ , i.e.,

$$C_{xy}(t_1, t_2) = R_{\tilde{x}\tilde{y}}(t_1, t_2) = \langle \tilde{x}(t_1) \tilde{y}^*(t_2) \rangle.$$

- $|C_{xy}(t_1, t_2)|^2 \leq C_{xx}(t_1, t_1) C_{yy}(t_2, t_2)$ .

## Cross–Correlation Coefficient

Cross–correlation coefficient  $r_{xy}(t_1, t_2)$  of two complex random processes  $x(t)$  and  $y(t)$  at times  $t_1$  and  $t_2$  is defined as:

$$r_{xy}(t_1, t_2) = \frac{C_{xy}(t_1, t_2)}{\sqrt{C_{xx}(t_1, t_1) C_{yy}(t_2, t_2)}}. \quad (24)$$

It is evident that for any cross–correlation coefficient we always have

- $|r_{xy}(t_1, t_2)| \leq 1$ .

## Normal (Gaussian) Process

As an example of the probability density introduced in equations (5), (7), and (8), we consider here probability density of a particularly important class of random process, namely normal (or Gaussian) process, which is known to be a good model of signals from astronomical radio sources, as well as of noises produced in antenna–receiving systems or in environments.

Real random process  $x(t)$ , with expectation  $\eta(t)$  and autocovariance  $C(t_1, t_2)$ , is called “normal (or Gaussian) process”, if, at any times  $t_1, t_2, \dots, t_n$  for any  $n$ , random variables  $x(t_1), x(t_2), \dots, x(t_n)$  are jointly normal (or Gaussian), i.e., they are characterized by following probability densities.

- First–order Gaussian probability density:

$$f(x_1; t_1) = \frac{1}{\sigma_1 \sqrt{2\pi}} e^{-\frac{[x_1 - \eta_1]^2}{2\sigma_1^2}}, \quad (25)$$

where  $\eta_1 \equiv \eta(t_1)$  and  $\sigma_1^2 \equiv C(t_1, t_1)$  are expectation and dispersion, respectively, of  $x(t)$  at time  $t_1$ .

- Second-order Gaussian probability density:

$$f(x_1, x_2; t_1, t_2) = \frac{1}{2\pi\sigma_1\sigma_2\sqrt{1-r^2}} e^{-\frac{1}{2(1-r^2)}\left(\frac{(x_1-\eta_1)^2}{\sigma_1^2} - 2r\frac{(x_1-\eta_1)(x_2-\eta_2)}{\sigma_1\sigma_2} + \frac{(x_2-\eta_2)^2}{\sigma_2^2}\right)}, \quad (26)$$

where we introduced notations:  $\eta_1 \equiv \eta(t_1)$ ,  $\eta_2 \equiv \eta(t_2)$ ,  $\sigma_1^2 \equiv C(t_1, t_1)$ ,  $\sigma_2^2 \equiv C(t_2, t_2)$ , and correlation coefficient:

$$r \equiv \frac{C(t_1, t_2)}{\sqrt{C(t_1, t_1)C(t_2, t_2)}}.$$

- $n$ -th-order Gaussian probability density:

$$f(x_1, \dots, x_n; t_1, \dots, t_n) = \frac{1}{\sqrt{(2\pi)^n \Delta}} e^{-\frac{1}{2} \sum_{i=1}^n \sum_{j=1}^n [x_i - \eta_i] C_{ij}^{-1} [x_j - \eta_j]}, \quad (27)$$

where  $\eta_i \equiv \eta(t_i)$ ,  $\eta_j \equiv \eta(t_j)$ ,  $C_{ij} \equiv C(t_i, t_j)$  is autocovariance matrix,  $C_{ij}^{-1}$  is its inverse, and  $\Delta \equiv \det\{C_{ij}\}$  is its determinant.

When  $n = 1$  and  $n = 2$ , equation (27) is reduced to equations (25) and (26). Therefore, the first- and second-order Gaussian probability densities given in equations (25) and (26), respectively, are special cases of the more general expression of the  $n$ -th-order normal (or Gaussian) probability density given in equation (27).

Likewise, we can conceive a number of normal (or Gaussian) processes which are jointly normal with each other.

- Two real normal processes  $x(t)$  and  $y(t)$  are called “jointly normal (or Gaussian) processes”, if, at any times  $t_1$  and  $t_2$ , random variables  $x(t_1)$  and  $y(t_2)$  are jointly normal, i.e., they are characterized by following joint probability density:

$$f(x, y; t_1, t_2) = \frac{1}{2\pi\sigma_x\sigma_y\sqrt{1-r_{xy}^2}} e^{-\frac{1}{2(1-r_{xy}^2)}\left(\frac{(x-\eta_x)^2}{\sigma_x^2} - 2r_{xy}\frac{(x-\eta_x)(y-\eta_y)}{\sigma_x\sigma_y} + \frac{(y-\eta_y)^2}{\sigma_y^2}\right)}, \quad (28)$$

where we introduced expectations of  $x(t_1)$  and  $y(t_2)$ :  $\eta_x \equiv \eta_x(t_1)$  and  $\eta_y \equiv \eta_y(t_2)$ , dispersions of  $x(t_1)$  and  $y(t_2)$ :  $\sigma_x^2 \equiv C_{xx}(t_1, t_1)$ ,  $\sigma_y^2 \equiv C_{yy}(t_2, t_2)$ , and cross-correlation coefficient:

$$r_{xy} \equiv \frac{C_{xy}(t_1, t_2)}{\sqrt{C_{xx}(t_1, t_1) C_{yy}(t_2, t_2)}}.$$

Here  $C_{xx}(t_1, t_1)$ ,  $C_{yy}(t_2, t_2)$  and  $C_{xy}(t_1, t_2)$  are autocovariances and cross-covariance of  $x(t_1)$  and  $y(t_2)$ , correspondingly.

- An arbitrary number  $m$  of normal processes  $x_{(1)}(t)$ ,  $x_{(2)}(t)$ ,  $\dots$ ,  $x_{(m)}(t)$  are called “jointly normal (or Gaussian) processes”, if, at any times  $t_1$ ,  $t_2$ ,  $\dots$ ,  $t_m$ , random variables  $x_{(1)}(t_1)$ ,  $x_{(2)}(t_2)$ ,  $\dots$ ,  $x_{(m)}(t_m)$  are jointly normal, i.e., they are characterized by following joint probability density:

$$\begin{aligned} f(x_{(1)}, \dots, x_{(m)}; t_1, \dots, t_m) \\ = \frac{1}{\sqrt{(2\pi)^m \Delta}} e^{-\frac{1}{2} \sum_{i=1}^m \sum_{j=1}^m [x_{(i)} - \eta_{(i)}(t_i)] C_{(i)(j)}^{-1} [x_{(j)} - \eta_{(j)}(t_j)]}, \end{aligned} \quad (29)$$

where  $\eta_{(i)}(t)$  is expectation of  $x_{(i)}(t)$ ,  $C_{(i)(j)} \equiv C_{x_{(i)}x_{(j)}}(t_i, t_j)$  is cross-covariance matrix,  $C_{(i)(j)}^{-1}$  is inverse matrix of  $C_{(i)(j)}$ , and  $\Delta \equiv \det\{C_{(i)(j)}\}$  is determinant of  $C_{(i)(j)}$ .

Of course, equation (28) is a special case of equation (29) with  $m = 2$ .

- In the above statement, some random variables among  $x_{(1)}(t_1)$ ,  $x_{(2)}(t_2)$ ,  $\dots$ ,  $x_{(m)}(t_m)$  could be values of the same normal process taken at different times. In such a case, some elements of matrix  $C_{(i)(j)}$  are autocovariances, rather than cross-covariances.

In this sense, joint probability densities of a single normal (or Gaussian) process given in equations (25), (26), and (27) can be regarded as special cases of the joint probability density of the jointly normal (or Gaussian) processes given in equation (29).

It is not difficult to confirm that the joint probability densities of jointly normal (or Gaussian) processes given in equations (25) – (29) are consistent with general properties of joint probability densities, as well as with definitions of the expectation and the covariances, as explained in standard textbooks. For this purpose, we can use well-known integration formulae:

$$\int_{-\infty}^{\infty} e^{-ax^2} dx = \sqrt{\frac{\pi}{a}}, \quad (30)$$

$$\int_{-\infty}^{\infty} x e^{-ax^2} dx = 0, \quad (31)$$

$$\int_{-\infty}^{\infty} x^2 e^{-ax^2} dx = \frac{1}{2} \sqrt{\frac{\pi}{a^3}}, \quad (32)$$

for  $a > 0$ .

For example, if we take the form of the joint normal (or Gaussian) probability density given in equation (28), we can confirm following formulae.

- $\int_{-\infty}^{\infty} f(x, y; t_1, t_2) dy = f(x; t_1)$ :

$$\begin{aligned} & \int_{-\infty}^{\infty} f(x, y; t_1, t_2) dy \\ &= \frac{1}{2\pi\sigma_x\sigma_y\sqrt{1-r_{xy}^2}} \int_{-\infty}^{\infty} e^{-\frac{1}{2(1-r_{xy}^2)}\left(\frac{(x-\eta_x)^2}{\sigma_x^2} - 2r_{xy}\frac{(x-\eta_x)(y-\eta_y)}{\sigma_x\sigma_y} + \frac{(y-\eta_y)^2}{\sigma_y^2}\right)} dy \\ &= \frac{1}{2\pi\sigma_x\sqrt{1-r_{xy}^2}} \int_{-\infty}^{\infty} e^{-\frac{1}{2(1-r_{xy}^2)}\left(\frac{(x-\eta_x)^2}{\sigma_x^2} - 2r_{xy}\frac{(x-\eta_x)}{\sigma_x}y' + y'^2\right)} dy' \\ &= \frac{1}{2\pi\sigma_x\sqrt{1-r_{xy}^2}} \int_{-\infty}^{\infty} e^{-\frac{1}{2(1-r_{xy}^2)}\left[(1-r_{xy}^2)\frac{(x-\eta_x)^2}{\sigma_x^2} + (y' - r_{xy}\frac{x-\eta_x}{\sigma_x})^2\right]} dy' \\ &= \frac{1}{2\pi\sigma_x\sqrt{1-r_{xy}^2}} e^{-\frac{(x-\eta_x)^2}{2\sigma_x^2}} \int_{-\infty}^{\infty} e^{-\frac{y''^2}{2(1-r_{xy}^2)}} dy'' \\ &= \frac{1}{\sigma_x\sqrt{2\pi}} e^{-\frac{(x-\eta_x)^2}{2\sigma_x^2}} = f(x; t_1), \end{aligned} \quad (33)$$

in view of equation (30), where we introduced variable transformations:

$$y' = \frac{y - \eta_y}{\sigma_y}, \quad y'' = y' - r_{xy} \frac{x - \eta_x}{\sigma_x}.$$

- Expectation:

$$\begin{aligned} \langle x \rangle &= \int_{-\infty}^{\infty} \int_{-\infty}^{\infty} x f(x, y; t_1, t_2) dx dy = \int_{-\infty}^{\infty} x \int_{-\infty}^{\infty} f(x, y; t_1, t_2) dy dx \\ &= \int_{-\infty}^{\infty} x f(x; t_1) dx = \frac{1}{\sigma_x\sqrt{2\pi}} \int_{-\infty}^{\infty} x e^{-\frac{(x-\eta_x)^2}{2\sigma_x^2}} dx \end{aligned}$$

$$\begin{aligned}
&= \frac{1}{\sigma_x \sqrt{2\pi}} \int_{-\infty}^{\infty} [(x - \eta_x) + \eta_x] e^{-\frac{(x - \eta_x)^2}{2\sigma_x^2}} dx \\
&= \frac{\eta_x}{\sigma_x \sqrt{2\pi}} \int_{-\infty}^{\infty} e^{-\frac{(x - \eta_x)^2}{2\sigma_x^2}} dx = \eta_x,
\end{aligned} \tag{34}$$

in view of equations (30) and (31).

- Covariance:

$$\begin{aligned}
&\langle (x - \eta_x)(y - \eta_y) \rangle \\
&= \int_{-\infty}^{\infty} \int_{-\infty}^{\infty} (x - \eta_x)(y - \eta_y) f(x, y; t_1, t_2) dx dy \\
&= \frac{1}{2\pi\sigma_x\sigma_y\sqrt{1-r_{xy}^2}} \\
&\times \int_{-\infty}^{\infty} \int_{-\infty}^{\infty} (x - \eta_x)(y - \eta_y) e^{-\frac{1}{2(1-r_{xy}^2)}\left(\frac{(x-\eta_x)^2}{\sigma_x^2} - 2r_{xy}\frac{(x-\eta_x)(y-\eta_y)}{\sigma_x\sigma_y} + \frac{(y-\eta_y)^2}{\sigma_y^2}\right)} dx dy \\
&= \frac{\sigma_x\sigma_y}{2\pi\sqrt{1-r_{xy}^2}} \int_{-\infty}^{\infty} \int_{-\infty}^{\infty} x' y' e^{-\frac{1}{2(1-r_{xy}^2)}(x'^2 - 2r_{xy}x'y' + y'^2)} dx' dy' \\
&= \frac{\sigma_x\sigma_y}{2\pi\sqrt{1-r_{xy}^2}} \int_{-\infty}^{\infty} \int_{-\infty}^{\infty} (x'' + r_{xy}y'') y'' e^{-\frac{1}{2(1-r_{xy}^2)}[x''^2 + (1-r_{xy}^2)y''^2]} dx'' dy'' \\
&= \frac{\sigma_x\sigma_y r_{xy}}{2\pi\sqrt{1-r_{xy}^2}} \int_{-\infty}^{\infty} e^{-\frac{x''^2}{2(1-r_{xy}^2)}} dx'' \int_{-\infty}^{\infty} y''^2 e^{-\frac{y''^2}{2}} dy'' \\
&= \frac{\sigma_x\sigma_y r_{xy}}{2\pi\sqrt{1-r_{xy}^2}} \sqrt{2\pi(1-r_{xy}^2)} \sqrt{2\pi} = r_{xy}\sigma_x\sigma_y = C_{xy}(t_1, t_2),
\end{aligned} \tag{35}$$

in view of equations (30), (31), and (32), where we introduced variable transformations:

$$\begin{aligned}
x' &= \frac{x - \eta_x}{\sigma_x}, & y' &= \frac{y - \eta_y}{\sigma_y}, \\
x'' &= x' - r_{xy}y', & y'' &= y'.
\end{aligned}$$

In following discussions, we will mainly use general properties of expectations and correlations, without specifying explicit forms of probability densities. However, when necessary, we will assume jointly normal (or Gaussian) processes, and explicitly use expressions of the normal probability density given in equations (25) – (29).

## 1.2.2 Random Processes in Linear Systems

### Definition of Linear Systems

Let us consider a system of two complex functions  $x(t)$  and  $y(t)$  of time  $t$ , which are related with each other by an operator  $L$ :

$$y(t) = L[x(t)], \quad (36)$$

where  $x(t)$  is called “input” and  $y(t)$  is called “output” of the operator  $L$ .

Such a system is called “linear system”, if the operator  $L$  satisfies

$$L[a_1 x_1(t) + a_2 x_2(t)] = a_1 L[x_1(t)] + a_2 L[x_2(t)], \quad (37)$$

for any complex coefficients  $a_1, a_2$  and for any functions  $x_1(t), x_2(t)$ .

The linear system is also called as “linear filter”, which linearly “filters” the input  $x(t)$  to yield the output  $y(t)$ .

### Impulse Response

If the input of an operator  $L$  is a delta function  $\delta(t)$  of time  $t$ , the output is called “impulse response” of the operator, which we denote as  $h(t)$ :

$$h(t) = L[\delta(t)]. \quad (38)$$

Here, we introduce “convolution”  $f(t) * g(t)$  of functions  $f(t)$  and  $g(t)$ , which is defined by a following infinite integration:

$$f(t) * g(t) = \int_{-\infty}^{\infty} f(t - \alpha) g(\alpha) d\alpha, \quad (39)$$

where symbol “\*” stands for the operation of the convolution. Convolution has following properties:

$$f(t) * g(t) = g(t) * f(t) \quad (\text{commutative}),$$

because

$$g(t) * f(t) = \int_{-\infty}^{\infty} g(t - \beta) f(\beta) d\beta = \int_{-\infty}^{\infty} f(\beta) g(t - \beta) d\beta = \int_{-\infty}^{\infty} f(t - \alpha) g(\alpha) d\alpha,$$

where we used a transformation of the argument of the integration:  $\alpha = t - \beta$  and hence  $d\beta = -d\alpha$ ,

and

$$f(t) * g(-t) = \int_{-\infty}^{\infty} f(t - \beta) g(-\beta) d\beta = \int_{-\infty}^{\infty} f(t + \alpha) g(\alpha) d\alpha,$$

where we used  $\alpha = -\beta$  and  $d\beta = -d\alpha$ .

Then, the output of the linear system can be represented as a convolution of the input and the impulse response, i.e.,

$$y(t) = x(t) * h(t) = \int_{-\infty}^{\infty} x(t - \alpha) h(\alpha) d\alpha. \quad (40)$$

This equation is easily proven, based on the definition of the delta function, in the following way:

$$\begin{aligned} y(t) &= L[x(t)] = L\left[\int_{-\infty}^{\infty} x(\beta) \delta(t - \beta) d\beta\right] = \int_{-\infty}^{\infty} x(\beta) L[\delta(t - \beta)] d\beta \\ &= \int_{-\infty}^{\infty} x(\beta) h(t - \beta) d\beta = \int_{-\infty}^{\infty} x(t - \alpha) h(\alpha) d\alpha = x(t) * h(t). \end{aligned}$$

Note that  $L$  operates only on a function of time  $t$ .

## Linear Systems with Random Processes as Inputs

Hereafter, we will consider linear systems having random processes as inputs. Then, we have following general properties.

- If  $x(t)$  and  $y(t)$  are input and output of a linear system, their expectations  $\langle x(t) \rangle$  and  $\langle y(t) \rangle$  are also related with each other as input and output of the same linear system, i.e.,

$$\begin{aligned} \langle L[x(t)] \rangle &= L[\langle x(t) \rangle], \\ \text{or} \\ \langle x(t) * h(t) \rangle &= \langle x(t) \rangle * h(t), \\ \text{or} \\ \eta_y(t) &= L[\eta_x(t)]. \end{aligned} \quad (41)$$

*Proof :*

$$\begin{aligned} \langle x(t) * h(t) \rangle &= \left\langle \int_{-\infty}^{\infty} x(t - \alpha) h(\alpha) d\alpha \right\rangle = \int_{-\infty}^{\infty} \langle x(t - \alpha) \rangle h(\alpha) d\alpha \\ &= \langle x(t) \rangle * h(t). \end{aligned}$$

Note that the impulse response  $h(t)$  is a deterministic function of time, and, hence, not affected by the ensemble average.

- Autocorrelation of the output:

$$R_{yy}(t_1, t_2) = R_{xx}(t_1, t_2) * h(t_1) * h^*(t_2),$$

or

$$R_{yy}(t_1, t_2) = \int_{-\infty}^{\infty} \int_{-\infty}^{\infty} R_{xx}(t_1 - \alpha, t_2 - \beta) h(\alpha) h^*(\beta) d\alpha d\beta. \quad (42)$$

*Proof:*

1. Cross-correlation of the input and the output is

$$\begin{aligned} R_{xy}(t_1, t_2) &= \langle x(t_1) y^*(t_2) \rangle = \langle x(t_1) x^*(t_2) * h^*(t_2) \rangle \\ &= \langle x(t_1) x^*(t_2) \rangle * h^*(t_2) = R_{xx}(t_1, t_2) * h^*(t_2), \end{aligned}$$

or

$$R_{xy}(t_1, t_2) = \int_{-\infty}^{\infty} R_{xx}(t_1, t_2 - \beta) h^*(\beta) d\beta.$$

2. Autocorrelation of the output is

$$\begin{aligned} R_{yy}(t_1, t_2) &= \langle y(t_1) y^*(t_2) \rangle = \langle x(t_1) * h(t_1) y^*(t_2) \rangle \\ &= \langle x(t_1) y^*(t_2) \rangle * h(t_1) = R_{xy}(t_1, t_2) * h(t_1), \end{aligned}$$

or

$$R_{yy}(t_1, t_2) = \int_{-\infty}^{\infty} R_{xy}(t_1 - \alpha, t_2) h(\alpha) d\alpha.$$

3. From 1. and 2. above, we have

$$\begin{aligned} R_{yy}(t_1, t_2) &= R_{xx}(t_1, t_2) * h^*(t_2) * h(t_1) \\ &= R_{xx}(t_1, t_2) * h(t_1) * h^*(t_2), \end{aligned}$$

or

$$R_{yy}(t_1, t_2) = \int_{-\infty}^{\infty} \int_{-\infty}^{\infty} R_{xx}(t_1 - \alpha, t_2 - \beta) h(\alpha) h^*(\beta) d\alpha d\beta.$$

### 1.2.3 Stationary Random Processes

#### Definitions

- A random process  $z(t)$  is called “stationary” (or, more specifically, “wide-sense stationary”), if the expectation does not depend on time, and the autocorrelation is a function of time difference only:

$$\begin{aligned}\langle z(t) \rangle &= \eta = \text{const}, \\ \langle z(t_1) z^*(t_2) \rangle &= R(\tau),\end{aligned}\tag{43}$$

where  $\tau \equiv t_1 - t_2$ .

- Random processes  $x(t)$  and  $y(t)$  are called “jointly stationary”, if both of them are stationary, and their cross-correlation is a function of time difference only:

$$\langle x(t_1) y^*(t_2) \rangle = R_{xy}(\tau),\tag{44}$$

where  $\tau \equiv t_1 - t_2$ .

Of course, it is not easy to find actual physical processes which strictly satisfy these conditions. For example, some of quasars or astronomical masers are known to exhibit significant time variations in yearly, or shorter, time scales. In a practical sense, however, physical processes are well approximated by the stationary random processes, if equations (43) and (44) are fulfilled during time scales, which are sufficient to estimate their statistical properties (see discussions on ergodicity in section 1.2.4). In this sense, many physical processes can be successfully modeled as stationary random processes.

## Properties

Following formulae can be easily derived, by applying general properties of correlations, covariances, and so on, to the particular case of the stationary random processes as defined above.

- $R(-\tau) = R^*(\tau)$ .
- $R(0) = \langle |z(t)|^2 \rangle \geq 0$ .
- Positive definiteness:

$$\sum_{i=1}^n \sum_{j=1}^n a_i a_j^* R(t_i - t_j) \geq 0, \quad \text{for any } a_i.$$

- $|R(\tau)| \leq R(0)$ .
- $C(\tau) = R(\tau) - |\eta|^2$ , autocovariance.

- $r(\tau) = C(\tau)/C(0)$ , correlation coefficient.
- $|r(\tau)| \leq 1$ .
- $R_{xy}(-\tau) = R_{yx}^*(\tau)$ .
- $|R_{xy}(\tau)|^2 \leq R_{xx}(0) R_{yy}(0)$ .
- $C_{xy}(\tau) = R_{xy}(\tau) - \eta_x \eta_y^*$ , cross-covariance.
- $r_{xy} = C_{xy}(\tau) / \sqrt{C_{xx}(0) C_{yy}(0)}$ , cross-correlation coefficient.
- $|r_{xy}(\tau)| \leq 1$ .

### 1.2.4 Ergodicity

How can we estimate various statistical properties of a random process, if we are given with a single sample of time series only, which is an outcome of a single trial?

- Definition.  
A random process  $z(t)$  is called “ergodic” if its ensemble averages are equal to appropriate time averages.

This implies that we can estimate any statistical property of  $z(t)$ , using time average of the single sample, if the random process is ergodic.

- Mean-ergotic process.  
A random process  $z(t)$ , with constant expectation:

$$\eta = \langle z(t) \rangle,$$

is called “mean-ergotic”, if its time average tends to  $\eta$  as averaging time tends to infinity:

$$\eta_T = \frac{1}{2T} \int_{-T}^T z(t) dt \rightarrow \eta \quad \text{as } T \rightarrow \infty.$$

- A condition for the mean-ergotic process.  
It is evident that

$$\langle \eta_T \rangle = \frac{1}{2T} \int_{-T}^T \langle z(t) \rangle dt = \eta.$$

Therefore,  $z(t)$  is mean-ergodic, if its “variance”, or “dispersion”,  $\sigma_T^2$  tends to 0 as  $T \rightarrow \infty$ , i.e.,

$$\sigma_T^2 \equiv \langle | \eta_T - \eta |^2 \rangle \rightarrow 0 \text{ as } T \rightarrow \infty.$$

Since

$$\begin{aligned} \sigma_T^2 = \langle | \eta_T - \eta |^2 \rangle &= \frac{1}{(2T)^2} \int_{-T}^T \int_{-T}^T \langle (z(t_1) - \eta) (z(t_2) - \eta)^* \rangle dt_1 dt_2 \\ &= \frac{1}{(2T)^2} \int_{-T}^T \int_{-T}^T C(t_1, t_2) dt_1 dt_2, \end{aligned}$$

where  $C(t_1, t_2)$  is the autocovariance, and we used here equation (20), the above condition is equivalent to

$$\frac{1}{(2T)^2} \int_{-T}^T \int_{-T}^T C(t_1, t_2) dt_1 dt_2 \rightarrow 0 \text{ as } T \rightarrow \infty.$$

- In the stationary random case.

If  $z(t)$  is a stationary random process, and, therefore, the autocovariance is a function of time difference  $\tau = t_1 - t_2$  only:

$$C(t_1, t_2) = C(\tau),$$

the double integral in the above condition is reduced to a single integral:

$$\frac{1}{2T} \int_{-2T}^{2T} C(\tau) \left(1 - \frac{|\tau|}{2T}\right) d\tau \rightarrow 0 \text{ as } T \rightarrow \infty, \quad (45)$$

because

$$\int_{-T}^T \int_{-T}^T C(t_1, t_2) dt_1 dt_2 = \int_{-2T}^{2T} C(\tau) (2T - |\tau|) d\tau, \quad (46)$$

as we can easily see from Figure 8. In fact, in the rectangular range of integration  $-T \leq t_1 \leq T$  and  $-T \leq t_2 \leq T$  in Figure 8, the autocovariance  $C(\tau)$  is constant along a line  $t_1 - t_2 = \tau$ , and an area of the hatched region, put between two lines  $t_1 - t_2 = \tau$  and  $t_1 - t_2 = \tau + \Delta\tau$  is nearly equal to the area of the enclosing parallelogram, which is equal to  $(2T - |\tau|) \Delta\tau$ , in the linear approximation with respect to small  $\Delta\tau$ .

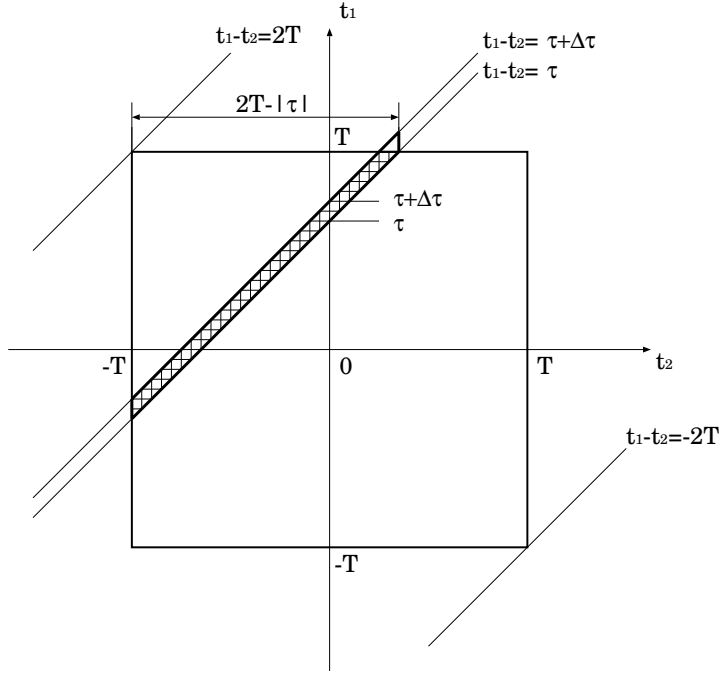


Figure 8: Geometry of the integration.

- Correlation-ergodic process.

A stationary random process  $z(t)$  with an autocorrelation

$$R(\xi) = \langle z(t + \xi) z^*(t) \rangle,$$

is called “correlation-ergodic”, if the corresponding process  $u_\xi(t)$ :

$$u_\xi(t) = z(t + \xi) z^*(t),$$

is mean-ergodic, i.e., if

$$R_T \equiv \frac{1}{2T} \int_{-T}^T u_\xi(t) dt \rightarrow R(\xi) \text{ as } T \rightarrow \infty.$$

Similarly to the case of the mean-ergodic process,  $z(t)$  is correlation-ergodic, if the variance, or dispersion,  $\sigma_{R_T}^2 \equiv \langle |R_T - R(\xi)|^2 \rangle$  tends to 0 as  $T \rightarrow \infty$ , or, equivalently, if an autocovariance of  $u_\xi(t)$ :

$$C_{uu}(\tau) = R_{uu}(\tau) - R^2(\xi),$$

where  $R_{uu}(\tau)$  is an autocorrelation of  $u_\xi(t)$ :

$$R_{uu}(\tau) = \langle u_\xi(t + \tau) u_\xi^*(t) \rangle = \langle z(t + \xi + \tau) z^*(t + \tau) z^*(t + \xi) z(t) \rangle,$$

satisfies the condition in equation (45) for any  $\xi$ , i.e.,

$$\frac{1}{2T} \int_{-2T}^{2T} C_{uu}(\tau) \left(1 - \frac{|\tau|}{2T}\right) d\tau \rightarrow 0 \text{ as } T \rightarrow \infty. \quad (47)$$

For actual physical processes, which are approximated by the stationary random processes, it is likely that autocovariances are finite everywhere and tend to 0 when  $\tau \rightarrow \pm\infty$ . Therefore, equations (45) and (47) appear well satisfied in the most cases. In the followings, we assume that these equations are fulfilled, and, hence, we can estimate both expectation and correlation of our physical process in terms of the time averaging of a single sample.

It is known that the power or the correlation of a moderately strong signal from an astronomical radio source, which is estimated by time averaging in a square-law detector or in a correlator, usually reaches a sufficiently high signal-to-noise ratio, that means a small enough dispersion, after averaging during seconds to hours, depending on telescope or array sensitivity. The detected power or correlation is usually almost time-invariant during time-scales from hours to months. Therefore, radio astronomical data are mostly consistent with assumptions of the stationary random process and the ergodicity.

### 1.2.5 Stationary Random Processes in Linear Systems

Let us consider cases when inputs of linear systems are stationary random processes. Then, we have following properties.

- If an input  $x(t)$  in a linear system  $y(t) = L[x(t)]$  is a stationary random process, then an output  $y(t)$  is also a stationary random process.

*Proof:*

1. Expectation  $\eta_y(t)$  of the output  $y(t)$  is constant in time, because

$$\eta_y(t) = \int_{-\infty}^{\infty} \eta_x(t - \alpha) h(\alpha) d\alpha = \eta_x \int_{-\infty}^{\infty} h(\alpha) d\alpha = \text{const},$$

since  $x(t)$  is stationary, and hence,  $\eta_x(t) = \eta_x$  is constant in time. Thus, we have

$$\eta_y = \eta_x \int_{-\infty}^{\infty} h(\alpha) d\alpha. \quad (48)$$

2. Autocorrelation  $R_{yy}(t_1, t_2)$  of the output  $y(t)$  is a function of time difference  $\tau = t_1 - t_2$  only, because

$$\begin{aligned} R_{yy}(t_1, t_2) &= \int_{-\infty}^{\infty} \int_{-\infty}^{\infty} R_{xx}(t_1 - \alpha, t_2 - \beta) h(\alpha) h^*(\beta) d\alpha d\beta \\ &= \int_{-\infty}^{\infty} \int_{-\infty}^{\infty} R_{xx}(\tau - \alpha + \beta) h(\alpha) h^*(\beta) d\alpha d\beta, \end{aligned}$$

since  $x(t)$  is stationary, and hence,

$$R_{xx}(t_1 - \alpha, t_2 - \beta) = R_{xx}(t_1 - \alpha - (t_2 - \beta)) = R_{xx}(\tau - \alpha + \beta).$$

Then, the above formula is now expressed as:

$$R_{yy}(\tau) = R_{xx}(\tau) * h(\tau) * h^*(-\tau). \quad (49)$$

- If an input  $x(t)$  in a linear system  $y(t) = L[x(t)]$  is a stationary random process, then the input  $x(t)$  and the output  $y(t)$  are jointly stationary.

*Proof:*

1. We have proven above that, if the input is stationary, then the output is also stationary, i.e., both  $x(t)$  and  $y(t)$  are stationary.
2. Cross-correlation  $R_{xy}(t_1, t_2)$  of the input  $x(t)$  and the output  $y(t)$  is a function of time difference  $\tau = t_1 - t_2$  only, because

$$\begin{aligned} R_{xy}(t_1, t_2) &= \langle x(t_1) y^*(t_2) \rangle = \int_{-\infty}^{\infty} \langle x(t_1) x^*(t_2 - \alpha) \rangle h^*(\alpha) d\alpha \\ &= \int_{-\infty}^{\infty} R_{xx}(\tau + \alpha) h^*(\alpha) d\alpha = R_{xx}(\tau) * h^*(-\tau). \end{aligned}$$

Thus, we have

$$R_{xy}(\tau) = R_{xx}(\tau) * h^*(-\tau). \quad (50)$$

- Likewise, we can prove an equation:

$$R_{yy}(\tau) = R_{xy}(\tau) * h(\tau), \quad (51)$$

which, together with equation (50), offers another derivation of equation (49).

- If  $x_1(t)$  and  $x_2(t)$  are jointly stationary random processes, then outputs  $y_1(t)$  and  $y_2(t)$ , which are obtained from  $x_1(t)$  and  $x_2(t)$  through arbitrary linear operators  $L_1$  and  $L_2$ , respectively, are also jointly stationary.

*Proof:*

Let the two linear operators  $L_1$  and  $L_2$  correspond to impulse responses  $h_1(t)$  and  $h_2(t)$ , respectively. Then we have

$$y_1(t) = L_1[x_1(t)] = x_1(t) * h_1(t) = \int_{-\infty}^{\infty} x_1(t - \alpha) h_1(\alpha) d\alpha,$$

$$y_2(t) = L_2[x_2(t)] = x_2(t) * h_2(t) = \int_{-\infty}^{\infty} x_2(t - \alpha) h_2(\alpha) d\alpha.$$

Both  $y_1(t)$  and  $y_2(t)$  are, of course, stationary, and their cross-correlation:

$$\begin{aligned} R_{y_1 y_2}(t_1, t_2) &= \langle y_1(t_1) y_2^*(t_2) \rangle \\ &= \int_{-\infty}^{\infty} \int_{-\infty}^{\infty} \langle x_1(t_1 - \alpha) x_2^*(t_2 - \beta) \rangle h_1(\alpha) h_2^*(\beta) d\alpha d\beta \\ &= \int_{-\infty}^{\infty} \int_{-\infty}^{\infty} R_{x_1 x_2}(\tau - \alpha + \beta) h_1(\alpha) h_2^*(\beta) d\alpha d\beta, \end{aligned}$$

is a function of time difference  $\tau = t_1 - t_2$  only. This proves the joint stationarity of  $y_1(t)$  and  $y_2(t)$ , and yields

$$R_{y_1 y_2}(\tau) = R_{x_1 x_2}(\tau) * h_1(\tau) * h_2^*(-\tau). \quad (52)$$

## 1.2.6 Spectra of Stationary Random Processes

### Definitions

- Fourier transform  $S(\omega)$  of an autocorrelation  $R(\tau)$  of a stationary random process is called “power spectrum” (or “spectral density”) of the process. Here,  $\omega$  is an angular frequency, which is related to a linear

frequency  $\nu$  as  $\omega = 2\pi\nu$ . Thus, the power spectrum and the autocorrelation are related to each other by the Fourier- and inverse Fourier transforms:

$$S(\omega) = \int_{-\infty}^{\infty} R(\tau)e^{-i\omega\tau} d\tau, \quad (53)$$

$$R(\tau) = \frac{1}{2\pi} \int_{-\infty}^{\infty} S(\omega)e^{i\omega\tau} d\omega. \quad (54)$$

Hereafter, we express a Fourier transform pair by a symbol “ $\Leftrightarrow$ ”. Then,

$$S(\omega) \Leftrightarrow R(\tau).$$

- Fourier transform  $S_{xy}(\omega)$  of a cross-correlation  $R_{xy}(\tau)$  of jointly stationary random processes  $x(t)$  and  $y(t)$  is called “cross-power spectrum”. Thus,

$$S_{xy}(\omega) = \int_{-\infty}^{\infty} R_{xy}(\tau)e^{-i\omega\tau} d\tau, \quad (55)$$

$$R_{xy}(\tau) = \frac{1}{2\pi} \int_{-\infty}^{\infty} S_{xy}(\omega)e^{i\omega\tau} d\omega, \quad (56)$$

and

$$S_{xy}(\omega) \Leftrightarrow R_{xy}(\tau).$$

Note that convergence of Fourier integrals in equations (53) and (55), and therefore in their inverses in equations (54) and (56), too, is usually guaranteed, since, for actual physical processes,  $R(\tau)$  and  $R_{xy}(\tau)$  are mostly finite everywhere, and tend to zero as  $\tau \rightarrow \pm\infty$ .

## Properties

- Power  $\langle |z(t)|^2 \rangle$  of a stationary random process  $z(t)$  is equal to an integrated power spectrum over the whole frequency range:

$$\langle |z(t)|^2 \rangle = R(0) = \frac{1}{2\pi} \int_{-\infty}^{\infty} S(\omega) d\omega = \int_{-\infty}^{\infty} S(\omega) d\nu, \quad (57)$$

where  $\nu = \omega/(2\pi)$  is a frequency, corresponding to the angular frequency  $\omega$ .

- Power spectrum  $S(\omega)$  is a real function.

*Proof :*

Since  $R(-\tau) = R^*(\tau)$ ,

$$S^*(\omega) = \int_{-\infty}^{\infty} R^*(\tau)e^{i\omega\tau} d\tau = \int_{-\infty}^{\infty} R(-\tau)e^{i\omega\tau} d\tau = \int_{-\infty}^{\infty} R(\tau)e^{-i\omega\tau} d\tau = S(\omega).$$

- For any cross-power spectrum,  $S_{xy}(\omega) = S_{yx}^*(\omega)$ .

*Proof :*

Since  $R_{xy}(-\tau) = R_{yx}^*(\tau)$ ,

$$S_{yx}^*(\omega) = \int_{-\infty}^{\infty} R_{yx}^*(\tau)e^{i\omega\tau} d\tau = \int_{-\infty}^{\infty} R_{xy}(-\tau)e^{i\omega\tau} d\tau = \int_{-\infty}^{\infty} R_{xy}(\tau)e^{-i\omega\tau} d\tau = S_{xy}(\omega).$$

- A power spectrum  $S(\omega)$  corresponding to a real autocorrelation  $R(\tau)$  is an even function of  $\omega$  (see Figure 9):

$$S(-\omega) = S(\omega). \quad (58)$$

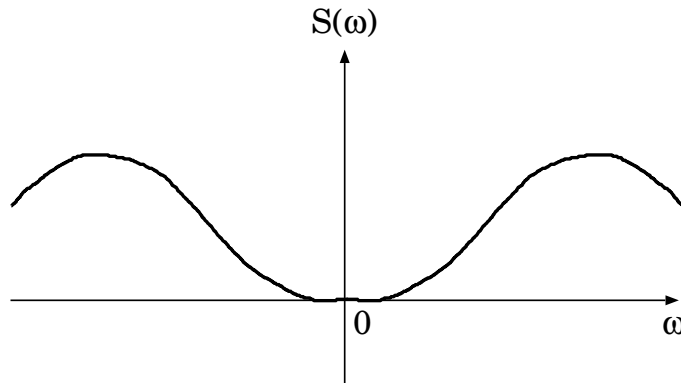


Figure 9: Power spectrum is even when autocorrelation is real.

*Proof :*

Since, in this case,  $R(-\tau) = R(\tau)$  (the real autocorrelation is an even function of  $\tau$ ),

$$S(-\omega) = \int_{-\infty}^{\infty} R(\tau)e^{i\omega\tau} d\tau = \int_{-\infty}^{\infty} R(-\tau)e^{i\omega\tau} d\tau = \int_{-\infty}^{\infty} R(\tau)e^{-i\omega\tau} d\tau = S(\omega).$$

- A cross-power spectrum corresponding to a real cross-correlation satisfies

$$S_{xy}(-\omega) = S_{yx}(\omega), \quad (59)$$

and, therefore, is Hermitian symmetric:

$$S_{xy}(-\omega) = S_{xy}^*(\omega), \quad (60)$$

(see Figure 10).

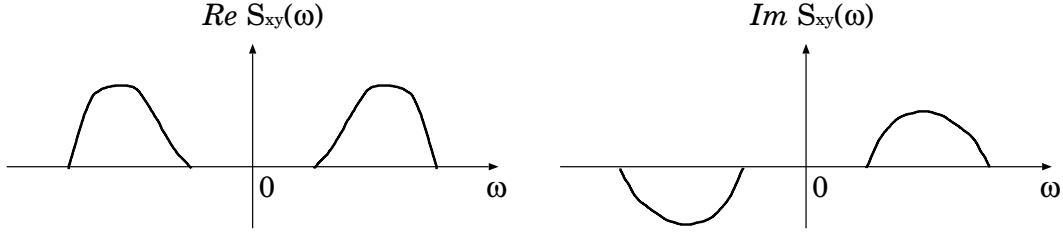


Figure 10: Cross-power spectrum is Hermitian symmetric (i.e., real part is even and imaginary part is odd) when cross-correlation is real.

*Proof:*

Since, in this case,  $R_{xy}(-\tau) = R_{yx}(\tau)$ ,

$$\begin{aligned} S_{xy}(-\omega) &= \int_{-\infty}^{\infty} R_{xy}(\tau) e^{i\omega\tau} d\tau = \int_{-\infty}^{\infty} R_{xy}(-\tau) e^{-i\omega\tau} d\tau = \int_{-\infty}^{\infty} R_{yx}(\tau) e^{-i\omega\tau} d\tau \\ &= S_{yx}(\omega), \end{aligned}$$

and, in view of the general property  $S_{xy}(\omega) = S_{yx}^*(\omega)$ , we also have

$$S_{xy}(-\omega) = S_{xy}^*(\omega).$$

- Real autocorrelation can be described solely by the positive frequency range of the power spectrum.

*Proof:*

Since  $S(\omega) = S(-\omega)$ , in this case,

$$R(\tau) = \frac{1}{2\pi} \int_{-\infty}^{\infty} S(\omega) e^{i\omega\tau} d\omega = \frac{1}{2\pi} \left[ \int_{-\infty}^0 S(\omega) e^{i\omega\tau} d\omega + \int_0^{\infty} S(\omega) e^{i\omega\tau} d\omega \right]$$

$$\begin{aligned}
&= \frac{1}{2\pi} \int_0^{\infty} [S(-\omega)e^{-i\omega\tau} + S(\omega)e^{i\omega\tau}] d\omega = \frac{1}{2\pi} \int_0^{\infty} S(\omega)[e^{-i\omega\tau} + e^{i\omega\tau}] d\omega \\
&= \frac{1}{\pi} \int_0^{\infty} S(\omega) \cos(\omega\tau) d\omega = \frac{1}{\pi} \Re \left[ \int_0^{\infty} S(\omega)e^{i\omega\tau} d\omega \right]. \tag{61}
\end{aligned}$$

- Real cross-correlation can be described solely by the positive frequency range of the cross-power spectrum.

*Proof :*

Since  $S_{xy}(-\omega) = S_{xy}^*(\omega)$ , in this case,

$$\begin{aligned}
R_{xy}(\tau) &= \frac{1}{2\pi} \int_{-\infty}^{\infty} S_{xy}(\omega)e^{i\omega\tau} d\omega = \frac{1}{2\pi} \left[ \int_{-\infty}^0 S_{xy}(\omega)e^{i\omega\tau} d\omega + \int_0^{\infty} S_{xy}(\omega)e^{i\omega\tau} d\omega \right] \\
&= \frac{1}{2\pi} \int_0^{\infty} [S_{xy}(-\omega)e^{-i\omega\tau} + S_{xy}(\omega)e^{i\omega\tau}] d\omega \\
&= \frac{1}{2\pi} \int_0^{\infty} [S_{xy}^*(\omega)e^{-i\omega\tau} + S_{xy}(\omega)e^{i\omega\tau}] d\omega \\
&= \frac{1}{\pi} \Re \int_0^{\infty} S_{xy}(\omega)e^{i\omega\tau} d\omega. \tag{62}
\end{aligned}$$

- White noise: if the spectrum is flat throughout the whole frequency range, then the correlation is proportional to the delta function of  $\tau$ .

If  $S(\omega) = S = \text{const}$ , then

$$R(\tau) = \frac{1}{2\pi} \int_{-\infty}^{\infty} S(\omega)e^{i\omega\tau} d\omega = S \frac{1}{2\pi} \int_{-\infty}^{\infty} e^{i\omega\tau} d\omega = S \delta(\tau). \tag{63}$$

If  $S_{xy}(\omega) = S_{xy} = \text{const}$ , then

$$R_{xy}(\tau) = \frac{1}{2\pi} \int_{-\infty}^{\infty} S_{xy}(\omega)e^{i\omega\tau} d\omega = S_{xy} \frac{1}{2\pi} \int_{-\infty}^{\infty} e^{i\omega\tau} d\omega = S_{xy} \delta(\tau). \tag{64}$$

Here we used a formula

$$\int_{-\infty}^{\infty} e^{i\omega\tau} d\omega = 2\pi\delta(\tau), \tag{65}$$

which is known as one of the definitions of the delta function.

Thus, if spectra of random processes are completely flat (white), then their correlations are non-zero, only when  $\tau = 0$ .

- Convolution theorem: Fourier transform of a convolution of two functions is equal to a product of Fourier transforms of those functions, i.e., if  $a(\tau) \Leftrightarrow A(\omega)$  and  $b(\tau) \Leftrightarrow B(\omega)$ , then

$$a(\tau) * b(\tau) \Leftrightarrow A(\omega) B(\omega). \quad (66)$$

*Proof:*

$$\begin{aligned} \int_{-\infty}^{\infty} a(\tau) * b(\tau) e^{-i\omega\tau} d\tau &= \int_{-\infty}^{\infty} \int_{-\infty}^{\infty} a(\tau - \alpha) b(\alpha) e^{-i\omega\tau} d\alpha d\tau \\ &= \int_{-\infty}^{\infty} \int_{-\infty}^{\infty} a(\tau') e^{-i\omega\tau'} b(\tau'') e^{-i\omega\tau''} d\tau' d\tau'' = A(\omega) B(\omega), \end{aligned}$$

where we introduced transformations  $\tau' = \tau - \alpha$  and  $\tau'' = \alpha$ .

- Another convolution theorem holds for a product of functions  $a(\tau)$  and  $b(\tau)$ :

$$a(\tau) b(\tau) \Leftrightarrow \frac{1}{2\pi} A(\omega) * B(\omega), \quad (67)$$

because

$$\begin{aligned} &\int_{-\infty}^{\infty} a(\tau) b(\tau) e^{-i\omega\tau} d\tau \\ &= \frac{1}{(2\pi)^2} \int_{-\infty}^{\infty} \left[ \int_{-\infty}^{\infty} A(\omega') e^{i\omega'\tau} d\omega' \right] \left[ \int_{-\infty}^{\infty} B(\omega'') e^{i\omega''\tau} d\omega'' \right] e^{-i\omega\tau} d\tau \\ &= \frac{1}{(2\pi)^2} \int_{-\infty}^{\infty} \int_{-\infty}^{\infty} A(\omega') B(\omega'') \left[ \int_{-\infty}^{\infty} e^{-i(\omega - \omega' - \omega'')\tau} d\tau \right] d\omega' d\omega'' \\ &= \frac{1}{2\pi} \int_{-\infty}^{\infty} \int_{-\infty}^{\infty} A(\omega') B(\omega'') \delta(\omega - \omega' - \omega'') d\omega' d\omega'' \\ &= \frac{1}{2\pi} \int_{-\infty}^{\infty} A(\omega - \omega') B(\omega') d\omega' = \frac{1}{2\pi} A(\omega) * B(\omega), \end{aligned}$$

we used here the relation

$$\int_{-\infty}^{\infty} e^{-i\omega\tau} d\tau = \int_{-\infty}^{\infty} e^{i\omega\tau} d\tau = 2\pi\delta(\omega).$$

- Shift theorem:  
If  $a(\tau) \Leftrightarrow A(\omega)$ , then

$$\begin{aligned} a(\tau - \tau_0) &\Leftrightarrow A(\omega) e^{-i\omega\tau_0}, \\ a(\tau)e^{i\omega_0\tau} &\Leftrightarrow A(\omega - \omega_0). \end{aligned} \quad (68)$$

*Proof:*

$$\begin{aligned} \int_{-\infty}^{\infty} a(\tau - \tau_0) e^{-i\omega\tau} d\tau &= \int_{-\infty}^{\infty} a(\tau') e^{-i\omega(\tau'+\tau_0)} d\tau' \\ &= \left[ \int_{-\infty}^{\infty} a(\tau') e^{-i\omega\tau'} d\tau' \right] e^{-i\omega\tau_0} = A(\omega) e^{-i\omega\tau_0}, \end{aligned}$$

and,

$$\int_{-\infty}^{\infty} a(\tau) e^{i\omega_0\tau} e^{-i\omega\tau} d\tau = \int_{-\infty}^{\infty} a(\tau) e^{-i(\omega-\omega_0)\tau} d\tau = A(\omega - \omega_0). \quad (69)$$

### 1.2.7 Spectra of Outputs of Linear Systems

Let us call a Fourier transform  $H(\omega)$  of an impulse response  $h(t)$  of a linear system as the “system function”:

$$H(\omega) = \int_{-\infty}^{\infty} h(t) e^{-i\omega t} dt, \quad (70)$$

or

$$H(\omega) \Leftrightarrow h(t).$$

For the system function, we have

$$H^*(\omega) \Leftrightarrow h^*(-t),$$

because

$$H^*(\omega) = \int_{-\infty}^{\infty} h^*(t) e^{i\omega t} dt = \int_{-\infty}^{\infty} h^*(-t) e^{-i\omega t} dt.$$

Now, let us consider stationary random processes as inputs of a linear system  $y(t) = L[x(t)]$  with the impulse response  $h(t)$  and the system function  $H(\omega)$ .

- Expectation of the output.

$$\eta_y = \eta_x \int_{-\infty}^{\infty} h(\alpha) d\alpha = \eta_x H(0). \quad (71)$$

- Power spectra of the output  $S_{yy}(\omega)$  and the inputs  $S_{xx}(\omega)$  are mutually related to each other as

$$S_{yy}(\omega) = S_{xx}(\omega) |H(\omega)|^2. \quad (72)$$

*Proof:*

In view of the convolution theorem given in equation (66), and properties of correlations,

$$R_{xy}(\tau) = R_{xx}(\tau) * h^*(-\tau) \Leftrightarrow S_{xy}(\omega) = S_{xx}(\omega) H^*(\omega),$$

$$R_{yy}(\tau) = R_{xy}(\tau) * h(\tau) \Leftrightarrow S_{yy}(\omega) = S_{xy}(\omega) H(\omega),$$

and, hence

$$R_{yy}(\tau) = R_{xx}(\tau) * h(\tau) * h^*(-\tau) \Leftrightarrow S_{yy}(\omega) = S_{xx}(\omega) |H(\omega)|^2.$$

- Autocorrelations of the outputs:

$$R_{yy}(\tau) = \langle y(t+\tau) y^*(t) \rangle = \frac{1}{2\pi} \int_{-\infty}^{\infty} S_{xx}(\omega) |H(\omega)|^2 e^{i\omega\tau} d\omega,$$

and, in particular,

$$R_{yy}(0) = \langle |y(t)|^2 \rangle = \frac{1}{2\pi} \int_{-\infty}^{\infty} S_{xx}(\omega) |H(\omega)|^2 d\omega. \quad (73)$$

- If the impulse response  $h(t)$  is real, then

$$H^*(\omega) = \int_{-\infty}^{\infty} h(t) e^{i\omega t} dt = H(-\omega), \quad (74)$$

and, therefore,  $|H(\omega)|^2$  is an even function of  $\omega$ , because

$$|H(-\omega)|^2 = H(-\omega) H^*(-\omega) = H^*(\omega) H(\omega) = |H(\omega)|^2. \quad (75)$$

- Cross-power spectrum of outputs  $y_1(t) = x_1(t) * h_1(t)$  and  $y_2(t) = x_2(t) * h_2(t)$  of jointly stationary inputs  $x_1(t)$  and  $x_2(t)$  through two linear systems with impulse responses  $h_1(t)$  and  $h_2(t)$ .

As we saw earlier in equation (52), the cross-correlation  $R_{y_1 y_2}(\tau)$  of the outputs is expressed through the cross-correlation of the inputs  $R_{x_1 x_2}(\tau)$  as

$$R_{y_1 y_2}(\tau) = R_{x_1 x_2}(\tau) * h_1(\tau) * h_2^*(-\tau).$$

Therefore, the convolution theorem in equation (66) gives us the cross-power spectrum:

$$S_{y_1 y_2}(\omega) = S_{x_1 x_2}(\omega) H_1(\omega) H_2^*(\omega), \quad (76)$$

where  $S_{x_1 x_2}(\omega) \Leftrightarrow R_{x_1 x_2}(\tau)$  is a cross-power spectrum of the inputs.

- Cross-correlation of the outputs.

$$R_{y_1 y_2}(\tau) = \langle y_1(t + \tau) y_2^*(t) \rangle = \frac{1}{2\pi} \int_{-\infty}^{\infty} S_{x_1 x_2}(\omega) H_1(\omega) H_2^*(\omega) e^{i\omega\tau} d\omega,$$

and, hence,

$$R_{y_1 y_2}(0) = \langle y_1(t) y_2^*(t) \rangle = \frac{1}{2\pi} \int_{-\infty}^{\infty} S_{x_1 x_2}(\omega) H_1(\omega) H_2^*(\omega) d\omega. \quad (77)$$

### 1.2.8 Two Designs of Spectrometers

As an example of applications of the theory of the stationary random process, let us consider principles of two types of spectrometers which have been widely used in the radio astronomy (Figures 11 and 12).

In the filterbank spectrometer (Figure 11), received voltage from a radio source is equally fed to  $n$  identical analog narrow-band BPF's (band-pass-filters), which are called "filterbank" with successive center frequencies  $\nu_1, \nu_2, \dots, \nu_n$ . Outputs of the BPF's are squared and averaged by SQ (square-law) detectors and resultant powers yield a spectral shape of the source at the above frequencies.

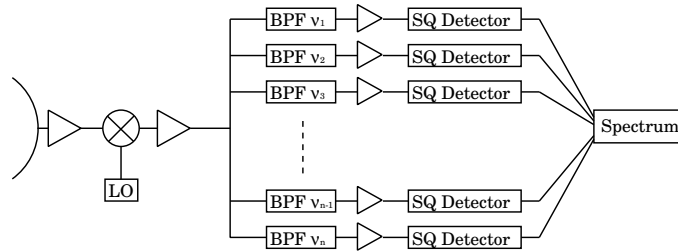


Figure 11: Basic design of a filterbank spectrometer.

In the autocorrelation spectrometer (Figure 12), on the other hand, the received voltage is first digitized by an analog-to-digital converter (A/D), and then equally divided into two digital signals, which are fed to  $n$  multipliers and integrators, one directly, and another with successive time delays  $0, \tau, 2\tau, \dots, (n - 1)\tau$ . The resultant ‘autocorrelation’ as a function of time delay is then Fourier transformed, and converted to a power spectrum.

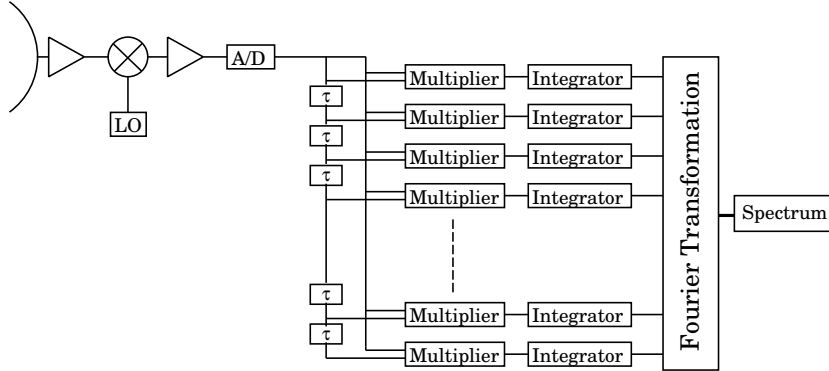


Figure 12: Basic design of an autocorrelation spectrometer.

The principles of the two designs look quite different. Do they really produce the same spectrum?

As far as the ergodicity holds, it is clear that the autocorrelation spectrometer must closely approximate the calculation of the power spectrum of the input signal (received voltage) as the Fourier transform of the autocorrelation, as we have described so far.

For the filterbank spectrometer, let us consider  $i$ -th narrow-band BPF as a linear system, which has an input stationary random process  $x(t)$ , which is the received voltage in this case, an output  $y_i(t)$ , and an impulse response  $h_i(t)$ , corresponding to a rectangular sytem function  $H_i(\omega)$ :

$$H_i(\omega) = \begin{cases} \sqrt{\frac{2\pi}{\Delta\omega}} & \omega_i - \frac{\Delta\omega}{2} \leq \omega \leq \omega_i + \frac{\Delta\omega}{2}, \\ 0 & \text{otherwise,} \end{cases}$$

where  $\omega_i = 2\pi\nu_i$  is the  $i$ -th center angular frequency, and  $\Delta\omega$  is the frequency bandwidth of the BPF. If the power spectrum of the input is  $S_{xx}(\omega)$ , then, according to equation (72), the power spectrum of the output  $S_{yy}(\omega)$  is

$$S_{yy}(\omega) = S_{xx}(\omega) |H_i(\omega)|^2,$$

(Figure 13). Since, in view of the ergodicity, the time averaging in a square-

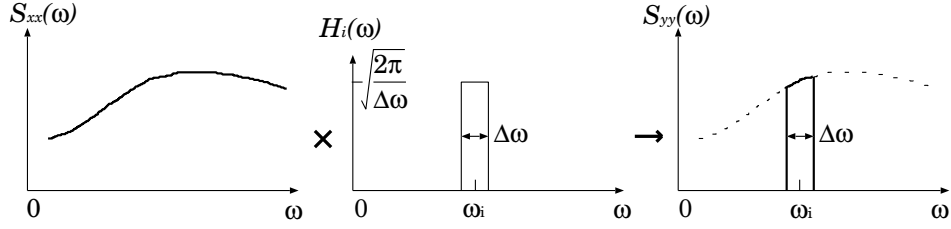


Figure 13: Band-pass filter passes a segment of the input power spectrum.

law detector must yield the power, or the autocorrelation at  $\tau = 0$ , of the output signal, if the averaging time is sufficiently long, we obtain

$$\begin{aligned} \langle |y_i(t)|^2 \rangle &= \frac{1}{2\pi} \int_{-\infty}^{\infty} S_{yy}(\omega) d\omega = \frac{1}{2\pi} \int_{-\infty}^{\infty} S_{xx}(\omega) |H_i(\omega)|^2 d\omega \\ &= \frac{1}{\Delta\omega} \int_{\omega_i - \frac{\Delta\omega}{2}}^{\omega_i + \frac{\Delta\omega}{2}} S_{xx}(\omega) d\omega. \end{aligned}$$

This “power passed by a BPF” is nothing but a mean of the power spectrum of the received voltage  $S_{xx}(\omega)$ , involved in the spectral range  $\omega_i - \frac{\Delta\omega}{2} \leq \omega \leq \omega_i + \frac{\Delta\omega}{2}$ . Therefore, if  $\Delta\omega$  is sufficiently narrow, and  $S_{xx}(\omega)$  is continuous around  $\omega_i$ , then we approximately have

$$\langle |y_i(t)|^2 \rangle \simeq S_{xx}(\omega_i).$$

Thus two spectrometers really yield the same power spectrum of the received voltage.

This example gives us a clear feel, that the power spectrum, defined as a Fourier transform of the autocorrelation of the input signal, is really a “spectrum of the power” of the signal.

### 1.2.9 Fourier Transforms of Stationary Random Processes

So far, we have considered Fourier transformation of correlations of the stationary random processes. Now, let us proceed to considerations of the Fourier transformation of the stationary random processes themselves.

Assume that a Fourier integral of a random process  $z(t)$  is expressed as

$$Z(\omega) = \int_{-\infty}^{\infty} z(t) e^{-i\omega t} dt. \quad (78)$$

Since  $z(t)$  is a random process in time  $t$ , it is natural to consider that  $Z(\omega)$  is a random process in angular frequency  $\omega$ , i.e., it is a function of  $\omega$ , and its value at any  $\omega$  is a random variable, which may vary from trial to trial.

If we apply the inverse Fourier transform to equation (78), we would have

$$z(t) = \frac{1}{2\pi} \int_{-\infty}^{\infty} Z(\omega) e^{i\omega t} d\omega, \quad (79)$$

i.e., we could express any random process in time  $t$  as a superposition of infinite number of frequency components, which are themselves random processes in angular frequency  $\omega$ .

Strictly speaking, however, we must be aware that the convergence of the integrals in equations (78) and (79) is not, in general, guaranteed, since the random processes may have finite amplitudes from the infinite past to the infinite future. Of course, we could restrict the actual integration range to  $-T < t \leq T$  with sufficiently large  $T$ . In fact, durations of actual physical processes are most likely to be shorter than the age of our Universe. However, a too strong emphasis on this point may cause difficulties when we require stationarity to the random processes. Special integral forms are often introduced in the literature to assure the convergence. We will, however, just assume some kind of convergence of the above integrals, without being heavily involved in the mathematical strictness. Instead, we will concentrate our attentions to several simple but useful statistical relations between the random process  $z(t)$  and its Fourier transform  $Z(\omega)$ .

### Properties of Fourier transforms of the random processes.

- Expectation of  $Z(\omega)$  is a Fourier transform of the expectation  $\eta(t)$  of  $z(t)$ .

*Proof:*

Taking ensemble average of the two sides of the Fourier transformation in equation (78), we have

$$\langle Z(\omega) \rangle = \int_{-\infty}^{\infty} \langle z(t) \rangle e^{-i\omega t} dt = \int_{-\infty}^{\infty} \eta(t) e^{-i\omega t} dt.$$

- If  $z(t)$  is a stationary random process, the expectation of  $Z(\omega)$  has a delta-function form with respect to  $\omega$ .

*Proof :*

Since

$$\langle z(t) \rangle = \eta = \text{const},$$

we have

$$\langle Z(\omega) \rangle = \int_{-\infty}^{\infty} \eta e^{-i\omega t} dt = 2\pi \eta \delta(\omega), \quad (80)$$

according to equation (65).

- An autocorrelation of  $Z(\omega)$ , defined as  $\langle Z(\omega_1) Z^*(\omega_2) \rangle$ , is related to a two-dimensional Fourier transform  $\Gamma(\omega_1, \omega_2)$  of an autocorrelation  $R(t_1, t_2) = \langle z(t_1) z^*(t_2) \rangle$  of  $z(t)$ , which is

$$\Gamma(\omega_1, \omega_2) = \int_{-\infty}^{\infty} \int_{-\infty}^{\infty} R(t_1, t_2) e^{-i(\omega_1 t_1 + \omega_2 t_2)} dt_1 dt_2,$$

by a formula:

$$\langle Z(\omega_1) Z^*(\omega_2) \rangle = \Gamma(\omega_1, -\omega_2). \quad (81)$$

*Proof :*

From equation (78),

$$\begin{aligned} \langle Z(\omega_1) Z^*(\omega_2) \rangle &= \int_{-\infty}^{\infty} \int_{-\infty}^{\infty} \langle z(t_1) z^*(t_2) \rangle e^{-i(\omega_1 t_1 - \omega_2 t_2)} dt_1 dt_2 \\ &= \int_{-\infty}^{\infty} \int_{-\infty}^{\infty} R(t_1, t_2) e^{-i(\omega_1 t_1 - \omega_2 t_2)} dt_1 dt_2 = \Gamma(\omega_1, -\omega_2). \end{aligned}$$

- If  $z(t)$  is a stationary random process, having a power spectrum  $S(\omega)$ , we have

$$\langle Z(\omega_1) Z^*(\omega_2) \rangle = 2\pi S(\omega_1) \delta(\omega_1 - \omega_2). \quad (82)$$

*Proof :*

Since, in view of the stationarity of  $z(t)$ , its autocorrelation  $\langle z(t_1) z^*(t_2) \rangle = R(t_1, t_2) = R(\tau)$  is a function of time difference  $\tau = t_1 - t_2$  only. Therefore,

$$\begin{aligned} \langle Z(\omega_1) Z^*(\omega_2) \rangle &= \int_{-\infty}^{\infty} \int_{-\infty}^{\infty} R(t_1, t_2) e^{-i(\omega_1 t_1 - \omega_2 t_2)} dt_1 dt_2 \\ &= \int_{-\infty}^{\infty} \int_{-\infty}^{\infty} R(\tau) e^{-i\omega_1 \tau - i(\omega_1 - \omega_2) t_2} d\tau dt_2 \end{aligned}$$

$$\begin{aligned}
&= \int_{-\infty}^{\infty} R(\tau) e^{-i\omega_1\tau} d\tau \int_{-\infty}^{\infty} e^{-i(\omega_1-\omega_2)t_2} dt_2 \\
&= 2\pi S(\omega_1) \delta(\omega_1 - \omega_2).
\end{aligned}$$

- If  $x(t)$  and  $y(t)$  are jointly stationary random processes, having a cross-power spectrum  $S_{xy}(\omega)$ , a cross-correlation of their Fourier transforms:

$$X(\omega) = \int_{-\infty}^{\infty} x(t) e^{-i\omega t} dt, \quad \text{and} \quad Y(\omega) = \int_{-\infty}^{\infty} y(t) e^{-i\omega t} dt,$$

is equal to

$$\langle X(\omega_1) Y^*(\omega_2) \rangle = 2\pi S_{xy}(\omega_1) \delta(\omega_1 - \omega_2). \quad (83)$$

*Proof:*

Since the cross-correlation  $\langle x(t_1) y^*(t_2) \rangle = R_{xy}(t_1, t_2) = R_{xy}(\tau)$  is a function of time difference  $\tau = t_1 - t_2$  only, we have

$$\begin{aligned}
\langle X(\omega_1) Y^*(\omega_2) \rangle &= \int_{-\infty}^{\infty} \int_{-\infty}^{\infty} R_{xy}(t_1, t_2) e^{-i(\omega_1 t_1 - \omega_2 t_2)} dt_1 dt_2 \\
&= \int_{-\infty}^{\infty} \int_{-\infty}^{\infty} R_{xy}(\tau) e^{-i\omega_1\tau - i(\omega_1 - \omega_2)t_2} d\tau dt_2 \\
&= \int_{-\infty}^{\infty} R_{xy}(\tau) e^{-i\omega_1\tau} d\tau \int_{-\infty}^{\infty} e^{-i(\omega_1 - \omega_2)t_2} dt_2 \\
&= 2\pi S_{xy}(\omega_1) \delta(\omega_1 - \omega_2).
\end{aligned}$$

Thus, the autocorrelation and the cross-correlation of the Fourier transforms of the stationary random processes are uniquely related to their power and cross-power spectra by equations (82) and (83). Therefore, the Fourier transforms of the stationary random processes can be regarded as useful tools for calculating the spectra. The FX-type correlators are the realizations of this principle.

Note that the expectation of  $Z(\omega)$ , which is the Fourier transform of a stationary random process  $z(t)$ , has a delta-function form with respect to the angular frequency  $\omega$ , that means not altogether constant in  $\omega$ , except for a special case when  $\langle z(t) \rangle = \eta = 0$ . Also, the RHS of equations (82) and (83) are not functions of angular-frequency difference  $\omega_1 - \omega_2$  only, because of the dependence on  $\omega_1$  in  $S(\omega_1)$  and  $S_{xy}(\omega_1)$ , except for special cases of the complete white spectra, where  $S(\omega) = \text{const}$  or  $S_{xy}(\omega) = \text{const}$ . Therefore,

the Fourier transforms of the stationary random processes are not wide-sense stationary, in general, with respect to  $\omega$ .

## 1.3 The White Fringe

### 1.3.1 A Simple Interferometer

A radio interferometer, in its simplest form, can be illustrated as Figure 14.

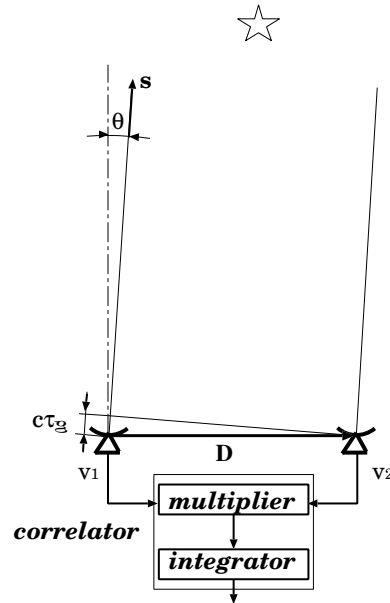


Figure 14: A simple interferometer.

This is a two-element interferometer consisting of identical antennas, identical receivers and a correlator, which is a combination of a multiplier and an integrator (a time-averager). We ignore here details of receiving systems, including the frequency conversion, just regarding as if the correlation processing is performed at RF (radio frequency) band.

Important information which is derived from interferometric observations is the geometric delay  $\tau_g$ . For an infinitely distant point radio source, which we assume in this simplified case, the geometric delay is expressed in a form:

$$\tau_g = \frac{\mathbf{D} \cdot \mathbf{s}}{c} = \frac{D \sin \theta}{c}, \quad (84)$$

where  $\mathbf{D}$  is a “baseline vector” connecting reference points of two antennas,  $\mathbf{s}$  is a “source vector” which is a unit vector directed towards the point radio

source,  $c$  is the light velocity, and  $\theta$  is an angle of the source direction  $\mathbf{s}$  from a plane perpendicular to the baseline vector  $\mathbf{D}$ . For simplicity, we assume that the same wavefront of the electromagnetic wave from an astronomical radio source arrive at two antennas with a time delay, which is equal to the geometric delay  $\tau_g$ , ignoring atmospheric and other delay factors.

We assume a case when the beam centers of the two antennas are exactly oriented towards the radio source. Also, we assume that the source direction is close to the plane perpendicular to the baseline, i.e.,  $\theta \approx 0$ , and the geometric delay  $\tau_g$  is within a small range around zero. Also, we ignore effects of diurnal motion of an observed radio source, just assuming that the source is at rest or moving very slowly.

We ignore, at this stage, any contribution of the system noise, in order to concentrate our attention to the basic characteristics of the correlated radio source signals only.

In summary, we assume following properties for our simple interferometer:

- point-like radio source,
- identical antennas,
- identical receivers,
- correlation at RF-band,
- source diurnal motion is neglected,
- no delay other than the geometric,
- no system noise contribution.

### 1.3.2 Received Voltages as Stationary Random Processes

Let us assume that the received voltage  $v(t)$ , as well as the electric field intensity  $E(t)$  of the radio wave which generates the voltage, are real stationary random processes, satisfying the ergodicity. Here, we used a scalar function  $E(t)$  for the electric field intensity, since any antenna can receive only one polarization component of the electric field intensity vector  $\mathbf{E}(t)$ . Therefore,  $E(t)$  here stands for a single polarization component of  $\mathbf{E}(t)$  in a plane perpendicular to the direction of propagation of the transversal electromagnetic wave, which is commonly received by two antennas of the interferometer.

In actual radio astronomical observations, we usually see that the received voltage oscillates around zero value and its time average is just zero, i.e., time invariant. Also, the outputs of the correlators, which are time-averaged

products of the received voltages, are almost time invariant, as far as we neglect the slow intrinsic time variability of the radio source. At the same time, the correlator outputs vary when we artificially insert different time delays between the two voltage time series, implying that they are functions of the time delay (i.e., of the time difference).

Therefore, the situation, which we experience in our observations, is just consistent with the stationarity and ergodicity assumptions.

Let us consider that the received voltage  $v(t)$  and the electric field intensity  $E(t)$ , generating the voltage, are related to each other by a linear system with a real impulse response  $q(t)$ :

$$v(t) = E(t) * q(t) = \int_{-\infty}^{\infty} E(t - \alpha) q(\alpha) d\alpha. \quad (85)$$

Here  $q(t)$  expresses the response of the antenna–receiver system to the incident radio wave, which, in particular, determines the frequency characteristics of the system as a BPF (band–pass–filter) passing a limited frequency range with a bandwidth  $\Delta\omega$  centered at  $\omega_0$ .

As we stated above, we assume that the responses of the antenna–receiver systems, in the two antennas of our simple interferometer, are identical, for simplicity.

### 1.3.3 Cross–Correlation of Received Voltages

Let us denote the received voltages of the two antennas as  $v_1(t)$  and  $v_2(t)$ . Since they are generated by the same electromagnetic wave from a radio source, but arrived at two antennas at different times due to the geometric delay  $\tau_g$ , we can express them through a common electric field intensity  $E(t)$  as:

$$\begin{aligned} v_1(t) &= \int_{-\infty}^{\infty} E(t - \tau_g - \alpha) q(\alpha) d\alpha, \\ v_2(t) &= \int_{-\infty}^{\infty} E(t - \alpha) q(\alpha) d\alpha, \end{aligned} \quad (86)$$

following equation (85). It is evident that  $v_1(t)$  and  $v_2(t)$  are jointly stationary random processes, because they are the outputs of linear systems (here, we assumed identical) with the same input stationary random process  $E(t)$ .

Now, let us consider that  $v_1(t)$  and  $v_2(t)$  are fed to the correlator shown in Figure 14. Since the correlation processing is the multiplication and inte-

gration of the signals, the correlator output  $\mathcal{R}$  can be modeled as

$$\mathcal{R} = \frac{1}{2T} \int_{-T}^T v_1(t)v_2(t)dt. \quad (87)$$

Of course,  $\langle \mathcal{R} \rangle = \langle v_1(t)v_2(t) \rangle$ , as far as  $v_1(t)$  and  $v_2(t)$  are jointly stationary random processes, and, in view of the ergodicity,  $\mathcal{R}$  tends to  $\langle v_1(t)v_2(t) \rangle$  as the integration time  $T$  increases to the infinity:

$$\mathcal{R} \rightarrow \langle \mathcal{R} \rangle = \langle v_1(t)v_2(t) \rangle, \quad \text{as } T \rightarrow \infty. \quad (88)$$

Therefore, assuming that the integration time is sufficiently long, we can approximate the output as

$$\mathcal{R} \cong \langle v_1(t)v_2(t) \rangle = R_{v_1v_2}(0), \quad (89)$$

where  $R_{v_1v_2}(0)$  is the cross-correlation of the two jointly stationary random processes  $v_1(t)$  and  $v_2(t)$ :

$$R_{v_1v_2}(\tau) = \langle v_1(t)v_2(t - \tau) \rangle, \quad (90)$$

at the time difference  $\tau = 0$ .

Since  $v_1(t)$  and  $v_2(t)$  satisfy equation (86), we have

$$\begin{aligned} R_{v_1v_2}(\tau) &= \int_{-\infty}^{\infty} \int_{-\infty}^{\infty} \langle E(t - \tau_g - \alpha)E(t - \tau - \beta) \rangle q(\alpha) q(\beta) d\alpha d\beta \\ &= \int_{-\infty}^{\infty} \int_{-\infty}^{\infty} R_{EE}(\tau - \tau_g - \alpha + \beta) q(\alpha) q(\beta) d\alpha d\beta, \end{aligned} \quad (91)$$

where  $R_{EE}(\tau)$  is the autocorrelation of  $E(t)$ :

$$R_{EE}(\tau) = \langle E(t)E(t - \tau) \rangle. \quad (92)$$

Let us introduce the cross-power spectrum  $S_{v_1v_2}(\omega)$  of the received voltages  $v_1(t)$  and  $v_2(t)$ , which forms a Fourier transform pair with the cross-correlation  $R_{v_1v_2}(\tau)$ , i.e.,  $R_{v_1v_2}(\tau) \Leftrightarrow S_{v_1v_2}(\omega)$ , where  $\omega$  is the angular frequency. Using the Fourier transformation equation (55), and the shift theorem given in equation (68), we have

$$S_{v_1v_2}(\omega) = \int_{-\infty}^{\infty} R_{v_1v_2}(\tau) e^{-i\omega\tau} d\tau$$

$$\begin{aligned}
&= \int_{-\infty}^{\infty} \left[ \int_{-\infty}^{\infty} \int_{-\infty}^{\infty} R_{EE}(\tau - \tau_g - \alpha + \beta) q(\alpha) q(\beta) d\alpha d\beta \right] e^{-i\omega\tau} d\tau \\
&= \left\{ \int_{-\infty}^{\infty} \left[ \int_{-\infty}^{\infty} \int_{-\infty}^{\infty} R_{EE}(\tau' - \alpha + \beta) q(\alpha) q(\beta) d\alpha d\beta \right] e^{-i\omega\tau'} d\tau' \right\} e^{-i\omega\tau_g} \\
&= \left[ \int_{-\infty}^{\infty} R_{EE}(\tau') * q(\tau') * q(-\tau') e^{-i\omega\tau'} d\tau' \right] e^{-i\omega\tau_g}.
\end{aligned}$$

Furthermore, let us introduce the power spectrum  $S_{EE}(\omega)$  of the incident electric field intensity  $E(t)$ ,  $S_{EE}(\omega) \Leftrightarrow R_{EE}(\tau)$ :

$$S_{EE}(\omega) = \int_{-\infty}^{\infty} R_{EE}(\tau) e^{-i\omega\tau} d\tau, \quad (93)$$

and the system function  $\mathcal{Q}(\omega)$  of the impulse response  $q(t)$ ,  $\mathcal{Q}(\omega) \Leftrightarrow q(t)$ :

$$\mathcal{Q}(\omega) = \int_{-\infty}^{\infty} q(t) e^{-i\omega t} dt. \quad (94)$$

Note that  $S_{EE}(\omega)$  is a real and even function of  $\omega$ , since  $E(t)$  is a real process, and also  $\mathcal{Q}^*(\omega) = \mathcal{Q}(-\omega)$  for the real impulse response  $q(t)$ .

Then, in view of the convolution theorem in the Fourier transformation (see equations (66) and (72)), we obtain

$$S_{v_1 v_2}(\omega) = S_{EE}(\omega) \mathcal{Q}(\omega) \mathcal{Q}(-\omega) e^{-i\omega\tau_g} = S_{EE}(\omega) |\mathcal{Q}(\omega)|^2 e^{-i\omega\tau_g}. \quad (95)$$

Applying the inverse Fourier transformation to this equation, we obtain a formula for the cross-correlation  $R_{v_1 v_2}(\tau)$ :

$$R_{v_1 v_2}(\tau) = \frac{1}{2\pi} \int_{-\infty}^{\infty} S_{v_1 v_2}(\omega) e^{i\omega\tau} d\omega = \frac{1}{2\pi} \int_{-\infty}^{\infty} S_{EE}(\omega) |\mathcal{Q}(\omega)|^2 e^{i\omega(\tau - \tau_g)} d\omega. \quad (96)$$

Taking  $\tau = 0$  in this equation, we obtain

$$\mathcal{R} \cong R_{v_1 v_2}(0) = \frac{1}{2\pi} \int_{-\infty}^{\infty} S_{EE}(\omega) |\mathcal{Q}(\omega)|^2 e^{-i\omega\tau_g} d\omega. \quad (97)$$

This is an equation which gives a relation between the expectation of the correlator output  $\langle \mathcal{R} \rangle = R_{v_1 v_2}(0)$  of our simple interferometer, and the spectrum of the radio wave coming from an astronomical source  $S_{EE}(\omega)$ , filtered by the frequency response  $|\mathcal{Q}(\omega)|^2$  of the antenna-receiver systems.

As the simplest case of the frequency response  $|\mathcal{Q}(\omega)|^2$ , let us assume a rectangular filter:

$$|\mathcal{Q}(\omega)|^2 = \begin{cases} G & \text{if } \omega_0 - \frac{\Delta\omega}{2} \leq \omega \leq \omega_0 + \frac{\Delta\omega}{2}, \\ 0 & \text{otherwise,} \end{cases} \quad (98)$$

where  $\omega_0$  is the band-center angular frequency,  $\Delta\omega$  is the bandwidth in angular frequency, and  $G$  is a constant coefficient, as shown in Figure 15. On

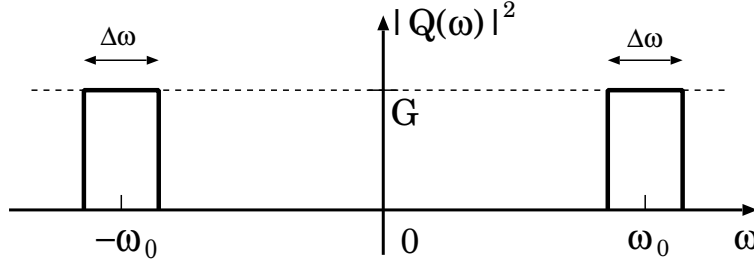


Figure 15: Rectangular frequency response of the antenna-receiver system.

the other hand, we can assume, for a continuum spectrum source, that the power spectrum of the radio wave  $S_{EE}(\omega)$  is flat, or “white-noise”, in the filter passband:

$$S_{EE}(\omega) = S(\omega_0) = S(-\omega_0) = \text{const.} \quad (99)$$

In such a case, from equations (97), (98) and (99), the expectation of the correlator output  $\mathcal{R}$  is expressed as:

$$\begin{aligned} \langle \mathcal{R} \rangle &= \frac{1}{\pi} \Re \left[ \int_0^\infty S_{EE}(\omega) |\mathcal{Q}(\omega)|^2 e^{-i\omega\tau_g} d\omega \right] \\ &= \frac{S(\omega_0) G}{\pi} \Re \left[ \int_{\omega_0 - \frac{\Delta\omega}{2}}^{\omega_0 + \frac{\Delta\omega}{2}} e^{-i\omega\tau_g} d\omega \right] \\ &= \frac{S(\omega_0) G}{\pi} \Re \left[ e^{-i\omega_0\tau_g} \int_{-\frac{\Delta\omega}{2}}^{\frac{\Delta\omega}{2}} e^{-i\omega'\tau_g} d\omega' \right] \\ &= 2 B S(\omega_0) G \frac{\sin(\pi B \tau_g)}{\pi B \tau_g} \cos(\omega_0 \tau_g), \end{aligned} \quad (100)$$

where  $\Re$  stands for the real part of the complex quantity,  $B = \Delta\omega/(2\pi)$  is the frequency bandwidth, and  $\omega'$  is chosen to satisfy  $\omega = \omega_0 + \omega'$ . In deriving the above equation, we used a well-known integration formula:

$$\frac{1}{2} \int_{-x}^x e^{-ix'} dx' = \sin x.$$

A function of a form  $\frac{\sin x}{x}$  is known as “sinc function”.

### 1.3.4 Fringe Pattern Enclosed by Bandwidth Pattern

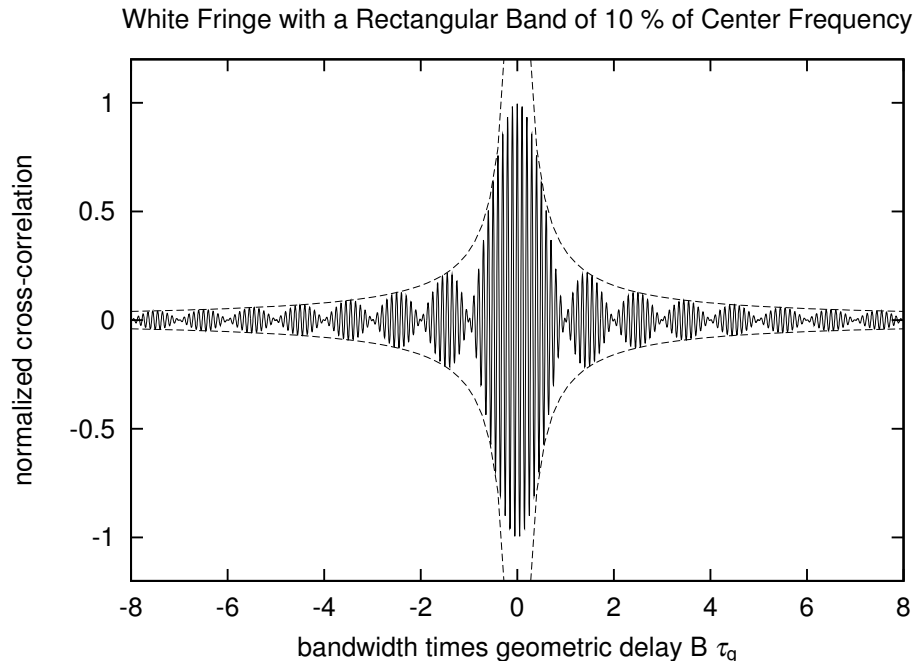


Figure 16: A normalized white fringe of a noise signal limited within a rectangular frequency band of width  $B$ , equal to 10 % of central frequency (solid line). Horizontal axis shows  $B\tau_g$ , i.e. the geometric delay multiplied by the bandwidth. Also shown by dashed lines is the behaviour of the  $1/(\pi B\tau_g)$  term which quickly suppresses the fringe amplitude with increasing  $\tau_g$ .

Figure (16) shows the expectation of the correlator output  $\langle \mathcal{R} \rangle$  of a white noise signal from the radio source, which is limited within a rectangular passband of width  $B$ , according to equation (100). The vertical axis shows

amplitude normalized by  $2BS(\omega_0)G$ , and the horizontal axis shows the geometric delay  $\tau_g$  normalized by  $1/B$ , i.e.,  $B\tau_g$ . In this figure, the bandwidth  $B$  is chosen to be equal to 10 % of the central frequency ( $B = 0.1\omega_0/2\pi$ ). We again have a fringe pattern  $\cos(\omega_0\tau_g)$  enclosed by an envelope, which, in this case, has a sinc function form, and takes the maximum value at  $\tau_g = 0$ . The enclosed fringe pattern, obtained from the band-limited white noise spectrum, is called the “white fringe”.

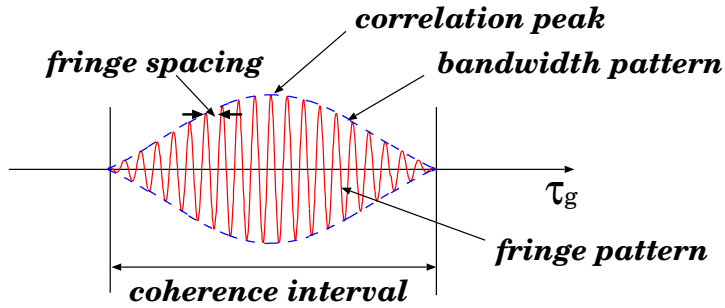


Figure 17: Technical terms describing the white fringe.

Figure 17 shows basic characteristics of the white fringe. The envelope, enclosing the rapidly oscillating fringe pattern, is called “bandwidth pattern”. A particular case of the rectangular band gives the sinc function pattern, as we saw already. Other band shapes give different shapes of the bandwidth pattern. But in any case, we always have the common feature, that the interferometric fringes of finite amplitude are obtained within a limited range of the geometric delay, enclosed by a bandwidth pattern, as far as the noise signal is band-limited.

Such a limited range of the geometric delay  $\Delta\tau_B$ , where the fringe pattern has finite amplitude, is called “coherence interval”, and is roughly represented by an equation  $\Delta\tau_B = 2/B$ , where  $B$ , in a general band-shape case, is a quantity which effectively characterizes a bandwidth.

The fringe spacing  $\Delta\tau_F$ , in terms of the geometric delay, is determined by a condition  $\omega_0\Delta\tau_F = 2\pi$ , therefore,  $\Delta\tau_F \simeq 1/\nu_0$ .

The peak of the bandwidth pattern, which gives a precise observable for the geodetic VLBI, is called “correlation peak”. Of course, the peak is the sharper, the wider the bandwidth  $B$ , and therefore the narrower the coherence interval is (see Figure 18).

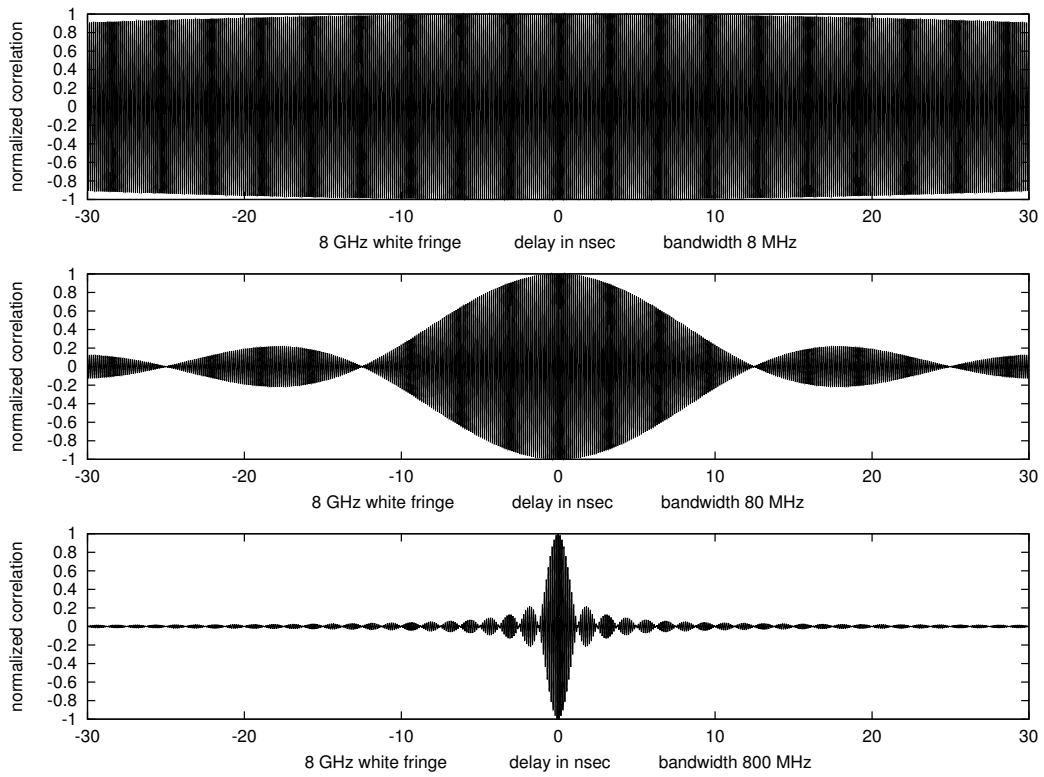


Figure 18: White fringes with center frequency 8 GHz and various bandwidths:  $B = 8$  MHz (top),  $B = 80$  MHz (middle), and  $B = 800$  MHz (bottom). Horizontal axes show geometric delays covering a range from  $-30$  to  $30$  nsec.

### 1.3.5 Amplitude and Phase Spectra of the Correlated Signals

Equation (95) shows, that the cross-power spectrum  $S_{v_1 v_2}(\omega)$  of the voltage signals  $v_1(t)$  and  $v_2(t)$ , received by two antennas, is described through the power spectrum  $S_{EE}(\omega)$  of the radio wave coming from a source, and the frequency response, assumed rectangular here, of the antenna-receiver system  $|Q(\omega)|^2$ , as:

$$S_{v_1 v_2}(\omega) = S_{EE}(\omega) |Q(\omega)|^2 e^{-i\omega\tau_g}.$$

Therefore, if we assume that the real, and even, power spectrum  $S_{EE}(\omega)$

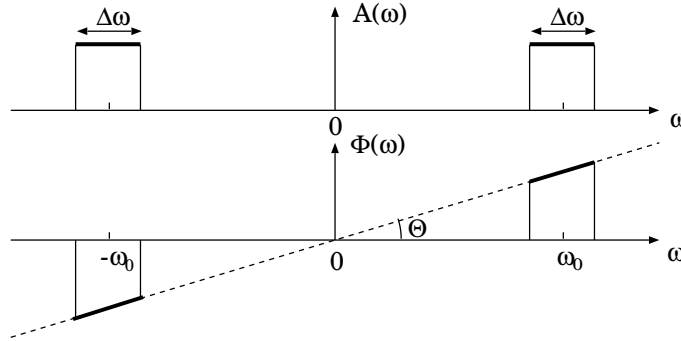


Figure 19: Amplitude (top) and phase (bottom) spectra of the cross-power spectrum.

is nearly constant in the receiving frequency band, the amplitude  $A(\omega)$  and phase  $\Phi(\omega)$  of the cross-power spectrum, which we define as

$$S_{v_1 v_2}(\omega) = A(\omega) e^{-i\Phi(\omega)}, \quad (101)$$

are expressed as:

$$A(\omega) = S_{EE}(\omega) |Q(\omega)|^2 \cong \text{const}, \quad (102)$$

$$\Phi(\omega) = \omega\tau_g, \quad (103)$$

within the passband (see Figure 19). Note, that the phase spectrum is expressed by a straight line, crossing the origin and having an inclination  $\tan \Theta$ , which is equal to the geometric delay  $\tau_g$ , i.e.,  $\tan \Theta = \tau_g$ , in the present simple interferometer model. This is a general feature of the phase spectra of the continuum spectrum sources observed by interferometers.

### 1.3.6 Coherence Interval in the Sky

The coherence interval  $\Delta\tau_B = 2/B$ , in terms of the geometric delay, corresponds to a certain angular extent  $\Delta\theta_B$  in the sky (Figure 20). Following the assumption we made earlier, we consider only a region of the sky which is close to the direction perpendicular to the baseline of an interferometer with length  $D$ .

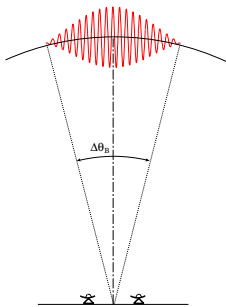


Figure 20: Coherence interval in the sky.

For a source in the sky, which is separated from a plane perpendicular to the baseline by an angle  $\theta$ , the geometric delay  $\tau_g$  is equal to

$$\tau_g = \frac{D \sin \theta}{c}, \quad \text{and, hence,} \quad \theta = \arcsin \left( \frac{c \tau_g}{D} \right), \quad (104)$$

where  $c$  is the light velocity. Therefore, the angular extent  $\Delta\theta_B$  is

$$\Delta\theta_B = 2 \arcsin \left( \frac{c \Delta\tau_B}{2D} \right) \simeq \frac{c \Delta\tau_B}{D} = \frac{2c}{DB}. \quad (105)$$

The coherence intervals for several values of  $D$  and  $B$  are listed in Table 1. It is evident from this table that the coherence interval in the sky is fairly narrow for modern interferometers, especially for VLBI. Therefore, the passive observational mode, which would just “wait for” the passage of a source through the narrow coherence interval with  $\tau_g \approx 0$ , is extremely ineffective and unrealistic, except in the “classical” systems with  $\sim 100$  m, or shorter, baselines and  $\sim$  a few MHz, or narrower, bandwidths. Consequently, modern radio interferometers are usually equipped with a special mechanism, which compensates the delay, by time-shifting one of two received signals, so that the signals corresponding to the same wave front are fed to the correlation processing simultaneously, as we will see later.

bandwidth $B$		200 kHz	2 MHz	200 MHz	2 GHz
$\Delta\tau_B$		10 $\mu\text{sec}$	1 $\mu\text{sec}$	10 nsec	1 nsec
$\Delta\theta_B$	$D = 100 \text{ m}$	$> 180^\circ$	$> 180^\circ$	1. $^\circ$ 7	0. $^\circ$ 17
	$D = 10 \text{ km}$	17 $^\circ$	1. $^\circ$ 7	1.'0	6.''2
	$D = 1000 \text{ km}$	0. $^\circ$ 17	1.'0	0.''62	0.''062

Table 1: Coherence interval values for various baseline length  $D$  and bandwidth  $B$ .

In VLBI, it is very important to know accurate positions of the radio sources and accurate coordinates of the baseline vectors, for successful prediction and compensation of the delay, which allow us to detect the fringe within the quite narrow coherence interval.

### 1.3.7 Fringe Spacing in the Sky

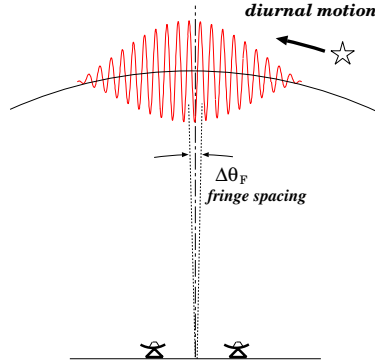


Figure 21: Fringe spacing in the sky.

Since the fringe spacing is  $\Delta\tau_F = 1/\nu_0$ , in terms of the geometric delay, equation (104) gives the fringe spacing in the sky  $\Delta\theta_F$ , in the direction nearly perpendicular to the baseline, as:

$$\Delta\theta_F = \frac{\lambda_0}{D}, \quad (106)$$

where  $\lambda_0 = c/\nu_0$  is the wave length at the central frequency  $\nu_0$  of the receiving band (see Figure 21 and Table 2).

central frequency $\nu_0$	100 MHz	10 GHz	100 GHz
wave length $\lambda_0$	3 m	3 cm	3 mm
D = 100 m	1. $^{\circ}$ 7	1.'0	6.''2
D = 10 km	1.'0	0.''62	0.''062
D = 1000 km	0.''62	0.''0062	0.''00062

Table 2: Fringe spacing values for various baseline length  $D$  and central frequency  $\nu_0$ .

The angular resolution of an interferometer is usually expressed by equation (106), since the resolution is essentially determined by the fringe spacing.

Since every radio source diurnally moves across the dense fringe pattern in the sky with the very short fringe spacing, the phase of the cosine term  $\omega_0\tau_g$  in equation (100) changes very rapidly. Therefore, the correlator output of the signals of our simple interferometer must oscillate also very rapidly. This would make mostly impossible to integrate the multiplier output for a duration of time, which is long enough to detect the white fringe with a sufficiently high signal-to-noise ratio, since any simple time averaging (integration) of an oscillating signal results in almost zero signal only (Figure 22). Therefore, modern radio interferometers are usually equipped with a special mechanism to compensate (or stop) the rapid phase change, as we will see later.

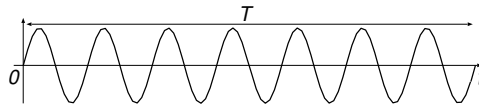


Figure 22: What will come out, if we integrate (time average) this?

## 2 A Realistic Radio Interferometer

The simple interferometer, which we discussed in the previous section, was helpful for understanding one of the most important concepts for radio inter-

ferometry, the white fringe. Nevertheless, the simple model is far from real modern radio interferometers in following aspects.

First, radio sources are not mere points. They usually show structures, or intensity distributions, in the sky. One of the main purposes of the VLBI, or radio interferometry in general, is to obtain images of the radio source structures. But if the source is not point-like, the delayed voltage model in equation (86), which was described through a single geometric delay of a point source, must be no longer valid. Moreover, if the source structures are extended, we have to take into account the beam patterns of element antennas, as well.

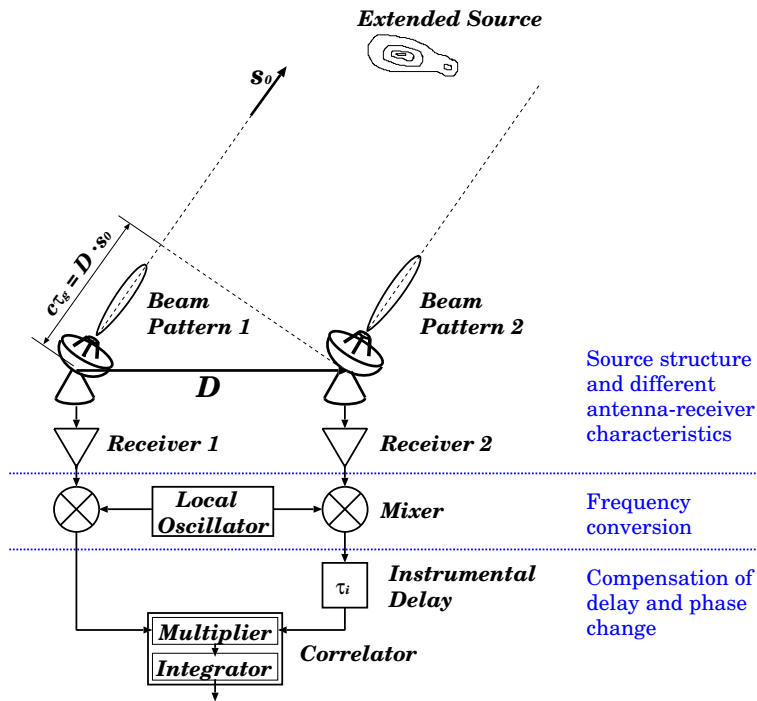


Figure 23: A realistic interferometer.

Second, the antennas and receiving systems in a radio interferometer are not identical, in general. Therefore, the beam patterns and the frequency responses of the antenna-receiver systems may differ from each other, unlike in the simple interferometer model.

Third, receiving systems in modern interferometers are usually based on the superheterodyne design, and correlation processings are performed for IF (intermediate frequency) signals after the frequency conversion, but not for RF signals, as assumed in the simple interferometer model.

Finally, we have to introduce the special mechanisms in order to compensate the geometric delay and the rapid phase change in the correlator output, as we noted in the last two paragraphs of the previous section. This should be done so that we can always observe a radio source whenever it is above the horizon, but not just within a very short duration of time, while the source happens to pass the very narrow coherence interval.

However, we still neglect, for a while, atmospheric and instrumental delays, other than the geometric delay. Also, we ignore, as before, any contribution of the system noise, in order to concentrate our attention to the characteristics of the correlated radio source signals only.

Figure 23 illustrates a “more realistic” 2–element interferometer. In the following subsections, we will examine effects of the source structure and different antenna–receiver characteristics, the frequency conversion, and the compensation of the delay and the phase change, in turn.

## 2.1 Source Structure, Visibility and Intensity

### 2.1.1 Source Coherence Function

How the correlator output of an interferometer is related to the intensity (or brightness) distribution of a radio source in the sky?

In order to answer to this question, we must consider how the electromagnetic field from a source, which is received and converted to the voltage signal by each antenna of the interferometer, is related to the intensity distribution of the source. For this purpose, we first address ourselves to a problem regarding properties of radio waves from an extended radio source, namely, whether radio waves coming from different points of a radio source are mutually correlated, or not.

Let us choose a certain direction in the source (for example, the direction of the maximum intensity), which is denoted by a unit vector  $\mathbf{s}_0$ , as a reference direction. Then a unit vector  $\mathbf{s}$ , pointing towards an arbitrary direction in the source, may be expressed as  $\mathbf{s} = \mathbf{s}_0 + \boldsymbol{\sigma}$ , and we can use the “offset vector from the reference direction”  $\boldsymbol{\sigma} \equiv \mathbf{s} - \mathbf{s}_0$ , as a vector, which is almost confined in the celestial sphere and indicates the direction  $\mathbf{s}$ . See Figure 24 for the geometry.

As a quantity representing the electromagnetic wave from the source, we again choose a single polarization component of the electric field intensity  $E(t)$ , to be received by the antennas. Since the source is now extended, we denote a component of the electric field intensity, which comes from a unit solid angle around a direction  $\boldsymbol{\sigma}$ , as  $e(\boldsymbol{\sigma}, t)$ . Then the incident electric field

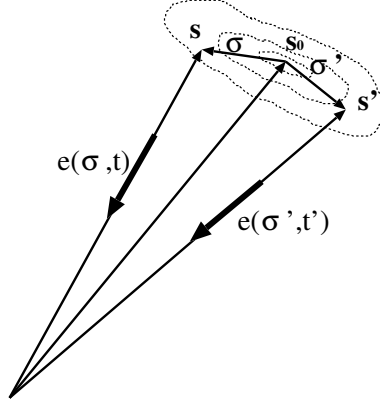


Figure 24: Radio waves coming from different directions in a radio source.

from the whole source  $E(t)$  is expressed through  $e(\boldsymbol{\sigma}, t)$  as

$$E(t) = \int_{\text{source}} e(\boldsymbol{\sigma}, t) d\Omega, \quad (107)$$

where  $d\Omega$  is an infinitesimal solid angle element. Now, let us consider a cross-correlation of electric field components  $e(\boldsymbol{\sigma}, t)$  and  $e(\boldsymbol{\sigma}', t')$ , coming from different directions  $\boldsymbol{\sigma}$  and  $\boldsymbol{\sigma}'$ , and taken at different times  $t$  and  $t'$ :

$$\langle e(\boldsymbol{\sigma}, t) e(\boldsymbol{\sigma}', t') \rangle,$$

(see Figure 24).

Assuming again that  $e(\boldsymbol{\sigma}, t)$  and  $e(\boldsymbol{\sigma}', t')$  are jointly stationary random processes, we express the cross-correlation as a function of time difference  $\tau = t - t'$ :

$$\gamma(\boldsymbol{\sigma}, \boldsymbol{\sigma}', \tau) = \langle e(\boldsymbol{\sigma}, t) e(\boldsymbol{\sigma}', t') \rangle. \quad (108)$$

This function  $\gamma(\boldsymbol{\sigma}, \boldsymbol{\sigma}', \tau)$  is called “source coherence function”.

Using this source coherence function, we define a cross-correlation coefficient, which is called “normalized source coherence function”:

$$\gamma_N(\boldsymbol{\sigma}, \boldsymbol{\sigma}', \tau) = \frac{\gamma(\boldsymbol{\sigma}, \boldsymbol{\sigma}', \tau)}{\sqrt{\gamma(\boldsymbol{\sigma}, \boldsymbol{\sigma}, 0)\gamma(\boldsymbol{\sigma}', \boldsymbol{\sigma}', 0)}}, \quad (109)$$

(here, we assume that the expectation of the electric field  $\langle e(\boldsymbol{\sigma}, t) \rangle = 0$ , and, therefore, the cross-correlation is equal to the cross-covariance). According to the general property of the cross-correlation coefficient, the normalized source coherence function always satisfies

$$0 \leq |\gamma_N(\boldsymbol{\sigma}, \boldsymbol{\sigma}', \tau)| \leq 1.$$

Now we use following definitions.

1. Radio waves from different directions  $\boldsymbol{\sigma}$  and  $\boldsymbol{\sigma}'$  are called “completely coherent” if  $|\gamma_N(\boldsymbol{\sigma}, \boldsymbol{\sigma}', \tau)| = 1$  for any  $\tau$ , and “completely incoherent” if  $|\gamma_N(\boldsymbol{\sigma}, \boldsymbol{\sigma}', \tau)| = 0$  for any  $\tau$ .
2. A radio source is called “coherent” if radio waves from any different directions  $\boldsymbol{\sigma}$  and  $\boldsymbol{\sigma}'$  in the source are completely coherent, and “incoherent” if the waves are completely incoherent. In all other cases, the radio source is called “partially coherent”.

If someone puts many transmission antennas in a town, and broadcasts a TV program, then any “poor-reception-level” problem would simply disappear. Instead, however, we would suffer from a serious “ghost” problem, since TV signals from different antennas are mutually coherent. The “ghost” images would drastically change when we slightly shift or rotate our TV reception antenna to an extent, comparable with the wavelength of the TV signal. Therefore, it would even become difficult to know directions of transmission antennas in the easy way, by just rotating the reception antenna and watching the screen. But if the TV broadcasting is turned off, and only incoherent (independent) noises are emitted from transmission antennas, it would get much easier to know their directions.

Fortunately, most of actual astronomical radio sources are known to be incoherent, and, therefore, can be imaged relatively simply. This is because radio waves emitted from the source regions are just mutually independent noises generated by random microscopic processes occurring there. Therefore, in following discussions, we assume that radio sources are incoherent.

Then, the source coherence function must be expressed as

$$\gamma(\boldsymbol{\sigma}, \boldsymbol{\sigma}', \tau) = \gamma(\boldsymbol{\sigma}, \tau)\delta(\boldsymbol{\sigma} - \boldsymbol{\sigma}'), \quad (110)$$

since radio waves from directions  $\boldsymbol{\sigma}$  and  $\boldsymbol{\sigma}'$  are correlated only when  $\boldsymbol{\sigma} = \boldsymbol{\sigma}'$ . The function  $\gamma(\boldsymbol{\sigma}, \tau)$ , defined by equation (110), is called “self-coherence function”.

### 2.1.2 Power of Electric Field Incident from a Certain Direction

The autocorrelation of the electric field  $E(t)$  is expressed through the self-coherence function as:

$$\begin{aligned} \langle E(t)E(t') \rangle &= \int \int_{source} \langle e(\boldsymbol{\sigma}, t)e(\boldsymbol{\sigma}', t') \rangle d\Omega d\Omega' \\ &= \int \int_{source} \gamma(\boldsymbol{\sigma}, \tau)\delta(\boldsymbol{\sigma} - \boldsymbol{\sigma}') d\Omega d\Omega' = \int_{source} \gamma(\boldsymbol{\sigma}, \tau) d\Omega. \end{aligned} \quad (111)$$

Therefore, we obtain, for a mean square value of the electric field  $E(t)$ ,

$$\langle E(t)^2 \rangle = \int_{source} \gamma(\boldsymbol{\sigma}, 0) d\Omega, \quad (112)$$

which implies that  $\gamma(\boldsymbol{\sigma}, 0)$  is a “density per solid angle” of the mean square electric field in the direction of  $\boldsymbol{\sigma}$ .

Consequently, if we consider a total electric field vector  $\mathbf{E}(t)$ , which comes from a small solid angle element  $\Delta\Omega$  towards a direction  $\boldsymbol{\sigma}$ , and includes both of the two independent polarization components, then its mean square value (or power) is related to the self-coherence function at  $\tau = 0$  as:

$$\frac{1}{2} \langle |\mathbf{E}(\boldsymbol{\sigma})|^2 \rangle = \gamma(\boldsymbol{\sigma}, 0) \Delta\Omega, \quad (113)$$

where the coefficient  $1/2$  corresponds to the fact that  $\gamma(\boldsymbol{\sigma}, 0)$  includes only a single polarization component of the electric field.

### 2.1.3 Poynting Flux

Now we proceed to the relation between the incident electric field and the source intensity (or brightness) distribution. First, we consider a quantity, characterizing the incident electromagnetic wave, which we call “Poynting flux through a cross section”.

Let us consider the Poynting vector  $\mathbf{S}(\boldsymbol{\sigma})$  of an electromagnetic wave, which comes from the same small solid angle element  $\Delta\Omega$  towards the direction  $\boldsymbol{\sigma}$ , as in equation (113). Let  $\Delta\Omega$  be small enough that the wave is well approximated by a superposition of monochromatic plane waves propagating along the same direction, with individual frequencies contained in a finite bandwidth of the incident wave.

As we saw in Chapter 2, the Poynting vector  $\mathbf{S}_m(\boldsymbol{\sigma})$  of a monochromatic plane wave is given, in terms of the corresponding electric field intensity  $\mathbf{E}_m(\boldsymbol{\sigma})$ , by an equation:

$$\mathbf{S}_m(\boldsymbol{\sigma}) = \frac{1}{Z} \mathbf{n} |\mathbf{E}_m(\boldsymbol{\sigma})|^2, \quad (114)$$

where  $Z$  is the intrinsic impedance of the medium, and  $\mathbf{n} = -\mathbf{s} = -(\mathbf{s}_0 + \boldsymbol{\sigma})$  is a unit vector along a direction of the wave propagation.

The term  $|\mathbf{E}_m(\boldsymbol{\sigma})|^2$ , in equation (114), corresponds to a power of the electric field, contained within an infinitesimally narrow frequency band of a monochromatic plane wave. Such a power is equal to the power spectrum at the frequency of the band, multiplied by the bandwidth, as we discussed

in subsection 1.2.8. On the other hand, the power  $|\mathbf{E}(\boldsymbol{\sigma})|^2$ , contained in a finite bandwidth, is simply equal to the integral of the power spectrum over the bandwidth. Hence, we obtain the power  $|\mathbf{E}(\boldsymbol{\sigma})|^2$ , by just summing up all monochromatic plane wave components  $|\mathbf{E}_m(\boldsymbol{\sigma})|^2$  over the bandwidth:

$$|\mathbf{E}(\boldsymbol{\sigma})|^2 = \sum |\mathbf{E}_m(\boldsymbol{\sigma})|^2.$$

Meanwhile, the Poynting vector  $\mathbf{S}(\boldsymbol{\sigma})$ , with the finite bandwidth, is a vector sum of all monochromatic plane wave components  $\mathbf{S}_m(\boldsymbol{\sigma})$ :

$$\mathbf{S}(\boldsymbol{\sigma}) = \sum \mathbf{S}_m(\boldsymbol{\sigma}).$$

Therefore, an equation, with the same form as the one in the monochromatic plane wave case, given in equation (114), holds also for the Poynting vector  $\mathbf{S}(\boldsymbol{\sigma})$  and the power of the electric field  $|\mathbf{E}(\boldsymbol{\sigma})|^2$ , having the finite bandwidth:

$$\mathbf{S}(\boldsymbol{\sigma}) = \frac{1}{Z} \mathbf{n} |\mathbf{E}(\boldsymbol{\sigma})|^2. \quad (115)$$

Let us now consider ‘‘Poynting flux through a cross section’’, or simply ‘‘Poynting flux’’, which we define as equal to the energy of the electromagnetic wave passing through a certain cross section of unit area, per unit duration

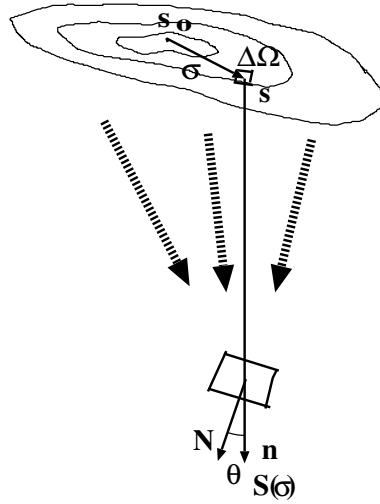


Figure 25: Poynting flux through a cross section.

of time. If we denote a unit vector normal to the cross section as  $\mathbf{N}$ , the Poynting flux of the wave coming from the direction  $\boldsymbol{\sigma}$  is given by a projection of the Poynting vector on the direction  $\mathbf{N}$ :

$$\mathbf{S}(\boldsymbol{\sigma}) \cdot \mathbf{N} = \frac{1}{Z} |\mathbf{E}(\boldsymbol{\sigma})|^2 \cos \theta, \quad (116)$$

where  $\theta$  is an angle between the normal unit vector  $\mathbf{N}$  of the cross section and the direction  $\mathbf{n}$  of the wave propagation (see Figure 25).

Now we consider the Poynting flux  $S$  of the wave not only from a small solid angle towards  $\boldsymbol{\sigma}$ , but from the all source area:

$$S = \sum_n \mathbf{S}(\boldsymbol{\sigma}_n) \cdot \mathbf{N} = \frac{1}{Z} \sum_n |\mathbf{E}(\boldsymbol{\sigma}_n)|^2 \cos \theta_n, \quad (117)$$

where  $\sum_n$  means a summation of all small solid angle elements towards directions  $\boldsymbol{\sigma}_1, \boldsymbol{\sigma}_2, \dots, \boldsymbol{\sigma}_n, \dots$ , covering the whole source area, and  $\theta_n$  is an angle between the normal to the cross section  $\mathbf{N}$  and the direction of propagation  $\mathbf{n}_n = -(\mathbf{s}_0 + \boldsymbol{\sigma}_n)$ .

Combining this equation with equation (113), we obtain an equation relating a mean Poynting flux to the self-coherence function:

$$\langle S \rangle = \frac{1}{Z} \sum_n \langle |\mathbf{E}(\boldsymbol{\sigma}_n)|^2 \rangle \cos \theta_n = \frac{2}{Z} \sum_n \gamma(\boldsymbol{\sigma}_n, 0) \cos \theta_n \Delta\Omega_n, \quad (118)$$

where  $\Delta\Omega_n$  is a small solid angle element towards a direction  $\boldsymbol{\sigma}_n$ . If we replace the summation, with respect to the small solid angles, by an integration, the relation between the mean Poynting flux  $\langle S \rangle$  and the self-coherence function  $\gamma(\boldsymbol{\sigma}, \tau)$  is given by:

$$\langle S \rangle = \frac{2}{Z} \int_{source} \gamma(\boldsymbol{\sigma}, 0) \cos \theta d\Omega. \quad (119)$$

If we further introduce the Fourier transform  $\tilde{\gamma}(\boldsymbol{\sigma}, \omega)$  of the self-coherence function  $\gamma(\boldsymbol{\sigma}, \tau)$  in the angular frequency  $\omega$  space, i.e.,  $\gamma(\boldsymbol{\sigma}, \tau) \Leftrightarrow \tilde{\gamma}(\boldsymbol{\sigma}, \omega)$ :

$$\begin{aligned} \tilde{\gamma}(\boldsymbol{\sigma}, \omega) &= \int_{-\infty}^{\infty} \gamma(\boldsymbol{\sigma}, \tau) e^{-i\omega\tau} d\tau, \\ \gamma(\boldsymbol{\sigma}, \tau) &= \frac{1}{2\pi} \int_{-\infty}^{\infty} \tilde{\gamma}(\boldsymbol{\sigma}, \omega) e^{i\omega\tau} d\omega, \end{aligned} \quad (120)$$

then, we have

$$\gamma(\boldsymbol{\sigma}, 0) = \int_{-\infty}^{\infty} \tilde{\gamma}(\boldsymbol{\sigma}, \omega) d\nu,$$

where  $\nu$  is a frequency corresponding to the angular frequency  $\omega$ , i.e.,  $\nu = \omega/(2\pi)$ . Since Fourier transform of a real function is an even function of the frequency,  $\gamma(\boldsymbol{\sigma}, 0)$  is also given as:

$$\gamma(\boldsymbol{\sigma}, 0) = 2 \int_0^{\infty} \tilde{\gamma}(\boldsymbol{\sigma}, \omega) d\nu. \quad (121)$$

Therefore, the mean Poynting flux in equation (119) is now given as:

$$\langle S \rangle = \frac{4}{Z} \int_0^{\infty} \int_{source} \tilde{\gamma}(\boldsymbol{\sigma}, \omega) \cos \theta d\Omega d\nu. \quad (122)$$

#### 2.1.4 Electric Field and Radio Source Intensity — Electromagnetics and Astronomy

As we saw in Chapter 1, results of radio astronomical observations are characterized by a number of quantities, such as, “intensity”  $I_\nu$ , “spectral flux density”  $S_\nu$ , and “power flux density”  $S$ . These quantities are phenomenologically defined in astronomy. For example, the intensity is defined as “the quantity of radiation energy incoming from a certain direction in the sky, per unit solid angle, per unit time, per unit area perpendicular to this direction, and per unit frequency bandwidth with center frequency  $\nu$ ”. As we see, no electromagnetic quantity, such as electric field intensity  $\mathbf{E}$ , or voltage  $v$ , appears in such a phenomenological definition. Therefore, we must precisely define a certain relationship between the electromagnetic and radioastronomical quantities, in order to describe radioastronomical results in terms of the electromagnetic quantities, which we actually measure in our radio telescopes.

Such a relationship was defined by IEEE (Institute of Electrical and Electronics Engineers) in 1977. According to the definition, the power flux density in astronomy is equal to the time average of the Poynting vector in electromagnetics.

The power flux density  $S$  is defined in astronomy as “the quantity of radiation energy, over the whole frequency range, incoming through a cross section of unit area, per unit time”. This quantity is related to the spectral flux density  $S_\nu$ , and to the intensity  $I_\nu$  as:

$$S = \int_0^{\infty} S_\nu d\nu = \int_0^{\infty} \int_{source} I_\nu(\boldsymbol{\sigma}) \cos \theta d\Omega d\nu, \quad (123)$$

because the spectral flux density is defined as “the quantity of radiation energy incoming through a cross section of unit area, per unit frequency bandwidth, and per unit time”, and the intensity is defined as we saw above.

Since the power flux density is given with respect to a certain cross section of unit area, we interpret the “Poynting vector”, in the IEEE definition as a Poynting flux, through the cross section.

Then, the definition of IEEE (1977) requires that the mean Poynting flux  $\langle S \rangle$  must be equal to the power flux density  $S$ :

$$\langle S \rangle = S, \quad (124)$$

since, in view of the Ergodicity, the time average must be equal to the statistical mean, provided that the averaging time is sufficiently long. Therefore, from equations (122) and (123), we have

$$\int_0^{\infty} \int_{source} I_{\nu}(\boldsymbol{\sigma}) \cos \theta d\Omega d\nu = \frac{4}{Z} \int_0^{\infty} \int_{source} \tilde{\gamma}(\boldsymbol{\sigma}, \omega) \cos \theta d\Omega d\nu. \quad (125)$$

Generally speaking, equal integrals do not necessarily mean equal integrands, of course. However, in our case of the stationary random signal from an incoherent source, we can equate integrands of the both sides of equation (125). In fact, the total power of the electric field intensity is simply equal to a sum of contributions from all elements in frequency bands and spatial solid angles. To make this point more evident, let us imagine a virtual source which emits radiation only in limited frequency and spatial solid-angle ranges of the actual radio source. The average Poynting flux and the power flux density from this virtual source are equal to those of the actual source in the respective frequency and solid-angle ranges. They must be expressed through the self-coherence function and the intensity, just in the same forms as those given in equations (122) and (123), but with limited frequency and solid-angle ranges of the integrations. Since the definition of IEEE (1977) requires their equality, for this virtual source as well, equation (125) must hold for arbitrary frequency range  $\Delta\nu$  and arbitrary spatial solid-angle range  $\Delta\Omega$ , i.e.,

$$\int_{\Delta\nu} \int_{\Delta\Omega} I_{\nu}(\boldsymbol{\sigma}) \cos \theta d\Omega d\nu = \frac{4}{Z} \int_{\Delta\nu} \int_{\Delta\Omega} \tilde{\gamma}(\boldsymbol{\sigma}, \omega) \cos \theta d\Omega d\nu,$$

which implies that the integrands must be equal to each other. Therefore, we have

$$I_{\nu}(\boldsymbol{\sigma}) = \frac{4}{Z} \tilde{\gamma}(\boldsymbol{\sigma}, \omega). \quad (126)$$

This is a relation between the source intensity distribution and the spectrum of the self-coherence function, which is the density per solid angle of the power of the incident electric field, as we saw before. Thus, we succeeded to relate the source intensity distribution in astronomy to the incident electric field in electromagnetics.

### 2.1.5 Field of View of a Radio Telescope

The incident electric field is converted to the voltage in a radio telescope antenna, and this voltage is actually processed in our detecting devices (square-law detectors, or correlators). Then, how can we relate the received voltage

$v(t)$  to the source intensity distribution? Here, we must take into account that an antenna collects electric fields, coming from different directions in a radio source, weighting them according to its beam pattern, specifically the voltage reception pattern, which we saw in Chapter 2. This “field of view” effect must be properly corrected for, prior to inferring the source intensity distribution from detected signals (Figure 26).

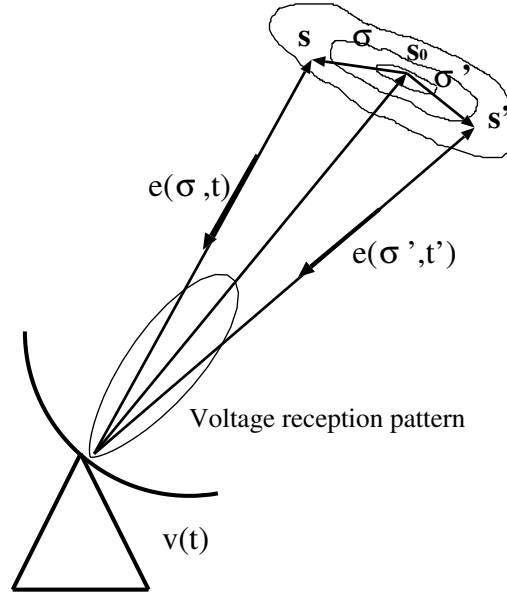


Figure 26: Voltage reception pattern.

In order to consider this problem, it is convenient to move from the time domain to the frequency domain, since, as we saw in Chapter 2, the beam pattern of an antenna is a function of frequency (the beam width is roughly proportional to  $\nu^{-1}$ ).

Let us consider Fourier transforms  $\tilde{e}(\boldsymbol{\sigma}, \omega)$  and  $\tilde{v}(\omega)$  of the single polarization component of the electric field intensity  $e(\boldsymbol{\sigma}, t)$ , coming from a unit solid angle of direction  $\boldsymbol{\sigma}$ , and the received voltage  $v(t)$ , respectively.

$$\tilde{e}(\boldsymbol{\sigma}, \omega) = \int_{-\infty}^{\infty} e(\boldsymbol{\sigma}, t) e^{-i\omega t} dt, \quad (127)$$

$$\tilde{v}(\omega) = \int_{-\infty}^{\infty} v(t) e^{-i\omega t} dt. \quad (128)$$

Since we assume that the electric field intensity  $e(\boldsymbol{\sigma}, t)$  and the received voltage  $v(t)$  are stationary random processes, these are examples of the

Fourier transforms of stationary random processes, which we discussed in subsection 1.2.9.

Without being involved in details of electromagnetics on wave reception, we just assume that the received voltage at a certain frequency is proportional to incident electric field intensity collected by the antenna beam at the same frequency. Then, we introduce the voltage reception pattern  $Q(\boldsymbol{\sigma}, \omega)$  as a function relating  $\tilde{v}(\omega)$  and  $\tilde{\mathbf{e}}(\boldsymbol{\sigma}, \omega)$  through an equation:

$$\tilde{v}(\omega) = \int_{\text{source}} \tilde{\mathbf{e}}(\boldsymbol{\sigma}, \omega) Q(\boldsymbol{\sigma}, \omega) d\Omega. \quad (129)$$

Note that the voltage reception pattern thus defined has a dimension of length (unit of voltage is V and unit of electric field intensity is  $\text{Vm}^{-1}$ ). The voltage reception pattern is, in general, a complex quantity, since the reception process might be associated with some energy dissipation.

### 2.1.6 Power Pattern of a Receiving Antenna

Let us now establish a relationship between the voltage reception pattern, as defined in equation (129), and the power pattern of a receiving antenna, which we empirically introduced in Chapter 2. Although this is a topic related to a single-dish radio telescope, following discussions will serve as useful preparations for further considerations of interferometers.

If we denote a resistance in the circuit of the receiving system as  $R$ , then averaged power  $W$  and received voltage  $v(t)$  are related to each other by an equation:

$$W = \frac{\langle v^2 \rangle}{R}. \quad (130)$$

Introducing an autocorrelation  $R_{vv}(\tau)$ :

$$R_{vv}(\tau) = \langle v(t)v(t') \rangle, \quad (131)$$

and power spectrum  $S_{vv}(\omega)$ :

$$S_{vv}(\omega) = \int_{-\infty}^{\infty} R_{vv}(\tau) e^{-i\omega\tau} d\tau, \quad (132)$$

$$R_{vv}(\tau) = \frac{1}{2\pi} \int_{-\infty}^{\infty} S_{vv}(\omega) e^{i\omega\tau} d\omega, \quad (133)$$

of the received voltage  $v(t)$ , we reexpress equation (130) as

$$W = \frac{R_{vv}(0)}{R} = \frac{2}{R} \int_0^{\infty} S_{vv}(\omega) d\nu. \quad (134)$$

Hence, the power per unit frequency bandwidth  $W_\nu$ , which satisfies

$$W = \int_0^\infty W_\nu d\nu,$$

is given by

$$W_\nu = \frac{2}{\mathbf{R}} S_{vv}(\omega). \quad (135)$$

Now, let us express the power spectrum  $S_{vv}(\omega)$  in terms of the incident electric field intensity. For this purpose, we first calculate the autocorrelation of the Fourier transform  $\tilde{v}(\omega)$  of the received voltage  $v(t)$ . In view of equation (129), we have

$$\langle \tilde{v}(\omega) \tilde{v}^*(\omega') \rangle = \int \int_{source} \langle \tilde{e}(\boldsymbol{\sigma}, \omega) \tilde{e}^*(\boldsymbol{\sigma}', \omega') \rangle Q(\boldsymbol{\sigma}, \omega) Q^*(\boldsymbol{\sigma}', \omega') d\Omega d\Omega'. \quad (136)$$

Here, the cross-correlation  $\langle \tilde{e}(\boldsymbol{\sigma}, \omega) \tilde{e}^*(\boldsymbol{\sigma}', \omega') \rangle$  of the Fourier transforms of the incident electric field intensities, must be in a form:

$$\langle \tilde{e}(\boldsymbol{\sigma}, \omega) \tilde{e}^*(\boldsymbol{\sigma}', \omega') \rangle = 2\pi \tilde{\gamma}(\boldsymbol{\sigma}, \boldsymbol{\sigma}', \omega) \delta(\omega - \omega'), \quad (137)$$

since we assume them as stationary random processes, which satisfy equation (83). In the right hand side of equation (137), we introduced a cross-power spectrum  $\tilde{\gamma}(\boldsymbol{\sigma}, \boldsymbol{\sigma}', \omega)$  of the electric field intensities, which is the Fourier transform of the source coherence function  $\gamma(\boldsymbol{\sigma}, \boldsymbol{\sigma}', \tau)$ , as defined in equation (108).

Since we assume an incoherent source, the source coherence function is expressed through the self-coherence function  $\gamma(\boldsymbol{\sigma}, \tau)$ , as given in equation (110). Therefore, the cross-power spectrum must be given as:

$$\tilde{\gamma}(\boldsymbol{\sigma}, \boldsymbol{\sigma}', \omega) = \tilde{\gamma}(\boldsymbol{\sigma}, \omega) \delta(\boldsymbol{\sigma} - \boldsymbol{\sigma}'). \quad (138)$$

Hence, equation (137) is rewritten as:

$$\langle \tilde{e}(\boldsymbol{\sigma}, \omega) \tilde{e}^*(\boldsymbol{\sigma}', \omega') \rangle = 2\pi \tilde{\gamma}(\boldsymbol{\sigma}, \omega) \delta(\boldsymbol{\sigma} - \boldsymbol{\sigma}') \delta(\omega - \omega'). \quad (139)$$

Inserting this equation to equation (136), we obtain

$$\langle \tilde{v}(\omega) \tilde{v}^*(\omega') \rangle = 2\pi \left[ \int_{source} \tilde{\gamma}(\boldsymbol{\sigma}, \omega) |Q(\boldsymbol{\sigma}, \omega)|^2 d\Omega \right] \delta(\omega - \omega'). \quad (140)$$

Now, on the other hand, the autocorrelation  $\langle \tilde{v}(\omega) \tilde{v}^*(\omega') \rangle$  must also be expressed through the power spectrum  $S_{vv}(\omega)$  of the voltage as:

$$\langle \tilde{v}(\omega) \tilde{v}^*(\omega') \rangle = 2\pi S_{vv}(\omega) \delta(\omega - \omega'), \quad (141)$$

in view of equation (82), which is a general property of Fourier transforms of the stationary random processes. Thus, from equations (140) and (141), we obtain

$$S_{vv}(\omega) = \int_{source} \tilde{\gamma}(\boldsymbol{\sigma}, \omega) |Q(\boldsymbol{\sigma}, \omega)|^2 d\Omega, \quad (142)$$

or, taking into account equations (126) and (135),

$$W_\nu = \frac{Z}{2R} \int_{source} I_\nu(\boldsymbol{\sigma}) |Q(\boldsymbol{\sigma}, \omega)|^2 d\Omega. \quad (143)$$

Equation (143) must be equivalent to the equation

$$W_\nu = \frac{1}{2} A_e \int_{source} I_\nu(\boldsymbol{\sigma}) P_n(\boldsymbol{\sigma}) d\Omega, \quad (144)$$

which we introduced in Chapter 2, in order to express the power per unit bandwidth received by an antenna with a normalized power pattern  $P_n(\boldsymbol{\sigma})$  and an effective aperture  $A_e$ . Noting again, that we can select arbitrary solid angle as the source range, we can equate integrands of equations (143) and (144), to obtain

$$|Q(\boldsymbol{\sigma}, \omega)|^2 = \frac{R}{Z} A_e P_n(\boldsymbol{\sigma}). \quad (145)$$

This is the relation between the voltage reception pattern and the normalized power pattern.

From equations (126) and (145), the power spectrum of the received voltage in equation (142) is now given as:

$$S_{vv}(\omega) = \frac{1}{4} A_e \int_{source} I_\nu(\boldsymbol{\sigma}) P_n(\boldsymbol{\sigma}) d\Omega. \quad (146)$$

### 2.1.7 New Dimensions of Voltage and Electric Field

For further discussions, it is convenient to redefine the voltage and the electric field intensity as

$$\begin{aligned} \frac{v(t)}{\sqrt{R}} &\longrightarrow v(t), \\ \frac{e(\boldsymbol{\sigma}, t)}{\sqrt{Z}} &\longrightarrow e(\boldsymbol{\sigma}, t), \end{aligned} \quad (147)$$

to eliminate constant coefficients of the resistance  $R$  and the intrinsic impedance  $Z$ , which may cause rather complicated appearances of our equations. Then, dimensions of the voltage and the electric field intensity change to

- voltage  $v$  [electric power]<sup>1/2</sup> (W<sup>1/2</sup>)
- electric field intensity  $e$  [power flux density]<sup>1/2</sup> (W<sup>1/2</sup> m<sup>-1</sup>),

and we have

$$\begin{aligned}\frac{S_{vv}(\omega)}{R} &\longrightarrow S_{vv}(\omega), \\ \frac{\tilde{\gamma}(\boldsymbol{\sigma}, \omega)}{Z} &\longrightarrow \tilde{\gamma}(\boldsymbol{\sigma}, \omega),\end{aligned}\tag{148}$$

for the power spectra of the voltage and the electric field intensity.

Let us further redefine the voltage reception pattern as

$$\sqrt{\frac{Z}{R}}Q(\boldsymbol{\sigma}, \omega) \longrightarrow Q(\boldsymbol{\sigma}, \omega).\tag{149}$$

Then, the voltage — field relation remain in the same form as equation (129):

$$\tilde{v}(\omega) = \int_{source} \tilde{e}(\boldsymbol{\sigma}, \omega)Q(\boldsymbol{\sigma}, \omega)d\Omega,$$

and we obtain simple expressions:

$$\begin{aligned}W_\nu &= 2S_{vv}(\omega), \\ I_\nu(\boldsymbol{\sigma}) &= 4\tilde{\gamma}(\boldsymbol{\sigma}, \omega), \\ A_e P_n(\boldsymbol{\sigma}) &= |Q(\boldsymbol{\sigma}, \omega)|^2,\end{aligned}\tag{150}$$

for the power per unit bandwidth, the source intensity, and the normalized power pattern.

### 2.1.8 How Does A Radio Interferometer View the Universe?

A radio interferometer can be regarded as an instrument which yields a cross-correlation or a cross-power spectrum of voltages received at antennas. We consider now the cross-correlation and cross-power spectrum of the voltages “just received”, which we will call hereafter “received voltages”. Although actual correlation processing is performed for voltages after frequency conversion and compensation of the delay and the phase change, present discussion is quite meaningful, since the final results are described through the spectrum of the received voltages, as we will see later.

Let us again consider a two-element interferometer, such as shown in Figure 27. Let a baseline vector  $\mathbf{D}$  be drawn from antenna 1 to antenna 2,

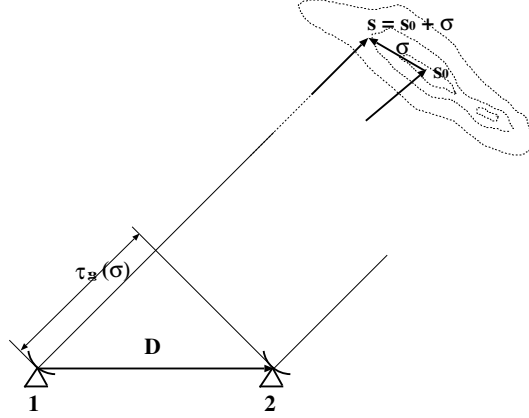


Figure 27: Geometry of a two element radio interferometer.

and let a unit vector  $\mathbf{s} = \mathbf{s}_0 + \boldsymbol{\sigma}$  point towards a certain direction within a radio source, where  $\mathbf{s}_0$  shows a reference direction of the source, as before.

Then, the geometric delay, between arrivals of the same wave front from the direction  $\mathbf{s}$  at two antennas, is given by

$$\tau_g(\boldsymbol{\sigma}) = \frac{\mathbf{D} \cdot \mathbf{s}}{c} = \tau_{g_0} + \frac{\mathbf{D} \cdot \boldsymbol{\sigma}}{c}, \quad (151)$$

where  $c$  is the light velocity,  $\tau_{g_0} \equiv \frac{\mathbf{D} \cdot \mathbf{s}_0}{c}$  is a geometric delay of the wave coming from the reference direction  $\mathbf{s}_0$ , and we use the offset vector  $\boldsymbol{\sigma} = \mathbf{s} - \mathbf{s}_0$  for denoting the direction  $\mathbf{s}$  within the source. For simplicity, we ignore here any atmospheric or instrumental delay effect, other than the geometric delay.

Now, the electric field intensities  $e_1(\boldsymbol{\sigma}, t)$  and  $e_2(\boldsymbol{\sigma}, t)$ , with a single polarization component, which arrive at two antennas at a certain time  $t$  from the same direction  $\boldsymbol{\sigma}$ , are described through a common incident field intensity  $e(\boldsymbol{\sigma}, t)$ , representing the same wave front, as

$$\begin{aligned} e_1(\boldsymbol{\sigma}, t) &= e(\boldsymbol{\sigma}, t - \tau_g(\boldsymbol{\sigma})), \\ e_2(\boldsymbol{\sigma}, t) &= e(\boldsymbol{\sigma}, t). \end{aligned} \quad (152)$$

Therefore, their Fourier transforms  $\tilde{e}_1(\boldsymbol{\sigma}, \omega)$  and  $\tilde{e}_2(\boldsymbol{\sigma}, \omega)$  are given by

$$\begin{aligned} \tilde{e}_1(\boldsymbol{\sigma}, \omega) &= \tilde{e}(\boldsymbol{\sigma}, \omega) e^{-i\omega\tau_g(\boldsymbol{\sigma})}, \\ \tilde{e}_2(\boldsymbol{\sigma}, \omega) &= \tilde{e}(\boldsymbol{\sigma}, \omega), \end{aligned} \quad (153)$$

where  $\tilde{e}(\boldsymbol{\sigma}, \omega)$  is the Fourier transform of  $e(\boldsymbol{\sigma}, t)$ . We used equation (68) of the shift theorem, in deriving the upper equation of equation (153).

These electric field intensities are converted to voltages at the two antennas:

$$\begin{aligned}\tilde{v}_1(\omega) &= \int_{source} \tilde{e}_1(\boldsymbol{\sigma}, \omega) Q_1(\boldsymbol{\sigma}, \omega) d\Omega, \\ \tilde{v}_2(\omega) &= \int_{source} \tilde{e}_2(\boldsymbol{\sigma}, \omega) Q_2(\boldsymbol{\sigma}, \omega) d\Omega,\end{aligned}\quad (154)$$

according to equation (129).

Therefore, their cross-correlation is given by

$$\langle \tilde{v}_1(\omega) \tilde{v}_2^*(\omega') \rangle = \int \int_{source} \langle \tilde{e}_1(\boldsymbol{\sigma}, \omega) \tilde{e}_2^*(\boldsymbol{\sigma}', \omega') \rangle Q_1(\boldsymbol{\sigma}, \omega) Q_2^*(\boldsymbol{\sigma}', \omega') d\Omega d\Omega'. \quad (155)$$

In view of equation (153), we can here express the electric field intensities at two antennas through the common incident electric field intensity  $\tilde{e}(\boldsymbol{\sigma}, \omega)$ :

$$\langle \tilde{e}_1(\boldsymbol{\sigma}, \omega) \tilde{e}_2^*(\boldsymbol{\sigma}', \omega') \rangle = \langle \tilde{e}(\boldsymbol{\sigma}, \omega) \tilde{e}^*(\boldsymbol{\sigma}', \omega') \rangle e^{-i\omega\tau_g(\boldsymbol{\sigma})}. \quad (156)$$

Since the electric field is regarded as a stationary random process, and the radio source is assumed to be incoherent, we have equation (139) again for  $\langle \tilde{e}(\boldsymbol{\sigma}, \omega) \tilde{e}^*(\boldsymbol{\sigma}', \omega') \rangle$ :

$$\langle \tilde{e}(\boldsymbol{\sigma}, \omega) \tilde{e}^*(\boldsymbol{\sigma}', \omega') \rangle = 2\pi \tilde{\gamma}(\boldsymbol{\sigma}, \omega) \delta(\boldsymbol{\sigma} - \boldsymbol{\sigma}') \delta(\omega - \omega').$$

Therefore, the cross-correlation of the Fourier transforms of the received voltages  $\langle \tilde{v}_1(\omega) \tilde{v}_2^*(\omega') \rangle$  in equation (155) are now given by

$$\langle \tilde{v}_1(\omega) \tilde{v}_2^*(\omega') \rangle = 2\pi \left[ \int_{source} \tilde{\gamma}(\boldsymbol{\sigma}, \omega) Q_1(\boldsymbol{\sigma}, \omega) Q_2^*(\boldsymbol{\sigma}, \omega) e^{-i\omega\tau_g(\boldsymbol{\sigma})} d\Omega \right] \delta(\omega - \omega'). \quad (157)$$

On the other hand, since the voltages received at two antennas are jointly stationary random processes (they originate from the same incident wave front), the cross-correlation of their Fourier transforms and their cross-power spectrum are related to each other by the general formula of equation (83):

$$\langle \tilde{v}_1(\omega) \tilde{v}_2^*(\omega') \rangle = 2\pi S_{v_1 v_2}(\omega) \delta(\omega - \omega'). \quad (158)$$

From equations (157) and (158), we obtain

$$S_{v_1 v_2}(\omega) = \int_{source} \tilde{\gamma}(\boldsymbol{\sigma}, \omega) Q_1(\boldsymbol{\sigma}, \omega) Q_2^*(\boldsymbol{\sigma}, \omega) e^{-i\omega\tau_g(\boldsymbol{\sigma})} d\Omega. \quad (159)$$

Now, equation (150) shows that the Fourier transform  $\tilde{\gamma}(\boldsymbol{\sigma}, \omega)$  of the self-coherence function and the source intensity  $I_\nu(\boldsymbol{\sigma})$  are related to each other as

$$\tilde{\gamma}(\boldsymbol{\sigma}, \omega) = \frac{1}{4} I_\nu(\boldsymbol{\sigma}).$$

Furthermore, equation (150) also shows that the voltage reception pattern  $Q(\boldsymbol{\sigma}, \omega)$  and the normalized power pattern  $P_n(\boldsymbol{\sigma})$  of an antenna are related to each other as

$$A_e P_n(\boldsymbol{\sigma}) = |Q(\boldsymbol{\sigma}, \omega)|^2,$$

where  $A_e$  is the effective aperture of the antenna. So, let us introduce here an analog of this equation in an interferometer case:

$$A_0 A_N(\boldsymbol{\sigma}) = Q_1(\boldsymbol{\sigma}, \omega) Q_2^*(\boldsymbol{\sigma}, \omega), \quad (160)$$

where  $A_0$  is a geometrical mean of effective apertures of two antennas:

$$A_0 = \sqrt{A_{e1} A_{e2}}, \quad (161)$$

and  $A_N(\boldsymbol{\sigma})$  is called “normalized power pattern of an interferometer”. When the two voltage reception patterns  $Q_1$  and  $Q_2$  are real quantities (i.e., there is no phase change associated with the field  $\rightarrow$  voltage conversion), or they have equal phases,  $A_N(\boldsymbol{\sigma})$  is described through the normalized power patterns  $P_{n1}$  and  $P_{n2}$  of the respective single-dish antennas as:

$$A_N(\boldsymbol{\sigma}) = \sqrt{P_{n1}(\boldsymbol{\sigma}) P_{n2}(\boldsymbol{\sigma})}. \quad (162)$$

Taking into account equations (150), (151) and (160), and denoting

$$\omega \frac{\mathbf{D} \cdot \boldsymbol{\sigma}}{c} = 2\pi \mathbf{D}_\lambda \cdot \boldsymbol{\sigma}, \quad (163)$$

where  $\mathbf{D}_\lambda = \mathbf{D}/\lambda$  is the baseline vector normalized by the wavelength  $\lambda = 2\pi c/\omega$ , we rewrite equation (159) in a form:

$$S_{v_1 v_2}(\omega) = \frac{1}{4} A_0 e^{-i\omega\tau_{g0}} \int_{source} A_N(\boldsymbol{\sigma}) I_\nu(\boldsymbol{\sigma}) e^{-i2\pi \mathbf{D}_\lambda \cdot \boldsymbol{\sigma}} d\Omega. \quad (164)$$

This equation gives a relationship between the cross-power spectrum of the received voltages and the intensity distribution of the radio source. This is an interferometer analog of the power-spectrum — intensity relationship in a single dish antenna, given in equation (146):

$$S_{vv}(\omega) = \frac{1}{4} A_e \int_{source} P_n(\boldsymbol{\sigma}) I_\nu(\boldsymbol{\sigma}) d\Omega.$$

In closing this subsection, it is worthwhile to notice an approximation made in our treatment of the geometric delay. In deriving equation (153) from equation (152), we implicitly assumed that the geometric delay  $\tau_g$  is constant in time, though, of course, the geometric delay must change in time due to the diurnal motion of the Earth. Such a quasi-static approach is good enough for our present purpose to understand basic features of radio interferometry, and we will continue to follow this approach hereafter. However, it should be noted that the quasi-static approach does not allow us to properly take account of some observable effects, such as Doppler shift in amplitude of cross-power spectrum of a radio source due to the Earth's rotation. Consequently, formulae we provide here lack these effects. More complete account of this problem will require some modification in our assumption of the stationary random nature of the received signals.

### 2.1.9 Complex Visibility

The cross-power spectrum of the received voltages  $S_{v_1 v_2}(\omega)$  is an observable quantity, which can be derived from the correlator output, as we will see in more detail, later. Equation (164) shows that the cross-power spectrum is a product of three terms: the geometric mean of the effective apertures  $A_0$ , the exponential term which depends on the geometric delay  $\tau_{g_0}$  at the reference direction  $\mathbf{s}_0$  of the observed source, and an integral over the solid angle of the source. The exponential term stands for the fringe pattern, which we discussed in section 1.3. Therefore, the integral term figures as a complex coefficient of the fringe pattern. We can derive this integral term from the observed cross-power spectrum, since  $A_0$  is almost constant and can be estimated independently, and the fringe pattern is known, as far as we know the source direction and the baseline vector with sufficient accuracies.

We call the integral, or the complex coefficient of the fringe pattern, “complex visibility”, “fringe visibility”, or just “visibility”, and denote it as  $\mathcal{V}(\omega)$ :

$$\mathcal{V}(\omega) = \oint A_N(\boldsymbol{\sigma}) I_\nu(\boldsymbol{\sigma}) e^{-i2\pi \mathbf{D}_\lambda \cdot \boldsymbol{\sigma}} d\Omega. \quad (165)$$

Here, we expanded the range of integration from the source region to the whole sky, since we expect  $I_\nu(\boldsymbol{\sigma}) = 0$  outside the source region, and radio sources far from the antenna beam direction do not contribute to the integral, simply because  $A_N(\boldsymbol{\sigma}) = 0$  for those sources.

Equation (165) shows the relationship between the complex visibility and the intensity distribution of the radio source. Amplitude  $|\mathcal{V}(\omega)|$  and phase  $\Phi_v$  of the complex visibility:

$$\mathcal{V}(\omega) = |\mathcal{V}(\omega)| e^{i\Phi_v(\omega)}, \quad (166)$$

are called “visibility amplitude” and “visibility phase”, respectively.

The complex visibility as shown in equation (165) has a dimension of the flux density ( $\text{w m}^{-2} \text{ Hz}^{-1}$ ). In fact, the complex visibility can be regarded as an analog of the effective flux density  $S_\nu$  received by a single-dish antenna:

$$S_\nu = \oint P_n(\boldsymbol{\sigma}) I_\nu(\boldsymbol{\sigma}) d\Omega, \quad (167)$$

which we introduced in Chapter 2. Thus, the visibility amplitude is also called as “correlated flux density”.

Although equations (165) and (167) show similar forms, and the similarity clearly comes from a common physical nature of the complex visibility and the effective flux density, there is a big difference between these quantities, as well. While angular resolution of a single-dish observation is determined by the normalized power pattern of an antenna  $P_n(\boldsymbol{\sigma})$  in equation (167), angular resolution of an interferometer observation is essentially determined by  $e^{-i2\pi\mathbf{D}_\lambda \cdot \boldsymbol{\sigma}}$  term in equation (165), which represents the fringe pattern of the interferometer, but not by the normalized power patterns of element antennas figuring in  $A_N(\boldsymbol{\sigma})$ . In this sense, the complex visibility could be regarded as the “intensity collected by a fringe pattern”, in contrast to the effective flux density, which is the “intensity collected by an antenna beam”.

The cross-power spectrum of the received voltages is given through the complex visibility as:

$$S_{v_1 v_2}(\omega) = \frac{1}{4} A_0 e^{-i\omega\tau_{g0}} \mathcal{V}(\omega). \quad (168)$$

This is an analog of the single-dish relation:

$$S_{vv}(\omega) = \frac{1}{2} W_\nu = \frac{1}{4} A_e S_\nu, \quad (169)$$

where  $A_e$  is the effective aperture of the antenna, and  $W_\nu$  is the received power per unit frequency, as before.

The complex visibility is an important quantity of the interferometry for inferring the structure, or “image”, of the observed source, as we will discuss later.

## 2.2 Frequency Conversion in Radio Interferometers

It has been technically impossible to cross-correlate received voltage signals at RF frequencies higher than  $\sim 1$  GHz. Therefore, in modern radio interferometers, the received RF signals have been frequency-converted to lower IF frequencies, before the correlation processing (Figure 28).

So, let us now consider how cross-power spectra  $S_{v_{I1}v_{I2}}(\omega)$  of IF signals are related to the cross-power spectra  $S_{v_1v_2}(\omega)$  of RF signals, which we have so far discussed (see, for example, equation (168)). It is interesting to examine, in particular, if the condition of stationary randomness of the RF

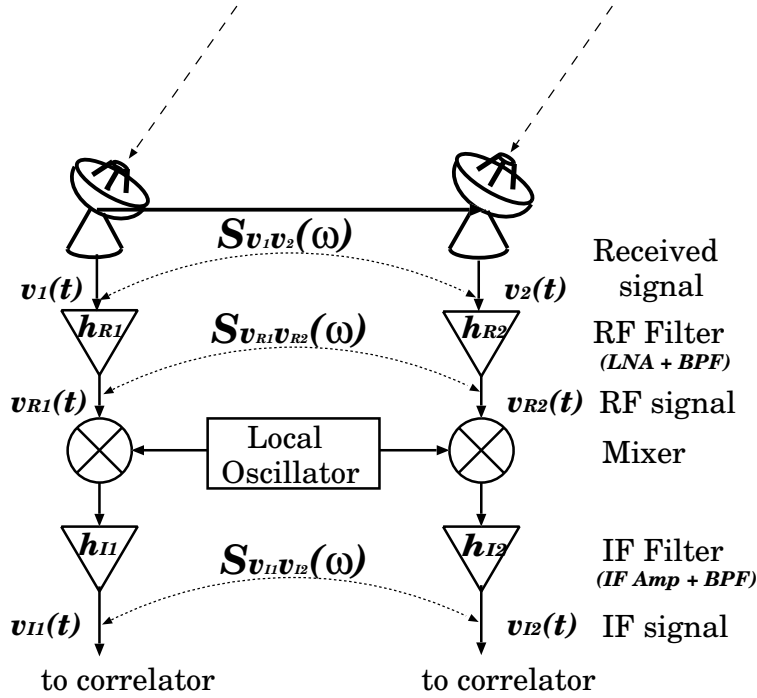


Figure 28: How the cross-power spectrum  $S_{v_{I1}v_{I2}}(\omega)$  of IF signals are related to the cross-power spectrum  $S_{v_1v_2}(\omega)$  of received signals?

signals are conserved after the frequency conversion, where the RF signals are “mixed” (multiplied and then band-pass filtered) with sinusoidal reference signals provided from LOs (local oscillators).

### 2.2.1 Response of RF Filters

The RF signals are usually amplified and band-pass filtered, before the frequency conversion, in cm- and long mm-wave observations. Therefore, we first take into account, in a general form, responses of the RF filters, which are usually composed of LNAs (low noise amplifiers) and BPFs (band-pass filters). In cases, when first stage devices in receiving systems are mixers, such as SIS mixers used in short mm-wave observations, this step must be simply omitted.

Let us consider that an RF filter is a linear system, whose input is the received voltage  $v(t)$ , output is a voltage denoted as  $v_R(t)$ , and filter response is described by a real impulse response  $h_R(t)$ .

Then, we have

$$v_R(t) = v(t) * h_R(t). \quad (170)$$

This means, in view of the convolution theorem given in equation (66), that Fourier transforms  $\tilde{v}(\omega)$  and  $\tilde{v}_R(\omega)$  of the stationary random processes  $v(t)$  and  $v_R(t)$ , respectively, and system function  $H_R(\omega)$  of the impulse response  $h_R(t)$ :

$$v(t) \Leftrightarrow \tilde{v}(\omega), \quad v_R(t) \Leftrightarrow \tilde{v}_R(\omega), \quad h_R(t) \Leftrightarrow H_R(\omega), \quad (171)$$

satisfy

$$\tilde{v}_R(\omega) = \tilde{v}(\omega) H_R(\omega). \quad (172)$$

The system function  $H_R(\omega)$  here stands for effects of the LNA gain and band-pass characteristics of the BPF.

Thus, for Fourier transforms of input voltage signals  $v_1(t)$  and  $v_2(t)$ , received at two antennas, and output voltages  $v_{R1}(t)$  and  $v_{R2}(t)$  of RF filters, with impulse responses  $h_{R1}(t)$  and  $h_{R2}(t)$ , respectively,

$$\begin{aligned} v_1(t) &\Leftrightarrow \tilde{v}_1(\omega), & v_{R1}(t) &\Leftrightarrow \tilde{v}_{R1}(\omega), & h_{R1}(t) &\Leftrightarrow H_{R1}(\omega), \\ v_2(t) &\Leftrightarrow \tilde{v}_2(\omega), & v_{R2}(t) &\Leftrightarrow \tilde{v}_{R2}(\omega), & h_{R2}(t) &\Leftrightarrow H_{R2}(\omega), \end{aligned} \quad (173)$$

we have

$$\begin{aligned} \tilde{v}_{R1}(\omega) &= \tilde{v}_1(\omega) H_{R1}(\omega), \\ \tilde{v}_{R2}(\omega) &= \tilde{v}_2(\omega) H_{R2}(\omega). \end{aligned} \quad (174)$$

Hence, cross-correlation of  $\tilde{v}_{R1}(\omega)$  and  $\tilde{v}_{R2}(\omega)$  is given by

$$\langle \tilde{v}_{R1}(\omega) \tilde{v}_{R2}^*(\omega') \rangle = \langle \tilde{v}_1(\omega) \tilde{v}_2^*(\omega') \rangle H_{R1}(\omega) H_{R2}^*(\omega'). \quad (175)$$

Now, in view of the general properties of cross-correlations of Fourier transforms of stationary random processes, given in equation (83), we have

$$\begin{aligned} \langle \tilde{v}_{R1}(\omega) \tilde{v}_{R2}^*(\omega') \rangle &= 2\pi S_{v_{R1}v_{R2}}(\omega) \delta(\omega - \omega'), \\ \langle \tilde{v}_1(\omega) \tilde{v}_2^*(\omega') \rangle &= 2\pi S_{v_1v_2}(\omega) \delta(\omega - \omega'), \end{aligned} \quad (176)$$

where  $S_{v_1v_2}(\omega)$  and  $S_{v_{R1}v_{R2}}(\omega)$  are cross-power spectra of input voltages  $v_1(t)$  and  $v_2(t)$ , and output voltages  $v_{R1}(t)$  and  $v_{R2}(t)$ , respectively, of the RF filters. Consequently, equation (175) yields a relation:

$$S_{v_{R1}v_{R2}}(\omega) = S_{v_1v_2}(\omega) H_{R1}(\omega) H_{R2}^*(\omega), \quad (177)$$

between the cross-power spectra of input and output signals of the RF filters (see Figure 28). Note that the cross-power spectrum of the received voltages  $S_{v_1v_2}(\omega)$  is related to the complex visibility of an observed source in equation (168).

### 2.2.2 Fourier Transform of IF Voltage Signal

Let us now proceed to the problem of the frequency conversion.

Actual frequency conversion is often performed through several steps, by sequentially shifting a spectral range, which contains observed data, from higher frequencies to lower frequencies, in turn. However, we assume here a simplified scheme, where single frequency conversion units down-convert RF signals to final IF signals, at once. Basically, multi-step conversion is equivalent to a single-step conversion, as long as the total frequency shifts and total band-pass characteristics are the same in both schemes. Therefore, our simplified assumption will not lower generality of following discussions.

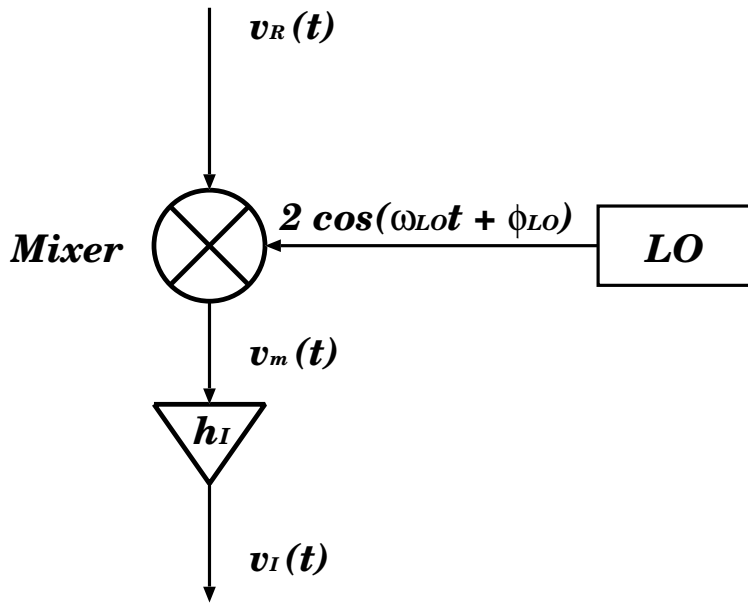


Figure 29: A simple image of a frequency converter.

Let us consider a simple frequency converter, as illustrated in Figure 29. Generally speaking, amplitude of the LO reference signal can be arbitrarily chosen. We adopted here  $2 \cos(\omega_{LO}t + \phi_{LO})$  as the reference signal, where  $\omega_{LO}$  is LO frequency and  $\phi_{LO}$  is initial phase, since the coefficient 2 results in a simple form of the IF signal after the down-conversion.

Then, an RF voltage signal  $v_R(t)$  is multiplied with the LO reference signal by a mixer, and a resulting signal  $v_m(t)$  has a form:

$$v_m(t) = v_R(t) 2 \cos(\omega_{LO}t + \phi_{LO}) = v_R(t) [e^{i(\omega_{LO}t + \phi_{LO})} + e^{-i(\omega_{LO}t + \phi_{LO})}]. \quad (178)$$

Therefore, in view of the shift theorem given in equation (68), a Fourier transform  $\tilde{v}_m(\omega)$  of  $v_m(t)$  (i.e.,  $v_m(t) \Leftrightarrow \tilde{v}_m(\omega)$ ) is given by

$$\tilde{v}_m(\omega) = \tilde{v}_R(\omega - \omega_{LO}) e^{i\phi_{LO}} + \tilde{v}_R(\omega + \omega_{LO}) e^{-i\phi_{LO}}, \quad (179)$$

where  $\tilde{v}_R(\omega)$  is again a Fourier transform of the random process  $v_R(t)$ .

An IF filter is usually composed of a BPF and an IF amplifier. So, let us denote an impulse response and a system function of such an IF filter as  $h_I(t)$  and  $H_I(\omega)$ , respectively. By definition, they form a Fourier transformation pair:

$$h_I(t) \Leftrightarrow H_I(\omega). \quad (180)$$

Then, an IF voltage signal  $v_I(t)$ , which is an output of the IF filter, is described through the impulse response  $h_I(t)$  as

$$v_I(t) = v_m(t) * h_I(t). \quad (181)$$

Therefore, in view of the convolution theorem given in equation (66), we obtain a Fourier transform  $\tilde{v}_I(\omega)$  of the IF voltage signal  $v_I(t)$  (i.e.,  $v_I(t) \Leftrightarrow \tilde{v}_I(\omega)$ ) in a form:

$$\begin{aligned} \tilde{v}_I(\omega) &= \tilde{v}_m(\omega) H_I(\omega) \\ &= [\tilde{v}_R(\omega - \omega_{LO}) e^{i\phi_{LO}} + \tilde{v}_R(\omega + \omega_{LO}) e^{-i\phi_{LO}}] H_I(\omega). \end{aligned} \quad (182)$$

### 2.2.3 Cross-Correlation of Fourier Transforms of IF Signals

Let us now consider the frequency conversion in an interferometer, as schematically shown in Figure 30.

All notations in the previous subsection are used here again, except for new suffices 1 and 2, which distinguish signals and devices in antennas 1 and 2. We assume here that reference signals with a common frequency  $\omega_{LO}$  are fed to two mixers, based on an image of a connected-element interferometer, which is equipped with a common frequency standard. In general, this assumption is not applicable to VLBI, as we will see later.

Now, the Fourier transforms of the IF voltage signals from antennas 1 and 2 are given by

$$\begin{aligned} \tilde{v}_{I1}(\omega) &= [\tilde{v}_{R1}(\omega - \omega_{LO}) e^{i\phi_{LO1}} + \tilde{v}_{R1}(\omega + \omega_{LO}) e^{-i\phi_{LO1}}] H_{I1}(\omega), \\ \tilde{v}_{I2}(\omega) &= [\tilde{v}_{R2}(\omega - \omega_{LO}) e^{i\phi_{LO2}} + \tilde{v}_{R2}(\omega + \omega_{LO}) e^{-i\phi_{LO2}}] H_{I2}(\omega). \end{aligned} \quad (183)$$

Therefore their cross-correlation is

$$\langle \tilde{v}_{I1}(\omega) \tilde{v}_{I2}^*(\omega') \rangle = \langle [\tilde{v}_{R1}(\omega - \omega_{LO}) e^{i\phi_{LO1}} + \tilde{v}_{R1}(\omega + \omega_{LO}) e^{-i\phi_{LO1}}] \rangle$$

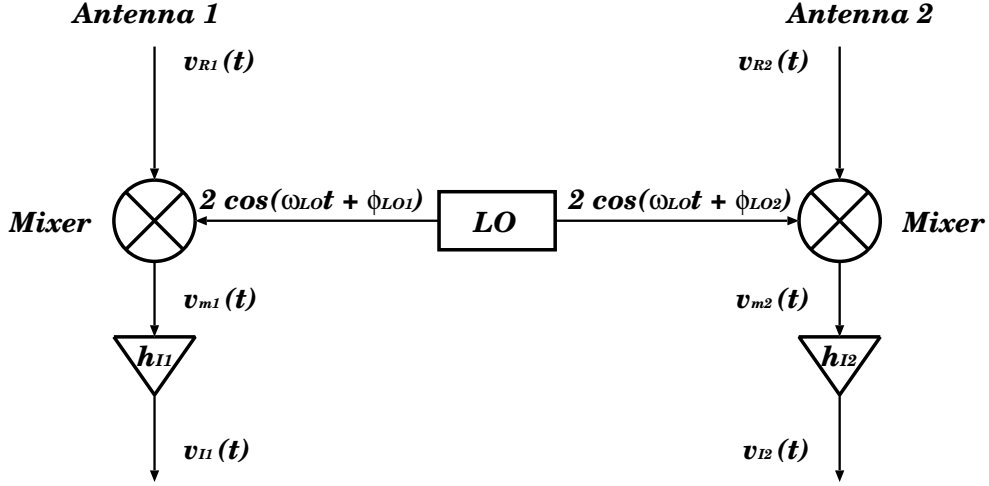


Figure 30: Frequency conversion in an interferometer.

$$\begin{aligned}
& \times [\tilde{v}_{R2}^*(\omega' - \omega_{LO}) e^{-i\phi_{LO2}} + \tilde{v}_{R2}^*(\omega' + \omega_{LO}) e^{i\phi_{LO2}}] \\
& \times H_{I1}(\omega) H_{I2}^*(\omega') \\
= & [ \langle \tilde{v}_{R1}(\omega - \omega_{LO}) \tilde{v}_{R2}^*(\omega' - \omega_{LO}) \rangle e^{i(\phi_{LO1} - \phi_{LO2})} \\
& + \langle \tilde{v}_{R1}(\omega + \omega_{LO}) \tilde{v}_{R2}^*(\omega' + \omega_{LO}) \rangle e^{-i(\phi_{LO1} - \phi_{LO2})} \\
& + \langle \tilde{v}_{R1}(\omega - \omega_{LO}) \tilde{v}_{R2}^*(\omega' + \omega_{LO}) \rangle e^{i(\phi_{LO1} + \phi_{LO2})} \\
& + \langle \tilde{v}_{R1}(\omega + \omega_{LO}) \tilde{v}_{R2}^*(\omega' - \omega_{LO}) \rangle e^{-i(\phi_{LO1} + \phi_{LO2})} ] \\
& \times H_{I1}(\omega) H_{I2}^*(\omega'). \tag{184}
\end{aligned}$$

Since RF voltage signals  $v_{R1}(t)$  and  $v_{R2}(t)$  are assumed to be jointly stationary random processes, their Fourier transforms must satisfy

$$\langle \tilde{v}_{R1}(\omega) \tilde{v}_{R2}^*(\omega') \rangle = 2\pi S_{v_{R1}v_{R2}}(\omega) \delta(\omega - \omega'), \tag{185}$$

as shown in equation (83), where  $S_{v_{R1}v_{R2}}(\omega)$  is the cross-power spectrum of RF voltages, which is given in equation (177). Therefore, we obtain

$$\begin{aligned}
& \langle \tilde{v}_{I1}(\omega) \tilde{v}_{I2}^*(\omega') \rangle \\
= & 2\pi [ S_{v_{R1}v_{R2}}(\omega - \omega_{LO}) e^{i(\phi_{LO1} - \phi_{LO2})} H_{I1}(\omega) H_{I2}^*(\omega) \delta(\omega - \omega') \\
& + S_{v_{R1}v_{R2}}(\omega + \omega_{LO}) e^{-i(\phi_{LO1} - \phi_{LO2})} H_{I1}(\omega) H_{I2}^*(\omega) \delta(\omega - \omega') \\
& + S_{v_{R1}v_{R2}}(\omega - \omega_{LO}) e^{i(\phi_{LO1} + \phi_{LO2})} H_{I1}(\omega) H_{I2}^*(\omega - 2\omega_{LO}) \\
& \quad \times \delta(\omega - \omega' - 2\omega_{LO}) \\
& + S_{v_{R1}v_{R2}}(\omega + \omega_{LO}) e^{-i(\phi_{LO1} + \phi_{LO2})} H_{I1}(\omega) H_{I2}^*(\omega + 2\omega_{LO}) \\
& \quad \times \delta(\omega - \omega' + 2\omega_{LO}) ].
\end{aligned}$$

(186)

First two terms in RHS of equation (186) are proportional to  $\delta(\omega - \omega')$ , and therefore, satisfy the condition of jointly stationary processes, given in equation (83). However, third and fourth terms in RHS of equation (186) are proportional to  $\delta(\omega - \omega' - 2\omega_{LO})$  and  $\delta(\omega - \omega' + 2\omega_{LO})$ , respectively, and therefore, do not satisfy the condition of equation (83). Consequently, generally speaking, IF voltage signals after the frequency conversion may not be jointly stationary, i.e. their cross-correlations may depend on time and LO frequency  $\omega_{LO}$ . This is not surprising, because the mixer output  $v_m(t)$  in equation (178) is a product of the RF signal with a LO reference signal, a regular cosine oscillation, which is not random, nor stationary.

#### 2.2.4 Roles of Low-Pass Filters

Nevertheless, if the cross-power spectrum of the RF signals is band-limited within a certain frequency range, and the IF filters are designed to pass a suitable low-frequency range only, we can make the third and fourth terms to be zero, so that resulting IF signals become jointly stationary.

In fact, if the cross-power spectrum of the RF signals is band-limited within a range:

$$0 < \omega_1 < |\omega| < \omega_2, \quad (187)$$

and IF filters  $H_{I1}(\omega)$  and  $H_{I2}(\omega)$  are both confined within, or proportional to, a rectangular low-pass filter  $H_{LP}(\omega)$ :

$$H_{LP}(\omega) = \begin{cases} 1 & \text{for } |\omega| \leq \omega_c, \\ 0 & \text{otherwise,} \end{cases} \quad (188)$$

with a cut-off frequency  $\omega_c$ , which satisfies conditions:

$$\begin{cases} \omega_2 - \omega_{LO} < \omega_c, \\ \omega_{LO} - \omega_1 < \omega_c, \\ \omega_c < \omega_1 + \omega_{LO}, \end{cases} \quad (189)$$

then, we can eliminate the third and fourth terms in RHS of equation (186), as illustrated in Figure 31.

Figure 31 shows real and imaginary spectral shapes of original complex cross-power spectrum  $S_{v_{R1}v_{R2}}(\omega)$  (solid line) in RF-band, and two spectral functions figuring in equation (186), namely,  $S_{v_{R1}v_{R2}}(\omega + \omega_{LO})$  (dotted line), and  $S_{v_{R1}v_{R2}}(\omega - \omega_{LO})$  (broken line).

$S_{v_{R1}v_{R2}}(\omega)$  is shown here as Hermitian symmetric, since corresponding cross-correlation  $R_{v_{R1}v_{R2}}(\tau)$  is real (equation (60)).  $S_{v_{R1}v_{R2}}(\omega + \omega_{LO})$  has the same spectral shape as the original  $S_{v_{R1}v_{R2}}(\omega)$ , but shifted by  $\omega_{LO}$  towards lower frequency side, while  $S_{v_{R1}v_{R2}}(\omega - \omega_{LO})$  also has the same spectral shape, but shifted by  $\omega_{LO}$  towards higher frequency side.

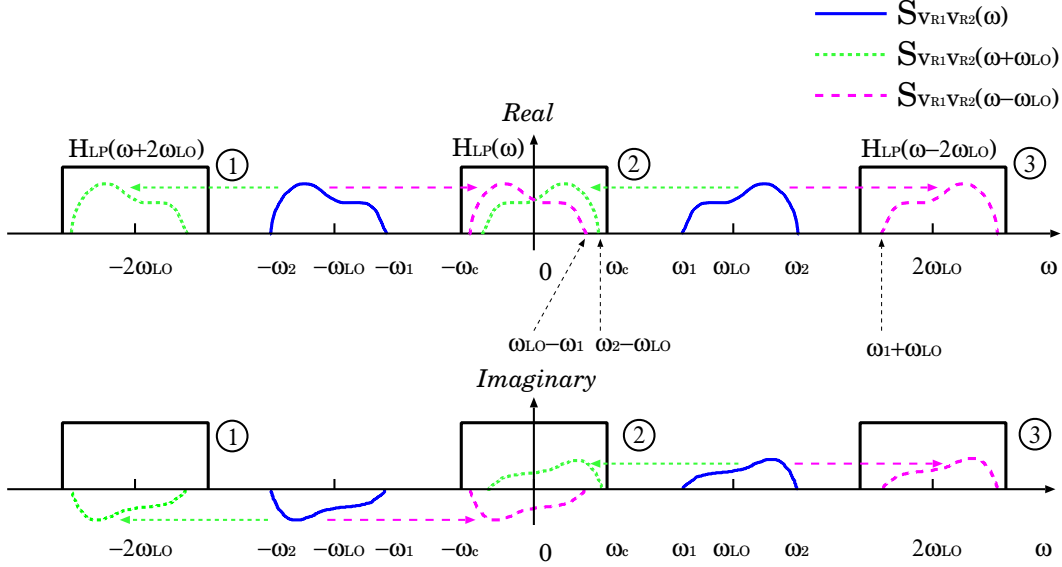


Figure 31: Original complex cross-power spectrum  $S_{v_{R1}v_{R2}}(\omega)$  (solid line), and shifted-in-frequency spectra  $S_{v_{R1}v_{R2}}(\omega + \omega_{LO})$  (dotted line) and  $S_{v_{R1}v_{R2}}(\omega - \omega_{LO})$  (broken line). Boxes assigned with numbers show frequency ranges corresponding to passbands of filters  $H_{LP}(\omega + 2\omega_{LO})$ ,  $H_{LP}(\omega)$ , and  $H_{LP}(\omega - 2\omega_{LO})$ , respectively. Only those parts of spectra which are confined within the central box can be passed through the product of IF filters  $H_{I1}(\omega) H_{I2}^*(\omega)$  in equation (186).

Both spectral functions  $S_{v_{R1}v_{R2}}(\omega + \omega_{LO})$  and  $S_{v_{R1}v_{R2}}(\omega - \omega_{LO})$  consist of lower-frequency and higher-frequency parts, corresponding to negative-frequency and positive-frequency parts of the original band-limited RF cross-power spectrum  $S_{v_{R1}v_{R2}}(\omega)$ . They are confined in three frequency ranges shown by boxes ①, ②, and ③ in Figure 31. These frequency ranges correspond to passbands of rectangular filters  $H_{LP}(\omega + 2\omega_{LO})$ ,  $H_{LP}(\omega)$ , and  $H_{LP}(\omega - 2\omega_{LO})$ , respectively, which are defined by equations (188) and (189).

Let us now examine contributions from 4 terms in RHS of equation (186), one by one.

1. In the first term, the lower-frequency part of  $S_{v_{R1}v_{R2}}(\omega - \omega_{LO})$ , which

is inside the box ②, can be passed through the product of IF filters  $H_{I1}(\omega) H_{I2}^*(\omega)$ , but the higher frequency part, which is inside the box ③, is cut off by the same filter product.

2. In the second term, the higher-frequency part of  $S_{v_{R1}v_{R2}}(\omega + \omega_{LO})$ , which is inside the box ②, can be passed through the product of IF filters  $H_{I1}(\omega) H_{I2}^*(\omega)$ , but the lower frequency part, which is inside the box ①, is cut off by the same filter product.
3. In the third term, the entire spectrum  $S_{v_{R1}v_{R2}}(\omega - \omega_{LO})$  is cut off by the product of IF filters  $H_{I1}(\omega) H_{I2}^*(\omega - 2\omega_{LO})$ , since the lower-frequency part, which is inside the box ②, is cut off by the filter  $H_{I2}^*(\omega - 2\omega_{LO})$ , while the higher-frequency part, which is in ③, is cut off by the filter  $H_{I1}(\omega)$ .
4. In the fourth term, again, the entire spectrum  $S_{v_{R1}v_{R2}}(\omega + \omega_{LO})$  is cut off by the product of IF filters  $H_{I1}(\omega) H_{I2}^*(\omega + 2\omega_{LO})$ , since the lower-frequency part, which is inside the box ①, is cut off by the filter  $H_{I1}(\omega)$ , while the higher-frequency part, which is in ②, is cut off by the filter  $H_{I2}^*(\omega + 2\omega_{LO})$ .

Thus, in the RHS of equation (186), the third and fourth terms are reduced to zero, and only first 2 terms, with the higher-frequency part of  $S_{v_{R1}v_{R2}}(\omega + \omega_{LO})$  and lower-frequency part of  $S_{v_{R1}v_{R2}}(\omega - \omega_{LO})$ , are left.

Therefore, equation (186) now results in:

$$\begin{aligned}
& \langle \tilde{v}_{I1}(\omega) \tilde{v}_{I2}^*(\omega') \rangle \\
&= 2\pi [S_{v_{R1}v_{R2}}(\omega + \omega_{LO}) e^{-i(\phi_{LO1} - \phi_{LO2})} \\
&\quad + S_{v_{R1}v_{R2}}(\omega - \omega_{LO}) e^{i(\phi_{LO1} - \phi_{LO2})}] \\
&\quad \times H_{I1}(\omega) H_{I2}^*(\omega) \delta(\omega - \omega'). \quad (190)
\end{aligned}$$

This equation has a proper form of a cross-correlation of Fourier transforms of jointly stationary random processes, which is proportional to  $\delta(\omega - \omega')$ , as given in equation (83). Consequently, the IF voltage signals  $v_{I1}(t)$  and  $v_{I2}(t)$  can now be regarded as jointly stationary random processes.

### 2.2.5 Relationship between RF Spectrum and IF Spectrum

The result of the previous section means that we can now define a cross-power spectrum  $S_{v_{I1}v_{I2}}(\omega)$  of the IF voltage signals  $v_{I1}(t)$  and  $v_{I2}(t)$ , according to equation (55), as we usually do for jointly stationary random processes. In

view of equation (83), the cross-power spectrum must be related to the cross-correlation of the Fourier transforms  $\langle \tilde{v}_{I1}(\omega) \tilde{v}_{I2}^*(\omega') \rangle$  by the general formula:

$$\langle \tilde{v}_{I1}(\omega) \tilde{v}_{I2}^*(\omega') \rangle = 2\pi S_{v_{I1}v_{I2}}(\omega) \delta(\omega - \omega'). \quad (191)$$

Equating RHSs of equations (190) and (191), we obtain

$$\begin{aligned} S_{v_{I1}v_{I2}}(\omega) = & [S_{v_{R1}v_{R2}}(\omega + \omega_{LO}) e^{-i(\phi_{LO1} - \phi_{LO2})} \\ & + S_{v_{R1}v_{R2}}(\omega - \omega_{LO}) e^{i(\phi_{LO1} - \phi_{LO2})}] \\ & \times H_{I1}(\omega) H_{I2}^*(\omega), \end{aligned} \quad (192)$$

which is a relationship between a cross-power spectrum of IF voltage signals  $S_{v_{I1}v_{I2}}(\omega)$ , after the frequency conversion, and a cross-power spectrum of RF voltage signals  $S_{v_{R1}v_{R2}}(\omega)$ , before the frequency conversion.

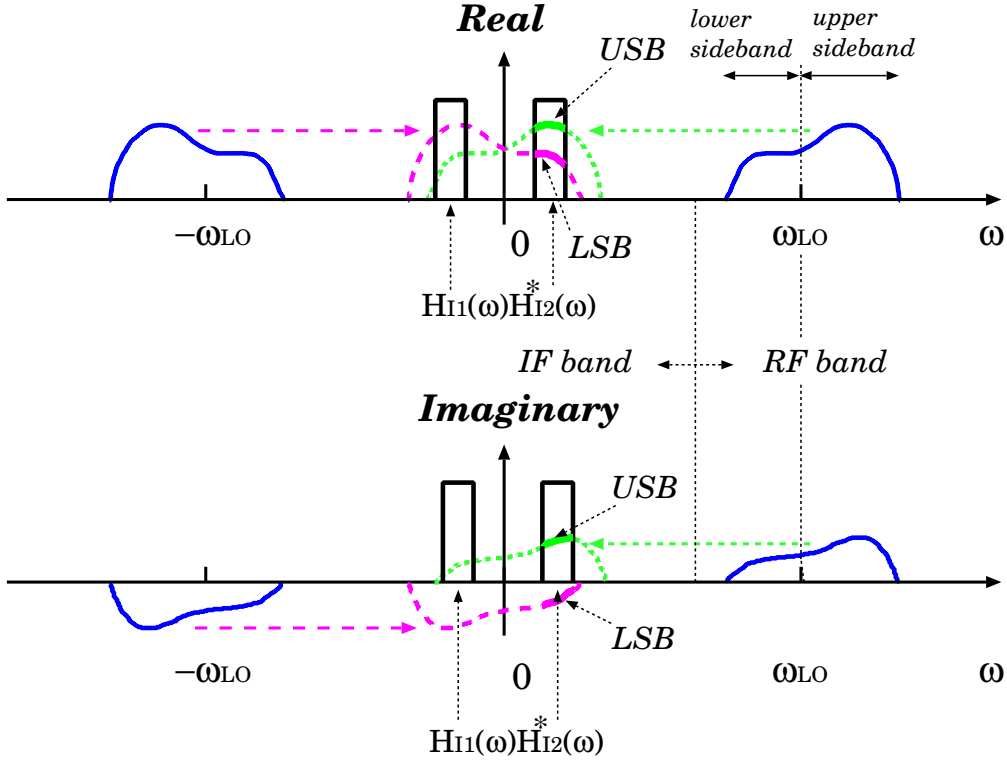


Figure 32: Upper sideband (USB) and lower sideband (LSB) contributions in a cross-power spectrum of IF voltage signals, which is confined in a passband of the product of IF filters  $H_{I1}(\omega) H_{I2}^*(\omega)$ .

The IF cross-power spectrum is shown in Figure 32, where we assumed same initial phases of local oscillators, i.e.,  $\phi_{LO1} - \phi_{LO2} = 0$  for simplicity.

The IF spectrum is Hermitian symmetric, according to the general property of a cross-power spectrum, which corresponds to a real cross-correlation, as shown in equation (60). In our case, the cross-correlation of IF voltage signals is surely real, simply because IF voltage signals themselves are real.

Since the cross-correlation can be described by the positive-frequency region of the Hermitian symmetric cross-power spectrum, as we saw in equation (62), we will pay our attention to the positive frequency region ( $\omega \geq 0$ ) of the IF spectrum. Then, the original RF cross-power spectrum, shown by solid lines in Figure 32, is down-converted to IF-band, and the upper sideband (USB) of  $S_{v_{R1}v_{R2}}(\omega + \omega_{LO})$  (shown by a broken line), and the lower sideband (LSB) of  $S_{v_{R1}v_{R2}}(\omega - \omega_{LO})$  (shown by a dotted line) are passed through the product of the IF filters  $H_{I1}(\omega) H_{I2}^*(\omega)$  in the positive IF frequency region, as we see in Figure 32.

Thus, we can notice here following properties of the IF spectrum:

- Spectral shape of the RF spectrum is preserved, and just shifted into the IF-band.
- Upper sideband (USB) and lower sideband (LSB) components are superposed in the IF passband of  $H_{I1}(\omega) H_{I2}^*(\omega)$ .
- In the positive frequency range of the IF spectrum,  $\omega \geq 0$ , spectrum of the LSB component is reversed, compared with the positive frequency part of the original RF spectrum.

Because of the Hermitian symmetry  $S_{xy}(-\omega) = S_{xy}^*(\omega)$  for real processes, as shown in equation (60), we can rewrite equation (192) in a form:

$$\begin{aligned}
 S_{v_{I1}v_{I2}}(\omega) = & [S_{v_{R1}v_{R2}}(\omega_{LO} + \omega) e^{-i(\phi_{LO1} - \phi_{LO2})} \\
 & + S_{v_{R1}v_{R2}}^*(\omega_{LO} - \omega) e^{i(\phi_{LO1} - \phi_{LO2})}] \\
 & \times H_{I1}(\omega) H_{I2}^*(\omega), \tag{193}
 \end{aligned}$$

using only positive-frequency part of the RF cross-power spectrum. The first term in the RHS of equation (193) shows USB component in the positive frequency side ( $\omega \geq 0$ ) and LSB component in the negative frequency side ( $\omega < 0$ ), while the second term shows LSB component in the positive frequency side ( $\omega \geq 0$ ) and USB component in the negative frequency side ( $\omega < 0$ ).

## 2.3 Delay Tracking and Fringe Stopping

In subsection 1.3, we saw, based on a simple interferometer model, that a radio interferometer can detect a radio source, only when the source is within the “coherence interval” of the white fringe, i.e., within a certain range, around zero, of the delay between arrival times of a common wave front, from an astronomical radio source, at antennas. The delay range is roughly equal to  $2/B$ , where  $B$  is a frequency bandwidth of the received signal. Table 1 of subsection 1.3.6 showed that the delay range corresponds to an angular interval in the sky, which is usually very narrow for modern interferometers, especially for VLBI. If we do not have any effective means to compensate the delay, this would imply that we can observe a source, only when the source happens to be within the very narrow region of the sky, where the geometric delay is nearly zero, that is, of course, highly ineffective and unrealistic.

Also, we saw that the diurnal motion of a radio source causes rapid oscillation of the correlator output due to the densely spaced fringe patterns, as schematically illustrated in Figure 21 and Table 2 of subsection 1.3.7. Such an oscillation would make it practically impossible to integrate the multiplier output for a duration of time, sufficient to get a signal to noise ratio, necessary for detecting the source.

Therefore, the modern interferometers must be equipped with special mechanisms, for compensating the delay and stopping the rapid oscillation of the correlator output. They are called “delay tracking” and “fringe stopping”, respectively. Now we would like to discuss how these functions are realized in a realistic interferometer.

### 2.3.1 General Form of Cross-Power Spectrum of IF Signals

In order to clarify meanings of the delay tracking and fringe stopping in more detail, we will first combine results of previous discussions, and derive a general description of the cross-power spectrum of IF voltage signals.

So far, we derived

1. the cross-power spectrum of received voltages:

$$S_{v_1 v_2}(\omega) = \frac{1}{4} A_0 e^{-i\omega\tau_{g0}} \mathcal{V}(\omega),$$

given in equation (168), where  $A_0$  is the geometrical mean of effective apertures of antennas, and  $\mathcal{V}(\omega)$  is the complex visibility:

$$\mathcal{V}(\omega) = \oint A_N(\boldsymbol{\sigma}) I_\nu(\boldsymbol{\sigma}) e^{-i2\pi\mathbf{D}_\lambda \cdot \boldsymbol{\sigma}} d\Omega,$$

given in equation (165), where  $A_N(\boldsymbol{\sigma})$  is the normalized power pattern of an interferometer,  $\boldsymbol{\sigma} = \mathbf{s} - \mathbf{s}_0$  is an offset vector showing a certain direction  $\mathbf{s}$  in a source with respect to the reference direction  $\mathbf{s}_0$ ,  $I_\nu(\boldsymbol{\sigma})$  is the source intensity distribution, and  $\mathbf{D}_\lambda = \mathbf{D}/\lambda$  is a baseline vector normalized by a wave length  $\lambda$ ,

2. the cross-power spectrum of RF voltage signals after the RF filters (amplifiers and BPFs) with system functions  $H_{R1}(\omega)$  and  $H_{R2}(\omega)$ :

$$S_{v_{R1}v_{R2}}(\omega) = S_{v_1v_2}(\omega) H_{R1}(\omega) H_{R2}^*(\omega),$$

given in equation (177),

3. the cross-power spectrum of IF voltage signals after the frequency conversion:

$$\begin{aligned} S_{v_{I1}v_{I2}}(\omega) &= [S_{v_{R1}v_{R2}}(\omega_{LO} + \omega) e^{-i(\phi_{LO1} - \phi_{LO2})} \\ &\quad + S_{v_{R1}v_{R2}}^*(\omega_{LO} - \omega) e^{i(\phi_{LO1} - \phi_{LO2})}] \\ &\quad \times H_{I1}(\omega) H_{I2}^*(\omega), \end{aligned}$$

given in equation (193), where  $\omega_{LO}$  is the LO reference frequency,  $\phi_{LO1}$  and  $\phi_{LO2}$  are initial phases of two local oscillators, and  $H_{I1}(\omega)$  and  $H_{I2}(\omega)$  are system functions of the IF filters.

Combining last two equations, i.e., equations (177) and (193), we have

$$\begin{aligned} S_{v_{I1}v_{I2}}(\omega) &= [H_{R1}(\omega_{LO} + \omega) H_{R2}^*(\omega_{LO} + \omega) S_{v_1v_2}(\omega_{LO} + \omega) e^{-i(\phi_{LO1} - \phi_{LO2})} \\ &\quad + H_{R1}^*(\omega_{LO} - \omega) H_{R2}(\omega_{LO} - \omega) S_{v_1v_2}^*(\omega_{LO} - \omega) e^{i(\phi_{LO1} - \phi_{LO2})}] \\ &\quad \times H_{I1}(\omega) H_{I2}^*(\omega). \end{aligned} \quad (194)$$

Here, system functions of real impulse responses of IF filters must satisfy equation (74):

$$H_{I1}(\omega) = H_{I1}^*(-\omega), \quad \text{and} \quad H_{I2}^*(\omega) = H_{I2}(-\omega).$$

Therefore, introducing new system functions  $H_1(\omega)$  and  $H_2(\omega)$  for responses of combined IF filters, composed of down-converted RF and original IF filters, in antenna 1 and antenna 2, respectively:

$$\begin{aligned} H_1(\omega) &= H_{R1}(\omega_{LO} + \omega) H_{I1}(\omega), \\ H_2(\omega) &= H_{R2}(\omega_{LO} + \omega) H_{I2}(\omega), \end{aligned} \quad (195)$$

we can rewrite equation (194) as:

$$\begin{aligned}
& S_{v_{I1}v_{I2}}(\omega) \\
&= H_1(\omega) H_2^*(\omega) S_{v_1v_2}(\omega_{LO} + \omega) e^{-i(\phi_{LO1}-\phi_{LO2})} \\
&\quad + H_1^*(-\omega) H_2(-\omega) S_{v_1v_2}^*(\omega_{LO} - \omega) e^{i(\phi_{LO1}-\phi_{LO2})}. \tag{196}
\end{aligned}$$

Hereafter, we call the complex function  $H_1(\omega) H_2^*(\omega)$  “bandpass characteristics of combined IF filters”.

Then, inserting equation (168) into equation (196), we obtain a general form of the cross-power spectrum of the IF voltage signals, which describes  $S_{v_{I1}v_{I2}}(\omega)$  in terms of source intensity distribution, geometry of observation, filter responses, and parameters of the frequency conversion:

$$\begin{aligned}
& S_{v_{I1}v_{I2}}(\omega) \\
&= \frac{1}{4} A_0 \{ e^{-i[(\omega_{LO}+\omega)\tau_{g0}+\phi_{LO1}-\phi_{LO2}]} \mathcal{V}(\omega_{LO} + \omega) H_1(\omega) H_2^*(\omega) \\
&\quad + e^{i[(\omega_{LO}-\omega)\tau_{g0}+\phi_{LO1}-\phi_{LO2}]} \mathcal{V}^*(\omega_{LO} - \omega) H_1^*(-\omega) H_2(-\omega) \}. \tag{197}
\end{aligned}$$

Of course, this equation satisfies the Hermitian symmetry condition:

$$S_{v_{I1}v_{I2}}(\omega) = S_{v_{I1}v_{I2}}^*(-\omega),$$

required for real processes  $v_{I1}(t)$  and  $v_{I2}(t)$ .

Representing the complex visibility in terms of visibility amplitude and visibility phase, as introduced in equation (166), we have

$$\begin{aligned}
\mathcal{V}(\omega_{LO} + \omega) &= |\mathcal{V}(\omega_{LO} + \omega)| e^{i\Phi_v(\omega_{LO}+\omega)}, \\
\mathcal{V}^*(\omega_{LO} - \omega) &= |\mathcal{V}(\omega_{LO} - \omega)| e^{-i\Phi_v(\omega_{LO}-\omega)}. \tag{198}
\end{aligned}$$

Also we represent the bandpass characteristics of combined IF filters in terms of its amplitude  $|H_1(\omega) H_2^*(\omega)|$  and phase  $\Phi_b(\omega)$ :

$$\begin{aligned}
H_1(\omega) H_2^*(\omega) &= |H_1(\omega) H_2^*(\omega)| e^{i\Phi_b(\omega)}, \\
H_1^*(-\omega) H_2(-\omega) &= |H_1(-\omega) H_2^*(-\omega)| e^{-i\Phi_b(-\omega)}. \tag{199}
\end{aligned}$$

Then, the cross-power spectrum of IF signals is now reduced to

$$\begin{aligned}
& S_{v_{I1}v_{I2}}(\omega) \\
&= \frac{1}{4} A_0 |\mathcal{V}(\omega_{LO} + \omega)| |H_1(\omega) H_2^*(\omega)| e^{-i[(\omega_{LO}+\omega)\tau_{g0}+\phi_{LO1}-\phi_{LO2}-\Phi_v(\omega_{LO}+\omega)-\Phi_b(\omega)]} \\
&\quad + \frac{1}{4} A_0 |\mathcal{V}(\omega_{LO} - \omega)| |H_1(-\omega) H_2^*(-\omega)| e^{i[(\omega_{LO}-\omega)\tau_{g0}+\phi_{LO1}-\phi_{LO2}-\Phi_v(\omega_{LO}-\omega)-\Phi_b(-\omega)]}. \tag{200}
\end{aligned}$$

Again, first term in the RHS of equation (200) shows USB component in the positive frequency range ( $\omega \geq 0$ ) and LSB component in the negative frequency range ( $\omega < 0$ ), while second term shows LSB component in the positive frequency range ( $\omega \geq 0$ ) and USB component in the negative frequency range ( $\omega < 0$ ).

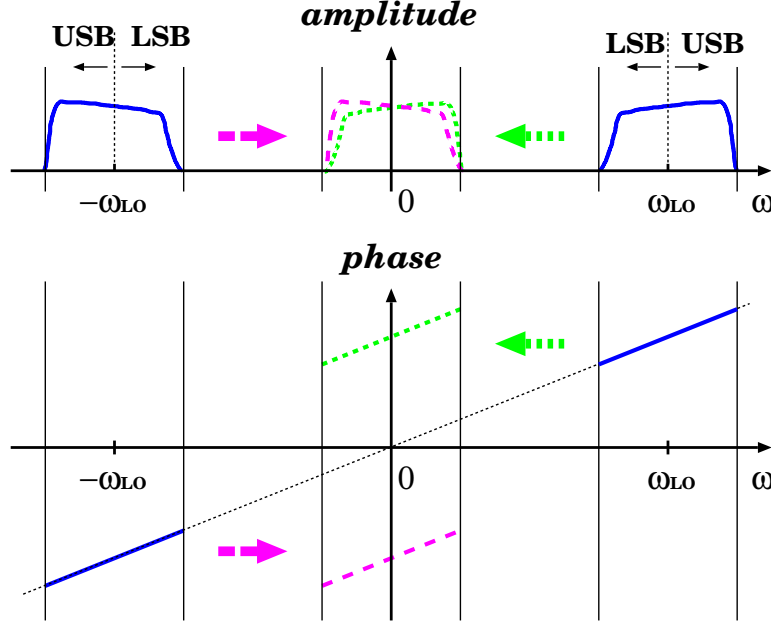


Figure 33: Amplitudes and phases of two terms in a cross-power spectrum of IF voltage signals. Solid lines show original RF spectrum, and dotted and broken lines correspond to first and second terms of the RHS of equation (200), respectively. For simplicity, only contribution of geometric delay is shown in phase spectrum.

If we denote amplitudes and phases of the first and second terms of the RHS of equation (200) as  $A_p(\omega)$ ,  $\Phi_p(\omega, t)$  and  $A_n(\omega)$ ,  $\Phi_n(\omega, t)$ , respectively, we have

$$S_{v_{I1}v_{I2}}(\omega) = A_p(\omega) e^{-i\Phi_p(\omega, t)} + A_n(\omega) e^{-i\Phi_n(\omega, t)}, \quad (201)$$

with

$$\begin{aligned} A_p(\omega) &= \frac{1}{4} A_0 | \mathcal{V}(\omega_{LO} + \omega) | | H_1(\omega) H_2^*(\omega) |, \\ A_n(\omega) &= \frac{1}{4} A_0 | \mathcal{V}(\omega_{LO} - \omega) | | H_1(-\omega) H_2^*(-\omega) |, \end{aligned} \quad (202)$$

and

$$\begin{aligned}
\Phi_p(\omega, t) &= (\omega_{LO} + \omega)\tau_{g_0} + \phi_{LO1} - \phi_{LO2} - \Phi_v(\omega_{LO} + \omega) - \Phi_b(\omega), \\
\Phi_n(\omega, t) &= -(\omega_{LO} - \omega)\tau_{g_0} - \phi_{LO1} + \phi_{LO2} + \Phi_v(\omega_{LO} - \omega) + \Phi_b(-\omega).
\end{aligned} \tag{203}$$

Here, we took into account that phases are functions of both frequency and time, in view of the time-variable geometric delay  $\tau_{g_0}$ . This shows amplitude and phase spectra of the cross-power spectrum of IF signals, which can be contrasted to those given in equations (101), (102), and (103), for a simple interferometer model. Again, first term in the RHS of equation (200) shows USB component in the positive frequency range ( $\omega \geq 0$ ) and LSB component in the negative frequency range ( $\omega < 0$ ), while second term shows LSB component in the positive frequency range ( $\omega \geq 0$ ) and USB component in the negative frequency range ( $\omega < 0$ ).

Figure 33 shows the amplitude and phase spectra of two terms of the IF cross-power spectrum in the RHS of equation (200), which can be compared with Figure 19 for a simple interferometer. For simplicity, we showed only contribution of geometric delay  $\tau_{g_0}$  in this figure, ignoring small effects of  $\phi_{LO1}$ ,  $\phi_{LO2}$ ,  $\Phi_v$ , and  $\Phi_b$  terms. The IF band here is assumed to be a “video-band” (or “baseband”), which includes zero frequency, or “DC (direct current)”, component with  $\omega = 0$ .

### 2.3.2 “Expected Correlation” of IF Signals

If we had an idealized correlator, which would be capable of multiplying two IF voltage signals, and immediately calculating a statistical mean of the product, such a correlator would yield the cross-correlation of the IF voltage signals  $R_{v_{I1}v_{I2}}(\tau)$  at time difference  $\tau = 0$ :

$$\langle v_{I1}(t) v_{I2}(t) \rangle = R_{v_{I1}v_{I2}}(0).$$

According to equation (197), we expect that this “instantaneous correlator output” is described by an inverse Fourier transformation of the cross-power spectrum  $S_{v_{I1}v_{I2}}(\omega)$ , with  $\tau = 0$ :

$$\begin{aligned}
R_{v_{I1}v_{I2}}(0) &= \frac{1}{2\pi} \int_{-\infty}^{\infty} S_{v_{I1}v_{I2}}(\omega) d\omega = \frac{1}{\pi} \Re \int_0^{\infty} S_{v_{I1}v_{I2}}(\omega) d\omega \\
&= \frac{A_0}{4\pi} \Re \left[ e^{-i(\omega_{LO}\tau_{g_0} + \phi_{LO1} - \phi_{LO2})} \int_0^{\infty} \mathcal{V}(\omega_{LO} + \omega) e^{-i\omega\tau_{g_0}} H_1(\omega) H_2^*(\omega) d\omega \right. \\
&\quad \left. + e^{i(\omega_{LO}\tau_{g_0} + \phi_{LO1} - \phi_{LO2})} \int_0^{\infty} \mathcal{V}^*(\omega_{LO} - \omega) e^{-i\omega\tau_{g_0}} H_1^*(-\omega) H_2(-\omega) d\omega \right], \tag{204}
\end{aligned}$$

where we used the property of a Hermitian symmetric cross-power spectrum given in equation (74), in order to restrict range of integration to the positive frequency side only.

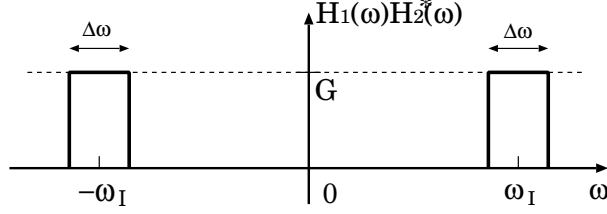


Figure 34: Rectangular response of a real filter.

If we assume, similarly to what we did in the case of a simple interferometer model in Section 1.3, a real, even, and rectangular system functions of the combined IF filters, with a gain factor  $G$ , bandwidth  $\Delta\omega = 2\pi B$  and center frequency  $\omega_I$ , as shown in Figure 34, i.e.,

$$H_1(\omega) H_2^*(\omega) = H_1^*(-\omega) H_2(-\omega) = \begin{cases} G & \text{if } \omega_I - \frac{\Delta\omega}{2} \leq |\omega| \leq \omega_I + \frac{\Delta\omega}{2}, \\ 0 & \text{otherwise,} \end{cases} \quad (205)$$

and also assume a continuum spectrum source, with almost constant complex visibility across the frequency bandwidth,

$$\mathcal{V}(\omega) \cong \mathcal{V} \quad \text{for } \omega_I - \frac{\Delta\omega}{2} \leq |\omega| \leq \omega_I + \frac{\Delta\omega}{2}, \quad (206)$$

then, we obtain from equation (204)

$$R_{v_{I1}v_{I2}}(0) = \frac{A_0 G}{4\pi} \Re \left[ e^{-i(\omega_{LO}\tau_{g0} + \phi_{LO1} - \phi_{LO2})} \mathcal{V} \int_{\omega_I - \frac{\Delta\omega}{2}}^{\omega_I + \frac{\Delta\omega}{2}} e^{-i\omega\tau_{g0}} d\omega + e^{i(\omega_{LO}\tau_{g0} + \phi_{LO1} - \phi_{LO2})} \mathcal{V}^* \int_{\omega_I - \frac{\Delta\omega}{2}}^{\omega_I + \frac{\Delta\omega}{2}} e^{-i\omega\tau_{g0}} d\omega \right]. \quad (207)$$

Since the integral in equation (207) is described in terms of the sinc function, as we saw in equation (100):

$$\frac{1}{\pi} \int_{\omega_I - \frac{\Delta\omega}{2}}^{\omega_I + \frac{\Delta\omega}{2}} e^{-i\omega\tau_{g0}} d\omega = 2B e^{-i\omega_I\tau_{g0}} \frac{\sin(\pi B\tau_{g0})}{\pi B\tau_{g0}},$$

and the complex visibility is represented in terms of its amplitude and phase:

$$\mathcal{V} = |\mathcal{V}| e^{i\Phi_v},$$

equation (207) is further reduced to

$$\begin{aligned} R_{v_{I1}v_{I2}}(0) &= \frac{A_0GB |\mathcal{V}| \sin(\pi B\tau_{g0})}{2 \pi B\tau_{g0}} \\ &\times [\cos(\omega_{LO}\tau_{g0} + \omega_I\tau_{g0} + \phi_{LO1} - \phi_{LO2} - \Phi_v) \\ &+ \cos(\omega_{LO}\tau_{g0} - \omega_I\tau_{g0} + \phi_{LO1} - \phi_{LO2} - \Phi_v)]. \end{aligned} \quad (208)$$

This equation is an analog of equation (100), which we derived for a simple interferometer model observing a continuum spectrum source. The sinc function stands for a bandwidth pattern, and two cosine terms are fringe patterns corresponding to center frequencies of USB and LSB, respectively. Evidently, first cosine term shows contribution of USB component, while second cosine term shows contribution of LSB component.

Equation (208) again shows that we can detect fringe pattern of a continuum spectrum source within a narrow coherence interval, roughly represented by  $\Delta\tau_B = 2/B$ . Also, time variation of the geometric delay  $\tau_{g0}$  in the fringe patterns causes rapid sinusoidal oscillation of  $R_{v_{I1}v_{I2}}(0)$ , which makes it almost impossible to integrate (time-average) the product of voltage signals for a meaningful duration of time. Therefore, we definitely need the delay tracking and fringe stopping for a realistic interferometer.

There is no widely-accepted name for the ‘‘instantaneous correlator output’’  $R_{v_{X1}v_{X2}}(0)$ , where  $v_{X1}(t)$  and  $v_{X2}(t)$  could be any voltages in radio interferometry, i.e., they could be received voltages, RF voltages, or IF voltages. This is not an actual correlator output, since any correlator output is obtained only after integration of a product of voltages, or a multiplier output, for some duration of time in an integrator. This is not the product of individual voltages, either. This is a statistical expectation of the product of voltages, or the multiplier output, at a certain instance of time.

An important point here is the following. We consider that an actual product of voltages consists of a signal component and a noise component, and the signal component is described by this quantity:  $R_{v_{X1}v_{X2}}(0)$ . We apply the fringe stopping, in order to stop the rapid oscillation of this signal quantity, so that we can suppress the noise and detect the signal by time averaging.

Hereafter, we call this quantity as an ‘‘expected correlation’’ in a radio interferometer.

### 2.3.3 Radio Source Tracking by an Interferometer

What is needed is to compensate the geometric delay  $\tau_{g0}$  to get the same effect, which would be obtained, if we move one of the antennas along the surface of a sphere of diameter equal to the baseline length, such that  $\tau_{g0}$  is always maintained equal to zero, as illustrated in Figure 35. Such compensa-

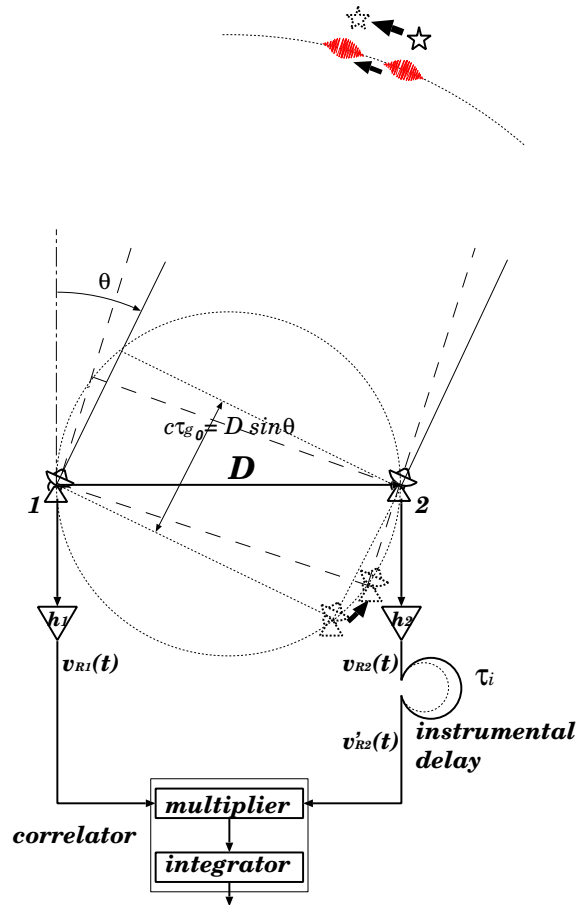


Figure 35: How to track a radio source by an interferometer? Insertion of an instrumental delay, which compensates the geometric delay, in the RF-band can do the job.

tion of the geometric delay enables an interferometer to “track” the motion of a radio source, in order to keep the source in its “interferometer beam”, just as a single-dish radio telescope does with its antenna beam.

A time-variable delay circuit, which is inserted into the transmission system of one of the antennas at RF-band, and provides an instrumental delay

$\tau_i$  equal to the geometric delay  $\tau_{g_0}$ , as illustrated in Figure 35, can realize, at least theoretically, the required tracking.

Although this statement must be intuitively obvious, it would be still useful to logically trace the effect of delay insertion, in the following way.

Insertion of an instrumental delay  $\tau_i$ , in the RF signal transmission system of antenna 2, would make the RF voltage signal  $v'_{R2}(t)$ , after the delay circuit, and its Fourier transform  $\tilde{v}'_{R2}(\omega)$ , to be equal to

$$v'_{R2}(t) = v_{R2}(t - \tau_i), \quad \text{and therefore,} \quad \tilde{v}'_{R2}(\omega) = \tilde{v}_{R2}(\omega) e^{-i\omega\tau_i}, \quad (209)$$

where  $v_{R2}(t)$ , and  $\tilde{v}_{R2}(\omega)$ , correspond to the RF voltage signal before the instrumental delay. We used the shift theorem given in equation (68), in deriving equation (209).

Therefore, taking a cross-correlation of Fourier transforms  $\tilde{v}_{R1}(\omega)$  and  $\tilde{v}'_{R2}(\omega)$  of RF voltage signals, we see

$$\langle \tilde{v}_{R1}(\omega) \tilde{v}'_{R2}(\omega') \rangle = \langle \tilde{v}_{R1}(\omega) \tilde{v}_{R2}(\omega') \rangle e^{i\omega'\tau_i}. \quad (210)$$

Since we assumed that the RF signals  $v_{R1}(t)$  and  $v_{R2}(t)$  are jointly stationary random processes,  $v_{R1}(t)$  and  $v'_{R2}(t)$  must also be jointly stationary random processes. Hence, the cross-correlations of their Fourier transforms and cross-power spectra must be related to each other as:

$$\begin{aligned} \langle \tilde{v}_{R1}(\omega) \tilde{v}'_{R2}(\omega') \rangle &= 2\pi S_{v_{R1}v'_{R2}}(\omega) \delta(\omega - \omega'), \\ \langle \tilde{v}_{R1}(\omega) \tilde{v}_{R2}(\omega') \rangle &= 2\pi S_{v_{R1}v_{R2}}(\omega) \delta(\omega - \omega'), \end{aligned} \quad (211)$$

in view of equation (83). Comparing equations (210) and (211), we obtain a relation between the cross-power spectrum  $S_{v_{R1}v'_{R2}}(\omega)$  of the RF voltage signal  $v_{R1}(t)$  of antenna 1 and the delay-inserted RF voltage signal  $v'_{R2}(t)$  of antenna 2, and the cross-power spectrum  $S_{v_{R1}v_{R2}}(\omega)$  of the RF voltages without delay insertion:

$$S_{v_{R1}v'_{R2}}(\omega) = S_{v_{R1}v_{R2}}(\omega) e^{i\omega\tau_i}, \quad (212)$$

which leads to

$$\begin{aligned} S_{v_{R1}v'_{R2}}(\omega) &= S_{v_1v_2}(\omega) H_{R1}(\omega) H_{R2}^*(\omega) e^{i\omega\tau_i} \\ &= \frac{1}{4} A_0 e^{-i\omega\Delta\tau_g} \mathcal{V}(\omega) H_{R1}(\omega) H_{R2}^*(\omega), \end{aligned} \quad (213)$$

where

$$\Delta\tau_g = \tau_{g_0} - \tau_i.$$

We used here equations (168) and (177) for expressions of the cross-power spectra of RF voltages  $S_{v_{R1}v_{R2}}(\omega)$ , and received voltages  $S_{v_1v_2}(\omega)$ .

As we see, an only different point between combined equations (168) and (177) and this equation (213) is that the geometric delay  $\tau_{g0}$  is replaced by the delay difference  $\Delta\tau_g = \tau_{g0} - \tau_i$ . Therefore, we can easily derive an expected correlation of an IF voltage  $v_{I1}(t)$  of antenna 1 and an IF voltage with delay inserted at RF-band  $v''_{I2}$  of antenna 2,  $R_{v_{I1}v''_{I2}}(0)$ , from equation (208), assuming again a rectangular filter, given in equation (205), and constant visibility over receiving bandwidth, given in equation (206). The result is

$$\begin{aligned}
R_{v_{I1}v''_{I2}}(0) &= \frac{A_0GB |\mathcal{V}| \sin(\pi B\Delta\tau_g)}{2 \pi B\Delta\tau_g} \\
&\times [\cos(\omega_{LO}\Delta\tau_g + \omega_I\Delta\tau_g + \phi_{LO1} - \phi_{LO2} - \Phi_v) \\
&+ \cos(\omega_{LO}\Delta\tau_g - \omega_I\Delta\tau_g + \phi_{LO1} - \phi_{LO2} - \Phi_v)].
\end{aligned} \tag{214}$$

Thus, as long as  $\tau_i = \tau_{g0}$ , no delay effect is left in the RF cross-power spectrum, given in equation (213), and, therefore, also in the expected correlation of IF voltages in equation (214). This means that the insertion of an instrumental delay, exactly equal to the geometric delay, at RF-band could effectively reduce  $\tau_g$  in equation (100), or  $\tau_{g0}$  in equation (208), to zero. This would allow us to find fringes always at the center of the coherence interval, and to integrate the product of voltage signals, as long as we wish. Or, otherwise speaking, we could realize both delay tracking and fringe stopping by a single operation, namely by the insertion of a time variable instrumental delay, if we were allowed to do this at RF-band.

Unfortunately, it is almost impossible, in the current level of technology, to realize any delay insertion at RF frequencies, higher than several GHz. Therefore, the delay insertion is usually performed at IF-band.

### 2.3.4 Requirements to the Delay Tracking and Fringe Stopping

Before proceeding with discussions on actual realization of the delay tracking and fringe stopping, let us here estimate the ranges of variations, and accuracies required to theoretical predictions, of the geometric delay  $\tau_{g0}$  and its time rate  $\dot{\tau}_{g0}$ . For simplicity, we will implicitly rely upon an image of the delay insertion at RF-band discussed above, since this does not cause any loss of generality in present discussions.

If we denote the baseline vector and the unit vector directed to the radio source as  $\mathbf{D}$  and  $\mathbf{s}_0$ , respectively, the geometric delay  $\tau_{g0}$  and its time rate

$\dot{\tau}_{g_0}$ , due to the diurnal rotation of the Earth, are given by:

$$\tau_{g_0} = \frac{\mathbf{D} \cdot \mathbf{s}_0}{c}, \quad (215)$$

$$\dot{\tau}_{g_0} = \frac{\dot{\mathbf{D}} \cdot \mathbf{s}_0}{c} = \frac{(\boldsymbol{\omega} \times \mathbf{D}) \cdot \mathbf{s}_0}{c}, \quad (216)$$

where  $\boldsymbol{\omega}$  is the angular velocity vector of the rotation of the Earth ( $|\boldsymbol{\omega}| \simeq 7.3 \times 10^{-5}$  rad/sec) and  $c \simeq 3 \times 10^8$  m/sec is the light velocity. Of course, equation (216) is valid for ground-based interferometers only, and not valid for space-VLBI baselines.

For a connected-element radio interferometer (CERI) of 300 m baseline, say, the maximum geometric delay:

$$\tau_{g_{max}} = \frac{D}{c} = 1 \mu\text{sec},$$

is obtained when the source direction is parallel to the baseline, and the maximum delay rate:

$$\dot{\tau}_{g_{max}} = \frac{\omega D}{c} = 70 \text{ psec/sec},$$

is obtained when  $\boldsymbol{\omega} \perp \mathbf{D}$  and  $(\boldsymbol{\omega} \times \mathbf{D}) \parallel \mathbf{s}_0$ .

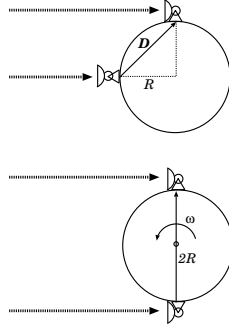


Figure 36: The maximum geometric delay (top) and maximum delay rate (bottom) of the ground-based VLBI.

For the ground-based VLBI, the maximum geometric delay and the maximum delay rate are obtained in cases shown in Figure 36. If we denote the Earth's radius as  $R_{\oplus} = 6300$  km, the maximum values are

$$\tau_{g_{max}} = \frac{R_{\oplus}}{c} = 21 \text{ msec}, \quad (217)$$

$$\dot{\tau}_{g_{max}} = \frac{2R_{\oplus}\omega}{c} = 3.1 \mu\text{sec/sec}. \quad (218)$$

If we observe at 22 GHz, equations (208) and (218) implies that the expected correlation, defined in subsection 2.1.8, may oscillate with frequency as high as  $22 \text{ GHz} \times 3.1 \times 10^{-6} = 68.2 \text{ kHz}$ , or 68,200 cycles per second(!), due to the diurnal motion of the source across the fringe pattern. Indeed, no meaningful integration of the multiplier output is possible, unless we stop such an oscillation.

The ranges of variations of geometric delay and its rate, as examined above, and resulting variations of the phase in the cross-power spectrum of voltage signals, such as shown in equation (200), are orders of magnitude larger, than those caused by other delay effects (clock offset, atmospheric propagation delay, cable delay, etc.), and by other phase terms (LO initial phase, visibility phase, phase of bandpass characteristics, etc.). Therefore, the delay tracking and fringe stopping are, primarily, means for compensation of geometric delay. Although some other, much smaller, effects are also taken into account in highly precise delay tracking and fringe stopping, performed in VLBI correlators, we will postpone discussion of this problem, until we consider correlation processings in VLBI.

We use an appropriate theoretical prediction of the time-variable geometric delay, in order to determine length and rate of the instrumental delay, to be applied to actual delay tracking and fringe stopping. Hence, the theoretical prediction itself, for the geometric delay  $\tau_{g_0}$ , has been traditionally denoted as  $\tau_i$ , and called “instrumental delay”.

Let us estimate accuracies required to such an instrumental delay  $\tau_i$  and its rate  $\dot{\tau}_i$ .

In order to get a white fringe near the peak of the bandwidth pattern, a difference  $\Delta\tau_g$  between the actual geometric delay  $\tau_{g_0}$  and the predicted instrumental delay  $\tau_i$ , which we call hereafter “residual delay”:

$$\Delta\tau_g = \tau_{g_0} - \tau_i, \quad (219)$$

must be kept well smaller than the coherence interval  $\Delta\tau_B = 2/B$ , where  $B$  is an observing bandwidth:

$$\Delta\tau_g \ll \Delta\tau_B = \frac{2}{B}. \quad (220)$$

Therefore, the accuracy of the instrumental delay must be much better than 1  $\mu\text{sec}$  when  $B = 2 \text{ MHz}$ , and much better than 1 nsec when  $B = 2 \text{ GHz}$ , as Table 1 shows. We now compare these required accuracies with maximum delay values  $\tau_{g_{max}}$ , estimated above for 300 m baseline connected-element radio interferometer (CERI), and for VLBI. Table 3 shows relative accuracy, in terms of  $\Delta\tau_g/\tau_{g_{max}}$ , required to the instrumental delay. The Table shows

	300 m CERI	VLBI
	$\tau_{g_{max}} = 1 \mu\text{sec}$	$\tau_{g_{max}} = 21 \text{ msec}$
$B = 2 \text{ MHz}$ ( $\Delta\tau_g \ll 1 \mu\text{sec}$ )	$\ll 1$	$\ll 5 \times 10^{-5}$
$B = 2 \text{ GHz}$ ( $\Delta\tau_g \ll 1 \text{ nsec}$ )	$\ll 10^{-3}$	$\ll 5 \times 10^{-8}$

Table 3: Relative accuracy of  $\Delta\tau_g/\tau_{g_{max}}$  required to the instrumental delay.

that the required accuracy is rather high, for VLBI.

On the other hand, in order to carry out integration of the multiplier output in a correlator, for a duration of time sufficient to get high enough  $S/N$  ratio, we must apply an accurate theoretical model  $\tau_i(t)$  to compensate for time variation of the geometric delay  $\tau_{g_0}$ . If integration time is  $\tau_a$  and observing frequency is  $\nu$ , a requirement to  $\Delta\dot{\tau}_g = (\dot{\tau}_{g_0} - \dot{\tau}_i)$  for successful integration, is traditionally given by

$$2\pi\nu\Delta\dot{\tau}_g\tau_a \leq 1. \quad (221)$$

This requirement corresponds to a condition that an accumulated change of the phase of the cross-power spectrum of voltage signals, such as shown in equation (213), or of the phase in cosine terms of the expected correlation in equation (214), does not exceed 1 radian during the integration time  $\tau_a$ . Table 4 shows required accuracy of the residual delay rate  $\Delta\dot{\tau}_g$ , according to

	300 m CERI	VLBI
	$\tau_a = 1000 \text{ s}, \dot{\tau}_{g_{max}} = 70 \text{ ps/s}$	$\tau_a = 1 \text{ s}, \dot{\tau}_{g_{max}} = 3.1 \mu\text{s/s}$
$\nu = 10 \text{ GHz}$	$\leq 1.6 \times 10^{-2} \text{ ps/s}$ ( $\leq 2.3 \times 10^{-4}$ )	$\leq 16 \text{ ps/s}$ ( $\leq 5.2 \times 10^{-6}$ )
$\nu = 100 \text{ GHz}$	$\leq 1.6 \times 10^{-3} \text{ ps/s}$ ( $\leq 2.3 \times 10^{-5}$ )	$\leq 1.6 \text{ ps/s}$ ( $\leq 5.2 \times 10^{-7}$ )

Table 4: Required accuracy of  $\Delta\dot{\tau}_g$  and relative accuracy of  $\Delta\dot{\tau}_g/\dot{\tau}_{g_{max}}$  (in parentheses) for a 300 m baseline CERI with integration time  $\tau_a = 1000 \text{ s}$  and maximum delay rate  $\dot{\tau}_{g_{max}} = 70 \text{ ps/s}$ , and a VLBI with integration time  $\tau_a = 1 \text{ s}$  and maximum delay rate  $\dot{\tau}_{g_{max}} = 3.1 \mu\text{s/s}$ .

equation (221), and its ratio to the maximum delay rate, estimated above, for a 300 m baseline CERI with a typical integration time  $\tau_a = 1000 \text{ s}$ , and a VLBI with a typical hardware integration time with a VLBI correlator  $\tau_a = 1 \text{ s}$ , at two cases of observing frequency,  $\nu = 10 \text{ GHz}$  and  $\nu = 100 \text{ GHz}$ .

The required accuracies are fairly high, especially in VLBI. Therefore, theoretical prediction of the instrumental delay is usually based on state-of-the-art geophysical and astronomical models of station coordinates, radio source coordinates, and irregularities in the rotational motion of the Earth.

### 2.3.5 Insertion of Instrumental Delay at IF Band

Let us consider a case, when a time-variable instrumental delay  $\tau_i$  is inserted in the IF-band signal transmission system of antenna 2, as illustrated in Figure 37.

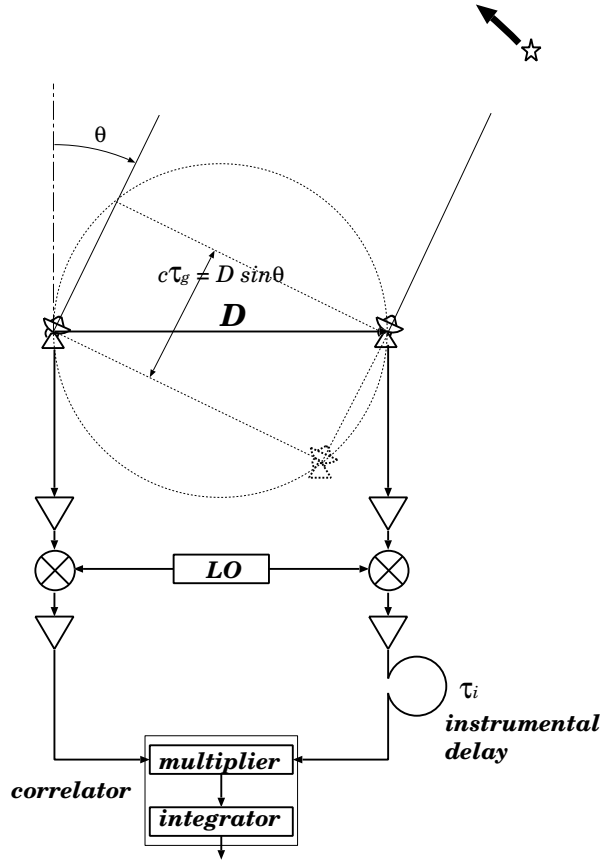


Figure 37: Time-variable instrumental delay inserted at IF-band.

After the insertion of the delay circuit, IF voltage signal  $v'_{I2}(t)$ , and its Fourier transform  $\tilde{v}'_{I2}(\omega)$ , are changed to

$$v'_{I2}(t) = v_{I2}(t - \tau_i), \quad \text{and, therefore,} \quad \tilde{v}'_{I2}(\omega) = \tilde{v}_{I2}(\omega) e^{-i\omega\tau_i}, \quad (222)$$

where  $v_{I2}(t)$ , and  $\tilde{v}_{I2}(\omega)$ , correspond to the IF voltage signal before the instrumental delay. We again used the shift theorem given in equation (68), for deriving equation (222).

Following discussions in Subsection 2.3.3, we take a cross-correlation of Fourier transforms  $\tilde{v}_{I1}(\omega)$  and  $\tilde{v}'_{I2}(\omega)$  of IF voltage signals, to obtain

$$\langle \tilde{v}_{I1}(\omega) \tilde{v}'_{I2}(\omega') \rangle = \langle \tilde{v}_{I1}(\omega) \tilde{v}_{I2}^*(\omega') \rangle e^{i\omega'\tau_i}. \quad (223)$$

Since the IF signals  $v_{I1}(t)$  and  $v'_{I2}(t)$ , as well as  $v_{I1}(t)$  and  $v_{I2}(t)$ , are assumed to be jointly stationary random processes, the cross-correlations of their Fourier transforms and cross-power spectra are related to each other, by equation (83), as:

$$\begin{aligned} \langle \tilde{v}_{I1}(\omega) \tilde{v}'_{I2}(\omega') \rangle &= 2\pi S_{v_{I1}v'_{I2}}(\omega) \delta(\omega - \omega'), \\ \langle \tilde{v}_{I1}(\omega) \tilde{v}_{I2}^*(\omega') \rangle &= 2\pi S_{v_{I1}v_{I2}}(\omega) \delta(\omega - \omega'). \end{aligned} \quad (224)$$

Comparing equations (223) and (224), we see that the cross-power spectrum  $S_{v_{I1}v'_{I2}}(\omega)$  of the IF voltage signal  $v_{I1}(t)$  of antenna 1 and the delay-inserted IF voltage signal  $v'_{I2}(t)$  of antenna 2, and the cross-power spectrum  $S_{v_{I1}v_{I2}}(\omega)$  of the IF voltages without delay insertion, are related to each other as:

$$S_{v_{I1}v'_{I2}}(\omega) = S_{v_{I1}v_{I2}}(\omega) e^{i\omega\tau_i}. \quad (225)$$

Inserting equation (197) to this equation, we have

$$\begin{aligned} &S_{v_{I1}v'_{I2}}(\omega) \\ &= \frac{1}{4} A_0 \{ e^{-i[\omega_{LO}\tau_{g0} + \omega\Delta\tau_g + \phi_{LO1} - \phi_{LO2}]} \mathcal{V}(\omega_{LO} + \omega) H_1(\omega) H_2^*(\omega) \\ &\quad + e^{i[\omega_{LO}\tau_{g0} - \omega\Delta\tau_g + \phi_{LO1} - \phi_{LO2}]} \mathcal{V}^*(\omega_{LO} - \omega) H_1^*(-\omega) H_2(-\omega) \}, \end{aligned} \quad (226)$$

where, again,  $\Delta\tau_g = \tau_{g0} - \tau_i$  is the residual delay. Contrary to equation (213), which describes the effect of the delay insertion at RF-band, we cannot here completely compensate for the geometric delay  $\tau_{g0}$ , even if we insert an instrumental delay which is exactly equal to the geometric delay  $\tau_i = \tau_{g0}$ . In fact, a term  $\omega_{LO}\tau_{g0}$  is still left uncompensated in the exponential functions of equation (226).

In order to see this point more clearly, let us derive the expected correlation  $R_{v_{I1}v'_{I2}}(0)$ , as we did in equation (207), assuming again a rectangular filter, given in equation (205), and constant visibility over receiving bandwidth, given in equation (206). Since everything is the same as given in

equation (207), except for a coefficient of  $\omega$  term in the exponential functions, namely  $\omega\Delta\tau_g$  instead of  $\omega\tau_{g0}$ , we obtain the result of integration:

$$\begin{aligned}
R_{v_{I1}v'_{I2}}(0) &= \frac{A_0GB |\mathcal{V}| \sin(\pi B\Delta\tau_g)}{2 \pi B\Delta\tau_g} \\
&\times [\cos(\omega_{LO}\tau_{g0} + \omega_I\Delta\tau_g + \phi_{LO1} - \phi_{LO2} - \Phi_v) \\
&+ \cos(\omega_{LO}\tau_{g0} - \omega_I\Delta\tau_g + \phi_{LO1} - \phi_{LO2} - \Phi_v)],
\end{aligned} \tag{227}$$

where  $\omega_I$  is the IF band center frequency, which is similar to equation (208), except in the argument of sinc function and in the coefficient of  $\omega_I$  term in cosine functions.

It is evident, from this equation, that insertion of an instrumental delay  $\tau_i$ , which is equal to the geometric delay  $\tau_{g0}$ , at IF-band, enables us to detect a white fringe at the center of the coherence interval. However,  $\omega_{LO}\tau_{g0}$  terms in arguments of cosine functions are left uncompensated, which will cause enormously rapid oscillations of the expected correlation. Therefore, insertion of an instrumental delay at IF-band can perform the delay tracking, **but not** the fringe stopping.

### 2.3.6 Separation of Delay Tracking and Fringe Stopping Due to Frequency Conversion

The reason, why the insertion of the instrumental delay at IF-band can perform only the delay tracking, but not the fringe stopping, may be easily understood by examining Figure 38, which illustrates a time variation of the phase spectrum of IF voltage signals shown in Figure 33, in a particular case of a single-sideband reception of USB component.

Let us consider phase spectra in cross-power spectra of voltage signals without delay insertion, and compare the phase spectrum in IF-band with the one in RF band. In doing so, we ignore minor phase terms, such as LO initial phase, visibility phase, and phase of bandpass characteristics, which figure in equation (200), leaving only the main term due to the geometric delay.

Then, the phase spectrum in RF-band is a straight line crossing the origin, with inclination equal to the geometric delay  $\tau_{g0}$ , as shown in equation (103) and Figure 19 for a simple interferometer model, or in equations (168), and (177), for a more realistic interferometer.

However, after the frequency conversion, the phase spectrum in the IF-band no longer crosses the origin, since the frequency conversion shifts the

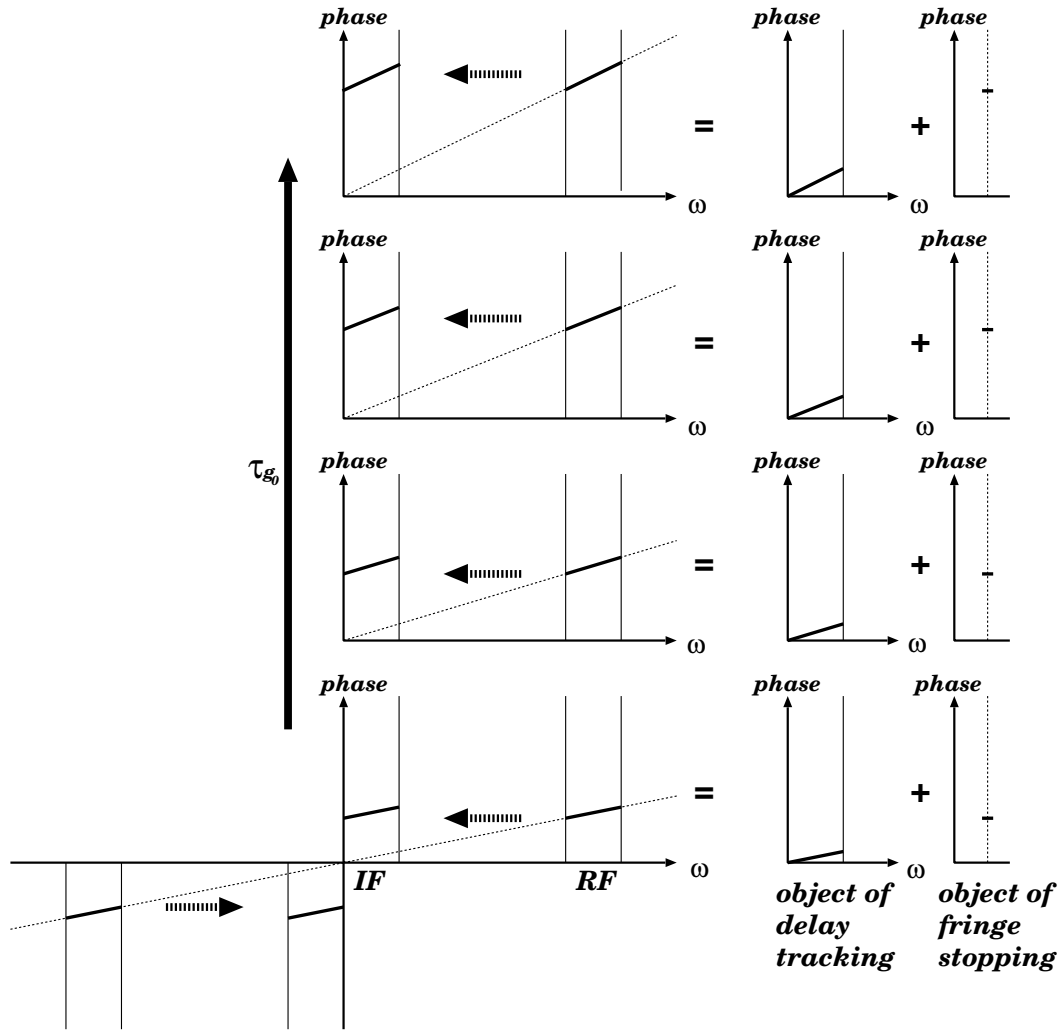


Figure 38: Necessity of fringe stopping, besides delay tracking in IF-band. We assume here a USB single-sideband reception, and show only positive frequency range of the phase spectrum, except in the bottom panel.

band-limited spectrum at RF-band to IF band without changing its shape, as shown in Figures 32, 33, and 38.

Therefore, the frequency converted phase spectrum in IF-band is now represented by a sum of two components, namely an inclined straight line  $\omega\tau_{g_0}$ , crossing the origin, **plus** a frequency-independent phase shift equal to  $\omega_{LO}\tau_{g_0}$ , where  $\omega_{LO}$  is the LO frequency, as illustrated in the right panels of Figure 38 and in equation (200). This phase shift rapidly changes in time, with the speed as high as several tens kHz (as we saw in the example of an intercontinental VLBI observation with 22 GHz), due to the diurnal variation of the geometric delay  $\tau_{g_0}$ .

The insertion of the instrumental delay at the IF-band compensates for the first component, i.e. reduces the phase slope across the frequency band to nearly zero, and thus makes it possible to get a white fringe in the middle of the coherence interval, as evident from equation (208). However, the instrumental delay in the IF-band does not compensate for the second component at all. Therefore, we still need to compensate for the rapid phase shift in the second component, by somehow controlling the interferometer phase. This operation is the “fringe stopping”, which is separated from the “delay tracking” after the frequency conversion.

### 2.3.7 Actual Implementations of Delay Tracking

In early history of radio interferometry, analog delay cables, as schematically

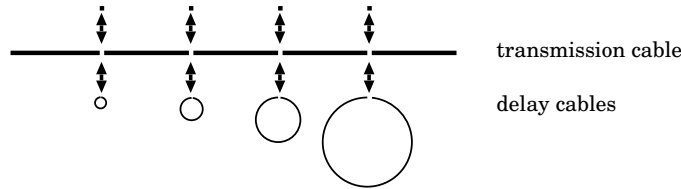


Figure 39: Analog delay cables used for delay tracking in early history of radio interferometry.

illustrated in Figure 39, were used for delay tracking.  $N$  delay cables with lengths  $\tau_0, 2\tau_0, 4\tau_0, 8\tau_0, \dots, 2^{N-1}\tau_0$ , were mechanically inserted into, and removed from, a signal transmission cable of an interferometer, to realize a time variable instrumental delay  $\tau_i$  with a range of variation:  $\tau_0 \leq \tau_i \leq (2^N - 1)\tau_0$ . Of course, the longest delay cable must have a length as large as about a half of baseline length of the interferometer. Therefore, such

analog delay cables could be used for connected–element interferometers with baseline lengths of several hundreds meters, but definitely not for VLBI.

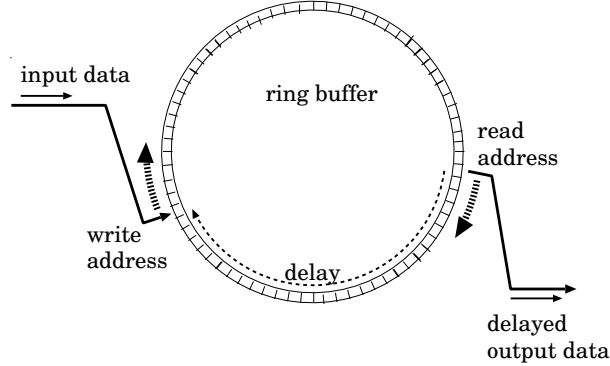


Figure 40: A “ring buffer” used for digital delay tracking.

Recently, most of radio interferometers, including VLBI, use digital delay circuits for delay tracking. In order to use this technique, data signal is first digitized, and then fed to a bulk memory, which is a kind of “ring buffer”, schematically shown in Figure 40.

Data are written to, and read from, the ring buffer at different addresses, and these write and read addresses are incremented by one at each “clock timing pulse” of digital circuit. An interval of successive clock timing pulses corresponds to a sampling interval  $t_s$  of digitization of the data. Thus, if the difference between the write and read addresses in the ring buffer is  $n$ , an instrumental delay equal to  $nt_s$  is realized in this way. And further shifting the write (or read) address periodically, once per a certain number of clock timing pulses, we can vary this instrumental delay in time. We will examine this digital delay tracking in more detail, when we will discuss VLBI correlators.

### 2.3.8 Actual Implementations of Fringe Stopping

In connected–element interferometers, the fringe stopping is often carried out by actively controlling the initial phases  $\phi_{LO1}$  and  $\phi_{LO2}$  of the LO reference signals, as illustrated in Figure 41, so that

$$\phi_{LO1}(t) - \phi_{LO2}(t) = -\omega_{LO} \tau_i(t) + \psi_{LO1} - \psi_{LO2}, \quad (228)$$

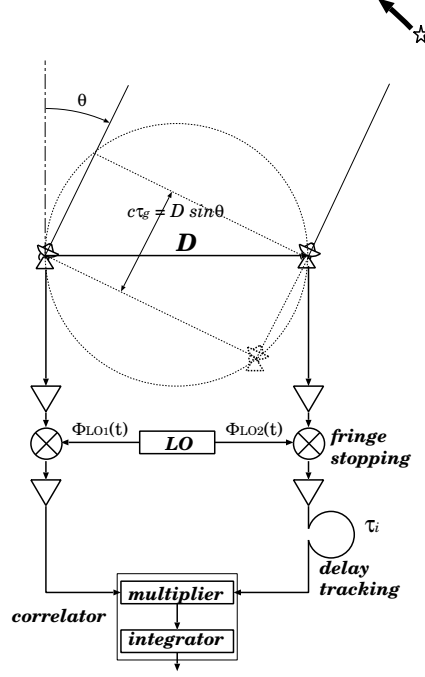


Figure 41: Fringe stopping by active control of LO initial phases.

where  $\psi_{LO1} - \psi_{LO2}$  is a nearly constant part of the difference of the initial phases of the LO signals, and  $\tau_i$  is the instrumental delay, i.e., the theoretical prediction of the geometric delay  $\tau_{g0}$ .

Assuming quasi-static LO initial phases, similarly to what we did in subsection 2.1.8 for the geometric delay, we can just insert equation (228) to equation (226) for the cross-power spectrum of IF voltages, and to equation (227) for the expected correlation in the case of a continuum flat spectrum source and rectangular filters, after the delay tracking at IF-band. Then, we obtain the cross-power spectrum of IF voltages:

$$\begin{aligned}
 S_{v_{I1}v'_{I2}}^f(\omega) &= \frac{1}{4} A_0 \{ e^{-i[\omega_{LO} \Delta\tau_g + \omega \Delta\tau_g + \psi_{LO1} - \psi_{LO2}]} \mathcal{V}(\omega_{LO} + \omega) H_1(\omega) H_2^*(\omega) \\
 &\quad + e^{i[\omega_{LO} \Delta\tau_g - \omega \Delta\tau_g + \psi_{LO1} - \psi_{LO2}]} \mathcal{V}^*(\omega_{LO} - \omega) H_1^*(-\omega) H_2(-\omega) \},
 \end{aligned} \tag{229}$$

and expected correlation:

$$R_{v_{I1}v'_{I2}}^f(0) = \frac{A_0 G B |\mathcal{V}| \sin(\pi B \Delta\tau_g)}{2 \pi B \Delta\tau_g}$$

$$\begin{aligned}
& \times [\cos(\omega_{LO}\Delta\tau_g + \omega_I\Delta\tau_g + \psi_{LO1} - \psi_{LO2} - \Phi_v) \\
& + \cos(\omega_{LO}\Delta\tau_g - \omega_I\Delta\tau_g + \psi_{LO1} - \psi_{LO2} - \Phi_v)],
\end{aligned}
\tag{230}$$

respectively.

Now we can stop the rapid phase changes in the cross-power spectrum, as well as in the expected correlation, provided that we can always keep the residual delay to be nearly zero:

$$\Delta\tau_g = \tau_{g\{0\}} - \tau_i \cong 0.$$

Note that this active control of LO initial phases can stop the phase changes both in USB and LSB components of the cross-power spectrum and expected correlation of IF voltages, as evidenced by equations (229) and (230). In particular, arguments of first and second cosine terms in the RHS of equation (230), which show USB and LSB contributions, respectively, are both stopped by this operation.

Another method for fringe stopping, which has been applied to VLBI digital correlators, in particular, uses multiplication of a sinusoidal function of time to an IF voltage, as shown in Figure 42.

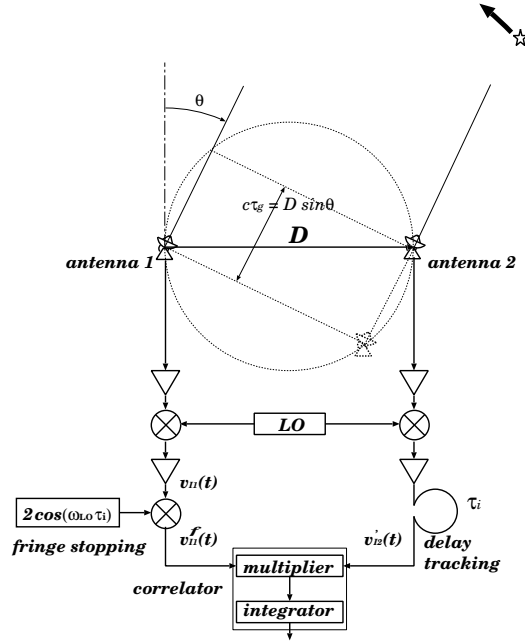


Figure 42: Fringe stopping by multiplication of a sinusoidal function.

In this method, a sinusoidal function

$$2 \cos(\omega_{LO}\tau_i), \quad (231)$$

where  $\omega_{LO}$  is the LO frequency, and  $\tau_i$  is the theoretically predicted instrumental delay, is multiplied to IF voltage  $v_{I1}(t)$  of antenna 1.

Assuming again that  $\omega_{LO}\tau_i$  is a quasi-static quantity, we obtain for a new IF voltage  $v_{I1}^f(t)$  of antenna 1 after the multiplication of  $2 \cos(\omega_{LO}\tau_i)$ :

$$v_{I1}^f(t) = v_{I1}(t)2 \cos(\omega_{LO}\tau_i) = v_{I1}(t)(e^{i\omega_{LO}\tau_i} + e^{-i\omega_{LO}\tau_i}), \quad (232)$$

and for its Fourier transform  $\tilde{v}_{I1}^f(\omega)$ :

$$\tilde{v}_{I1}^f(\omega) = \tilde{v}_{I1}(\omega)(e^{i\omega_{LO}\tau_i} + e^{-i\omega_{LO}\tau_i}), \quad (233)$$

where  $\tilde{v}_{I1}^f(\omega)$  is a Fourier transform of  $v_{I1}(t)$ . Then we have a cross-correlation of Fourier transforms of IF voltages:

$$\langle \tilde{v}_{I1}^f(\omega) \tilde{v}_{I2}^{\prime*}(\omega') \rangle = \langle \tilde{v}_{I1}(\omega) \tilde{v}_{I2}^{\prime*}(\omega') \rangle (e^{i\omega_{LO}\tau_i} + e^{-i\omega_{LO}\tau_i}), \quad (234)$$

where  $\tilde{v}_{I2}'(\omega)$  is the IF voltage of antenna 2 after the delay insertion. Assuming jointly stationary random processes, we obtain for a cross-power spectrum of IF voltages  $v_{I1}^f(t)$  and  $v_{I2}'(t)$ :

$$S_{v_{I1}^f v_{I2}'}(\omega) = S_{v_{I1} v_{I2}'}(\omega)(e^{i\omega_{LO}\tau_i} + e^{-i\omega_{LO}\tau_i}), \quad (235)$$

where  $S_{v_{I1} v_{I2}'}(\omega)$  is the cross-power spectrum of IF voltages  $v_{I1}(t)$  and  $v_{I2}'(t)$ , which is given in equation (226). Then, inserting equation (226) to equation (235), we have

$$\begin{aligned} S_{v_{I1}^f v_{I2}'}(\omega) &= \frac{1}{4} A_0 \\ &\times \{ e^{-i[\omega_{LO} \Delta\tau_g + \omega \Delta\tau_g + \phi_{LO1} - \phi_{LO2}]} \mathcal{V}(\omega_{LO} + \omega) H_1(\omega) H_2^*(\omega) \\ &\quad + e^{-i[\omega_{LO}(\tau_{g0} + \tau_i) + \omega \Delta\tau_g + \phi_{LO1} - \phi_{LO2}]} \mathcal{V}(\omega_{LO} + \omega) H_1(\omega) H_2^*(\omega) \\ &\quad + e^{i[\omega_{LO} \Delta\tau_g - \omega \Delta\tau_g + \phi_{LO1} - \phi_{LO2}]} \mathcal{V}^*(\omega_{LO} - \omega) H_1^*(-\omega) H_2(-\omega) \\ &\quad + e^{i[\omega_{LO}(\tau_{g0} + \tau_i) - \omega \Delta\tau_g + \phi_{LO1} - \phi_{LO2}]} \mathcal{V}^*(\omega_{LO} - \omega) H_1^*(-\omega) H_2(-\omega) \}, \end{aligned} \quad (236)$$

where  $\Delta\tau_g = \tau_{g0} - \tau_i$ . In first and third terms in the RHS of this equation, rapid oscillations of exponential terms are almost stopped, as long as  $\tau_i \cong \tau_{g0}$ . But, in second and fourth terms in the RHS, even more rapid oscillations with almost doubled frequency  $\omega_{LO}(\tau_{g0} + \tau_i)$  remain. Contributions of these rapidly oscillating terms almost disappear when the product of IF voltages

are integrated for some duration of time in a correlator. Therefore, we have an “effective” cross-power spectrum of IF voltages,

$$\begin{aligned}
 S_{v_{I1} v_{I2}}^f(\omega) &= \frac{1}{4} A_0 \\
 &\times \{ e^{-i[\omega_{LO} \Delta\tau_g + \omega \Delta\tau_g + \phi_{LO1} - \phi_{LO2}]} \mathcal{V}(\omega_{LO} + \omega) H_1(\omega) H_2^*(\omega) \\
 &\quad + e^{i[\omega_{LO} \Delta\tau_g - \omega \Delta\tau_g + \phi_{LO1} - \phi_{LO2}]} \mathcal{V}^*(\omega_{LO} - \omega) H_1^*(-\omega) H_2(-\omega) \},
 \end{aligned}
 \tag{237}$$

which has essentially the same form as the one given in equation (229).

Note that, in this simple method of multiplication of a sinusoidal function to an IF voltage, phase drifts are stopped again in both USB and LSB components.

## 2.4 Correlator Outputs

### 2.4.1 Multiplier and Integrator

As we saw earlier, a key component of a correlator in an interferometer is a device with two inputs and one output, which is composed of a multiplier and an integrator (Figure 43). The expected correlation, which is the sta-

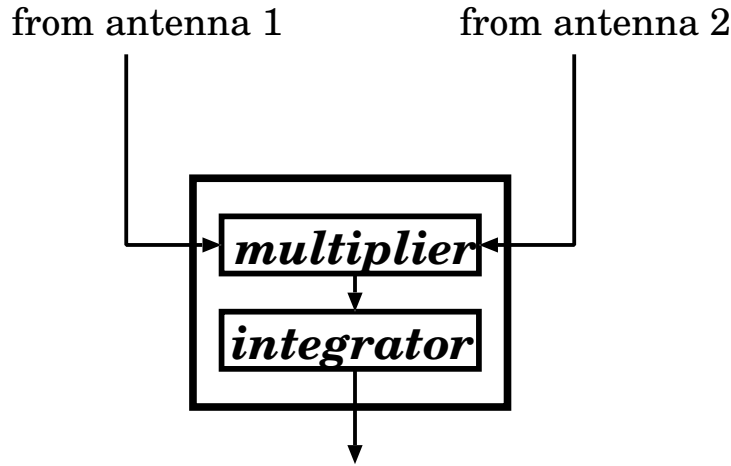


Figure 43: Multiplier and integrator as a key component of a correlator.

tistical expectation of the product of the voltage signals, must be contained as a signal component in a multiplier output of such a correlator. Since the expected correlation does not rapidly oscillate any more after the delay tracking and fringe stopping, we can integrate (time-average) the multiplier

output during some time to suppress the noise component, and detect this nearly constant expected correlation itself with a high signal to noise ratio. Therefore, an output of an actual correlator can be well approximated by the expected correlation after the delay tracking and fringe stopping. The expected correlation is easily derived from the cross-power spectrum (CPS) of the IF voltages by an inverse Fourier transformation, as we showed in equation (204).

Now we have slightly different notations for the CPS of IF voltages in equation (229) and in equation (237), depending on practical implementations of the fringe stopping, though they are essentially equivalent to each other. We adopt, hereafter, the expression given in equation (237), which is familiar in VLBI practice, for describing the CPS after the delay tracking and fringe stopping.

Then, the expected correlation, after the delay tracking and fringe stopping, is given by

$$R_{v_{I1}^f v_{I2}'}(0) = \frac{A_0}{4\pi} \Re \left[ e^{-i(\omega_{LO}\Delta\tau_g + \phi_{LO1} - \phi_{LO2})} \int_0^\infty \mathcal{V}(\omega_{LO} + \omega) e^{-i\omega\Delta\tau_g} H_1(\omega) H_2^*(\omega) d\omega \right. \\ \left. + e^{i(\omega_{LO}\Delta\tau_g + \phi_{LO1} - \phi_{LO2})} \int_0^\infty \mathcal{V}^*(\omega_{LO} - \omega) e^{-i\omega\Delta\tau_g} H_1^*(-\omega) H_2(-\omega) d\omega \right]. \quad (238)$$

In the special case of a continuum flat spectrum source and rectangular filters, the expected correlation will have essentially the same form as the one given in equation (230):

$$R_{v_{I1}^f v_{I2}'}(0) = \frac{A_0 G B |\mathcal{V}| \sin(\pi B \Delta\tau_g)}{2 \pi B \Delta\tau_g} \\ \times [\cos(\omega_{LO}\Delta\tau_g + \omega_I\Delta\tau_g + \phi_{LO1} - \phi_{LO2} - \Phi_v) \\ + \cos(\omega_{LO}\Delta\tau_g - \omega_I\Delta\tau_g + \phi_{LO1} - \phi_{LO2} - \Phi_v)]. \quad (239)$$

We will use expected correlations given in equations (238) and (239) as theoretical expressions of the correlator outputs.

In VLBI, no operation for delay tracking and fringe stopping is done, usually, in observing stations. Instead, they are done in VLBI correlators. Therefore, a VLBI correlator is a little more complicated than the mere multiplier and integrator, as we will see later.

### 2.4.2 Single Sideband (USB or LSB) Reception

So far, we considered a case of double sideband (DSB) reception, i.e. a case when we receive signals contained in both upper sideband (USB) and lower sideband (LSB) of LO frequency in original RF–band spectrum. In this case, the USB and LSB contributions are superposed in IF–band spectrum, as we saw earlier.

The DSB reception is not convenient for observing line spectrum sources, since different lines in USB and LSB are mixed up in the same IF spectrum. Also, the DSB reception causes additional complications in data calibrations. Therefore, in VLBI, we mostly use a single sideband (SSB), i.e., either of USB or LSB, reception.

Amplitude and phase spectra of IF voltage signals, which were shown in Figure 33 in the DSB reception case, now take simpler forms, in the SSB reception case, as shown in Figure 44.

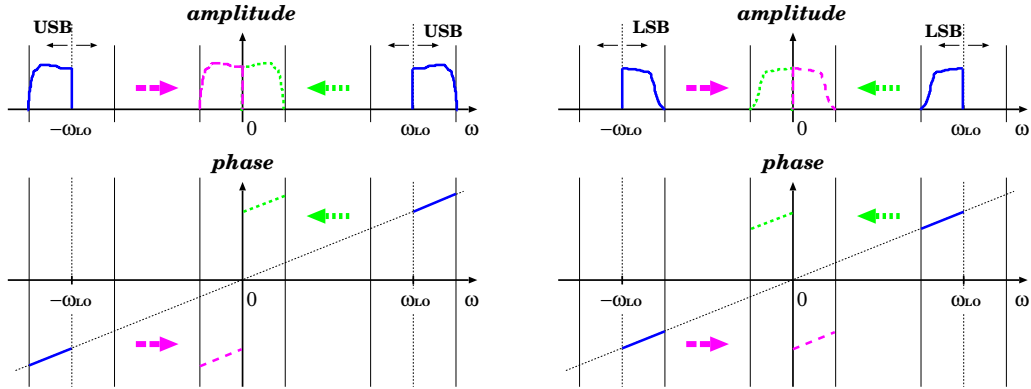


Figure 44: Amplitude and phase spectra of IF voltage signals in USB (left) and LSB (right) receptions. For simplicity, contributions of the geometric delay only are shown in the phase spectra.

Since, cross–power spectra (CPS) of IF voltages both in USB and LSB receptions are Hermitian symmetric, as illustrated in Figure 44, we do not lose generality if we confine ourselves to consider only positive frequency range ( $\omega \geq 0$ ) of the spectra.

In positive frequency range  $\omega \geq 0$ , cross–power spectra of IF voltages before the delay tracking and fringe stopping in USB and LSB receptions are given by

$$S_{v_{I1}v_{I2}}^{USB}(\omega) = \frac{1}{4} A_0 e^{-i[\omega_{LO} \tau_{g0} + \omega \tau_{g0} + \phi_{LO1} - \phi_{LO2}]} \mathcal{V}(\omega_{LO} + \omega) H_1(\omega) H_2^*(\omega), \quad (240)$$

$$S_{v_{I1}v_{I2}}^{LSB}(\omega) = \frac{1}{4} A_0 e^{i[\omega_{LO} \tau_{g0} - \omega \tau_{g0} + \phi_{LO1} - \phi_{LO2}]} \mathcal{V}^*(\omega_{LO} - \omega) H_1^*(-\omega) H_2(-\omega), \quad (241)$$

which correspond to positive frequency sides ( $\omega \geq 0$ ) of the USB and LSB spectra illustrated in Figure 44.

After the delay tracking and fringe stopping, they are reduced to

$$S_{v_{I1}v'_{I2}}^{USB}(\omega) = \frac{1}{4} A_0 e^{-i[\omega_{LO} \Delta\tau_g + \omega \Delta\tau_g + \phi_{LO1} - \phi_{LO2}]} \mathcal{V}(\omega_{LO} + \omega) H_1(\omega) H_2^*(\omega), \quad (242)$$

$$S_{v_{I1}v'_{I2}}^{LSB}(\omega) = \frac{1}{4} A_0 e^{i[\omega_{LO} \Delta\tau_g - \omega \Delta\tau_g + \phi_{LO1} - \phi_{LO2}]} \mathcal{V}^*(\omega_{LO} - \omega) H_1^*(-\omega) H_2(-\omega), \quad (243)$$

in the positive frequency range  $\omega \geq 0$ .

We can rewrite equations (240) and (241), as well as equations (242) and (243), using amplitudes and phases of the complex visibility and bandpass characteristics, which we introduced in equations (198) and (199).

Then, before the delay tracking and fringe stopping, the USB spectrum in  $\omega \geq 0$  is given by

$$S_{v_{I1}v_{I2}}^{USB}(\omega) = A_p(\omega) e^{-i\Phi_p(\omega, t)},$$

with amplitude:

$$A_p(\omega) = \frac{1}{4} A_0 | \mathcal{V}(\omega_{LO} + \omega) | | H_1(\omega) H_2^*(\omega) |,$$

and phase:

$$\Phi_p(\omega, t) = (\omega_{LO} + \omega)\tau_{g0} + \phi_{LO1} - \phi_{LO2} - \Phi_v(\omega_{LO} + \omega) - \Phi_b(\omega), \quad (244)$$

while the LSB spectrum in  $\omega \geq 0$  is given by

$$S_{v_{I1}v_{I2}}^{LSB}(\omega) = A_n(\omega) e^{-i\Phi_n(\omega, t)},$$

with amplitude:

$$A_n(\omega) = \frac{1}{4} A_0 | \mathcal{V}(\omega_{LO} - \omega) | | H_1(-\omega) H_2^*(-\omega) |,$$

and phase:

$$\Phi_n(\omega, t) = -(\omega_{LO} - \omega)\tau_{g0} - \phi_{LO1} + \phi_{LO2} + \Phi_v(\omega_{LO} - \omega) + \Phi_b(-\omega). \quad (245)$$

After the delay tracking and fringe stopping, the USB spectrum in  $\omega \geq 0$  becomes

$$S_{v'_{I1} v'_{I2}}^{USB}(\omega) = A_p(\omega) e^{-i\Delta\Phi_p(\omega, t)},$$

with amplitude:

$$A_p(\omega) = \frac{1}{4} A_0 | \mathcal{V}(\omega_{LO} + \omega) | | H_1(\omega) H_2^*(\omega) |,$$

and residual phase:

$$\Delta\Phi_p(\omega, t) = (\omega_{LO} + \omega)\Delta\tau_g + \phi_{LO1} - \phi_{LO2} - \Phi_v(\omega_{LO} + \omega) - \Phi_b(\omega), \quad (246)$$

while the LSB spectrum in  $\omega \geq 0$  becomes

$$S_{v'_{I1} v'_{I2}}^{LSB}(\omega) = A_n(\omega) e^{-i\Delta\Phi_n(\omega, t)},$$

with amplitude:

$$A_n(\omega) = \frac{1}{4} A_0 | \mathcal{V}(\omega_{LO} - \omega) | | H_1(-\omega) H_2^*(-\omega) |,$$

and residual phase:

$$\Delta\Phi_n(\omega, t) = -(\omega_{LO} - \omega)\Delta\tau_g - \phi_{LO1} + \phi_{LO2} + \Phi_v(\omega_{LO} - \omega) + \Phi_b(-\omega), \quad (247)$$

where  $\Delta\tau_g$  is the residual delay:  $\Delta\tau_g = \tau_{g0} - \tau_i$ .

### 2.4.3 Correlator Outputs in Single Sideband Reception

As we discussed earlier, correlator outputs are closely approximated by the expected correlations after the delay tracking and fringe stopping. Therefore, theoretical expressions for the correlator outputs in USB and LSB receptions are given by

$$R_{v'_{I1} v'_{I2}}^{USB}(0) = \frac{A_0}{4\pi} \Re[e^{-i(\omega_{LO}\Delta\tau_g + \phi_{LO1} - \phi_{LO2})} \int_0^\infty \mathcal{V}(\omega_{LO} + \omega) e^{-i\omega\Delta\tau_g} H_1(\omega) H_2^*(\omega) d\omega], \quad (248)$$

and

$$R_{v'_{I1} v'_{I2}}^{LSB}(0) = \frac{A_0}{4\pi} \Re[e^{i(\omega_{LO}\Delta\tau_g + \phi_{LO1} - \phi_{LO2})} \int_0^\infty \mathcal{V}^*(\omega_{LO} - \omega) e^{-i\omega\Delta\tau_g} H_1^*(-\omega) H_2(-\omega) d\omega], \quad (249)$$

respectively.

If we assume the case of rectangular filters and constant visibility, the above equations are reduced to

$$R_{v_{I1}^f v_{I2}^f}^{USB}(0) = \frac{A_0 G B |\mathcal{V}|}{2} \frac{\sin(\pi B \Delta \tau_g)}{\pi B \Delta \tau_g} \cos(\omega_{LO} \Delta \tau_g + \omega_I \Delta \tau_g + \phi_{LO1} - \phi_{LO2} - \Phi_v), \quad (250)$$

and

$$R_{v_{I1}^f v_{I2}^f}^{LSB}(0) = \frac{A_0 G B |\mathcal{V}|}{2} \frac{\sin(\pi B \Delta \tau_g)}{\pi B \Delta \tau_g} \cos(\omega_{LO} \Delta \tau_g - \omega_I \Delta \tau_g + \phi_{LO1} - \phi_{LO2} - \Phi_v). \quad (251)$$

For a more general case of an arbitrary filter shape, when the complex visibility is assumed to be constant only in each of USB and LSB receiving bandwidths, and the filters, with a passband:

$$\omega_I - \Delta\omega/2 \leq |\omega| \leq \omega_I + \Delta\omega/2,$$

are not necessarily rectangular, we have

$$\begin{aligned} & \int_0^\infty \mathcal{V}(\omega_{LO} + \omega) e^{-i\omega \Delta \tau_g} H_1(\omega) H_2^*(\omega) d\omega \\ &= \mathcal{V}(\omega_{LO} + \omega) \int_{\omega_I - \frac{\Delta\omega}{2}}^{\omega_I + \frac{\Delta\omega}{2}} e^{-i\omega \Delta \tau_g} H_1(\omega) H_2^*(\omega) d\omega \\ &= \mathcal{V}(\omega_{LO} + \omega) e^{-i\omega_I \Delta \tau_g} \int_{-\frac{\Delta\omega}{2}}^{\frac{\Delta\omega}{2}} e^{-i\omega' \Delta \tau_g} H_1(\omega_I + \omega') H_2^*(\omega_I + \omega') d\omega', \end{aligned} \quad (252)$$

in the USB reception, and

$$\begin{aligned} & \int_0^\infty \mathcal{V}^*(\omega_{LO} - \omega) e^{-i\omega \Delta \tau_g} H_1^*(-\omega) H_2(-\omega) d\omega \\ &= \mathcal{V}^*(\omega_{LO} - \omega) \int_{\omega_I - \frac{\Delta\omega}{2}}^{\omega_I + \frac{\Delta\omega}{2}} e^{-i\omega \Delta \tau_g} H_1^*(-\omega) H_2(-\omega) d\omega \\ &= \mathcal{V}^*(\omega_{LO} - \omega) e^{-i\omega_I \Delta \tau_g} \int_{-\frac{\Delta\omega}{2}}^{\frac{\Delta\omega}{2}} e^{-i\omega' \Delta \tau_g} H_1^*(-\omega_I - \omega') H_2(-\omega_I - \omega') d\omega', \end{aligned} \quad (253)$$

in the LSB reception.

Now, let us introduce “bandwidth patterns”  $\mathcal{B}_{12}$ :

$$\mathcal{B}_{12}^{USB}(B, \Delta\tau_g) = \frac{1}{4\pi} \int_{-\frac{\Delta\omega}{2}}^{\frac{\Delta\omega}{2}} e^{-i\omega'\Delta\tau_g} H_1(\omega_I + \omega') H_2^*(\omega_I + \omega') d\omega', \quad (254)$$

$$\mathcal{B}_{12}^{LSB}(B, \Delta\tau_g) = \frac{1}{4\pi} \int_{-\frac{\Delta\omega}{2}}^{\frac{\Delta\omega}{2}} e^{-i\omega'\Delta\tau_g} H_1^*(-\omega_I - \omega') H_2(-\omega_I - \omega') d\omega', \quad (255)$$

for USB reception and LSB reception, respectively. The suffix ‘12’ here accentuates that this pattern comes from bandpass characteristics of receiving systems in antennas 1 and 2. Then, if we represent complex visibilities and bandwidth patterns through their amplitudes and phases:

$$\mathcal{V}(\omega_{LO} + \omega_I) = |\mathcal{V}^U| e^{i\Phi^U_v} \quad \text{and} \quad \mathcal{V}(\omega_{LO} - \omega_I) = |\mathcal{V}^L| e^{i\Phi^L_v}, \quad (256)$$

and

$$\mathcal{B}_{12}^{USB}(B, \Delta\tau_g) = |\mathcal{B}_{12}^U| e^{i\Phi^U_B} \quad \text{and} \quad \mathcal{B}_{12}^{LSB}(B, \Delta\tau_g) = |\mathcal{B}_{12}^L| e^{i\Phi^L_B}, \quad (257)$$

equations (248) and (249) for theoretical expressions for correlator outputs are reduced to

$$R_{v_{11}^f v_{12}^f}^{USB}(0) = A_0 |\mathcal{V}^U| |\mathcal{B}_{12}^U| \cos(\omega_{LO}\Delta\tau_g + \omega_I\Delta\tau_g + \phi_{LO1} - \phi_{LO2} - \Phi_v^U - \Phi_B^U), \quad (258)$$

and

$$R_{v_{11}^f v_{12}^f}^{LSB}(0) = A_0 |\mathcal{V}^L| |\mathcal{B}_{12}^L| \cos(\omega_{LO}\Delta\tau_g - \omega_I\Delta\tau_g + \phi_{LO1} - \phi_{LO2} - \Phi_v^L + \Phi_B^L), \quad (259)$$

for USB reception and LSB reception, respectively.

#### 2.4.4 Fringe Amplitude and Fringe Phase

The above equations again show the white fringes, with bandwidth patterns in  $|\mathcal{B}_{12}|$  terms and fringe patterns in cosine terms.

In general, when a correlator output shows a sinusoidal fringe pattern  $\mathcal{A} \cos \Phi$  in the center of the coherence interval where  $\Delta\tau_g \approx 0$ , we call the amplitude  $\mathcal{A}$  of the fringe pattern the “**fringe (or correlation) amplitude**”, and the phase  $\Phi$  of the fringe pattern the “**fringe (or correlation) phase**”.

According to the theoretical expressions of correlator outputs in equations (258) and (259), theoretical expressions of fringe amplitude  $\mathcal{A}^U$  and fringe phase  $\Phi^U$  in USB reception are given by

$$\begin{aligned}\mathcal{A}^U &= A_0 |\mathcal{V}^U| |\mathcal{B}_{12}^U|, \\ \Phi^U &= \omega_{LO}\Delta\tau_g + \omega_I\Delta\tau_g + \phi_{LO1} - \phi_{LO2} - \Phi_v^U - \Phi_B^U,\end{aligned}\quad (260)$$

and theoretical expressions of fringe amplitude  $\mathcal{A}^L$  and fringe phase  $\Phi^L$  in LSB reception are given by

$$\begin{aligned}\mathcal{A}^L &= A_0 |\mathcal{V}^L| |\mathcal{B}_{12}^L|, \\ \Phi^L &= \omega_{LO}\Delta\tau_g - \omega_I\Delta\tau_g + \phi_{LO1} - \phi_{LO2} - \Phi_v^L + \Phi_B^L.\end{aligned}\quad (261)$$

In practice of interferometric observations, the fringe amplitude and fringe phase in the correlator outputs are often called as “visibility amplitude” and “visibility phase”. Strictly speaking, however, one must correct the fringe amplitude and fringe phase for the residual delay, bandwidth pattern, and other effects, in order to obtain proper visibility amplitude  $|\mathcal{V}|$  and visibility phase  $\Phi_v$  as defined in equations (165) and (166). Moreover, the fringe phase contains the residual delay  $\Delta\tau_g$  of the reference direction of the radio source, which could be a useful observable for high precision astrometry and geodesy, if one can resolve the cycle ambiguity and properly correct the atmospheric and other disturbing effects by means of a suitable phase compensation technique, while the visibility phase in equation (166) is defined to be free from the residual delay of the source reference direction. Therefore, we will henceforth distinguish the terms “fringe amplitude and phase” from the “visibility amplitude and phase”.

In the case of the rectangular filters and constant visibility, equations (258) and (259) are of course reduced to equations (250) and (251), since in this particular case,

$$\mathcal{V}(\omega_{LO} + \omega_I) = \mathcal{V}(\omega_{LO} - \omega_I) = |\mathcal{V}| e^{i\Phi_v},$$

and

$$\mathcal{B}_{12}^{USB}(B, \Delta\tau_g) = \mathcal{B}_{12}^{LSB}(B, \Delta\tau_g) = \frac{GB}{2} \frac{\sin(\pi B \Delta\tau_g)}{\pi B \Delta\tau_g}. \quad (262)$$

#### 2.4.5 Group Delay and Fringe Frequency

As we discussed so far, the delay tracking is aimed at reducing the slope of the phase spectrum in the observed bandwidth to nearly zero, thus facilitating the fringe detection in the middle of the coherence interval. Therefore, what is

needed for successful delay tracking is an accurate prediction or estimation of the phase slope, i.e. frequency derivative of the phase spectrum of the cross-power spectrum of voltage signals, which is to be used as the compensating instrumental delay. We call the frequency derivative of the phase spectrum  $\Phi(\omega, t)$  the “group delay”  $\tau_G$ :

$$\tau_G = \frac{\partial \Phi(\omega, t)}{\partial \omega}, \quad (263)$$

where  $\Phi(\omega, t)$  can be  $\Phi_p(\omega, t)$  of equation (244) in case of USB reception, or  $\Phi_n(\omega, t)$  of equation (245) in case of LSB reception. Thus, we need a good prediction or estimation of the group delay for successful delay tracking.

In an ideally simple case, the group delay is nothing but the geometric delay itself (see, for example, equation (103)). In actuality, however, equations (244) and (245) show phase terms other than the contribution of the geometric delay, which may depend on the frequency. Moreover, the phase slope may be affected by other effects as well, such as clock offsets among VLBI antennas, atmospheric propagation delays, cable delays in signal transmission systems, and so on, which we will see in discussions specific to VLBI. Furthermore, if some propagation delay is dispersive (i.e. frequency-dependent), then the phase slope will also depend on the frequency derivative of the dispersive delay. In general, the group delay is a quantity which includes all the effects mentioned above.

On the other hand, the fringe stopping is an operation to compensate the rapid time variation of the interferometer phase. This is done for the purpose to integrate the correlation results for some duration of time, which is sufficient to detect the white fringe with a good enough signal to noise ratio. Therefore, what is needed for successful fringe stopping is an accurate prediction or estimation of the time derivative of the phase spectrum of the correlated signals, which can be used for compensating the rapid phase shift. We call the time derivative of the phase spectrum  $\Phi(\omega, t)$  the “fringe frequency” or “fringe rate”, and denote it as  $F_r$ :

$$F_r = \frac{\partial \Phi(\omega, t)}{\partial t}, \quad (264)$$

where  $\Phi(\omega, t)$  can be  $\Phi_p(\omega, t)$  of equation (244) in case of USB reception, or  $\Phi_n(\omega, t)$  of equation (245) in case of LSB reception, as before. Thus, we need a good prediction or estimation of the fringe frequency for successful fringe stopping.

Again, the actual fringe frequency may include time derivatives of the clock offsets, propagation delays, cable delays, and other terms, besides the time derivative of the geometric delay.

For connected–element radio interferometers (CERI), a predicted instrumental delay  $\tau_i$ , usually based on the geometric delay model only, is accurate enough to make  $\Delta\tau_{g_0}$  almost zero. Therefore, the fringe is normally found within the coherence interval, and the correlated signals can be integrated for sufficiently long time, by applying the delay tracking and fringe stopping, based on the prediction.

In VLBI, accuracies required to delay tracking and fringe stopping are much higher than in CERI, as we saw earlier. Therefore, the theoretical prediction alone is usually not sufficient for obtaining fringes. Hence, one must first perform a special search for estimating the group delay and fringe frequency values, using the observed VLBI data themselves. If the search is successful, then the delay tracking and fringe stopping are done satisfactorily, and one can finally detect the correlation peak and the white fringe.

This is an additional labor imposed to VLBI, compared with CERI. But this “necessity” had led to the birth and the remarkable success of the geodetic VLBI.

#### 2.4.6 Complex Correlator

When we achieve a complete fringe stopping, the residual delay is kept always zero ( $\Delta\tau_g = 0$ ), and, therefore, the correlator outputs given in equations (258) and (259) become constants in time. For example, in case of USB reception, we have

$$R_{v'_{11}v'_{12}}^{USB}(0) = A_0 | \mathcal{V}^U | | \mathcal{B}_{12}^U | \cos(\phi_{LO1} - \phi_{LO2} - \Phi_v^U - \Phi_B^U), \quad (265)$$

where argument of cosine function (fringe phase) is constant in time.

This is not very convenient for further analysis, since, if the correlator output is just a constant, we cannot separately obtain the fringe amplitude and the fringe phase.

In order to get rid of this inconvenience, we use so–called complex correlators. Complex correlators are two sets of multipliers and integrators which provide two correlator outputs of the same signals, but with fringe phases different to each other by 90 degrees.

Figure 45 shows a design of a complex correlator which uses a quadrature phase–shift network. The quadrature phase–shift network is a special electric circuit which changes phases of all frequency components of a signal by 90 degrees. Then, in case of the USB reception, an output of “real correlator”  $\mathcal{R}^r$  will have a form such as given in equation (265), i.e.,

$$\mathcal{R}^r = A_0 | \mathcal{V} | | \mathcal{B}_{12} | \cos(\phi_{LO1} - \phi_{LO2} - \Phi_v - \Phi_B), \quad (266)$$

while an output of “imaginary correlator”  $\mathcal{R}^i$  will be 90 degrees shifted in phase, i.e.,

$$\mathcal{R}^i = -A_0 | \mathcal{V} | | \mathcal{B}_{12} | \sin(\phi_{LO1} - \phi_{LO2} - \Phi_v - \Phi_B). \quad (267)$$

Thus, it will be easy to separate fringe amplitude and fringe phase, by using outputs of these two correlators.

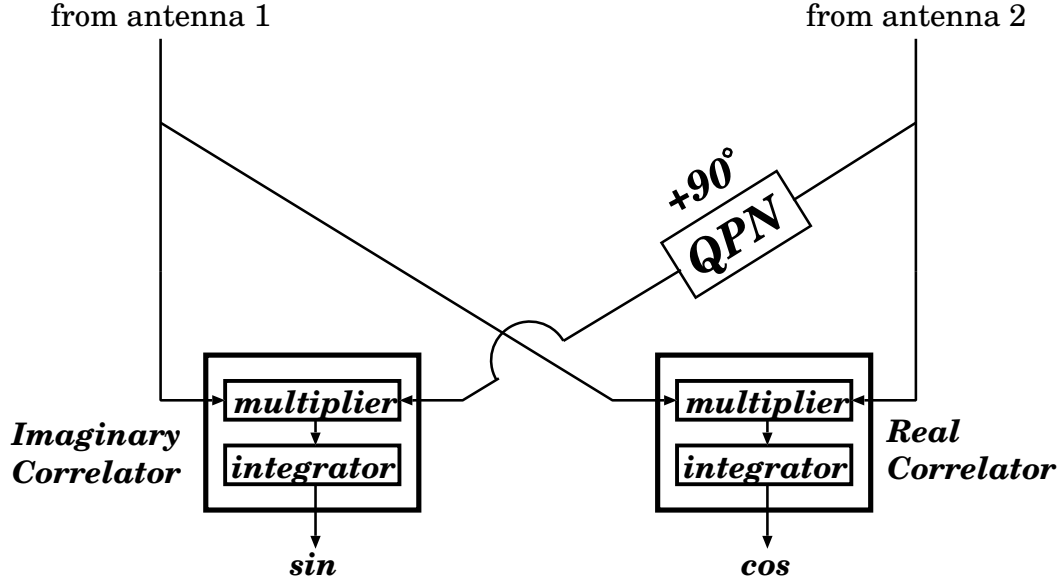


Figure 45: A complex correlator using a quadrature phase-shift network.

For a more general case when fringe is almost stopped but still a small residual delay  $\Delta\tau_g$  remains, we have, from equation (258),

$$\mathcal{R}^r = A_0 | \mathcal{V} | | \mathcal{B}_{12} | \cos((\omega_{LO} + \omega_I)\Delta\tau_g + \phi_{LO1} - \phi_{LO2} - \Phi_v - \Phi_B), \quad (268)$$

and

$$\mathcal{R}^i = -A_0 | \mathcal{V} | | \mathcal{B}_{12} | \sin((\omega_{LO} + \omega_I)\Delta\tau_g + \phi_{LO1} - \phi_{LO2} - \Phi_v - \Phi_B), \quad (269)$$

for real and imaginary correlator outputs in USB reception.

Instead of the quadrature phase-shift network, we can use two LO reference signals in the frequency conversion, shifted in phase by 90 degrees.

Also, we can use multiplications of cosine and sine functions of  $\omega_{LO}\tau_i$  in the fringe stopping, as we will see in discussions of VLBI correlators.

### 2.4.7 Projected Baseline

We discussed earlier the fringe pattern in the case when we observe a source at a direction nearly perpendicular to the interferometer baseline. When the delay tracking and fringe stopping are properly performed, however, we are in position to catch a source, within the coherence interval, at any direction of the sky.

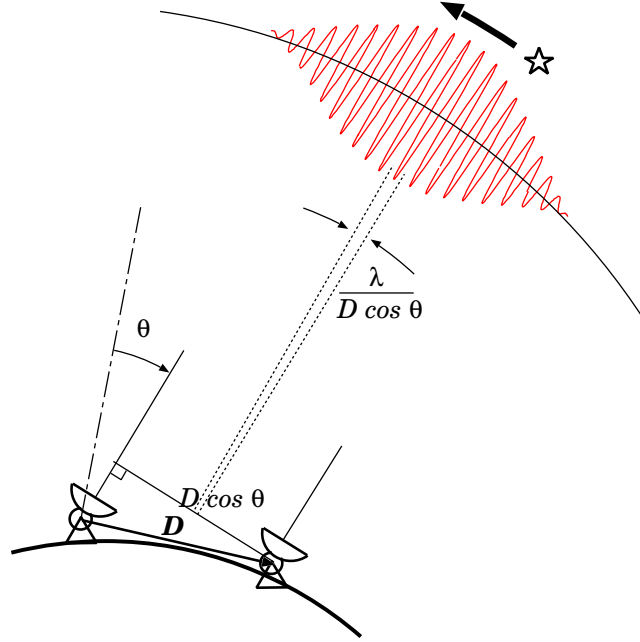


Figure 46: Fringe spacing at arbitrary direction of the sky with projected baseline length  $D \cos \theta$ .

In such a case, our interferometer is equivalent to the one having a baseline length  $D \cos \theta$  in Figure 46. This “effective baseline length viewed from the source” is called “projected baseline length”, since this is a length of a baseline projected onto a plane perpendicular to the source direction. The fringe pattern is now determined by the projected baseline, as illustrated in Figure 46. Therefore, the fringe pattern now varies in time, as we track a source, which moves in the sky changing the angle  $\theta$  due to the diurnal motion of the Earth. In particular, the fringe spacing in the sky is now expressed as

$$\Delta\theta_F = \frac{\lambda}{D \cos \theta}, \quad (270)$$

and also varies in time.

### 3 Source Structure and Correlated Flux Density

We saw earlier how a radio source structure (or, more specifically, intensity distribution) is related to an observable of radio interferometry, the complex visibility. Using this relationship, we can infer the radio source structure by analyzing observed complex visibilities.

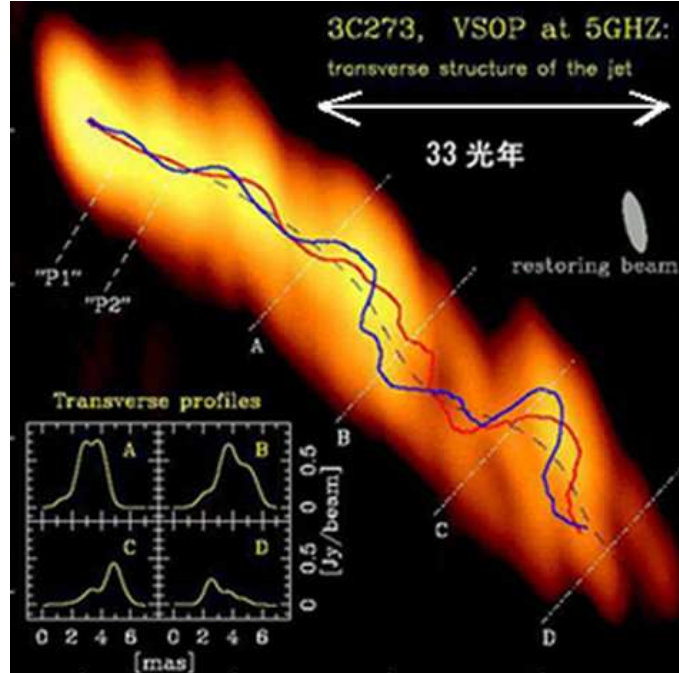


Figure 47: Helical structure of a jet ejected from a distant quasar 3C273 revealed by a VSOP (VLBI Space Observatory Program) observation.

This is the basis of an extensive field on the image synthesis of astronomical objects with radio interferometry, which has enabled us to produce high-resolution images of astronomical objects billions of light years away (as an example, see Figure 47). However, details of the image synthesis techniques are out of scope of this note. Here, we confine ourselves to a general formulation of the problem and a consideration of the effect of the finite angular size of the source on the correlator output.

### 3.1 Basic Equations of Image Synthesis

#### 3.1.1 Complex Visibility as an Observable

A complex correlator yields the fringe amplitude and fringe phase for an observed radio source, which enable us to derive the complex visibility of the source. In fact, in equations (268) and (269), we gave theoretical expressions for outputs of a complex correlator in a case of the USB reception:

$$\begin{aligned}\mathcal{R}^r &= A_0 |\mathcal{V}| |\mathcal{B}_{12}| \cos((\omega_{LO} + \omega_I)\Delta\tau_g + \phi_{LO1} - \phi_{LO2} - \Phi_v - \Phi_B), \\ \mathcal{R}^i &= -A_0 |\mathcal{V}| |\mathcal{B}_{12}| \sin((\omega_{LO} + \omega_I)\Delta\tau_g + \phi_{LO1} - \phi_{LO2} - \Phi_v - \Phi_B).\end{aligned}$$

Therefore, theoretical expressions of fringe amplitude and fringe phase are given by equation (260):

$$A = A_0 |\mathcal{V}| |\mathcal{B}_{12}|,$$

and

$$\Phi = (\omega_{LO} + \omega_I)\Delta\tau_g + \phi_{LO1} - \phi_{LO2} - \Phi_v - \Phi_B,$$

respectively.

Consequently, if we achieve a high enough  $S/N$  ratio, and if we are allowed to calibrate the observed fringe amplitude and fringe phase for geometric mean of effective apertures  $A_0$ , the bandwidth pattern  $|\mathcal{B}_{12}| e^{i\Phi_B}$ , the residual delay  $\Delta\tau_g$ , and the difference in LO initial phases  $\phi_{LO1} - \phi_{LO2}$ , on the basis of suitable measurements or estimations, we can derive the complex visibility of the observed source:

$$\mathcal{V}(\omega) = |\mathcal{V}(\omega)| e^{i\Phi_v(\omega)},$$

where we denote by  $\omega$  the center frequency of the RF band, i.e.,  $\omega = \omega_{LO} + \omega_I$ .

#### 3.1.2 Visibility and Intensity in EW–NS Coordinate System

We showed in equation (165), that the complex visibility  $\mathcal{V}(\omega)$  is related to the source intensity distribution  $I_\nu(\boldsymbol{\sigma})$  as

$$\mathcal{V}(\omega) = \oint A_N(\boldsymbol{\sigma}) I_\nu(\boldsymbol{\sigma}) e^{-i2\pi \mathbf{D}_\lambda \cdot \boldsymbol{\sigma}} d\Omega, \quad (271)$$

where  $A_N(\boldsymbol{\sigma})$  is the normalized power pattern of an interferometer,  $I_\nu(\boldsymbol{\sigma})$  is the source intensity distribution,  $\mathbf{D}_\lambda = \mathbf{D}/\lambda$  is the baseline vector  $\mathbf{D}$  normalized by the wavelength  $\lambda$  of the observation, and  $\boldsymbol{\sigma}$  is an offset vector of a direction  $\mathbf{s}$  in a radio source from a reference direction  $\mathbf{s}_0$ , i.e.,  $\boldsymbol{\sigma} = \mathbf{s} - \mathbf{s}_0$ .

The meaning of equation (271) becomes clearer if we introduce a rectangular coordinate system, whose 3-rd axis is chosen towards the reference direction  $\mathbf{s}_0$  of the source, and 1-st and 2-nd axes are chosen in the east (right ascension) and the north (declination) directions, respectively (Figure 48).

Taking into account that  $\boldsymbol{\sigma} = \mathbf{s} - \mathbf{s}_0$  is a vector difference of two unit vectors  $\mathbf{s}$  and  $\mathbf{s}_0$ , we denote components of the offset vector  $\boldsymbol{\sigma}$  in this new

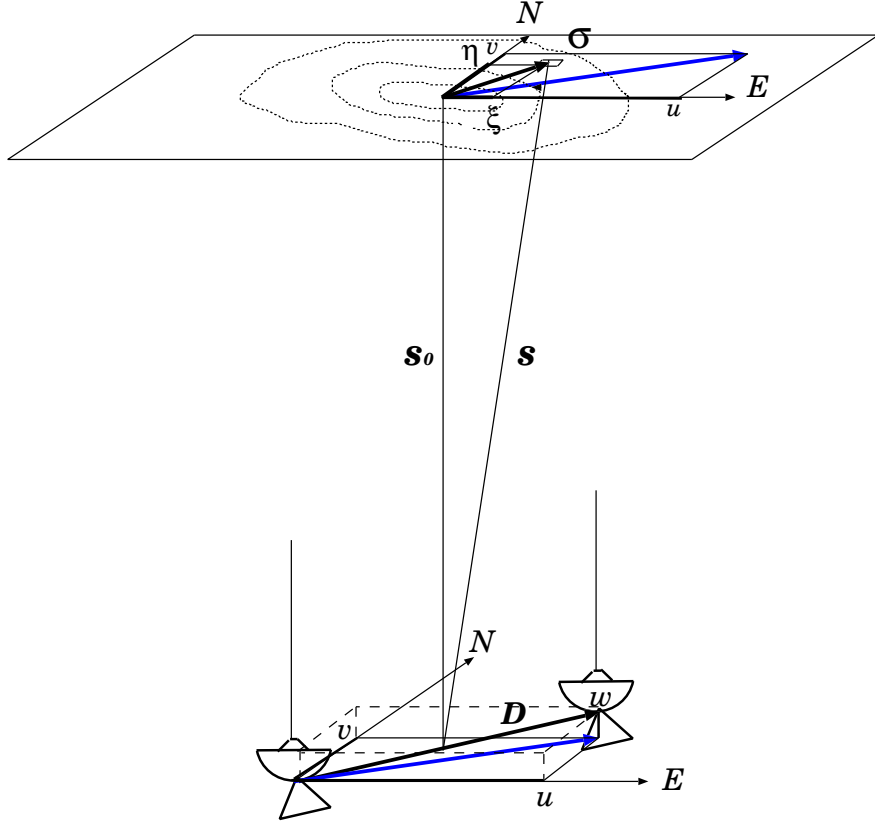


Figure 48: Source brightness distribution and projected baseline in an EW–NS plane perpendicular to the reference direction  $\mathbf{s}_0$  of the source.

coordinate system as:

$$\boldsymbol{\sigma} = (\xi, \eta, \sqrt{1 - \xi^2 - \eta^2} - 1). \quad (272)$$

Also, we denote components of the baseline vector  $\mathbf{D}$  and the normalized baseline vector  $\mathbf{D}_\lambda$  as:

$$\mathbf{D} = (u, v, w), \quad (273)$$

and

$$\mathbf{D}_\lambda = (u_\lambda, v_\lambda, w_\lambda), \quad (274)$$

respectively, in the same coordinate system, where

$$u_\lambda = \frac{u}{\lambda}, \quad v_\lambda = \frac{v}{\lambda}, \quad \text{and} \quad w_\lambda = \frac{w}{\lambda}.$$

Note that  $\xi$  and  $\eta$  are taken along right ascension and declination directions, respectively, in a celestial equatorial system. Note, also, that  $w$  is related to the geometric delay of the reference direction  $\tau_{g_0}$  by an equation:  $w = c\tau_{g_0}$ .

Then, we describe the argument of the exponential term in the complex visibility in equation (271) as:

$$2\pi \mathbf{D}_\lambda \cdot \boldsymbol{\sigma} = 2\pi [u_\lambda \xi + v_\lambda \eta + w_\lambda (\sqrt{1 - \xi^2 - \eta^2} - 1)]. \quad (275)$$

Also, we describe the solid angle element  $d\Omega$  in the same equation via  $d\xi d\eta$  as:

$$d\Omega = \frac{d\xi d\eta}{\sqrt{1 - \xi^2 - \eta^2}}, \quad (276)$$

since  $d\xi d\eta$  is the projection of  $d\Omega$  in the plane perpendicular to  $\mathbf{s}_0$  (Figure 49).

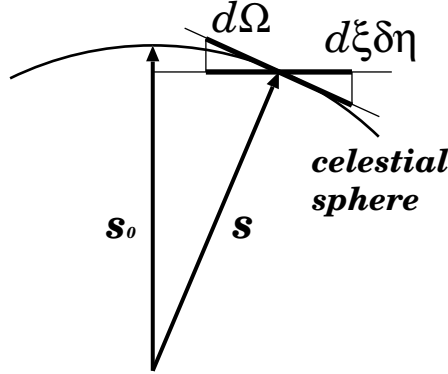


Figure 49: Solid angle element  $d\Omega$  and area element  $d\xi d\eta$  in a plane perpendicular to reference direction  $\mathbf{s}_0$ .

Then, the complex visibility in equation (271) is given in terms of  $\xi$ ,  $\eta$ ,  $u_\lambda$ ,  $v_\lambda$ , and  $w_\lambda$ , by

$$\mathcal{V}(\omega) = \int_{-\infty}^{\infty} \int_{-\infty}^{\infty} A_N(\xi, \eta) I_\nu(\xi, \eta) e^{-i2\pi [u_\lambda \xi + v_\lambda \eta + w_\lambda (\sqrt{1 - \xi^2 - \eta^2} - 1)]} \frac{d\xi d\eta}{\sqrt{1 - \xi^2 - \eta^2}}. \quad (277)$$

This equation can be regarded as an integral equation for the intensity distribution  $I_\nu(\xi, \eta)$  of a radio source with given complex visibility  $\mathcal{V}(\omega)$ . The purpose of the image synthesis is to get an intensity distribution (an “image”) of a radio source by solving this integral equation using observed complex visibilities.

### 3.1.3 Approximation of a Celestial Sphere by a Tangent Plane

It is not easy to solve the integral equation (277) in its general form. However, if we have a narrow range of mapping, where  $\xi \ll 1$  and  $\eta \ll 1$ , and second order terms  $\xi^2$  and  $\eta^2$  can be neglected, the equation becomes much simpler.

This narrow-range condition corresponds to an approximation of a small part of the celestial sphere, where we would like to draw an image map of a radio source, by a tangent plane at the reference direction  $\mathbf{s}_0$  (see Figure 50).

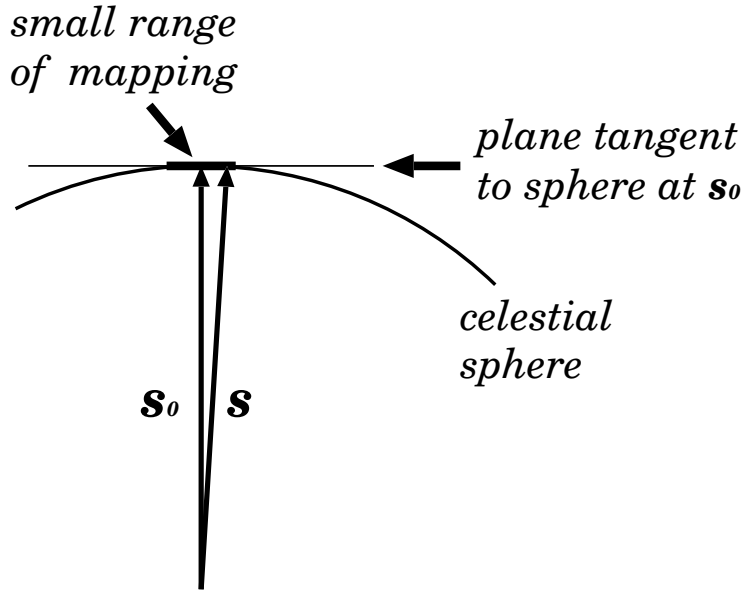


Figure 50: Celestial sphere can be approximated by a tangent plane for a small range of mapping.

Let us then examine conditions under which  $\xi^2$  and  $\eta^2$  terms can be actually neglected.

$\xi^2$  and  $\eta^2$  terms appear in two places of equation (277), namely in

$$\frac{d\xi d\eta}{\sqrt{1 - \xi^2 - \eta^2}}, \quad \text{and} \quad e^{-i2\pi[u_\lambda \xi + v_\lambda \eta + w_\lambda (\sqrt{1 - \xi^2 - \eta^2} - 1)]}.$$

In the first term:  $\frac{d\xi d\eta}{\sqrt{1-\xi^2-\eta^2}}$ , we can neglect  $\xi^2$  and  $\eta^2$ , provided only that  $|\xi| \ll 1$  and  $|\eta| \ll 1$ .

In the second term, which can be approximated by

$$e^{-i2\pi[u_\lambda \xi + v_\lambda \eta + w_\lambda (\sqrt{1-\xi^2-\eta^2} - 1)]} \cong e^{-i2\pi[u_\lambda \xi + v_\lambda \eta - \frac{1}{2} w_\lambda (\xi^2 + \eta^2)]}, \quad (278)$$

we must be a little careful. Here,  $\xi^2$  and  $\eta^2$  terms appear in a phase of a periodic function, for which only a residue of  $2\pi$  is meaningful. Therefore, it is not always possible to neglect a term in a phase even when it is much smaller than other phase terms. A phase term can be safely neglected only when it is absolutely small as a phase (for example, smaller than 0.1 radian, say). If we require this “ $\ll 0.1$  radian” condition, then  $\xi^2$  and  $\eta^2$  in equation (278) are negligible when

$$\pi w_\lambda (\xi^2 + \eta^2) \ll 0.1 \text{ radian}. \quad (279)$$

Let us now examine how this condition could be satisfied. Let us denote a

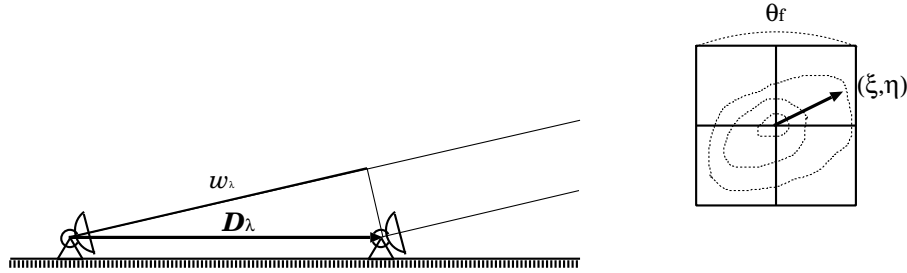


Figure 51: Length of  $w_\lambda$  (left) and a range of mapping (right).

full range of our intended image map (or, range of mapping) as  $\theta_f$ . Then, obviously

$$\xi^2 + \eta^2 \leq \left(\frac{\theta_f}{2}\right)^2,$$

(see Figure 51). Therefore, the condition in equation (279) is satisfied if

$$\pi w_\lambda \left(\frac{\theta_f}{2}\right)^2 \leq 0.1 \text{ radian}.$$

Adopting as a maximum value for  $w_\lambda$ :

$$w_{\lambda_{max}} = D_\lambda = \frac{D}{\lambda},$$

in view of Figure 51, we see that the condition in equation (279) is readily satisfied if

$$\pi \left( \frac{\theta_f}{2} \right)^2 \frac{D}{\lambda} \leq 0.1, \quad \text{and therefore} \quad \theta_f^2 \leq \frac{0.4}{\pi} \frac{\lambda}{D},$$

which is approximately equivalent to

$$\theta_f \leq \frac{1}{3} \sqrt{\frac{\lambda}{D}}. \quad (280)$$

Thus, the tangent plane approximation, where  $\xi^2$  and  $\eta^2$  are neglected, is adequate, if our range of mapping  $\theta_f$  satisfies the condition given in equation (280).

It is still left to us to examine whether equation (280) is a realistic condition in actual mappings of radio source images.

Angular resolution  $\theta_r$  of an interferometric observation is roughly given by the minimum fringe spacing:

$$\theta_r \approx \frac{\lambda}{D}.$$

Since number of grid points (“pixels”) required for an image mapping is proportional to  $(\theta_f/\theta_r)^2$ , a load of numerical processing becomes heavier, as the range of mapping  $\theta_f$  becomes much wider than the angular resolution  $\theta_r$ .

Moreover, it is usually meaningless to select a too wide range of mapping, since a radio source, which is much extended than the fringe spacing of an interferometer  $\theta_r$ , tends to be “resolved out” and becomes “invisible” for the interferometer, as we will see in more detail in later discussions.

Therefore, if we select a range, which is 30 times as large as the angular resolution, as a realistic range of mapping:

$$\theta_f \approx 30 \times \theta_r \approx 30 \times \frac{\lambda}{D},$$

then, the condition of equation (280) for the tangent-plane approximation becomes

$$30 \frac{\lambda}{D} \leq \frac{1}{3} \sqrt{\frac{\lambda}{D}}, \quad (281)$$

or

$$\sqrt{\frac{\lambda}{D}} \leq \frac{1}{90}, \quad \text{and, hence,} \quad \frac{\lambda}{D} \leq \frac{1}{8100} \approx 0.^\circ 007 \approx 25 \text{ arcsec}. \quad (282)$$

As we saw in Table 2, such a condition on the fringe spacing is generally satisfied in modern interferometers, except for m-wave or cm-wave CERI arrays of relatively short baselines. In VLBI, as far as our range of mapping is  $\leq 30 \times (\lambda/D)$ , we can safely use the tangent-plane approximation. Figure 47 gives an example, where the angular resolution is shown as an elliptical “restoring beam” in the right edge.

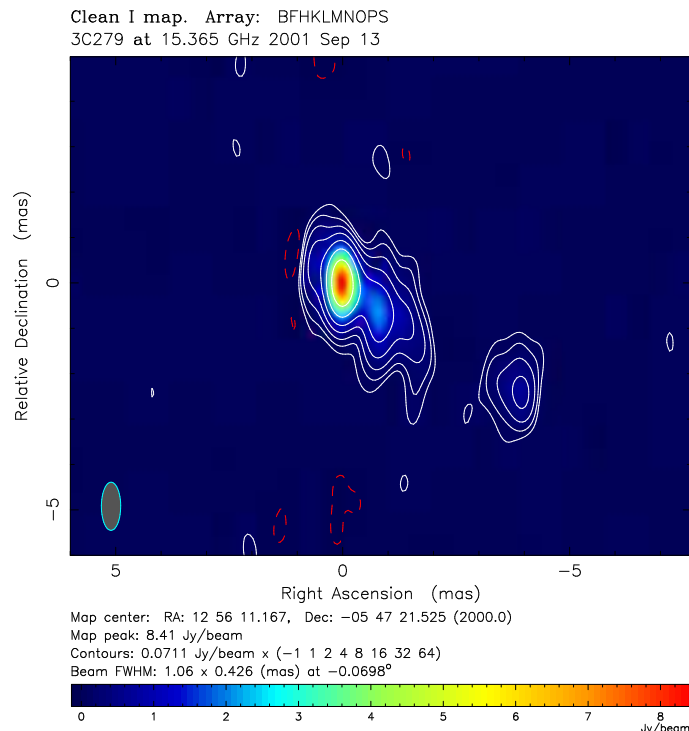


Figure 52: 15 GHz map of a quasar 3C279 observed with VLBA (Wajima and Iguchi, private communication in 2005).

Another example of a beautiful VLBI image of a quasar 3C279 observed at 15 GHz with VLBA (Wajima and Iguchi, private communication in 2005) also covers a range of mapping which is smaller than 30 times of the angular resolution (the full width half maximum (FWHM) of an interferometer beam is shown by an ellipse in the left bottom corner).

For typical CERI and VLBI, we have:

- CERI of  $\lambda = 1$  cm (30 GHz) and  $D = 2$  km:

$$\frac{\lambda}{D} = 5 \times 10^{-6} \text{ radian} = 1 \text{ arcsec},$$

$$\frac{1}{3} \sqrt{\frac{\lambda}{D}} = 7 \times 10^{-4} \text{ radian} = 140 \text{ arcsec.}$$

- VLBI of  $\lambda = 1.35 \text{ cm}$  (22 GHz) and  $D = 2300 \text{ km}$ :

$$\begin{aligned} \frac{\lambda}{D} &= 6.0 \times 10^{-9} \text{ radian} = 1.2 \text{ milliarcsec (mas)}, \\ \frac{1}{3} \sqrt{\frac{\lambda}{D}} &= 2.6 \times 10^{-5} \text{ radian} = 5.3 \text{ arcsec.} \end{aligned}$$

- VLBI of  $\lambda = 2.3 \text{ mm}$  (129 GHz) and  $D = 500 \text{ km}$ :

$$\begin{aligned} \frac{\lambda}{D} &= 4.6 \times 10^{-9} \text{ radian} = 1.0 \text{ milliarcsec (mas)}, \\ \frac{1}{3} \sqrt{\frac{\lambda}{D}} &= 2.3 \times 10^{-5} \text{ radian} = 4.7 \text{ arcsec.} \end{aligned}$$

In all above examples, the condition in equation (281) is well satisfied.

Important exceptions, where the tangent–plane approximation is not applicable, are wide–field mappings of maser sources in massive star–forming regions. They sometimes cover sky ranges of several tens arcseconds, yet individual maser features, of which they consist, are compact at milliarcsecond (mas) level, and thus well detectable with intercontinental VLBI. In such a case, the range of mapping  $\theta_f$  could be far larger than  $30 \theta_r$ . Therefore, one must properly take into account sphericity of the map surface in such wide–field mappings.

### 3.1.4 Interferometer is a Fourier Transformer

Under the tangent plane approximation, equation (277) is reduced to

$$\mathcal{V}(\omega) = \mathcal{V}(u_\lambda, v_\lambda) = \int_{-\infty}^{\infty} \int_{-\infty}^{\infty} A_N(\xi, \eta) I_\nu(\xi, \eta) e^{-i2\pi(u_\lambda \xi + v_\lambda \eta)} d\xi d\eta, \quad (283)$$

where we reexpressed  $\mathcal{V}(\omega)$  as  $\mathcal{V}(u_\lambda, v_\lambda)$ , stressing dependence of the visibility on “normalized projected baseline components”  $u_\lambda$  and  $v_\lambda$ .

Then, it is evident that the complex visibility  $\mathcal{V}(u_\lambda, v_\lambda)$ , as given in equation (283), is a two–dimensional Fourier transform of the source brightness distribution  $I_\nu(\xi, \eta)$  at “spatial frequency” values  $u_\lambda$  and  $v_\lambda$ .

Consequently, we can regard a radio interferometer as a “Fourier Transformation Device”, which yields, at the correlator output, a two–dimensional

Fourier component of the source brightness distribution on the sky, at spatial frequencies corresponding to two components of the normalized projected baseline,  $u_\lambda$  and  $v_\lambda$ . The Fourier transformation relation described in equation (283) is called “van Cittert–Zernike Theorem”.

Naturally, the source brightness distribution is restored from the measured visibilities by the inverse Fourier transformation:

$$A_N(\xi, \eta)I_\nu(\xi, \eta) = \int_{-\infty}^{\infty} \int_{-\infty}^{\infty} \mathcal{V}(u_\lambda, v_\lambda) e^{i2\pi(u_\lambda \xi + v_\lambda \eta)} du_\lambda dv_\lambda, \quad (284)$$

and then by correcting the normalized power pattern of the interferometer  $A_N(\xi, \eta)$ . This is the basis of the astrophysical imaging of the radio source structure by means of radio interferometry under the tangent plane approximation. This is important also for geodetic and astrometric VLBI, when we calibrate the effect of the source structure on the measured delay.

Of course, it is impossible to perform a complete inverse Fourier transformation, unless a continuous distribution of the visibility is available over the whole spatial frequency domain, the  $uv$ -plane. Nevertheless, a better restoration is achieved, with suitable image processing software, when the visibilities are sampled at many  $u_\lambda, v_\lambda$  points, which nearly homogeneously cover the  $uv$ -plane. It is therefore important to have a good coverage of  $uv$ -plane for radio interferometry observations aimed at astrophysical source imaging.

### 3.2 $uv$ -Coverage

The Earth’s diurnal rotation changes the direction and length of a projected baseline of a ground-based interferometer in the  $uv$ -plane, and thus helps us to sample visibilities at different  $u_\lambda, v_\lambda$  points. Since the interferometer baseline rotates around a nearly fixed spin axis of the Earth, the trajectory of the projected baseline is a circle, if the observed source is located at the celestial pole. The trajectory is a linear oscillation when the source is at the equator, and is an ellipse, for all other directions in between the celestial equator and the 2 celestial poles. For two stations 1 and 2 on the surface of the Earth, we have two baseline vectors with opposite directions  $\mathbf{D}_{12}$  and  $\mathbf{D}_{21} = -\mathbf{D}_{12}$  connecting these two stations. Therefore, in general, we have two point-symmetric arcs of ellipses on the  $uv$ -plane for a pair of stations (Figure 53).

Configurations of radio interferometer arrays are designed to achieve good coverages of the  $uv$ -plane, from the trajectories of projected baselines formed by their antennas.

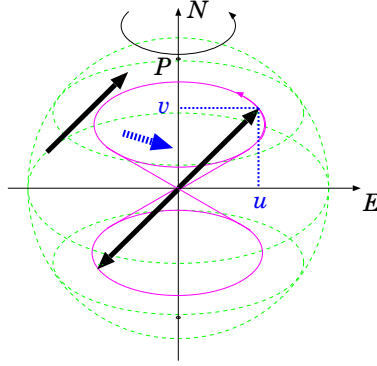


Figure 53: If we place an end of a baseline vector at the center of the rotating Earth, by a parallel translation, a tip of the vector draws an ellipse, in general, viewed from a radio source. EW and NS components of the projected baseline are the  $u$  and  $v$  components. Since we have two vectors of equal lengths and opposite directions which connect two stations, we have two point-symmetric elliptical trajectories.

### 3.2.1 $uv$ -Trajectories

Figure 54 shows geometry of the diurnal rotation of a baseline vector  $\mathbf{D}$ .

We use an Earth-fixed Cartesian  $X, Y, Z$  coordinate system with  $Z$  axis directed towards North Pole,  $X$  axis directed towards Greenwich Meridian, and  $Y$  axis which completes a right-handed system. Components of the baseline vector  $\mathbf{D}$  in this system are denoted by  $D_X$ ,  $D_Y$ , and  $D_Z$ . Direction of an observed radio source is given by the declination  $\delta$  and Greenwich hour angle  $H$  of the source with respect to this Earth-fixed coordinate system.

First, let us look at the baseline vector from a direction of the North Pole (bottom-left panel of Figure 54). We see two sets of rectangular axes  $X, Y$  and  $S, E$  in the equatorial plane, which is now perpendicular to our line of sight.  $S$  axis here is chosen along a plane containing both the North Pole axis and the radio source direction, which we call the “PS-plane”. We then consider  $S$  and  $E$  components of the baseline vector  $\mathbf{D}$  in the equatorial plane.  $E$  component is just equal to the  $u$  component, i.e. the EW-component of the baseline vector viewed from the radio source (top-left panel of Figure 54). As for  $S$  component of the baseline  $\mathbf{D}$ , we denote it as  $D_S$ . Since  $S, E$  and  $X, Y$  axes are inclined to each other by the Greenwich hour angle  $H$ , the  $u$  and  $D_S$  components and  $D_X$  and  $D_Y$  components of the baseline vector  $\mathbf{D}$  are related to each other by equations:

$$u = D_X \sin H + D_Y \cos H, \quad (285)$$

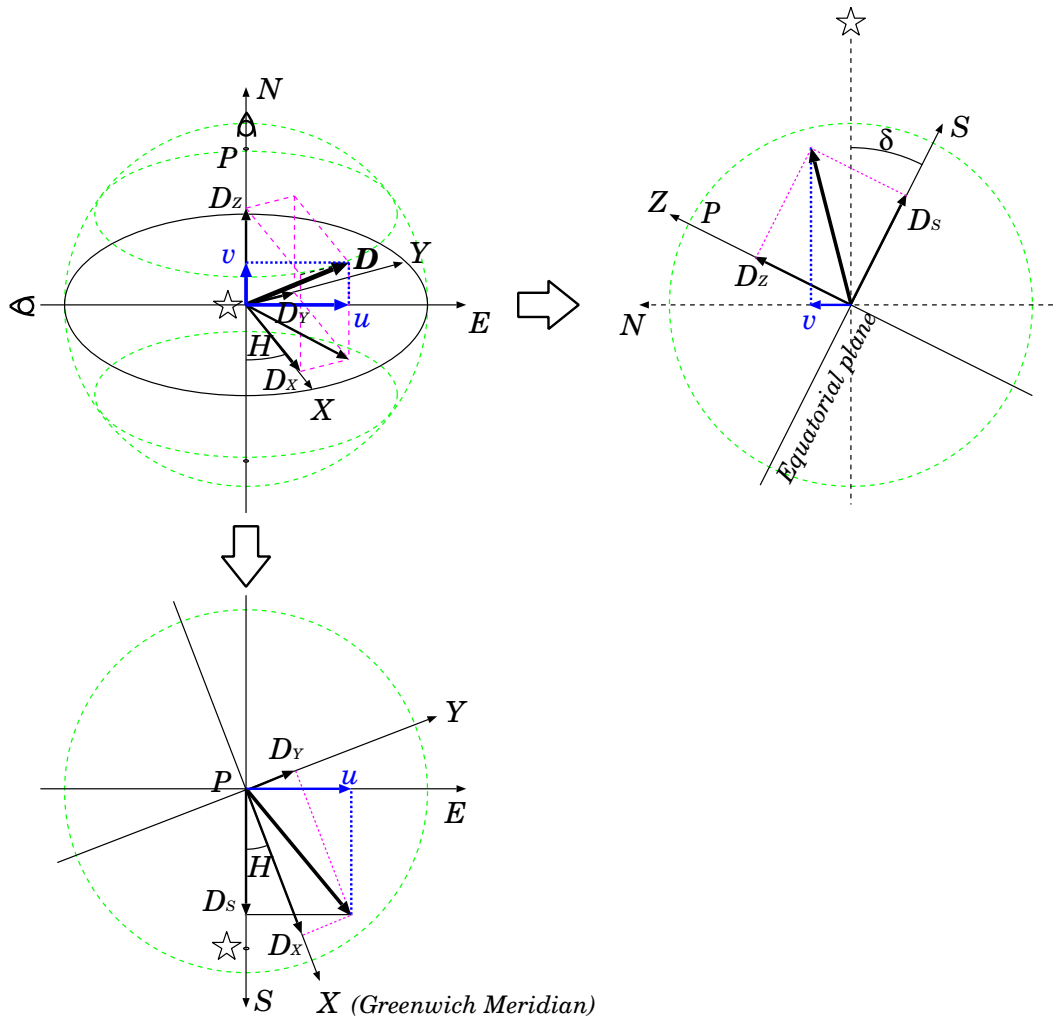


Figure 54: Geometrical relationship between  $D_X$ ,  $D_Y$ , and  $D_Z$  components of a baseline vector  $\mathbf{D}$  and  $u$ ,  $v$  coordinates. Here,  $X, Y, Z$  coordinate system is an Earth-fixed right-handed Cartesian system with  $Z$  axis towards the North Pole  $P$  and  $X$  axis towards Greenwich Meridian.  $H$  and  $\delta$  are Greenwich hour angle and declination of an observed radio source. The Earth-fixed baseline vector is shown as viewed from the radio source (top, left), viewed from west (top, left), and viewed from the North Pole (bottom).

and

$$D_S = D_X \cos H - D_Y \sin H. \quad (286)$$

Next, when we look at the baseline vector  $\mathbf{D}$  along the  $E$  axis from the west side (top-right panel of Figure 54), we see equatorial  $S$  axis and polar  $Z$  axis in the PS-plane, which is now perpendicular to the line of sight. The radio source direction is offset from the equatorial plane by the declination  $\delta$ . Therefore, the component of the baseline vector  $\mathbf{D}$  in an axis perpendicular to the source direction, which is nothing but the NS-component of the baseline vector viewed from the radio source (top-left panel of Figure 54), i.e. the  $v$  component, is related to the  $D_S$  and  $D_Z$  components by an equation:

$$v = -D_S \sin \delta + D_Z \cos \delta. \quad (287)$$

Combining equations (286) and (287), we obtain

$$v = -(D_X \cos H - D_Y \sin H) \sin \delta + D_Z \cos \delta, \quad (288)$$

for  $v$  component. Equations (285) and (288) allow us to calculate a  $uv$ -trajectory of a radio source with varying Greenwich hour angle  $H$ .

From equations (285) and (288), we obtain an equation of ellipse:

$$u^2 + \frac{(v - D_Z \cos \delta)^2}{\sin^2 \delta} = D_X^2 + D_Y^2, \quad (289)$$

which clearly shows that  $uv$ -trajectories are really ellipses.

In view of the point symmetry property mentioned above, a set of  $u$  and  $v$ :

$$\begin{aligned} u &= -D_X \sin H - D_Y \cos H, \\ v &= (D_X \cos H - D_Y \sin H) \sin \delta - D_Z \cos \delta, \end{aligned} \quad (290)$$

which satisfies an equation of another ellipse:

$$u^2 + \frac{(v + D_Z \cos \delta)^2}{\sin^2 \delta} = D_X^2 + D_Y^2, \quad (291)$$

is also a valid  $uv$ -trajectory of the same pair of stations.

When we calculate actual  $uv$ -trajectory of a radio source, we must take into account that the source can be observed by an interferometer baseline only when the source is “mutually visible” from two stations of the baseline, i.e. when the source is within lower and upper elevation limits of radio telescopes at the two stations. This condition is roughly formulated as follows.

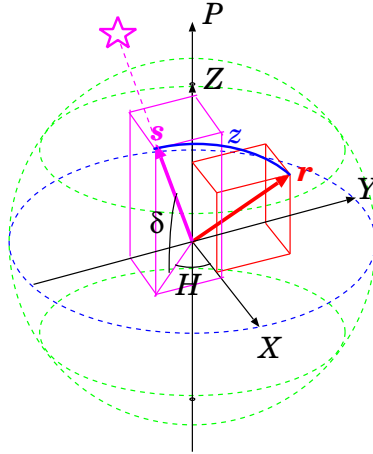


Figure 55: Zenith distance  $z$  of a radio source direction  $\mathbf{s}$  at a station in a direction  $\mathbf{r}$ . Also shown is an Earth-fixed Cartesian coordinate system with  $Z$ -axis towards the North Pole  $P$  and  $X$ -axis towards Greenwich Meridian.  $H$  and  $\delta$  are Greenwich hour angle and declination of the source, respectively.

If  $X, Y, Z$  coordinates of a station is  $\mathbf{R} = (R_X, R_Y, R_Z)$ , and if we approximate the Earth by a sphere, then a unit vector  $\mathbf{r}$  oriented towards zenith direction of the station is roughly given by

$$\mathbf{r} = \frac{\mathbf{R}}{R},$$

where

$$R = \sqrt{R_X^2 + R_Y^2 + R_Z^2}.$$

On the other hand, components of a unit vector  $\mathbf{s}$  towards a radio source are given in the  $X, Y, Z$  coordinates by

$$\mathbf{s} = (\cos \delta \cos H, -\cos \delta \sin H, \sin \delta),$$

(see Figure 55), where  $H$  is the Greenwich hour angle, and  $\delta$  is the declination of the source.

Therefore, cosine of the zenith distance  $z$ , i.e. the angle between the zenith direction  $\mathbf{r}$  and the source direction  $\mathbf{s}$ , is approximately given by

$$\cos z = \mathbf{r} \cdot \mathbf{s} = \frac{R_X \cos \delta \cos H - R_Y \cos \delta \sin H + R_Z \sin \delta}{R}. \quad (292)$$

Thus, if upper and lower elevation limits of a radio telescope at a station are  $E_u$  and  $E_l$ , respectively, then the radio source is visible with the telescope

when

$$\sin E_u \leq \cos z \leq \sin E_l. \quad (293)$$

Actual  $uv$ -trajectories can be calculated in terms of equations (285), (288), and (290), when the condition of equation (293) is satisfied at both ends of baselines.

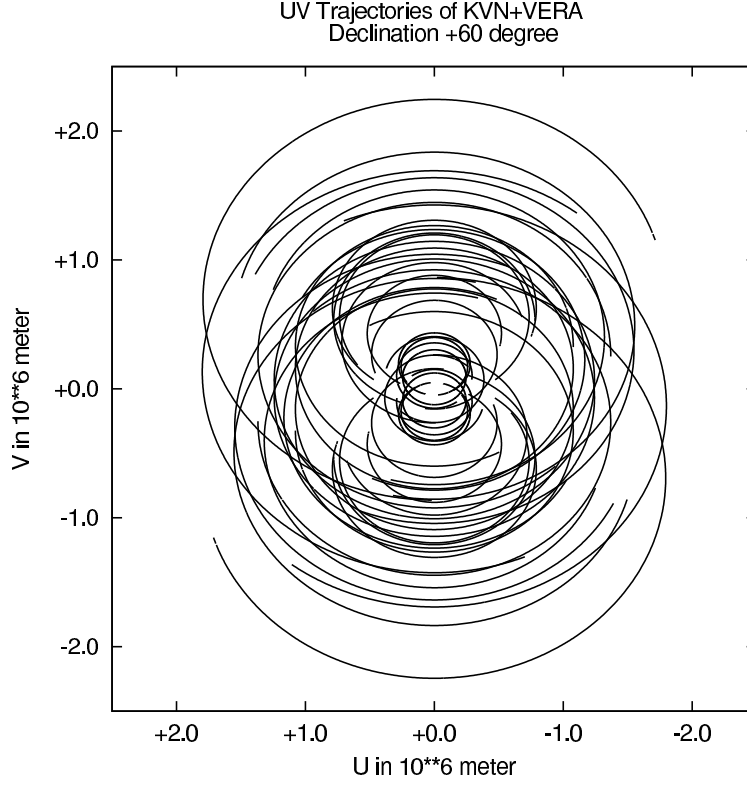


Figure 56:  $uv$ -trajectories of a combined KVN and VERA arrays, for a source at  $\delta = +60^\circ$ .

Figure 56 shows an example of the  $uv$ -coverage for the combined VERA and KVN VLBI arrays thus calculated, for a source located at  $+60^\circ$  declination.

### 3.2.2 Synthesized Beams

Let us consider a point source with flux density  $S_\nu$  located at the reference direction  $\mathbf{s}_0$  ( $\xi = 0$  and  $\eta = 0$ ). In this case, the intensity distribution, which we call here the “true intensity” and denote as  $I_\nu^{true}(\xi, \eta)$ , in order to

distinguish it from “synthesized” one to be introduced below, is given by

$$I_\nu^{true}(\xi, \eta) = S_\nu \delta(\xi) \delta(\eta), \quad (294)$$

where  $\delta(x)$  is the delta function.

For simplicity, we assume that the normalized power pattern of the interferometer is unity, i.e.  $A_N(\xi, \eta) = 1$ , everywhere in our range of mapping. Then, equation (283) gives the complex visibility which is constant at every  $u_\lambda, v_\lambda$  point:

$$\mathcal{V}(u_\lambda, v_\lambda) = S_\nu = \text{const.} \quad (295)$$

In an actual interferometer array, we can sample the complex visibility only along  $uv$ -trajectories. Therefore, the “synthesized intensity distribution” calculated by equation (284):

$$I_\nu^{synt}(\xi, \eta) = S_\nu \int_{-\infty}^{\infty} \int_{-\infty}^{\infty} e^{i2\pi(u_\lambda\xi + v_\lambda\eta)} du dv \Big|_{\text{along } uv}, \quad (296)$$

does not reproduce the point but yields some extended distribution. This “response of a synthesis interferometer array to a point source” is called the “synthesized beam” or the “dirty beam” of the array. This is analogous to the beam formation of a single dish antenna with a strange “aperture illumination” along elliptical arcs.

If we approximate the two-dimensional integration by a summation on meshes, equation (296) is reduced to

$$\begin{aligned} I_\nu^{synt}(\xi, \eta) &= S_\nu \sum_u \sum_v e^{i2\pi(u_\lambda\xi + v_\lambda\eta)} \Delta u_\lambda \Delta v_\lambda \Big|_{\text{along } uv} \\ &= S_\nu \sum_u \sum_v [e^{i2\pi(u_\lambda\xi + v_\lambda\eta)} + e^{-i2\pi(u_\lambda\xi + v_\lambda\eta)}] \Delta u_\lambda \Delta v_\lambda \Big|_{\text{along } uv1} \\ &= 2S_\nu \sum_u \sum_v \cos(2\pi[u_\lambda\xi + v_\lambda\eta]) \Delta u_\lambda \Delta v_\lambda \Big|_{\text{along } uv1}, \end{aligned} \quad (297)$$

where “*along uv*” means summation along  $uv$ -trajectories composed of point-symmetric elliptical arcs given in both equations (289) and (291), whereas “*along uv1*” means summation along  $uv$ -trajectories given by equation (289) only. We can further replace the two-dimensional summation on the  $uv$ -plane by a one-dimensional summation along the elliptical  $uv$ -trajectories with equal intervals of Greenwich hour angle  $\Delta H$ . Since an interval in Greenwich hour angle  $\Delta H$  corresponds to a length interval in the  $uv$ -plane

$$\sqrt{\left(\frac{du_\lambda}{dH}\right)^2 + \left(\frac{dv_\lambda}{dH}\right)^2} \Delta H,$$

we obtain from equation (297)

$$I_\nu^{synt}(\xi, \eta) \propto \sum_H \cos(2\pi[u_\lambda(H)\xi + v_\lambda(H)\eta]) \sqrt{\left(\frac{du_\lambda}{dH}\right)^2 + \left(\frac{dv_\lambda}{dH}\right)^2} \Delta H \Big|_{\text{along } uv1}. \quad (298)$$

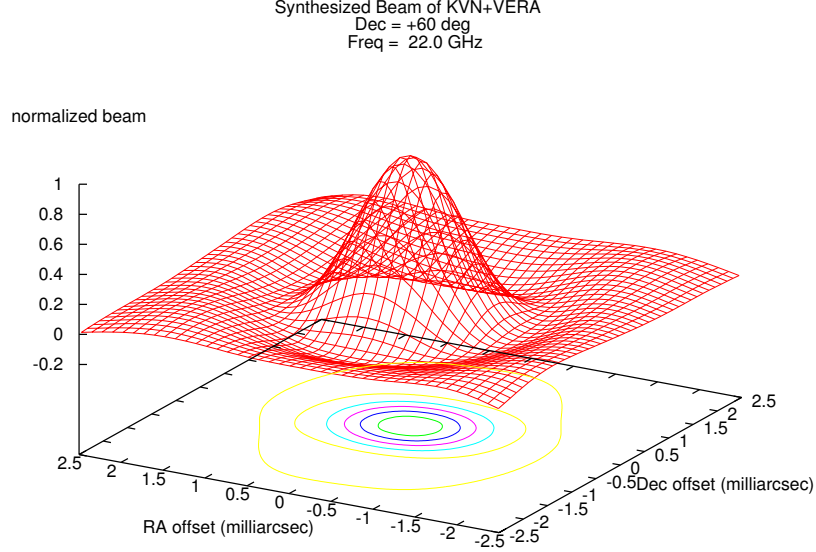


Figure 57: Normalized synthesized beam of the combined KVN and VERA VLBI arrays for a radio source at +60° declination with observing frequency 22 GHz.

$u_\lambda$ ,  $v_\lambda$  and their derivatives with respect to  $H$  in equation (298) are readily calculated for a radio source with declination  $\delta$  from equations (285) and (288), namely we have

$$u_\lambda = \frac{D_X \sin H + D_Y \cos H}{\lambda}, \quad (299)$$

$$v_\lambda = -\frac{D_X \cos H - D_Y \sin H}{\lambda} \sin \delta + \frac{D_Z}{\lambda} \cos \delta, \quad (300)$$

and

$$\frac{du_\lambda}{dH} = \frac{D_X \cos H - D_Y \sin H}{\lambda}, \quad (301)$$

$$\frac{dv_\lambda}{dH} = \frac{D_X \sin H + D_Y \cos H}{\lambda} \sin \delta. \quad (302)$$

Calculating these quantities with varying  $H$  while the source is mutually visible at two ends of baselines, inserting them into equation (298), and dividing the results by a maximum value, we obtain the synthesized beam normalized by its maximum value:

$$\frac{I_\nu^{synt}(\xi, \eta)}{I_\nu^{synt}_{max}}.$$

Figure 57 shows an example of the normalized synthesized beam for the combined KVN and VERA VLBI arrays for a radio source located at  $+60^\circ$  declination observed at 22 GHz.

### 3.3 Correlated Flux Density of a Source with Gaussian Intensity (Brightness) Distribution

How is the correlated flux density related to the size of an observed radio source? Let us consider this problem for a simple case, when the source has a circular Gaussian intensity (brightness) distribution (Figure 58):

$$I_\nu(\xi, \eta) = \frac{S_{T_\nu}}{\pi\Theta_s^2} e^{-\frac{\xi^2+\eta^2}{\Theta_s^2}}, \quad (303)$$

where  $S_{T_\nu}$  is the total flux density (note that  $\int_{-\infty}^{\infty} \int_{-\infty}^{\infty} e^{-\frac{\xi^2+\eta^2}{\Theta_s^2}} d\xi d\eta = \pi\Theta_s^2$ ),

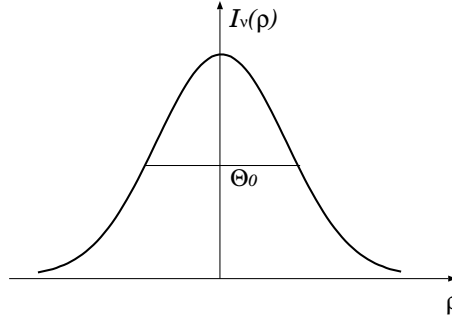


Figure 58: Circular Gaussian intensity distribution  $I_\nu(\rho)$  with  $\rho = \sqrt{\xi^2 + \eta^2}$ .

and  $\Theta_s$  is a parameter characterizing the source size. This parameter  $\Theta_s$  is related to the half-power width of the Gaussian distribution  $\Theta_0$  by a formula:

$$\Theta_s = \frac{\Theta_0}{2\sqrt{\ln 2}} \cong 0.60\Theta_0. \quad (304)$$

Then, in view of equation (283), the complex visibility of the source is given by

$$\begin{aligned}\mathcal{V}(u_\lambda, v_\lambda) &= \frac{S_{T_\nu}}{\pi \Theta_s^2} \int_{-\infty}^{\infty} \int_{-\infty}^{\infty} e^{-\frac{\xi^2 + \eta^2}{\Theta_s^2}} e^{-i2\pi(u_\lambda \xi + v_\lambda \eta)} d\xi d\eta \\ &= S_{T_\nu} e^{-\pi^2 \Theta_s^2 (u_\lambda^2 + v_\lambda^2)} = S_{T_\nu} e^{-[\pi \Theta_s (\frac{D \cos \theta}{\lambda})]^2} \quad (305)\end{aligned}$$

(see Figure 59 for geometry of the projected baseline), where we took  $A_N(\xi, \eta) \cong 1$ , for simplicity, assuming that the source is observed at beam centers of antennas. In deriving equation (305), we used an integration formula:

$$\int_{-\infty}^{\infty} e^{-x^2 - i a x} dx = \sqrt{\pi} e^{-\frac{a^2}{4}}.$$

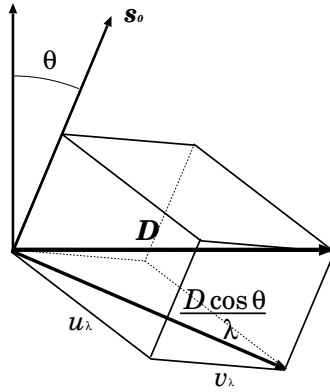


Figure 59: Projected baseline length:  $\sqrt{u_\lambda^2 + v_\lambda^2} = \frac{D \cos \theta}{\lambda}$ .

Thus, for a source with the circular Gaussian intensity distribution, we have

- correlated flux density =  $|\mathcal{V}(u_\lambda, v_\lambda)| = S_{T_\nu} e^{-[\pi \Theta_s (\frac{D \cos \theta}{\lambda})]^2}$ ,
- visibility phase = 0.

This means that the correlated flux density  $|\mathcal{V}(u_\lambda, v_\lambda)|$  is reduced to the half of the total flux density  $S_{T_\nu}$  when

$$\left[ \pi \Theta_s \left( \frac{D \cos \theta}{\lambda} \right) \right]^2 = \ln 2, \quad (306)$$

or, in view of equation (304), when the half-power width of the source distribution  $\Theta_0$  is equal to

$$\Theta_0 = \frac{2 \ln 2}{\pi} \frac{\lambda}{D \cos \theta} \cong 0.44 \frac{\lambda}{D \cos \theta}. \quad (307)$$

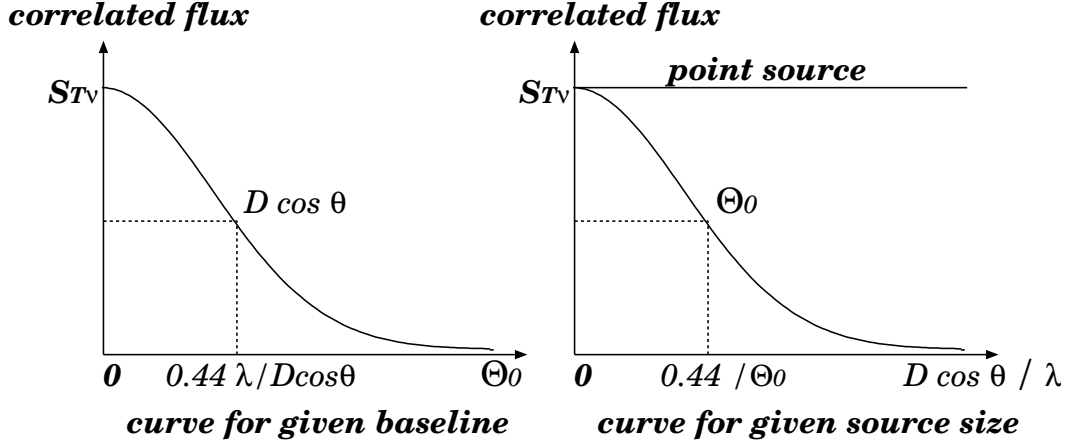


Figure 60: Correlated flux density of a source with Gaussian intensity distribution, as a function of the source size (left), and as a function of the projected baseline length (right).

Figure 60 shows the correlated flux density of the source, with a circular Gaussian intensity distribution, as a function of the half-power width  $\Theta_0$  of the source brightness distribution, assuming a fixed baseline length  $D$  (left panel); and as a function of the projected baseline length normalized by the wave length,  $D \cos \theta / \lambda$ , assuming a fixed source size (right panel), according to equation (305). This simple example shows that the source appears weak to an interferometer, or “resolved out”, when its size becomes comparable with or larger than the fringe spacing  $\lambda / (D \cos \theta)$ . In other words, interferometers are sensitive to the sources with angular sizes comparable to or smaller than their fringe spacings.

It is usual practice in VLBI to infer the size of a source by measuring its correlated flux densities at different projected baseline lengths, and fitting the results to a Gaussian model, as shown in the right panel of Figure 60. Figure 61 shows an example (Wajima and Iguchi, private communication in 2005).

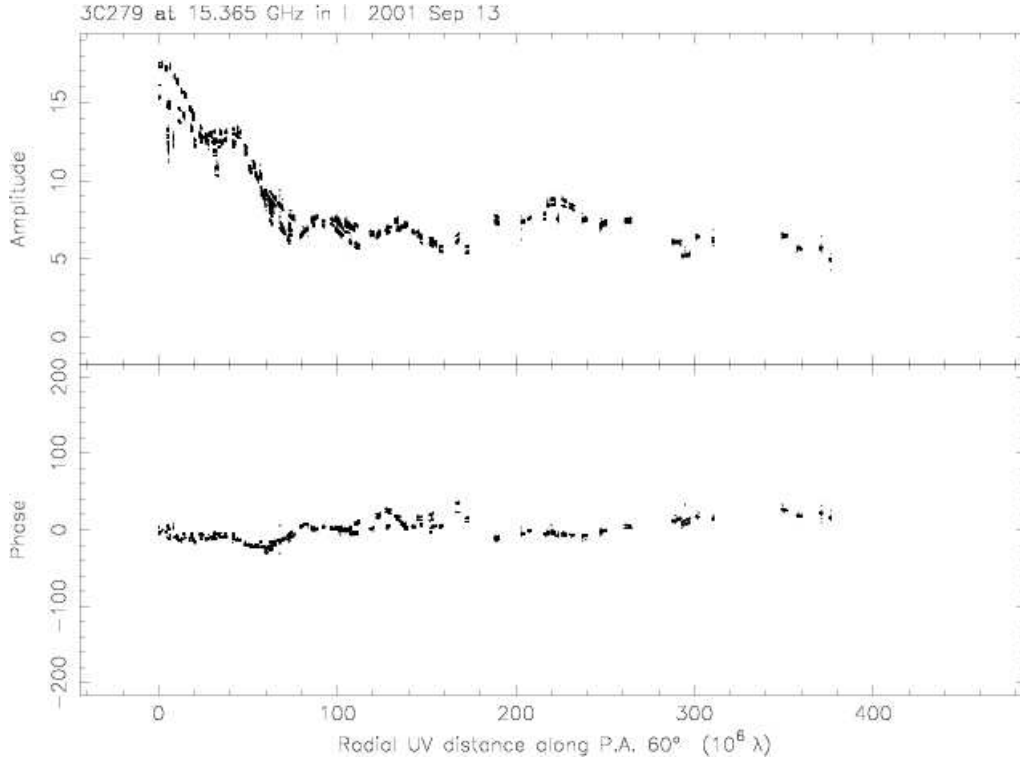


Figure 61: Visibility amplitude (top) and phase (bottom) versus  $uv$ -distance along a position angle (PA)  $60^\circ$  plot of a quasar 3C279 observed with VLBA at 15 GHz (Wajima and Iguchi, private communication in 2005). Visibility amplitude (top) decreases with  $uv$ -distance (projected baseline length) in a range from 0 to  $70 \times 10^6 \lambda$ , similarly to the curve in the right panel of Figure 60. However, visibility amplitude becomes almost flat in  $uv$ -distance range from  $70 \times 10^6$  to  $400 \times 10^6 \lambda$ , showing existence of a compact component which is not resolved even on the longest baseline  $400 \times 10^6 \lambda \simeq 8000 \text{ km}$ . This Figure can be compared with an image map of the same source shown in Figure 52.

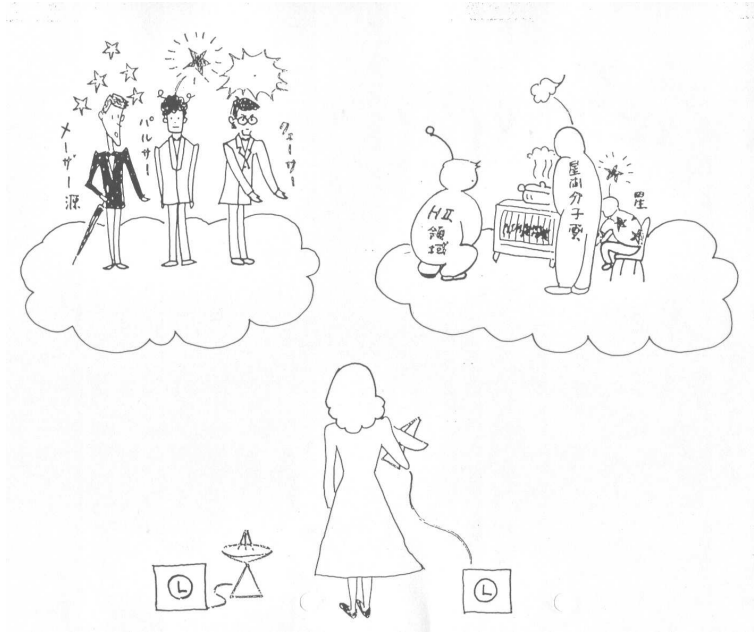


Figure 62: VLBI can observe very bright, compact objects only.

### 3.4 What Can VLBI Observe?

The above discussions show that a VLBI (or an interferometer, in general), with baseline length  $D$  and observing wavelength  $\lambda$ , can detect only compact sources with characteristic angular diameters  $\Theta_0$  comparable to or smaller than  $\lambda/D$ , i.e.,

$$\Theta_0 \leq \frac{\lambda}{D}.$$

If the brightness temperature of a source is  $T_B$ , then the intensity  $I_\nu$  and the flux density  $S_\nu$  are given by:

$$I_\nu = \frac{2kT_B}{\lambda^2}, \quad \text{and} \quad S_\nu = \frac{2kT_B \pi \Theta_0^2}{\lambda^2} \leq \frac{\pi k T_B}{2D^2},$$

where  $k = 1.381 \times 10^{-23} \text{ JK}^{-1}$  is the Boltzmann constant. Note that the last expression does not depend on the wavelength.

Now, if the minimum detectable flux density by VLBI is  $S_{\nu min}$ , we can impose a lower limit to the brightness temperature,  $T_{B min}$ , for the detectable source:

$$T_{B min} \cong \frac{2D^2}{\pi k} S_{\nu min}. \quad (308)$$

If  $D = 2300 \text{ km}$  and  $S_{\nu min} = 0.02 \text{ Jy}$ , then  $T_{B min} \cong 5 \times 10^7 \text{ K}$  (!).

Such a high lower limit of the brightness temperature precludes detection of almost all thermal sources, such as stars and molecular clouds with VLBI, leaving only very bright, compact non-thermal sources, e.g., AGNs, masers, and pulsars (see Figure 62), to be detected.

## 4 Signal-to-Noise Ratio in Radio Interferometry

So far, we approximated the result  $\mathcal{R}$  of the multiplication and integration in a correlator by the cross-correlation  $R_{U_1 U_2}(0)$  of the voltage signals  $U_1(t)$  and  $U_2(t)$  at input points of the correlator. In view of the ergodicity, this approximation should be good enough when the integration time is sufficiently long. Also, one can prove that the mathematical expectation of  $\mathcal{R}$  is equal to  $R_{U_1 U_2}(0)$ , if  $U_1(t)$  and  $U_2(t)$  are jointly stationary random processes. However, the actual correlator output, with some limited integration time, is inevitably accompanied with thermal noise fluctuations. Therefore, we have some finite signal-to-noise-ratio in the correlator output, which determines detectability of the radio source signal, i.e. the sensitivity (Figure 63).

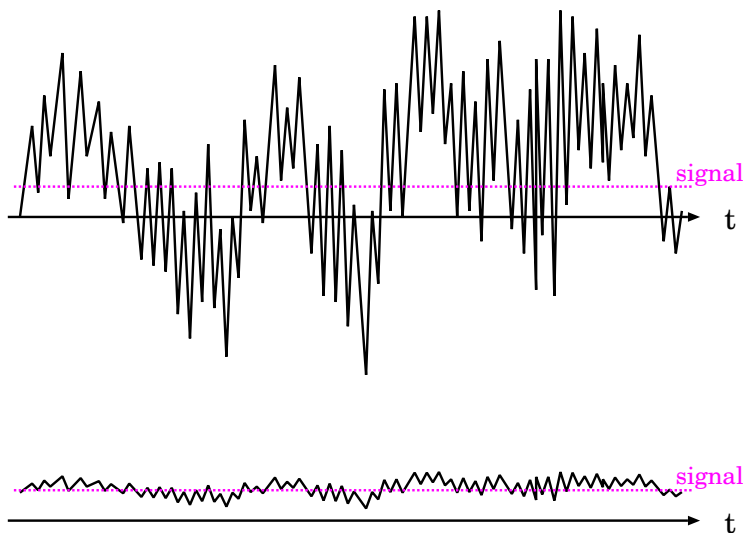


Figure 63: Signal-to-noise ratio of the correlator output determines the sensitivity of an interferometer.

We will see in the followings that a statistical theory of the dispersion of

the time-averaged product of random processes gives a theoretical expression for the signal-to-noise ratio  $S/N$  of the correlator output.

## 4.1 Statistical Model of a Correlator Output

### 4.1.1 Signal + Noise Inputs to a Correlator

Let us consider that the voltages from two antennas  $U_1(t)$  and  $U_2(t)$ , which are fed to input points of a correlator, consist of signals  $V_1(t)$ ,  $V_2(t)$  and

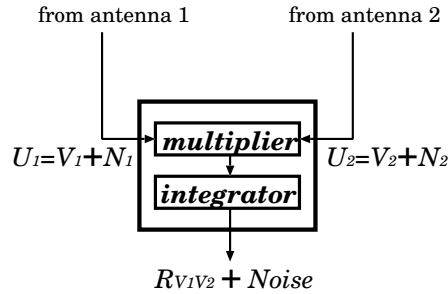


Figure 64: Input voltages to a correlator consist of signals and noises.

noises  $N_1(t)$ ,  $N_2(t)$  (see Figure 64):

$$\begin{aligned} U_1(t) &= V_1(t) + N_1(t), \\ U_2(t) &= U_2(t) + N_2(t). \end{aligned} \quad (309)$$

We assume that the delay tracking and fringe stopping were already successfully applied to the voltages  $U_1(t)$  and  $U_2(t)$ , so that we can integrate the multiplier output for an appropriate interval of time without losing signal power.

### 4.1.2 Integration of the Multiplier Output

If we denote an instantaneous output of the multiplier as  $y(t)$ :

$$y(t) = U_1(t)U_2(t), \quad (310)$$

an output of the integrator (i.e., correlator output)  $z(t)$  is related to the input  $y(t)$  by a linear system of time averaging with an impulse response  $a(t)$ :

$$z(t) = y(t) * a(t) = \int_{-\infty}^{\infty} y(t')a(t-t') dt', \quad (311)$$

where symbol ‘\*’ stands for a convolution, as before.

If an input  $y(t)$  is a constant  $y$  in time, the time averaging result must be equal to the constant  $y$ . Therefore, the impulse response  $a(t)$  must satisfy:

$$\int_{-\infty}^{\infty} a(t) dt = 1. \quad (312)$$

For example, if we take a simple running mean:

$$z(t) = \frac{1}{2T} \int_{t-T}^{t+T} y(t') dt', \quad (313)$$

then the impulse response  $a(t)$  is given by

$$a(t) = \begin{cases} \frac{1}{2T} & \text{for } -T \leq t \leq T, \\ 0 & \text{otherwise.} \end{cases}$$

### 4.1.3 Statistical Expectation of the Correlator Output

We assume that the noise components from two antennas are not correlated with each other, and are not correlated with signal components, either. Then, we have

$$\langle N_1(t) N_2(t) \rangle = 0, \quad \langle V_i(t) N_j(t) \rangle = 0 \quad \text{for } i = 1, 2 \text{ and } j = 1, 2, \quad (314)$$

where  $\langle \rangle$  stands for the ensemble average, as before. From equation (314), we obtain

$$\langle y(t) \rangle = \langle U_1 U_2 \rangle = \langle [V_1(t) + N_1(t)] [V_2(t) + N_2(t)] \rangle = \langle V_1(t) V_2(t) \rangle. \quad (315)$$

In next subsection, we will see that the multiplier output  $y(t) = U_1(t)U_2(t)$  is a stationary random process, provided that  $U_1(t)$  and  $U_2(t)$  are jointly stationary random processes obeying the zero-mean jointly normal (or Gaussian) probability density. If so,

$$\langle y(t) \rangle = \text{const},$$

and, therefore,

$$\langle z(t) \rangle = \int_{-\infty}^{\infty} \langle y(t') \rangle a(t-t') dt' = \langle y(t) \rangle \int_{-\infty}^{\infty} a(t-t') dt' = \langle y(t) \rangle, \quad (316)$$

in view of equation (312). Equations (315) and (316) show that the statistical expectation of the correlator output in radio interferometry does not contain system-noise contribution unlike in the single-dish radio telescope case.

#### 4.1.4 Dispersion of the Correlator Output

As we saw in the discussion of the correlation ergodicity in Subsection 1.2.4, a correlator output  $z(t)$  with finite integration time should be associated with noise-induced fluctuations around the expectation:

$$z(t) = \langle z(t) \rangle + \text{noise} = \langle V_1(t) V_2(t) \rangle + \text{noise}. \quad (317)$$

This fluctuation determines detection limit of radio sources as illustrated in Figure 64.

The magnitude of this fluctuation can be estimated by the dispersion  $\sigma_z^2$  of the correlator output  $z(t)$ , as we saw in the discussion of the correlation ergotic processes. The dispersion is given by

$$\begin{aligned} \sigma_z^2 &= \langle [z(t) - \langle z(t) \rangle]^2 \rangle \\ &= \langle [z^2(t) - 2z(t) \langle z(t) \rangle + \langle z(t) \rangle^2] \rangle \\ &= \langle z^2(t) \rangle - \langle z(t) \rangle^2, \end{aligned} \quad (318)$$

and, therefore, the standard deviation is given by

$$\sigma_z = \sqrt{\langle z^2(t) \rangle - \langle z(t) \rangle^2}. \quad (319)$$

This is a measure of strength of the noise in the correlator output.

On the other hand, strength of the signal in the correlator output is given by the theoretical expressions of the fringe amplitude  $\mathcal{A}^U$  and  $\mathcal{A}^L$  shown in equations (260) and (261) for USB and LSB receptions, respectively, for a continuum spectrum source.

Therefore, signal-to-noise ratio  $SNR$  for a continuum spectrum source is given by

$$SNR = \frac{\mathcal{A}}{\sigma_z}, \quad (320)$$

where  $\mathcal{A}$  is either  $\mathcal{A}^U$  or  $\mathcal{A}^L$ , depending on a choice of the single sideband actually received.

In following subsections, we will calculate the standard deviation of the correlator output  $\sigma_z$ , in order to get an explicit expression of the signal-to-noise ratio in terms of physical parameters characterizing the radio source and antenna-receiving systems.

## 4.2 Useful Formulae Related to the Correlator Output

In calculating the standard deviation of the correlator output  $\sigma_z$ , we will use following formulae relevant to the present problem.

### 4.2.1 Fourth Order Moment Relation

Let  $x_1, x_2, \dots, x_n$  are zero-mean random variables obeying to the jointly normal (or Gaussian) probability density given in equation (29):

$$f(x_1, \dots, x_n) = \frac{1}{\sqrt{(2\pi)^n \Delta}} e^{-\frac{1}{2} \sum_{i=1}^n \sum_{j=1}^n x_i C_{ij}^{-1} x_j}, \quad (321)$$

where expectation  $\eta_i$  of the random variable  $x_i$  figuring in equation (29) is zero by assumption for all  $i = 1, 2, \dots, n$ ;  $C_{ij} \equiv \langle x_i x_j \rangle$  is a covariance matrix,  $C_{ij}^{-1}$  is its inverse matrix, and  $\Delta \equiv \det\{C_{ij}\}$  is its determinant. In general, we denote an inverse matrix by a symbol  $( )^{-1}$  and a determinant by  $\det( )$ .

A very useful formula is known for such jointly normal random variables  $x_i$  ( $i = 1, \dots, n$ ):

$$\langle x_i x_j x_k x_l \rangle = \langle x_i x_j \rangle \langle x_k x_l \rangle + \langle x_i x_k \rangle \langle x_j x_l \rangle + \langle x_i x_l \rangle \langle x_j x_k \rangle, \quad (322)$$

which says that a fourth order statistical moment (a term “ $n$ -th order statistical moment” is used here to denote a statistical expectation of a product of  $n$  random variables)  $\langle x_i x_j x_k x_l \rangle$  is decomposed as a sum of products of second order statistical moment (correlations)  $\langle x_i x_j \rangle$ .

*Proof:*

1. Let us reformulate equation (321), using matrix notation of a row vector  $X$  and its transpose  $X^T$ :

$$X = \begin{pmatrix} x_1 \\ x_2 \\ \vdots \\ x_n \end{pmatrix}, \quad \text{and} \quad X^T = (x_1 \ x_2 \ \dots \ x_n),$$

where  $( )^T$  denotes a transpose matrix. Then we have

$$f(X) = \frac{1}{\sqrt{(2\pi)^n \Delta}} e^{-\frac{1}{2} X^T C^{-1} X}, \quad (323)$$

where  $C$  is the covariance matrix which is a positive-definite symmetric matrix with  $C_{ij} = \langle x_i x_j \rangle$  as  $ij$ -element.

2. Fourier transform of a probability density is called “characteristic function”. A characteristic function  $F(\Omega)$  of the joint probability density  $f(X)$  in equation (323), where  $\Omega$  is a row vector of angular frequencies  $\Omega^T = (\omega_1 \ \omega_2 \ \cdots \ \omega_n)$ , is given by

$$\begin{aligned} F(\Omega) &= \int_{-\infty}^{\infty} \cdots \int_{-\infty}^{\infty} f(X) e^{-i\Omega^T X} dx_1 \cdots dx_n = \langle e^{-i\Omega^T X} \rangle \\ &= \frac{1}{\sqrt{(2\pi)^n \Delta}} \int_{-\infty}^{\infty} \cdots \int_{-\infty}^{\infty} e^{-\frac{1}{2} X^T C^{-1} X - i\Omega^T X} dx_1 \cdots dx_n. \end{aligned} \quad (324)$$

3. According to the linear algebra, a symmetric matrix can be diagonalized by a suitable orthogonal transformation. So, let  $T$  be an orthogonal matrix, which diagonalizes the symmetric matrix  $C^{-1}$ :

$$T^T C^{-1} T = \begin{pmatrix} \lambda_1 & 0 & \cdots & 0 \\ 0 & \lambda_2 & \cdots & 0 \\ \vdots & \vdots & \ddots & \vdots \\ 0 & 0 & \cdots & \lambda_n \end{pmatrix}, \quad (325)$$

where  $\lambda_1, \lambda_2, \cdots, \lambda_n$  are eigen values of the matrix  $C^{-1}$ .

Since  $T$  is an orthogonal matrix, by definition we have

$$T^T T = T T^T = I, \quad T^{-1} = T^T, \quad \det T = 1, \quad (326)$$

where  $I$  is a unit matrix:

$$I = \begin{pmatrix} 1 & 0 & \cdots & 0 \\ 0 & 1 & \cdots & 0 \\ \vdots & \vdots & \ddots & \vdots \\ 0 & 0 & \cdots & 1 \end{pmatrix},$$

and, therefore,

$$T^T C T = (T^T C^{-1} T)^{-1} = \begin{pmatrix} \lambda_1^{-1} & 0 & \cdots & 0 \\ 0 & \lambda_2^{-1} & \cdots & 0 \\ \vdots & \vdots & \ddots & \vdots \\ 0 & 0 & \cdots & \lambda_n^{-1} \end{pmatrix}, \quad (327)$$

and

$$\Delta = \det C = \det T^T \det C \det T = \det(T^T C T) = \frac{1}{\lambda_1 \lambda_2 \cdots \lambda_n}. \quad (328)$$

4. If we introduce a new row vector  $Y$ :

$$Y^T = (y_1 \ y_2 \ \cdots \ y_n),$$

which is obtained by an orthogonal transformation of  $X$  with  $T$ :

$$Y = T^T X,$$

then we have

$$\begin{aligned} X = T Y, \quad \frac{\partial x_i}{\partial y_j} &= T_{ij}, \quad \frac{\partial(x_1 \ x_2 \ \cdots \ x_n)}{\partial(y_1 \ y_2 \ \cdots \ y_n)} = \det T = 1, \\ X^T C^{-1} X &= Y^T T^T C^{-1} T Y = \sum_{j=1}^n \lambda_j y_j^2, \\ \Omega^T X &= \Omega^T T Y = \sum_{i=1}^n \sum_{j=1}^n \omega_i T_{ij} y_j. \end{aligned} \quad (329)$$

Therefore, the characteristic function  $F(\Omega)$  given in equation (324) is reduced to

$$F(\Omega) = \frac{1}{\sqrt{(2\pi)^n \Delta}} \int_{-\infty}^{\infty} \cdots \int_{-\infty}^{\infty} e^{-\frac{1}{2} \sum_{j=1}^n \lambda_j y_j^2 - i \sum_{i=1}^n \sum_{j=1}^n \omega_i T_{ij} y_j} dy_1 \cdots dy_n. \quad (330)$$

If we further introduce new variables:

$$z_j = \sqrt{\frac{\lambda_j}{2}} y_j \quad (j = 1, \cdots, n),$$

then we have

$$\begin{aligned} F(\Omega) &= \frac{1}{\sqrt{(2\pi)^n \Delta}} \int_{-\infty}^{\infty} \cdots \int_{-\infty}^{\infty} \\ &e^{-\sum_{j=1}^n (z_j^2 + i \sum_{i=1}^n \omega_i T_{ij} \sqrt{\frac{2}{\lambda_j}} z_j)} \sqrt{\frac{2^n}{\lambda_1 \cdots \lambda_n}} dz_1 \cdots dz_n, \\ &= \frac{1}{\sqrt{\pi^n}} \int_{-\infty}^{\infty} \cdots \int_{-\infty}^{\infty} e^{-\sum_{j=1}^n (z_j^2 + i \sum_{i=1}^n \omega_i T_{ij} \sqrt{\frac{2}{\lambda_j}} z_j)} dz_1 \cdots dz_n. \end{aligned} \quad (331)$$

5. Applying the integration formula:

$$\int_{-\infty}^{\infty} e^{-x^2 - i a x} dx = \sqrt{\pi} e^{-\frac{a^2}{4}},$$

we reduce equation (331) to

$$\begin{aligned} F(\Omega) &= e^{-\frac{1}{4} \sum_{j=1}^n \left( \sum_{i=1}^n \omega_i T_{ij} \sqrt{\frac{2}{\lambda_j}} \right)^2} \\ &= e^{-\frac{1}{2} \sum_{i=1}^n \sum_{j=1}^n \sum_{k=1}^n \omega_i T_{ij} \frac{1}{\lambda_j} T_{kj} \omega_k} \\ &= e^{-\frac{1}{2} \Omega^T C \Omega}. \end{aligned} \quad (332)$$

6. From equations (324) and (332), we have

$$\langle e^{-i \Omega^T X} \rangle = e^{-\frac{1}{2} \Omega^T C \Omega}. \quad (333)$$

Expanding exponential functions in both sides of this equation into the Taylor series, we have

$$\begin{aligned} \langle e^{-i \Omega^T X} \rangle &= 1 - \frac{1}{2!} \langle (\Omega^T X)^2 \rangle + i \frac{1}{3!} \langle (\Omega^T X)^3 \rangle + \frac{1}{4!} \langle (\Omega^T X)^4 \rangle - \dots, \\ e^{-\frac{1}{2} \Omega^T C \Omega} &= 1 - \frac{1}{2} \Omega^T C \Omega + \frac{1}{2!} \left( \frac{1}{2} \Omega^T C \Omega \right)^2 - \dots. \end{aligned} \quad (334)$$

Terms with fourth order of  $\omega_i$ 's in the above equations are

$$\frac{1}{4!} \langle (\Omega^T X)^4 \rangle = \frac{1}{4!} \sum_{i=1}^n \sum_{j=1}^n \sum_{k=1}^n \sum_{l=1}^n \langle x_i x_j x_k x_l \rangle \omega_i \omega_j \omega_k \omega_l, \quad (335)$$

and

$$\begin{aligned} \frac{1}{2!} \left( \frac{1}{2} \Omega^T C \Omega \right)^2 &= \frac{1}{2!} \frac{1}{4} \sum_{i=1}^n \sum_{j=1}^n \sum_{k=1}^n \sum_{l=1}^n C_{ij} C_{kl} \omega_i \omega_j \omega_k \omega_l \\ &= \frac{1}{4!} \sum_{i=1}^n \sum_{j=1}^n \sum_{k=1}^n \sum_{l=1}^n (C_{ij} C_{kl} + C_{ik} C_{jl} + C_{il} C_{jk}) \omega_i \omega_j \omega_k \omega_l, \end{aligned} \quad (336)$$

respectively. Right hand sides of equations (335) and (336) are equal to each other in view of equation (333). Consequently, coefficients of  $\omega_i \omega_j \omega_k \omega_l$  in these equations, i.e.,  $\langle x_i x_j x_k x_l \rangle$  and  $C_{ij} C_{kl} + C_{ik} C_{jl} + C_{il} C_{jk}$ , must be equal to each other, too, since both of them are invariant in any substitution of  $i, j, k, l$ . Thus, we have

$$\langle x_i x_j x_k x_l \rangle = C_{ij} C_{kl} + C_{ik} C_{jl} + C_{il} C_{jk}. \quad (337)$$

Since  $C_{ij} = \langle x_i x_j \rangle$ , this completes the proof of equation (322).

### 4.2.2 Multiplier Output as a Stationary Random Process

If two voltage inputs  $U_1(t)$  and  $U_2(t)$  of a correlator are jointly stationary processes and if they obey the zero-mean jointly normal (or Gaussian) probability density such as given in equation (321), then their product  $y(t) = U_1(t) U_2(t)$  is also a stationary random process.

*Proof:*

1. Expectation of  $y(t)$  is a constant in time. In fact,

$$\langle y(t) \rangle = \langle U_1(t) U_2(t) \rangle = R_{U_1 U_2}(0), \quad (338)$$

where  $R_{U_1 U_2}(\tau) = \langle U_1(t) U_2(t - \tau) \rangle$  is a cross-correlation of jointly stationary random processes  $U_1(t)$  and  $U_2(t)$ , and, therefore,  $\langle y(t) \rangle$  does not depend on time  $t$ .

2. Autocorrelation of  $y(t)$  is a function of time difference only. In fact, in view of equation (322), we have

$$\begin{aligned} \langle y(t) y(t - \tau) \rangle &= \langle U_1(t) U_2(t) U_1(t - \tau) U_2(t - \tau) \rangle \\ &= \langle U_1(t) U_2(t) \rangle \langle U_1(t - \tau) U_2(t - \tau) \rangle \\ &\quad + \langle U_1(t) U_1(t - \tau) \rangle \langle U_2(t) U_2(t - \tau) \rangle \\ &\quad + \langle U_1(t) U_2(t - \tau) \rangle \langle U_2(t) U_1(t - \tau) \rangle \\ &= R_{U_1 U_2}^2(0) + R_{U_1 U_1}(\tau) R_{U_2 U_2}(\tau) + R_{U_1 U_2}(\tau) R_{U_1 U_2}(-\tau), \end{aligned} \quad (339)$$

where  $R_{U_1 U_1}(\tau) = \langle U_1(t) U_1(t - \tau) \rangle$  and  $R_{U_2 U_2}(\tau) = \langle U_2(t) U_2(t - \tau) \rangle$  are autocorrelations of input voltages  $U_1(t)$  and  $U_2(t)$ . This equation shows that  $\langle y(t) y(t - \tau) \rangle$  is a function of time difference  $\tau$  only.

Thus, we proved that the multiplier output  $y(t)$  is a stationary random process.

Since the integrator output (i.e., correlator output)  $z(t)$  is an output of a linear system of time averaging, given in equation (311), with the input  $y(t)$  which was shown to be a stationary random process, we conclude that  $z(t)$  is also a stationary random process.

Hereafter, we will denote autocorrelations of the multiplier output  $y(t)$  and the integrator output  $z(t)$  as functions of time difference  $\tau$ :

$$\begin{aligned} R_{yy}(\tau) &= \langle y(t) y(t - \tau) \rangle, \\ R_{zz}(\tau) &= \langle z(t) z(t - \tau) \rangle. \end{aligned} \quad (340)$$

### 4.2.3 Time Averaging Operator

Since the multiplier output  $y(t)$  and the integrator output  $z(t)$  are related to each other through the impulse response  $a(t)$  of the operator of time averaging, as shown in equation (311):

$$z(t) = y(t) * a(t),$$

their autocorrelations are related to each other as:

$$R_{zz}(\tau) = R_{yy}(\tau) * a(\tau) * a(-\tau), \quad (341)$$

in view of equation (42).

Therefore, if we denote power spectra of  $y(t)$  and  $z(t)$  as  $S_{yy}(\omega)$  and  $S_{zz}(\omega)$ :

$$\begin{aligned} S_{yy}(\omega) &\Leftrightarrow R_{yy}(\tau), \\ S_{zz}(\omega) &\Leftrightarrow R_{zz}(\tau), \end{aligned}$$

where symbol  $\Leftrightarrow$  stands for a Fourier transformation pair, and introduce a system function  $A(\omega)$  of  $a(t)$ :

$$A(\omega) \Leftrightarrow a(t),$$

then we have, in view of equation (72),

$$S_{zz}(\omega) = S_{yy}(\omega) |A(\omega)|^2. \quad (342)$$

Since

$$A(\omega) = \int_{-\infty}^{\infty} a(t) e^{-i\omega t} dt,$$

and, from equation (312),

$$\int_{-\infty}^{\infty} a(t) dt = 1,$$

the system function  $A(\omega)$  must always satisfy an equation:

$$A(0) = 1. \quad (343)$$

Note that, for the case of a simple running mean, the system function takes the sinc function form:

$$A(\omega) = \frac{1}{2T} \int_{-T}^T e^{-i\omega t} dt = \frac{\sin(\omega T)}{\omega T}. \quad (344)$$

In general,  $A(\omega)$  can be regarded as a low-pass filter with a narrow pass-band of about  $\pm 2\pi/T$ , as evident from the above simple case. If the integral time  $T$  is 1 s, for example, the passband is as narrow as  $\pm 1$  Hz.

#### 4.2.4 Power Spectrum of Multiplier Output

Let us now describe the power spectrum of the multiplier output  $S_{yy}(\omega)$  through power and cross-power spectra of voltages, which are the inputs to our correlator.

From equations (339) and (340), we have

$$R_{yy}(\tau) = R_{U_1U_2}^2(0) + R_{U_1U_1}(\tau) R_{U_2U_2}(\tau) + R_{U_1U_2}(\tau) R_{U_1U_2}(-\tau). \quad (345)$$

Therefore, Fourier transformation of this equation gives us the power spectrum  $S_{yy}(\omega)$ . Using convolution theorem in Fourier transformation, given in equation (67), for products of functions of  $\tau$ , we obtain

$$\begin{aligned} S_{yy}(\omega) &= \int_{-\infty}^{\infty} R_{yy}(\tau) e^{-i\omega\tau} d\tau \\ &= 2\pi R_{U_1U_2}^2(0) \delta(\omega) \\ &\quad + \frac{1}{2\pi} S_{U_1U_1}(\omega) * S_{U_2U_2}(\omega) + \frac{1}{2\pi} S_{U_1U_2}(\omega) * S_{U_1U_2}^*(\omega), \end{aligned} \quad (346)$$

where  $\delta(\omega)$  is the delta function of angular frequency  $\omega$ , and  $S_{U_1U_1}(\omega)$ ,  $S_{U_2U_2}(\omega)$ , and  $S_{U_1U_2}(\omega)$  are power and cross-power spectra of input voltages:

$$\begin{aligned} S_{U_1U_1}(\omega) &\Leftrightarrow R_{U_1U_1}(\tau), \\ S_{U_2U_2}(\omega) &\Leftrightarrow R_{U_2U_2}(\tau), \\ S_{U_1U_2}(\omega) &\Leftrightarrow R_{U_1U_2}(\tau). \end{aligned}$$

Here we used a relation:

$$\int_{-\infty}^{\infty} e^{-i\omega\tau} d\tau = 2\pi\delta(\omega),$$

which was given in equation (65), and for Fourier transform of a real function  $R_{U_1U_2}(-\tau)$ :

$$\begin{aligned} \int_{-\infty}^{\infty} R_{U_1U_2}(-\tau) e^{-i\omega\tau} d\tau &= \int_{-\infty}^{\infty} R_{U_1U_2}(\tau) e^{i\omega\tau} d\tau \\ &= \left( \int_{-\infty}^{\infty} R_{U_1U_2}(\tau) e^{-i\omega\tau} d\tau \right)^* = S_{U_1U_2}^*(\omega). \end{aligned}$$

### 4.2.5 Power and Cross-Power Spectra of Input Voltages

Power and cross-power spectra of input voltages figuring in equation (346) can be described as follows.

Assuming, as before, that signal and noise are not correlated with each other, and noises from different antennas are not correlated, either, we express autocorrelations and cross-correlation of input voltages  $U_1(t)$  and  $U_2(t)$  in terms of signal ( $V$ ) and noise ( $N$ ) components:

$$\begin{aligned} R_{U_1 U_1}(\tau) &= R_{V_1 V_1}(\tau) + R_{N_1 N_1}(\tau), \\ R_{U_2 U_2}(\tau) &= R_{V_2 V_2}(\tau) + R_{N_2 N_2}(\tau), \\ R_{U_1 U_2}(\tau) &= R_{V_1 V_2}(\tau), \end{aligned} \quad (347)$$

where

$$\begin{aligned} R_{V_1 V_1}(\tau) &= \langle V_1(t) V_1(t - \tau) \rangle, \\ R_{V_2 V_2}(\tau) &= \langle V_2(t) V_2(t - \tau) \rangle, \\ R_{V_1 V_2}(\tau) &= \langle V_1(t) V_2(t - \tau) \rangle, \end{aligned}$$

are auto- and cross-correlations of signal voltages  $V_1(t)$  and  $V_2(t)$ , while

$$\begin{aligned} R_{N_1 N_1}(\tau) &= \langle N_1(t) N_1(t - \tau) \rangle, \\ R_{N_2 N_2}(\tau) &= \langle N_2(t) N_2(t - \tau) \rangle, \end{aligned}$$

are autocorrelations of noise voltages  $N_1(t)$  and  $N_2(t)$ .

Therefore, the power and cross-power spectra are obtained by Fourier transformation of equations (347) as

$$\begin{aligned} S_{U_1 U_1}(\omega) &= S_{V_1 V_1}(\omega) + S_{N_1 N_1}(\omega), \\ S_{U_2 U_2}(\omega) &= S_{V_2 V_2}(\omega) + S_{N_2 N_2}(\omega), \\ S_{U_1 U_2}(\omega) &= S_{V_1 V_2}(\omega), \end{aligned} \quad (348)$$

where

$$\begin{aligned} S_{V_1 V_1}(\omega) &\Leftrightarrow R_{V_1 V_1}(\tau), \\ S_{V_2 V_2}(\omega) &\Leftrightarrow R_{V_2 V_2}(\tau), \\ S_{V_1 V_2}(\omega) &\Leftrightarrow R_{V_1 V_2}(\tau), \end{aligned}$$

are power and cross-power spectra of signal voltages, while

$$\begin{aligned} S_{N_1 N_1}(\omega) &\Leftrightarrow R_{N_1 N_1}(\tau), \\ S_{N_2 N_2}(\omega) &\Leftrightarrow R_{N_2 N_2}(\tau), \end{aligned}$$

are power spectra of noise voltages.

### 4.2.6 Antenna Temperature and System Noise Temperature

We saw in equation (169), that a power spectrum  $S_{v_i v_i}(\omega)$  of a received signal voltage  $v_i(t)$  ( $i = 1, 2$ ) at RF band, which is just received by  $i$ -th antenna, and has not yet gone through a receiving system, is given in terms of effective flux density  $S_\nu$  of an observed source and effective aperture of  $i$ -th antenna  $A_{e_i}$  by

$$S_{v_i v_i}(\omega) = \frac{1}{4} A_{e_i} S_\nu \quad (i = 1, 2).$$

Since the effective flux density and the antenna temperature  $T_{A_i}(\omega)$ , characterizing a received power from a radio source per unit bandwidth, are related to each other by an equation:

$$k T_{A_i}(\omega) = \frac{1}{2} A_{e_i} S_\nu,$$

as we saw in Chapter 2, where  $k = 1.381 \times 10^{-23} \text{ JK}^{-1}$  is Boltzmann's constant, the power spectrum of the received signal voltage is described through the antenna temperature as:

$$S_{v_i v_i}(\omega) = \frac{1}{2} k T_{A_i}(\omega) \quad (i = 1, 2). \quad (349)$$

Since the frequency conversion preserves the power spectrum of the received signal voltage, we can easily derive from equation (349) a power spectrum  $S_{V_i V_i}(\omega)$  of an IF signal voltage  $V_i(t)$  at an input of a correlator. Indeed, if we denote the system function of the receiving system as  $H_i(\omega)$ , as given in equation (195), and if we assume for definiteness upper sideband (USB) reception, we have

$$S_{V_i V_i}(\omega) = \frac{1}{2} k T_{A_i}(\omega_{LO} + \omega) |H_i(\omega)|^2 \quad (\text{for } \omega \geq 0, i = 1, 2), \quad (350)$$

where  $\omega$  is frequency in IF band and  $\omega_{LO}$  is local oscillator frequency of the frequency conversion. Here we showed only positive frequency side of the power spectrum, which is an essentially even function of frequency.

On the other hand, the noise component is described through the input equivalent system noise temperature  $T_{S_i}(\omega)$ , which is supposed to pass through the same receiving system as the radio source signal does. Thus, in the USB reception and in the positive frequency range, we have

$$S_{N_i N_i}(\omega) = \frac{1}{2} k T_{S_i}(\omega_{LO} + \omega) |H_i(\omega)|^2 \quad (\text{for } \omega \geq 0, i = 1, 2). \quad (351)$$

Therefore, from equations (348), (350), and (351), the power spectrum of the input voltage  $U_i(t)$  is given by

$$S_{U_i U_i}(\omega) = \frac{1}{2} k [T_{A_i}(\omega_{LO} + \omega) + T_{S_i}(\omega_{LO} + \omega)] |H_i(\omega)|^2 \quad (\text{for } \omega \geq 0, i = 1, 2), \quad (352)$$

in the USB reception and in the positive frequency range.

The cross-power spectrum of two input signal voltages  $V_i(t)$ , ( $i = 1, 2$ ) after delay tracking and fringe stopping is given in equation (242), for the case of the USB reception and in the positive frequency range of the Hermitian symmetric cross-power spectrum. Therefore, taking into account also equation (348), the cross-power spectrum of the input voltages  $U_i(t)$ , ( $i = 1, 2$ ) in the positive frequency range ( $\omega \geq 0$ ) is given by

$$S_{U_1 U_2}(\omega) = S_{V_1 V_2}(\omega) = \frac{1}{4} A_0 e^{-i(\phi_{LO1} - \phi_{LO2})} \mathcal{V}(\omega_{LO} + \omega) H_1(\omega) H_2^*(\omega), \quad (353)$$

where  $A_0$  is geometric mean of effective apertures of antennas,  $\phi_{LO1} - \phi_{LO2}$  is difference of initial phases of local oscillators, and we put  $\Delta\tau_g = 0$  in equation (242), assuming complete delay tracking and fringe stopping.

In a simple case of a point-like radio source with normalized power pattern of the interferometer  $A_N(\boldsymbol{\sigma}) = 1$  at centers of antenna beams, the complex visibility of the source is real and equal to its flux density,  $\mathcal{V}(\omega_{LO} + \omega) = S_\nu$ , as given in equation (295), and, therefore,

$$\frac{1}{4} A_0 \mathcal{V}(\omega_{LO} + \omega) = \frac{1}{4} \sqrt{A_{e1} A_{e2}} S_\nu = \frac{1}{2} k \sqrt{T_{A_1}(\omega_{LO} + \omega) T_{A_2}(\omega_{LO} + \omega)}. \quad (354)$$

In this case, we have, in  $\omega \geq 0$

$$S_{U_1 U_2}(\omega) = \frac{1}{2} k \sqrt{T_{A_1}(\omega_{LO} + \omega) T_{A_2}(\omega_{LO} + \omega)} e^{-i(\phi_{LO1} - \phi_{LO2})} H_1(\omega) H_2^*(\omega). \quad (355)$$

## 4.3 Sensitivity of a Radio Interferometer

### 4.3.1 Standard Deviation Due to the Noise

Now we are ready to calculate the standard deviation  $\sigma_z$  of the correlator output  $z(t)$  in equation (319), and then the signal-to-noise ratio in equation (320).

In equation (319):

$$\sigma_z = \sqrt{\langle z^2(t) \rangle - \langle z(t) \rangle^2},$$

the first term  $\langle z^2(t) \rangle$  in square root is given by inverse Fourier transformation at  $\tau = 0$  of the power spectrum  $S_{zz}(\omega)$ , which is related to  $S_{yy}(\omega)$  given in equation (346) through equation (342). Therefore, we have

$$\begin{aligned}
\langle z^2(t) \rangle &= \frac{1}{2\pi} \int_{-\infty}^{\infty} S_{zz}(\omega) d\omega = \frac{1}{2\pi} \int_{-\infty}^{\infty} S_{yy}(\omega) |A(\omega)|^2 d\omega \\
&= \frac{1}{2\pi} \int_{-\infty}^{\infty} \left[ 2\pi R_{U_1 U_2}^2(0) \delta(\omega) \right. \\
&\quad \left. + \frac{1}{2\pi} S_{U_1 U_1}(\omega) * S_{U_2 U_2}(\omega) + \frac{1}{2\pi} S_{U_1 U_2}(\omega) * S_{U_1 U_2}^*(\omega) \right] |A(\omega)|^2 d\omega \\
&= R_{U_1 U_2}^2(0) \\
&\quad + \frac{1}{(2\pi)^2} \int_{-\infty}^{\infty} \left[ S_{U_1 U_1}(\omega) * S_{U_2 U_2}(\omega) + S_{U_1 U_2}(\omega) * S_{U_1 U_2}^*(\omega) \right] |A(\omega)|^2 d\omega,
\end{aligned} \tag{356}$$

where  $A(\omega)$  is the system function of time averaging, and we used equation (343) for deriving the first term. On the other hand, second term  $\langle z(t) \rangle^2$  is equal to  $R_{U_1 U_2}^2(0)$ , since, in view of equations (317) and (338), we have

$$\langle z(t) \rangle = R_{U_1 U_2}(0).$$

Therefore, the first term of the right hand side of equation (356) is compensated by  $\langle z(t) \rangle^2$ , and hence we have

$$\sigma_z^2 = \frac{1}{(2\pi)^2} \int_{-\infty}^{\infty} \left[ S_{U_1 U_1}(\omega) * S_{U_2 U_2}(\omega) + S_{U_1 U_2}(\omega) * S_{U_1 U_2}^*(\omega) \right] |A(\omega)|^2 d\omega. \tag{357}$$

If we use explicit forms of convolution integrals, equation (357) is reduced to

$$\begin{aligned}
\sigma_z^2 &= \frac{1}{(2\pi)^2} \int_{-\infty}^{\infty} \int_{-\infty}^{\infty} \left[ S_{U_1 U_1}(\omega - \omega') S_{U_2 U_2}(\omega') \right. \\
&\quad \left. + S_{U_1 U_2}(\omega - \omega') S_{U_1 U_2}^*(\omega') \right] |A(\omega)|^2 d\omega' d\omega.
\end{aligned} \tag{358}$$

Since  $A(\omega)$  is a very narrow-band low-pass filter around  $\omega = 0$ , as we saw earlier,  $S_{U_1 U_1}(\omega - \omega')$  and  $S_{U_1 U_2}(\omega - \omega')$  can be replaced by  $S_{U_1 U_1}(-\omega') = S_{U_1 U_1}(\omega')$  and  $S_{U_1 U_2}(-\omega') = S_{U_1 U_2}^*(\omega')$ , and we can take them out of the integration with respect to  $\omega$ . Thus we obtain,

$$\sigma_z^2 = \frac{1}{(2\pi)^2} \int_{-\infty}^{\infty} \left[ S_{U_1 U_1}(\omega') S_{U_2 U_2}(\omega') + S_{U_1 U_2}^*(\omega') S_{U_1 U_2}(\omega') \right] d\omega' \int_{-\infty}^{\infty} |A(\omega)|^2 d\omega. \tag{359}$$

Taking into account that  $S_{U_1U_1}(\omega')$  is an even, and  $S_{U_1U_2}(\omega')$  is a Hermitian symmetric, functions, we can further reduce equation (359) to

$$\begin{aligned} \sigma_z^2 = & \frac{1}{2\pi^2} \int_0^\infty \{S_{U_1U_1}(\omega') S_{U_2U_2}(\omega') \\ & + \Re[S_{U_1U_2}(\omega') S_{U_1U_2}(\omega')]\} d\omega' \int_{-\infty}^\infty |A(\omega)|^2 d\omega. \end{aligned} \quad (360)$$

Now, assuming the USB reception, for definiteness, we apply equations (352) and (355) for spectra in positive frequency range ( $\omega \geq 0$ ) of input voltages to obtain

$$\begin{aligned} \sigma_z^2 = & \frac{k^2}{8\pi^2} \int_0^\infty \{(T_{A_1} + T_{S_1})(T_{A_2} + T_{S_2}) |H_1(\omega')|^2 |H_2(\omega')|^2 \\ & + \Re[(T_{A_1} T_{A_2}) e^{-2i(\phi_{LO_1} - \phi_{LO_2})} H_1(\omega') H_2^*(\omega') H_1(\omega') H_2^*(\omega')]\} d\omega' \\ & \times \int_{-\infty}^\infty |A(\omega)|^2 d\omega, \end{aligned} \quad (361)$$

where we omitted argument  $\omega_{LO} + \omega$  in  $T_{A_i}$  and  $T_{S_i}$  ( $i = 1, 2$ ) for simplicity.

Since, in actual observations of most of radio sources, antenna temperatures are much smaller than system noise temperatures:  $T_{A_i} \ll T_{S_i}$  ( $i = 1, 2$ ), we ignore terms with  $T_{A_i}$ , compared with terms with  $T_{S_i}$  ( $i = 1, 2$ ). Then, assuming a flat noise spectrum, we obtain an equation:

$$\sigma_z^2 = \frac{k^2 T_{S_1} T_{S_2}}{8\pi^2} \int_0^\infty |H_1(\omega')|^2 |H_2(\omega')|^2 d\omega' \int_{-\infty}^\infty |A(\omega)|^2 d\omega, \quad (362)$$

which describes the dispersion of noise fluctuations in the correlator output.

### 4.3.2 Signal in the Correlator Output

Now, if we assume a continuum spectrum source and USB reception, the signal in the correlator output is given by the theoretical expression of the fringe amplitude  $\mathcal{A}$  in equation (260):

$$\mathcal{A} = A_0 |\mathcal{V}| |\mathcal{B}_{12}|,$$

where  $A_0$  is the geometric mean of effective apertures of element antennas,  $|\mathcal{V}|$  is the visibility amplitude, and  $|\mathcal{B}_{12}|$  is the amplitude of the bandwidth

pattern defined in equation (254). In the simple case of the point-like source, for which the visibility  $\mathcal{V}$  is equal to the flux density  $S_\nu$ , we have

$$A_0 |\mathcal{V}| = \sqrt{A_{e_1} A_{e_2}} S_\nu = 2k \sqrt{T_{A_1} T_{A_2}},$$

and, therefore,

$$\mathcal{A} = 2k \sqrt{T_{A_1} T_{A_2}} |\mathcal{B}_{12}|. \quad (363)$$

### 4.3.3 Signal-to-Noise Ratio of the Correlator Output

Consequently, the signal-to-noise ratio is given by

$$\begin{aligned} SNR &= \frac{\mathcal{A}}{\sigma_z} \\ &= 8\pi \sqrt{\frac{T_{A_1} T_{A_2}}{T_{S_1} T_{S_2}}} \frac{|\mathcal{B}_{12}|}{\sqrt{2 \int_0^\infty |H_1(\omega')|^2 |H_2(\omega')|^2 d\omega'}} \frac{1}{\sqrt{\int_{-\infty}^\infty |A(\omega)|^2 d\omega}}. \end{aligned} \quad (364)$$

Let us first assume simple rectangular filters which are given in positive frequency range ( $\omega \geq 0$ ) by:

$$|H_i(\omega)|^2 = \begin{cases} G_i & \text{if } \omega_I - \frac{\Delta\omega}{2} \leq \omega \leq \omega_I + \frac{\Delta\omega}{2}, \\ 0 & \text{otherwise,} \end{cases} \quad (365)$$

where  $i = 1, 2$ ,  $G_i$  is a gain factor in a receiving system of  $i$ -th antenna,  $\omega_I$  is a center IF frequency of the filter passband, and  $\Delta\omega = 2\pi B$  is an angular frequency bandwidth, corresponding to a frequency bandwidth  $B$ .

In this case, the coefficient  $G$  of the bandwidth pattern given in equation (262) is equal to  $G = \sqrt{G_1 G_2}$ . Therefore, the amplitude of the bandwidth pattern  $|\mathcal{B}_{12}|$  is reduced to

$$\mathcal{B}_{12} = \frac{\sqrt{G_1 G_2} B}{2} \frac{\sin(\pi B \Delta\tau_g)}{\pi B \Delta\tau_g} = \frac{\sqrt{G_1 G_2} B}{2} \quad (\text{for } \Delta\tau_g = 0), \quad (366)$$

where we assumed complete delay tracking and fringe stopping with residual delay  $\Delta\tau_g = 0$ . On the other hand, we obviously have

$$\int_0^\infty |H_1(\omega')|^2 |H_2(\omega')|^2 d\omega' = 2\pi G_1 G_2 B. \quad (367)$$

Therefore, we obtain

$$\frac{8\pi |\mathcal{B}_{12}|}{\sqrt{2 \int_0^\infty |H_1(\omega')|^2 |H_2(\omega')|^2 d\omega'}} = \sqrt{4\pi B}. \quad (368)$$

For more general case of non-rectangular filters, we will adopt this equation (368) as a definition of bandwidth  $B$ .

On the other hand, if we assume the simple running mean of equation (313) for the time averaging, then an integration time  $\tau_a$  is equal to the interval of averaging  $\tau_a = 2T$ . In this case, equation (344) shows that the system function of time averaging  $A(\omega)$  has a simple sinc function form:

$$A(\omega) = \frac{\sin(\omega T)}{\omega T}.$$

Therefore,

$$\int_{-\infty}^{\infty} |A(\omega)|^2 d\omega = \int_{-\infty}^{\infty} \frac{\sin^2(\omega T)}{\omega^2 T^2} d\omega = \frac{\pi}{T} = \frac{2\pi}{\tau_a},$$

and, hence, we have

$$\frac{1}{\sqrt{\int_{-\infty}^{\infty} |A(\omega)|^2 d\omega}} = \sqrt{\frac{\tau_a}{2\pi}}. \quad (369)$$

For more general case of non-running-mean averaging, we will adopt this equation (369) as a definition of integration time  $\tau_a$ .

Inserting equations (368) and (369) to equation (364), we obtain an equation for the signal-to-noise ratio  $SNR$  in radio interferometry:

$$SNR = \frac{\mathcal{A}}{\sigma_z} = \sqrt{\frac{T_{A_1} T_{A_2}}{T_{S_1} T_{S_2}}} \sqrt{2 B \tau_a}. \quad (370)$$

This equation (370) is very similar to the one for the single dish telescope, which we mentioned in Chapter 2, except for an extra factor 2 in  $\sqrt{2B\tau_a}$ . The difference comes from the fact that, in case of the single baseline interferometry, the system noise contributions from 2 antennas are independent, and, therefore, not correlated, unlike in the single dish telescope case.

#### 4.3.4 Additional Remarks on the $SNR$ Formula

Although we derived equation (370) assuming a point-like and continuum spectrum source in a case of USB reception, the equation can be applied to more general cases, if we

- multiply a ratio of correlated flux density  $|\mathcal{V}|$  and total flux density  $S_{T\nu}$ , i.e.,  $|\mathcal{V}|/S_{T\nu}$ , to  $\sqrt{T_{A_1} T_{A_2}}$  for an extended source,
- take line width instead of the filter bandwidth for  $B$  for a line spectrum source,
- take LSB values of  $T_{A_i}$  and  $T_{S_i}$  ( $i = 1, 2$ ) in LSB reception.

An extra “efficiency factor”  $\eta_c$ , typically  $\eta_c \cong 0.5 \sim 0.9$ , is multiplied to the right hand side of equation (370) in case of digital data processing, in order to take into account losses associated with digitization and digital logics, as we will discuss later. Then, the signal-to-noise ratio  $SNR$  is usually given by:

$$SNR = \eta_c \sqrt{\frac{T_{A_1} T_{A_2}}{T_{S_1} T_{S_2}}} \sqrt{2 B \tau_a}. \quad (371)$$

#### 4.3.5 A Simple Interpretation of the $\sqrt{B \tau_a}$ Factor

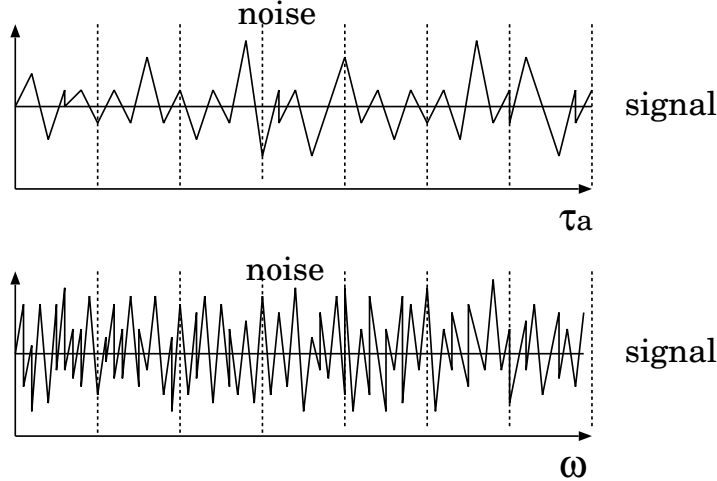


Figure 65: Schematic diagram explaining how the signal-to-noise ratio of a stationary signal with a continuum spectrum is improved by increasing the integration time  $\tau_a$  and the bandwidth  $B$ , in proportion to  $\sqrt{B \tau_a}$ .

Figure 65 gives a qualitative explanation why we have a factor  $\sqrt{B \tau_a}$  in a formula of signal-to-noise ratio. In fact, we can increase the number of independent measurements, by increasing the integration time  $\tau_a$  and the bandwidth  $B$  for a stationary source with a continuum spectrum, thus improving the signal-to-noise ratio in proportion to  $\sqrt{\tau_a}$  and  $\sqrt{B}$ .

### 4.3.6 Formulae for $SNR$ and Minimum Detectable Flux Density

If correlated flux density of an observed source is  $S_\nu$ , and effective apertures, aperture diameters, and aperture efficiencies of antennas are  $A_{e1}$ ,  $A_{e2}$ ,  $L_1$ ,  $L_2$ , and  $\eta_{A1}$ ,  $\eta_{A2}$ , respectively, we can rewrite equation (371) in a form:

$$SNR = \eta_c \frac{\sqrt{A_{e1} A_{e2}} S_\nu}{2k \sqrt{T_{S1} T_{S2}}} \sqrt{2 B \tau_a}, \quad (372)$$

or

$$SNR = \eta_c \frac{\pi}{8k} \frac{\sqrt{\eta_{A1} \eta_{A2}} L_1 L_2 S_\nu}{\sqrt{T_{S1} T_{S2}}} \sqrt{2 B \tau_a}. \quad (373)$$

Or, by introducing system equivalent flux densities (SEFDs) of the antennas,

$$SEFD_1 = \frac{2k T_{S1}}{A_{e1}}, \quad \text{and} \quad SEFD_2 = \frac{2k T_{S2}}{A_{e2}},$$

we have

$$SNR = \eta_c \frac{S_\nu}{\sqrt{SEFD_1 SEFD_2}} \sqrt{2 B \tau_a}. \quad (374)$$

For example, if we observe a source with correlated flux density 0.2 Jy, with antenna diameters of  $L_1 = L_2 = 20$  m,  $T_{S1} = T_{S2} = 120$  K,  $\eta_{A1} = \eta_{A2} = 0.5$ ,  $B = 256$  MHz,  $\eta_c = 0.88$ , and  $\tau_a = 100$  sec, then we expect to obtain a signal-to-noise ratio  $SNR \cong 19$ , which is clearly detectable.

On the other hand, if we denote a limiting  $SNR$  value, necessary for detection of a source by an interferometer, as  $(\mathcal{SNR})$ , we can derive from equation (373) the minimum correlated flux density  $S_{\nu min}$  detectable by the interferometer:

$$S_{\nu min} = (\mathcal{SNR}) \frac{8k}{\pi \eta_c} \frac{\sqrt{T_{S1} T_{S2}}}{\sqrt{\eta_{A1} \eta_{A2}} L_1 L_2 \sqrt{2 B \tau_a}}. \quad (375)$$

For VLBI,  $SNR \sim 6 - 7$  is usually adopted as the detection threshold. If we adopt  $\mathcal{SNR} = 7$ , and assume again  $L_1 = L_2 = 20$  m,  $T_{S1} = T_{S2} = 120$  K,  $\eta_{A1} = \eta_{A2} = 0.5$ ,  $B = 256$  MHz,  $\eta_c = 0.88$  and  $\tau_a = 100$  sec, then we obtain  $S_{\nu min} = 0.074$  Jy. We can observe many radio sources with such a sensitivity. In particular, almost all extragalactic continuum spectrum radio sources regularly observed in international geodetic VLBI observations are readily detected, since their flux densities are mostly  $S_\nu > 0.1$  Jy.

## References

- Papoulis, A., 1984, Probability, Random Variables, and Stochastic Processes, 2nd Edition, *McGraw-Hill* (New York).
- Thompson, A.R., Moran, J.M., and Swenson, G.W., Jr., 2001, Interferometry and Synthesis in Radio Astronomy, *John Wiley & Sons* (New York).